Award Number:
W81XWH-07-1-0215

TITLE:
Cellular Therapy to Obtain Rapid Endochondral Bone Formation

PRINCIPAL INVESTIGATOR: Elizabeth A. Olmsted-Davis, Ph.D.

CONTRACTING ORGANIZATION:
Baylor College of Medicine
Houston, TX 77030

REPORT DATE: February, 2011

TYPE OF REPORT: Final Year 4

PREPARED FOR: U.S. Army Medical Research and Materiel Command
Fort Detrick, Maryland 21702-5012

DISTRIBUTION STATEMENT:

distribution unlimited

REPORT DOCUMENTATION PAGE

Form Approved
OMB No. 0704-0188

1. REPORT DATE *(DD-MM-YYYY)*	2. REPORT TYPE	3. DATES COVERED *(From - To)*
28-FEB-2011	Final Year 4	1 MAR 2010 - 28 JAN 2011

4. TITLE AND SUBTITLE

Cellular Therapy to Obtain Rapid Endochondral Bone Formation

5a. CONTRACT NUMBER

5b. GRANT NUMBER
W81XWH-07-1-0215

5c. PROGRAM ELEMENT NUMBER

6. AUTHOR(S)
Elizabeth A. Olmsted-Davis, Ph.D.

edavis@bcm.tmc.edu

5d. PROJECT NUMBER
5e. TASK NUMBER
5f. WORK UNIT NUMBER

7. PERFORMING ORGANIZATION NAME(S) AND ADDRESS(ES)

Baylor College of Medicine
One Baylor Plaza, BCM505
Houston, Texas 77030

8. PERFORMING ORGANIZATION REPORT NUMBER

9. SPONSORING / MONITORING AGENCY NAME(S) AND ADDRESS(ES)

US ARMY MEDICAL RESEARCH AND
MATERIEL COMMAND
504 SCOTT STREET
FORT DETRICK, MD 21702-5012

10. SPONSOR/MONITOR'S ACRONYM(S)

11. SPONSOR/MONITOR'S REPORT NUMBER(S)

12. DISTRIBUTION / AVAILABILITY STATEMENT

distribution unlimited

13. SUPPLEMENTARY NOTES
N.A.

14. ABSTRACT The goal of this study is to provide a safe effective system for inducing bone formation for fracture healing in situations of significant trauma. This set of proposed experiments will provide significant knowledge to the field of bone tissue engineering. Proposed studies will provide essential biological information and involves the development of a novel biomaterial that can safely house the cells expressing the bone inductive factor to produce the new bone at which time the material is then selectively eliminated. Ultimately this system has significant applicability. Often bone graft must be surgically removed from the pelvis, to implant into the site of difficult fractures for proper healing. This additional surgery often results in significant pain, and long term healing. Further, this system would be applicable to orthopedic trauma situations that previously resulted in amputation. We propose in these studies to complete the development of this bone induction system and test it in a preclinical animal model. Validation of our hypothesis will provide a safe and efficacious material for the production of bone leading to reliable fracture healing, circumventing the need for bone grafts, or for direct administration of cells, viruses, or other materials that could lead to significant adverse reactions.

15. SUBJECT TERMS
BMP2, hydrogel, critical size defect, nonunion, gene therapy, adenovirus.

16. SECURITY CLASSIFICATION OF:			17. LIMITATION OF ABSTRACT	18. NUMBER OF PAGES	19a. NAME OF RESPONSIBLE PERSON
a. REPORT	b. ABSTRACT	c. THIS PAGE			19b. TELEPHONE NUMBER *(include area code)*
U	U	U	U	167	

Standard Form 298 (Rev. 8-98)
Prescribed by ANSI Std. Z39.18

Table of Contents

Introduction: This project, on the use of cell-based gene therapy for the production of rapid endochondral bone formation, and fracture healing is a collaborative effort between a bio-engineering/biomaterials group at Rice University and Baylor College of Medicine. Although bone possesses the rare capacity to continually renew and repair itself, more than 500,000 bone repair surgical procedures are performed annually within the United States alone. The need to enhance or initiate bone formation in a controlled clinical manner has brought tissue engineering to the forefront of orthopedic research. Much recent effort has been directed to the identification of factors essential to normal bone formation, and the development of new osteoconductive materials that can temporarily fill areas of missing osteoid. Still lacking are effective osteoinductive components that could be seeded into the osteoconductive materials to generate normal bone which this study will explore. The central hypothesis of this application is that rapid bone formation can be successfully achieved with only minimally invasive percutaneous techniques and without a scaffold, by using cells transduced with adenovirus vectors to express an osteoinductive factor (BMP2), which have been encapsulated in hydrogel material and later photopolymerized at the desired site.

The goal of this study is to provide a safe effective system for inducing bone formation for fracture healing. This set of proposed experiments will provide significant knowledge to the field of bone tissue engineering. Proposed studies will provide essential biological information and involves the development of a novel biomaterial that can safely house the cells expressing the bone inductive factor to produce the new bone at which time the material is then selectively eliminated. Ultimately this system has significant applicability. Often bone graft must be surgically removed from the pelvis, to implant into the site of difficult fractures for proper healing. This additional surgery often results in significant pain, and long term healing. Further, this system would be applicable to orthopedic trauma situations that previously resulted in amputation. We propose in these studies to complete the development of this bone induction system and test it in a preclinical animal model. Validation of our hypothesis will provide a safe and efficacious material for the production of bone leading to reliable fracture healing, circumventing the need for bone grafts, or for direct administration of cells, viruses, or other materials that could lead to significant adverse reactions.

Body: The central hypothesis of this application is that rapid bone formation can be successfully achieved with only minimally invasive percutaneous techniques and without a scaffold, by using cells transduced with adenovirus vectors to express an osteoinductive factor (BMP2), which have been encapsulated in hydrogel material and later photopolymerized at the desired site.

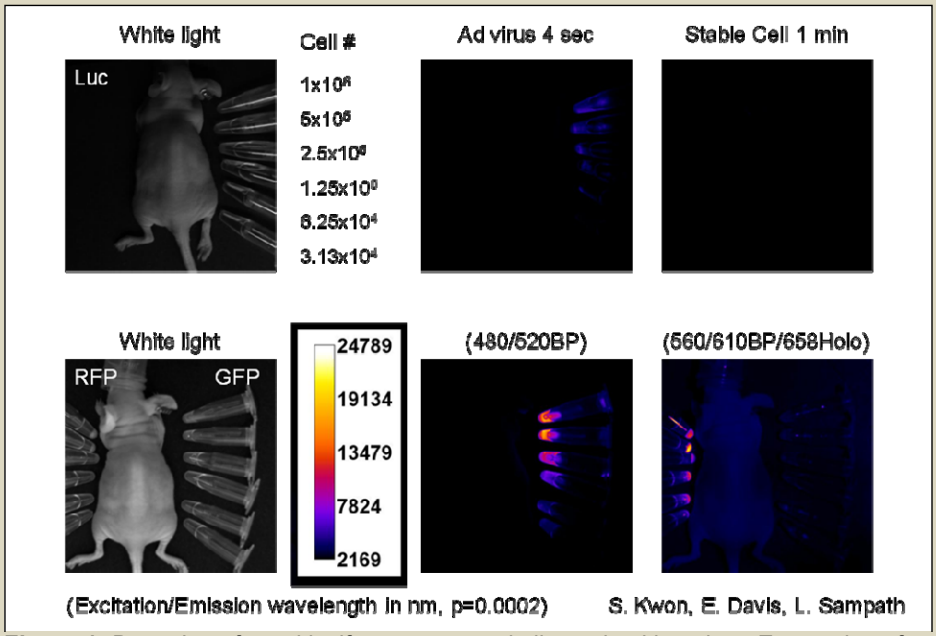

Figure 1: Detection of a red luciferase reporter in live animal imaging. Expression of a red shifted luciferase reporter was compared both in cells, and in live animals after subcutaneous intramuscular injection.Two types of cells were tested, one which was a cell line that had the reporter stably integrated, and the other cells which had been transduced with an AdCRBluc virus.

Task 1: *To determine the optimal levels of BMP2 for efficient rapid production of endochondral bone from human bone marrow mesenchymal stem cells (hBM-MSCs) transduced with a tetracycline regulated Ad5F35tet-BMP2 adenovirus carrying a red luciferase reporter gene.*

a. To determine if sustained expression of BMP2 is more efficient at inducing rapid bone formation than a pulse of expression using the tetracycline regulated vectors. **(Months 0-12)** Comparison studies were performed to determine the optimal method for tracking transgene expression *in vivo*.

As seen in figure 1, the originally described methodology using red luciferase reporter gene expression was compared to other red-shifted reporters to determine if we could obtain something more sensitive which would allow us to image the expression of the transgene during bone formation. In original experiments using luciferase (figure 1) we were unable to readily detect the reporter after intramuscular injection of our transduced cells at the levels routinely used for induction of bone formation. However, as seen in figure 2, when this was compared to dsRED, a red fluorescent protein, we could readily detect dsRED. Therefore we initiated studies using dsRED in place of the red luciferase.

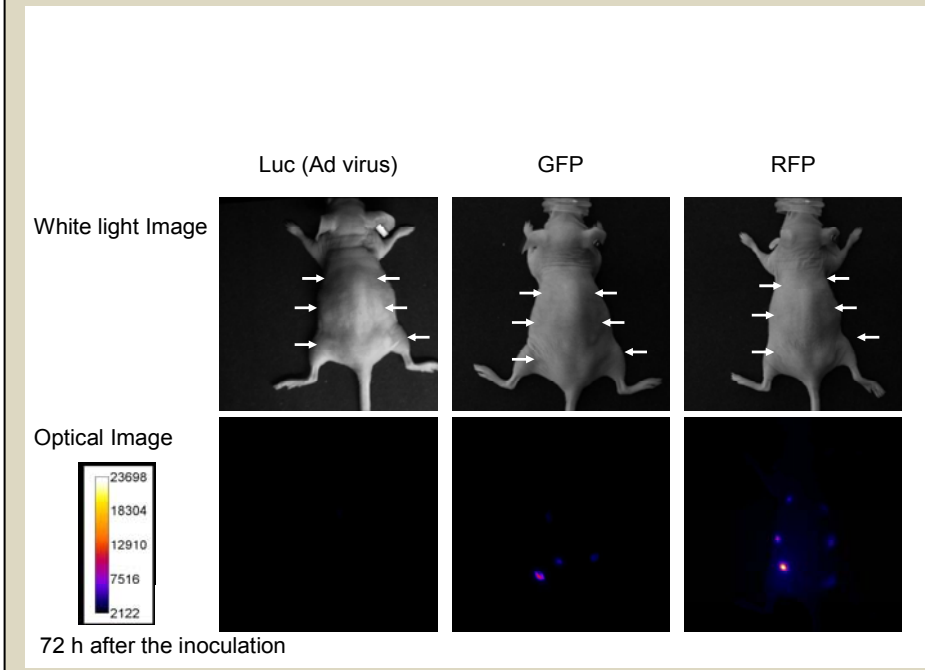

Figure 2: Comparison of reporter expression after intramuscular injection of dsRED, GFP, and CRBluc in live animals, through optical imaging.

In these studies, cells were transduced with Ad5dsRED (2500 vp/cell) and were encapsulated into microbead structures using PEGDA hydrogel (nondegradable). The microbeads were then injected into the hind limbs of the animal, and transgene expression compared to animals receiving the same Ad5dsRED transduced cells which have not been encapsulated.

Two days after the initial injection of cells, dsRED expression was readily detected whether cells were encapsulated or not and in no cases were cells or microspheres detected migrating from the injection site (Figure 3A). The dsRED expression, as measured by fluorescence intensity at 590 ± 10 nm, was significantly elevated in microencapsulated Ad5dsRED-transduced cells compared to other groups (Figure 3B). Microencapsulated control cells transduced with AdEmpty cassette had no fluorescent signal at 590 ± 10 nm, demonstrating that neither the cells nor the PEGDA were autofluorescing. Fluorescent intensity in animals receiving Ad5dsRED-transduced cells directly injected was substantially reduced after seven days and was indistinguishable from control. In microencapsulated Ad5dsRED-transduced cells, this 590 ± 10 nm dsRED fluorescent signal was significantly elevated over that of microencapsulated control cells for 15 days (Figure 3B). After 15 days, these levels dropped; however, signal was still detectable (Figure 3A, arrows) in some animals, suggesting that the microencapsulated cells remained viable to express the dsRED transgene. Statistical power to detect intensity over control ranged from 100% in microencapsulated cells to 99.7% in directly injected cells, and power to detect the difference between microencapsulated and unencapsulated cells was 88%.

Through these imaging experiments we are able to use dsRED to analyze bone formation after delivery of BMP2 short term or long term. **See following section.**

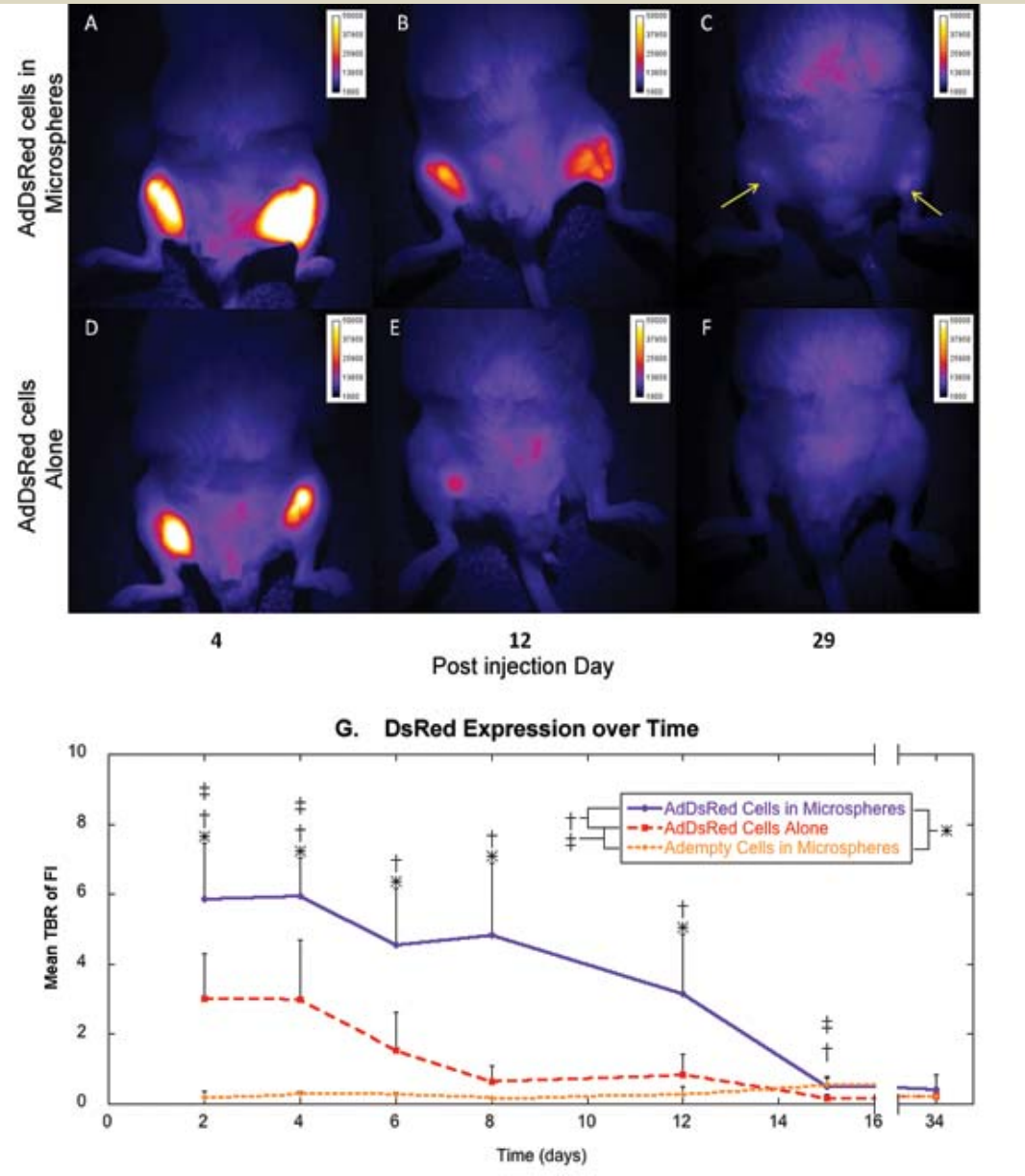

Figure 3: Optical fluorescence imaging of mice injected with cells expressing dsRed. Top panels (A through C) are images of a representative mouse (n=4) injected with dsRed-expressing cells encapsulated in microspheres and bottom panels (D through F) are of a mouse injected with dsRed-expressing cells directly, without microspheres. The images were taken at day 4, 12 and 29 post-injection of cells. By day 29, the fluorescent signal is at background levels or undetectable for the mouse given dsRed-expressing cells without microspheres (F). Whereas, the signal remains detectable in the mouse given dsRed-expressing cells encapsulated in microspheres (C).
G. Mean Target-to-Background Ratio (TBR) of Fluorescence Intensity (FI) in mice given unencapsulated dsRed cells, microencapsulated dsRed cells or microencapsulated control cells. * $p \leq 0.05$ for microencapsulated dsRed cells versus microencapsulated control cells; † $p \leq 0.05$ for microencapsulated dsRed cells versus unencapsulated dsRed cells; ‡ $p \leq 0.05$ for unencapsulated dsRed cells versus microencapsulated control cells.

b. ***To determine if longer expression times of BMP2 from cells embedded in hydrogel and longer cellular viability lead to more rapid bone formation than the rapid but short burst of BMP2 release obtained from the cells directly injected. (Months 9-12)***

We next set up similar experiments to track the dsRED in live animals during heterotopic ossification. In these experiments, we transduced the cells with an Ad5BMP2-dsRED virus, which was not tetracycline regulated. In these studies we look at the ability to detect the signal through the bone matrix that is forming. As seen in figure 4, dsRED could readily be detected above background for up to 16 days. Interestingly, the cells directly injected appeared to be readily detected, and stronger than the cells within the microbeads. Both the microbeads and directly injected cells were tracked up to 16 days, again which is odd, considering all previous experiments appeared to remove the cells rapidly after 6 -8 days. The data does suggest that we can track the reporter even in the presence of bone formation. Further, the signal is stronger in the directly injected cells, most likely because the microbeads, and bone itself that is forming, shield the signal as compared to the directly injected cells that are not necessarily encapsulated within the bone. Further, the bone formation as determined by micro CT was not as robust in the samples receiving the cells directly, thus less shield would also occur.

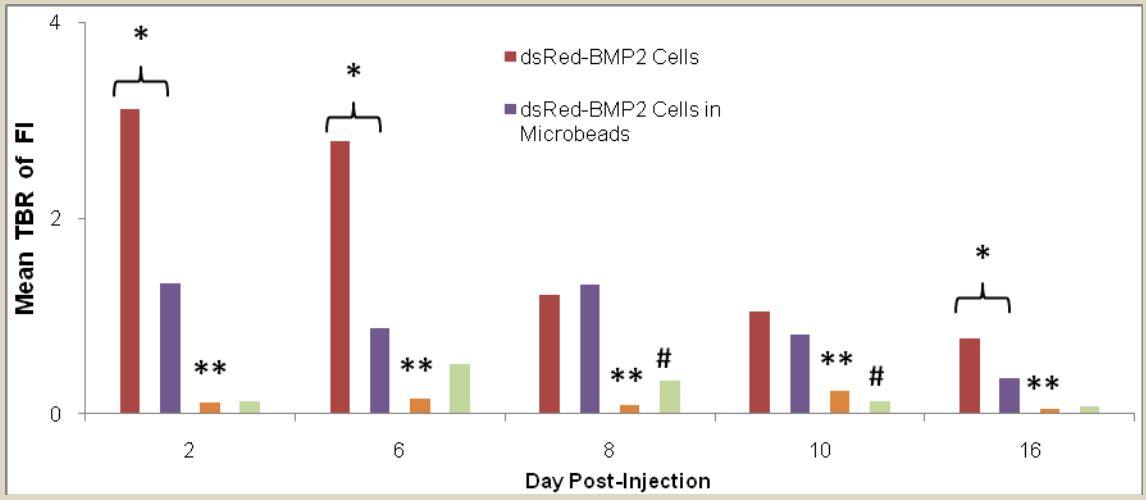

Figure 4: Mean Target-to-Background Ratio (TBR) of Fluorescence Intensity (FI) in mice given unencapsulated dsRed cells, microencapsulated dsRed cells or microencapsulated control cells.
*P < 0.05 for Ad5dsRED-BMP2 transduced cells versus Ad5dsRED-BMP2 cells in microbeads at days 2, 6, and 16 post-injection.
**P < 0.05 for Ad5dsRED-BMP2 cells transduced cells versus Ad5dsRED-BMP2 cells in microbeads at all time points.
# P < 0.05 for dsRED-BMP2 cells in microbeads versus Ad5empty cassette transduced cells (Control) in microbeads at days 8 and 10 after injection.

In these live animal imaging experiments we determined that the hydrogel greatly increased the length of expression time of the BMP2. Further, although the when similar numbers of cells are encapsulated in hydrogel microspheres (See Task 2), led to 3 fold more bone than was obtained when these cells were directly injected, the pattern of the new bone, suggested that this may be in part because the area of BMP2 expression was much greater, due to the addition of the polymer whereas the cells directly injected clumped between the muscle fibers and were encompassed a much smaller region. Further, dose curves done in rats (see Task 3) clearly show that there is a maximum amount of bone that can be obtained, and adding more BMP2 did not lead to a greater effect, presumably because the receptors may be saturated. ***This work has been published in Olabisi, R. et al, Tissue Engineering Part A. Dec 2010, 16(12):3727-36 and Lazard, Z.W. et al, J Cellular Biochemistry, In press).*** ***These two sub-aims are completed.***

c. To demonstrate the termination of BMP2 expression using an Ad5F35tet-BMP2-IRESCBRLuc vector in which expression can be tracked through live animal imaging. ***(Months 12-24). See above section.***

d.To determine what the responder cells to the BMP2 are proximal or more distal to the hydrogel encapsulated delivery cells by performing live animal confocal imaging which follows the translocation of a Smad 1 to the nucleus. ***(Months 24-48)***

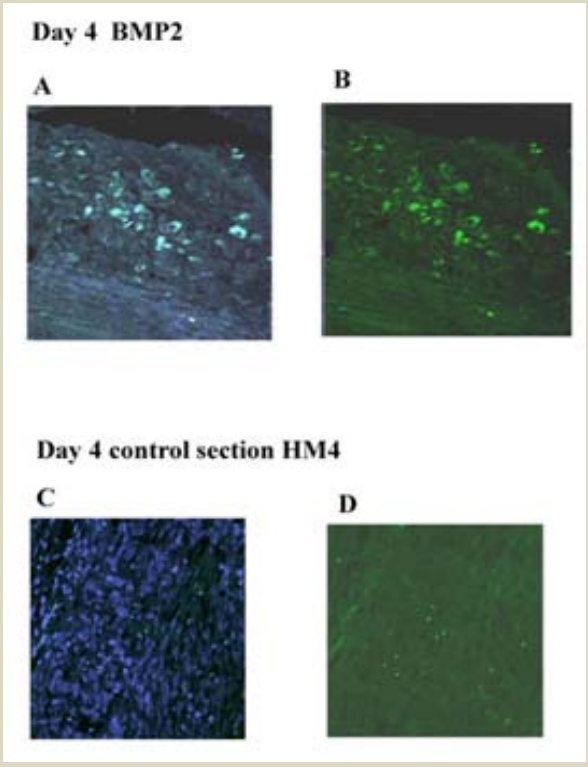

Figure 5: Immnuno-fluorescence staining on tissues isolated four days after receiving Ad5F35BMP2 transduced cells (A and B) or cells transduced with a control virus Ad4F35HM4 (C and D). Sections B and D are stained with Phospho-Smad1/5/8 antibody (1/100 dilution, Cell Signaling technology) and a secondary antibody anti-rabbit Alexa Fluor 488 conjugated. Sections A and C and stained with Phospho-Smad1/5/8 and counterstained with DAPI

could be one of the earliest responding cells to the BMP2.

Previous work in the literature suggests that the nerves respond to BMP2 by inducing neuroinflammation through the secretion of substance P and CGRP proteins. To determine if BMP2 directly activates expression of the neuroinflammatory proteins SP and CGRP during heterotopic ossification, proteins were isolated from tissues at daily intervals, starting 24 hours after delivery of AdBMP2 or Adempty (control virus) transduced cells, through the appearance of heterotopic bone. Quantification of protein levels of SP and CGRP within the tissues, through ELISA, is shown in figure 6A and B, respectively. Both proteins appear to be significantly elevated ($p \leq 0.0005$), compared to controls, within 24 hours after induction of HO, and again at 72 hours ($p \leq 0.005$) and 6 days ($p \leq 0.05$) after induction. Expression, therefore, appeared somewhat cyclical, and statistical analyses, using a one-way ANOVA

We generated the proposed mouse line, but were unable to detect the YFP expression most likely due to the nature of smad expression. This is a low copy number protein and without additional amplification, as with immunostaining, the expression was below the level of detection. We next switched the YFP to cyanin fluorescent protein and red fluorescent protein; neither provided high enough expression within the nucleus to provide unequivocal data. Therefore we went ahead and did some immuno staining with an antibody specific to phosphoSmad (figure 5). We localized positive expression to several cell types, however, in tissue sections isolated at 24 hours after delivery of BMP2, the expression was found associated with the peripheral nerves whereas, tissues receiving the control cells had no positive expression. Since BMP2 had previously been shown to have direct effects on peripheral nerves in culture, we next determined whether the nerve

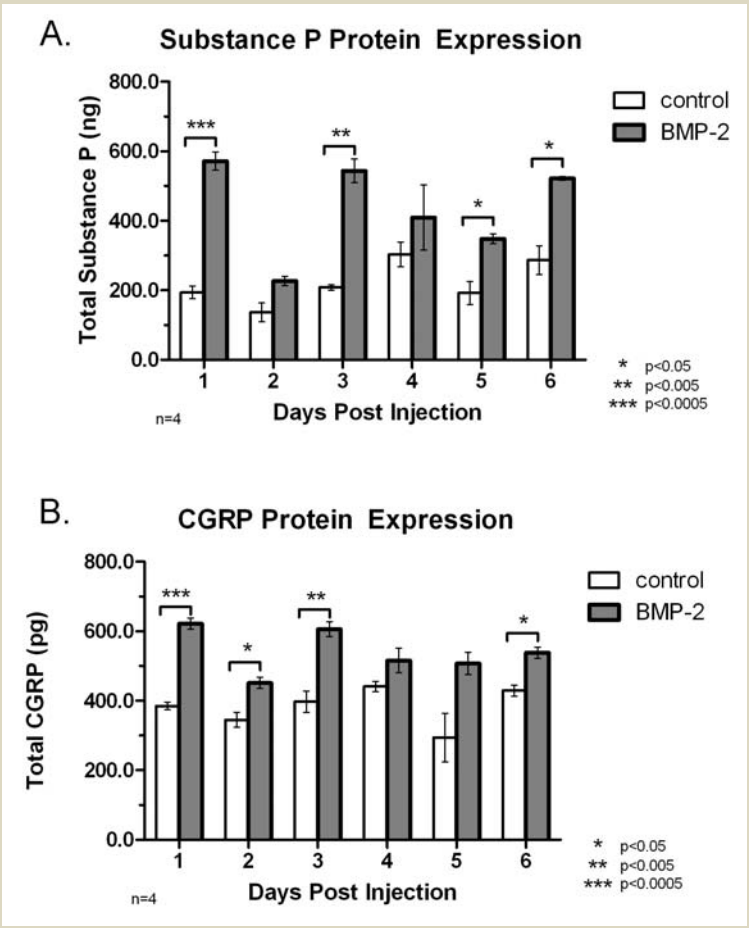

Figure 6: Quantitation of substance P and CGRP protein by ELISA. Soft tissues, which encompass the site of new bone formation, were isolated at daily intervals from animals receiving either AdBMP2 (BMP2) or Adempty (control) transduced cells, and protein extracts were generated. **A.)** Substance P total protein was quantified and statistically significant changes between the groups, as denoted by an asterisk, determined using a standard t-test; n=4. **B.)** CGRP total protein was quantified and statistically significant changes between the groups, as denoted by an asterisk, determined using a standard t-test; n=4. * denotes statistical significance.

with a post-hoc Bonferroni test for comparison between time points, verified a significant drop in SP and CGRP between days 1 and 2 ($p \leq 0.005$). This was followed by a significant rise between days 2 and 3 ($p \leq 0.005$). The data suggests that BMP2 induced a substantial and immediate release of these proteins, which was attenuated, but then continued for the remainder of endochondral bone formation, through the appearance of mineralized bone (Figure 6).

Tissues were next immunostained for the presence of SP and CGRP and analyzed to determine if the expression of these factors was associated with nerves throughout the entire hind limb, or limited to the region of new bone formation. Figure 7 shows representative images of the expression of SP and CGRP within the tissues isolated 4 days after receiving either AdBMP2 or Adempty transduced cells. By day 4 of HO, delivery cells are no longer found within the tissues, and the control appears as normal muscle (Figure 7D). However, there is a nidus of cartilage forming in tissues undergoing HO (Figure 7A). Figure 2 shows the positive expression of SP (green) or CGRP (red) in these tissues. As seen in figure 7, panels D-F, we observed a small amount of positive expression associated with a mature nerve structure within control tissues, but expression was not found within the muscle itself. In contrast, in tissue receiving BMP2, expression was co-localized with the region undergoing cartilage formation and was limited to this region. This suggests that the expression of these factors is associated with BMP2, as predicted, and the continued expression of these factors was localized to new cartilage and bone formation.

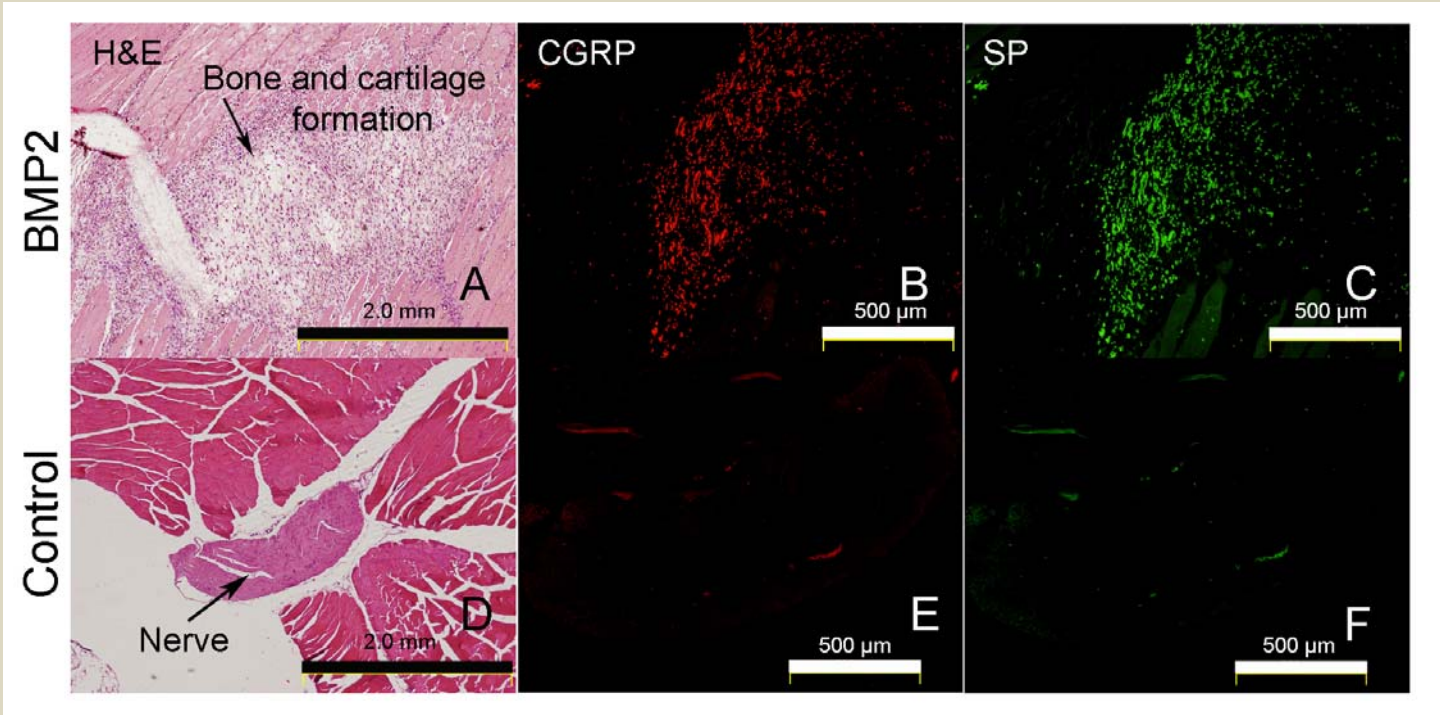

Figure 7: Photomicrographs of substance P and CGRP protein expression in tissues isolated four days after induction of HO. Tissues receiving cells transduced with AdBMP2 (BMP2) or Adempty cassette (control) were isolated four days after induction and immunostained with antibodies against substance P and CGRP. Expression of these factors was found to co-localize with the area of newly forming bone, but was minimal in tissues receiving the Adempty cassette transduced cells. Hematoxylin and eosin stained serial sections, adjacent to the section used for immunostaining four days after receiving **(A)** AdBMP2 transduced cells or **(D)** Adempty cassette transduced cells. Positive staining in the region of new bone (**B and C**) or nerve (**E and F**) for CGRP (B and E; red color) or substance P (C and F; green color).

The induction of neuroinflammatory mediators occurs through activation of sensory neurons by localized stimulus, or, in this case, secretion of BMP2. To determine if induction of neuroinflammation is contributing to HO, bone formation was quantified in animals that lacked TRPV1 ($TRVP1^{-/-}$), resulting in a functional loss of activity of sensory neurons. These $TRVP1^{-/-}$ animals lack a functional cationic channel on peripheral, sensory nerve terminals, which regulate neurogenic inflammation. We quantified the changes in SP and CGRP protein expression within tissues isolated from these knockout animals, and observed a significant suppression compared to the wild type counterpart, although we did observe a slight increase in their expression upon delivery of BMP2.

HO was induced in both TRVP1$^{-/-}$ and wild type mice (n=7), and, after 10 days, the resultant bone formation was quantified through micro-computed tomography (μCT). Figure 8A shows a representative three dimensional reconstruction of the bone formation. Heterotopic bone volume within TRVP1$^{-/-}$ mice was inhibited significantly ($p \leq 0.05$), as compared to wild type mice (Figure 8B).

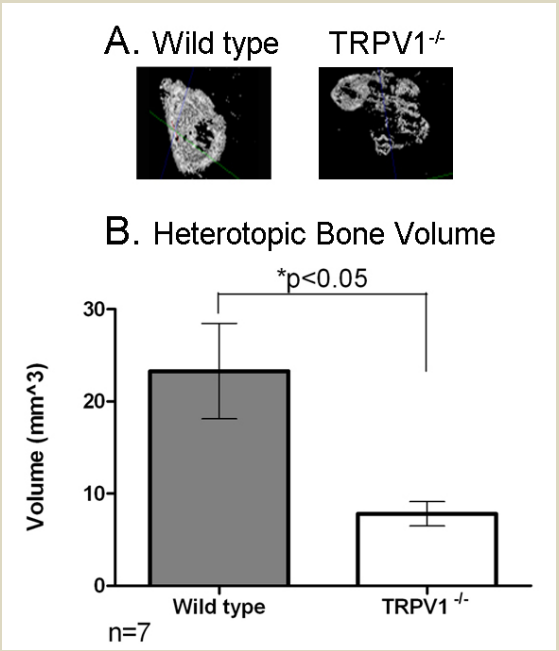

Figure 8: Microcomputational analysis of heterotopic ossification ten days after induction with AdBMP2 transduced cells, in C57/BL6, wild type or TRVP1$^{-/-}$ mice. **(A)** Three dimensional reconstructions of representative samples for each group. **(B)** Quantitation of bone volume and statistically significant changes between the groups was determined using a one-way analysis of variance; n=7. * denotes statistical significance.

for the release of SP and CGRP within the tissues, suggesting mast cells may be recruited after release of these factors.

Since mast cells are known to migrate throughout the tissues, co-localization with specific tissue structures was also noted. As seen in figure 9C, mast cells appeared to be scattered throughout the control tissues. However, within the tissues receiving AdBMP2 transduced cells, mast cells associated only with the nerves (figure 9B), in tissues isolated 2 days after induction of bone formation. As bone formation continues, the mast cells within the tissues receiving BMP2 continue to be localized within the nerve itself; however, a subset also appear within the vessel structures (data not shown). We did not see mast cells localizing within the nerve structures in control tissues at any time point.

The reduction of HO when there is a lack of functional TRVP1 signaling suggests that this pathway may be functionally important to the process of HO. The next step in neuroinflammatory signaling involves recruitment of mast cells and their resultant degranulation, for the release of key enzymes involved in processing proteins essential for inflammatory signaling and recruitment. To determine whether mast cells were recruited to the site of new bone formation, muscle tissues from the hind limbs of wild type mice injected with AdBMP2 or Adempty transduced cells were isolated at daily intervals and then serially sectioned in entirety for quantification. There appears to be a trend toward more mast cells within the tissues undergoing HO, as compared to the control tissues (figure 9A). However, only day 2 shows a statistically significant increase in the number of mast cells. It is intriguing that we observed the most significant difference at these early stages, since this appears to parallel our findings

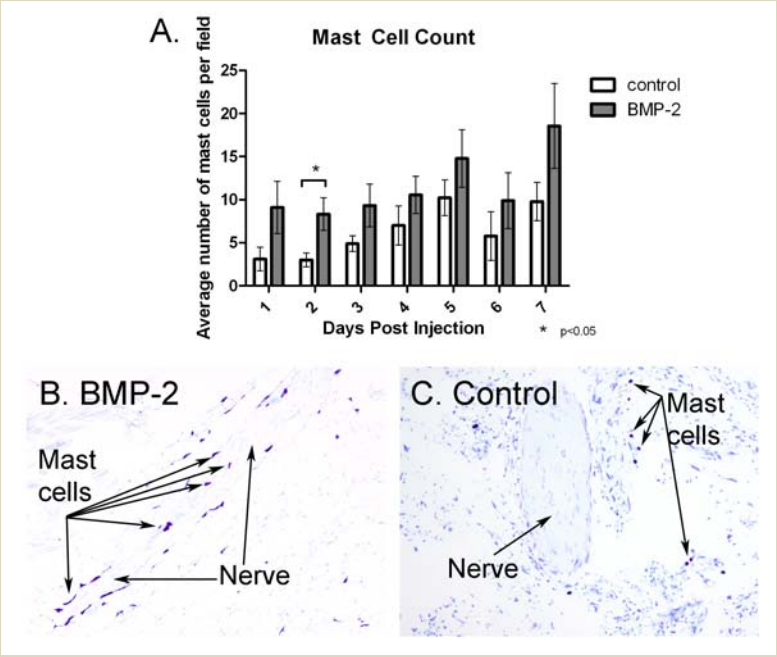

Figure 9: Quantitation of mast cells in tissues surrounding the area of new bone formation. Tissue sections were stained with the mast cell stain, toluidine blue. Photomicrographs of random fields (5 per section) were taken at 10X magnification, for every fifth slide, throughout the entire hind limb. Each field equals 5.2mm^2. **(A)** Quantification of the average number of mast cells within the tissues at daily intervals after induction of HO. Statistically significant changes were determined using a standard t-test; n=3 biological replicates. Seven slides were analyzed per tissue, and 5 fields per slide (35 images quantified per sample/time point). * denotes statistical significance. **(B)** Representative photomicrographs of tissues isolated two days after receiving AdBMP2 (BMP2) or Adempty (control) transduced cells, stained with toluidine blue. Positive cells are highlighted with arrows.

Mast cell degranulation leads to the release of degradative enzymes, such as tryptase and chymase. These enzymes are known to degrade or process other proteins, leading to their activation. Many of the enzymes are involved in tissue remodeling, including the nerve structure itself. To determine if mast cell degranulation could be a factor in heterotopic ossification, animals were pretreated with the drug sodium cromoglycate (cromolyn), which has been shown to prevent mast cell degranulation. Following the pretreatment with either cromolyn or a vehicle control (PBS), HO was induced and the resultant bone formation quantified 10 days later. Figure 10A shows representative images of three dimensional reconstructions of the resultant HO formation after cromolyn or control, PBS treatment. As can be seen in figure 10B, quantification of bone volume of the HO shows a significant ($p \leq 0.05$) decrease in animals after cromolyn treatment. The observed decrease in HO formation after cromolyn treatment was similar to that observed in the TRVP1 null mice, thus supporting the idea that suppression of this pathway inhibits HO.

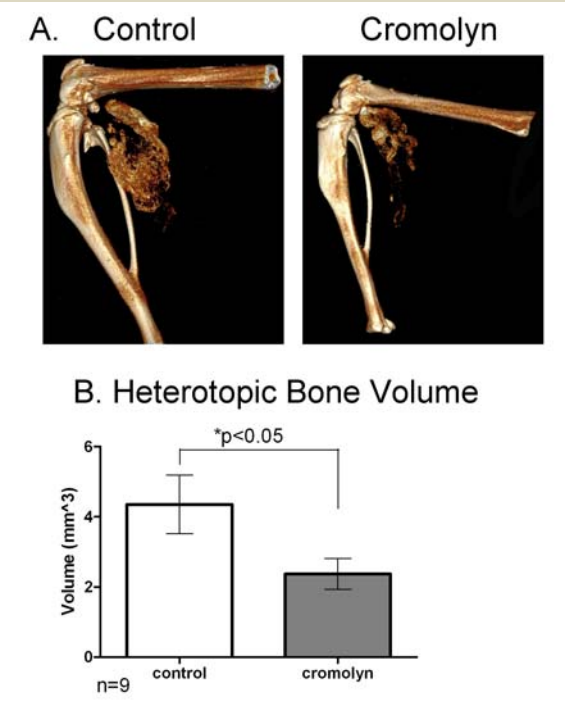

Figure 10: Microcomputational analysis of heterotopic ossification ten days after induction with AdBMP2 transduced cells, in mice pre-treated with either cromolyn or vehicle control (PBS). **(A)** Three dimensional reconstructions of representative samples for each group. **(B)** Quantitation of bone volume and statistically significant changes between the groups was determined using a one-way analysis of variance; n=9. * denotes statistical significance.

The data collectively suggests a molecular model in which sensory neurons signal to induce neuro-inflammatory mediator expression and mast cell migration and degranulation, which ultimately facilitate HO. Since others have shown that progenitors reside within the nerve sheath [30] and can expand upon nerve remodeling after injury, we analyzed the nerves isolated in hind limb tissues from cromolyn or vehicle treated animals after induction of HO. We hypothesized cromolyn treatment would block nerve remodeling, and thus, the ultimate release of progenitors perhaps residing within the nerve. The tissues were immunostained for expression of a variety of stem cell markers, and, intriguingly, we observed changes in the subset of markers related to pluripotency. Figure 11A shows representative photomicrographs of tissues immunostained for expression of Nanog and Krüppel-like family of transcription factor 4 (Klf4) within the tissues isolated two days after induction of HO. As seen in 11A, in animals that received cromolyn, cells positive for these factors were observed throughout the nerve (Fig 11A; c,d), as demonstrated by neurofilament staining (Fig 11A; b,f). However, in tissues isolated from animals that received vehicle, these markers were significantly reduced, to completely absent throughout the nerve (Fig 11A; g, h). We observed $nanog^+$ and $Klf4^+$ cells within tissues isolated from wild type animals undergoing HO, but such cells are rare and are often not co-localizing with the nerve. Both these markers have been implicated in maintenance of the pluripotential phenotype observed in embryonic stem (ES) cells, with Klf4 actually enhancing the expression of the nanog gene in ES cells. Interestingly, the osteoblast specific transcription factor osterix was also found associated with the nerve sheath (figure 11B). Osterix expression was observed in the nerve by co-staining with the neural marker neurofilament (figure 11B; g, h, i), in tissues isolated 2 days after BMP2 induction, in the presence of cromolyn. These osterix positive cells also appeared to co-localize with a portion of the primitive stem cell factors, suggesting that a subset of the cells may be undergoing differentiation (Figure 11B, panels a-f).

This work demonstrates the ability of the secreted BMP2 to induce neuro-inflammation which leads to

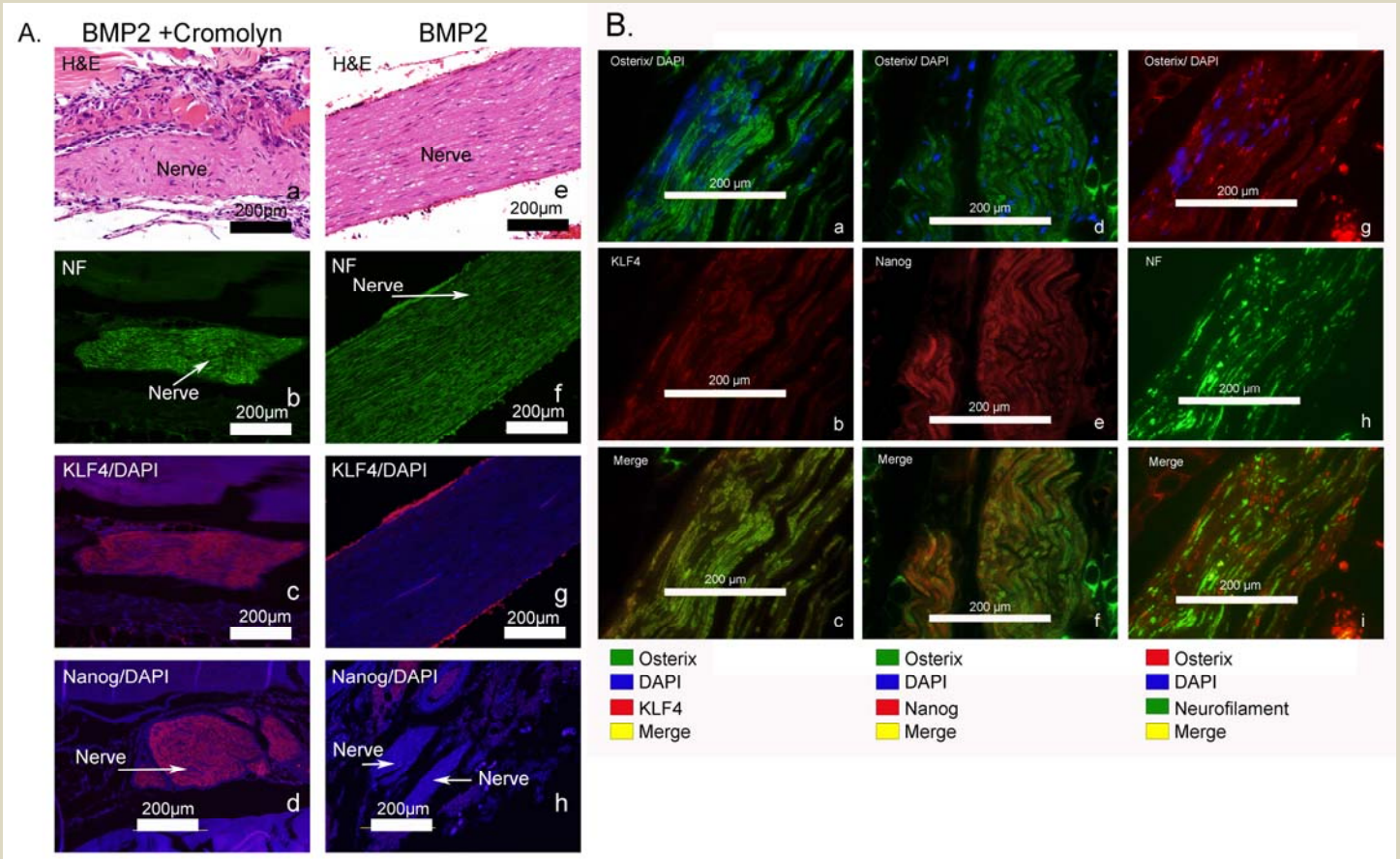

Figure 11. Peripheral nerves contain primitive stem cell markers and osterix after BMP2 induction in the presence of cromolyn. **A.** Photomicrographs of tissues isolated two days after induction of HO. Tissues from animals receiving cells transduced with AdBMP2 and pre-treated with either cromolyn (a-d) or vehicle control (e-h) were isolated two days after induction, and immunostained with antibodies against stem cell markers, Klf4 and Nanog. Expression of these factors was found to co-localize to nerves residing within the area of new bone formation. Nerves were identified by hematoxylin and eosin staining of a serial section adjacent to the immunostainned tissues (**a** and **e**) and by neurofilament (NF) staining (**b** and **f**; green color). Positive staining for Klf4 (**c**; red color) or Nanog (**d**; red color) was observed throughout the nerves in tissues isolated from animals receiving cromolyn at 2 days after induction. In comparison, the nerves in animals receiving vehicle control appeared to lack positive staining for either Klf 4 (**g**; red color) or nanog (**h**; red color). **B.** Photomicrographs of osterix expression within tissues isolated two days after BMP2 induction in the presence of cromolyn. Images of osterix expression (**g**; osterix red color, DAPI blue color) associated with the nerve (**h**; neurofilament, NF, green color). **i**, osterix and NF, is a merger of g and h. Images of the expression of **a, d** osterix (green, DAPI blue) and **b**, Klf4 (red) or **e**, nanog (red). **c**, osterix and Klf4, is a merger of a and b. **f**, osterix and nanog is a merger of d and e.

the release of factors and recruitment of mast cells for the remodeling of the local peripheral nerves. This appears to be critical to the process of de novo bone formation, in that inhibition of this process, led to a significant reduction in bone formation. Further, we demonstrate the appearance of osterix positive cells within the remodeling nerve. These cells appear to be expanding and trafficking off the nerve towards the region where new bone will be established. Interestingly, these cells appear 2-3 days prior to the appearance of any bone, suggesting that this marker may be expressed for other reasons than to induce the osteogenic phenotype or that these new osteoprogenitors may reside within the vessel structures until oxygen tension is restored through cartilage removal and vascular invasion (Shafer *et al,* 2007; Olmsted-Davis *et al,* 2007, and Fouletier-Dilling *et al*, 2010).

Conclusions: From the experiments in this aim, we have determined that the level of BMP2 in our experiments most likely is maximum and thus longer expression times do not appear to extend the reaction. However, the ability to target the exact placement of the material can not only increase the bone volume (Olabisi *et al*, 2010), but that it increased the area of responder tissues. Further we have identified one of the first direct immediate response to BMP2 within the localized tissues is from the peripheral nerve. This

activation of the nerve is **essential** to bone formation, and results in the migration of several cell populations from the nerve. One of these populations appears to be a pre-osteoblastic population that migrates towards the vessel structures, where it is housed until 2-3 days later when vessels infiltrate the hypertrophic condrocytes, and deposit the osteoblasts (Salisbury *et al*, In review, American Journal of Pathology). Further our data suggests that these nerves associated stem cells, are also the precursor for brown adipose, an essential tissue for vascularization, and patterning of the newly forming cartilage (Olmsted-Davis et al, 2007, Salisbury, In preparation). Therefore we propose that perhaps the early expression of osterix 2-3 days prior to the appearance of bone may be a mechanism to suppress the adipose phenotype in a sub-population of the cells. Further, the population of these stem cells which do not immediately associate with the vessels, but rather migrate into the adipose and muscle tissues, expresses the beta-adrenergic receptor 3 sub type, which has been shown to generate brown adipose. Isolation of these cells shows the co-expression of uncoupling protein 1 within these cells, and RNA studies of the tissues shows a significant increase in both mRNA's during this time, suggesting that activation of sensory neurons by BMP2, may launch of a cascade of events, that activates sympathetic neurons, presumably through release of serotonin by mast cells and platelets. Further, immediate recruitment of platelets to the local site, leads to the release of monocyte chemoattractant factors which can recruit myeloid cells necessary for vascular invasion, and bone formation. Therefore we have identified a pathway for BMP2 induced bone formation which requires both nerve and inflammatory signaling to occur, and demonstrated that ablation of this pathway will ultimately ablate bone formation and healing. **We currently have one published manuscript (Olabisi et al, 2010, Tissue Engineering), one manuscript in press (Salisbury, et al, 2011 Am. J Path), and a second manuscript in preparation which when published *will result in completion of the aims described in this Task.***

Task 2: To design an optimal hydrogel material that will rapidly promote endochondral bone formation and be capable of removal through bone remodeling processes. In addition to BMP2 transduced cells, we propose to include peptides essential to the recruitment and migration of osteoprogenitors for bone and cartilage. Selective protease sites will also be introduced into the hydrogel to allow for osteoclast selective degradation during bone remodeling. We propose to do this by incorporation of calcium into the material and inclusion of cathepsin K protease cleavage sites into the material. Inclusion of these factors in the hydrogel will provide a mechanism for removal of the hydrogel once bone has formed by using the normal bone remodeling process.

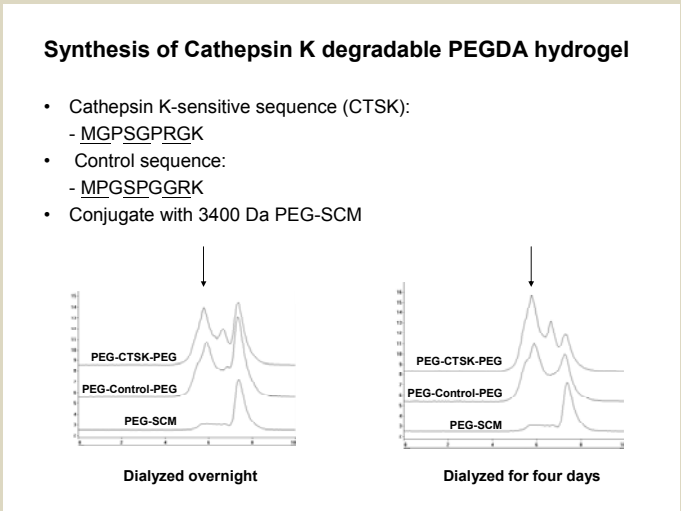

Figure 12: Results of HPLC analysis of the conjugation of peptide with the PEGDA hydrogel.

(Months 0-24)

We have synthesized the peptide MGPSGPRG (Gowen et a;1999) using a 431A solid-phase peptide synthesizer (Applied Biosystems, Foster City, CA). In order to make degradable PEG, we start with PEG-DA-SMC (succinimidyl carbonate). The PEG-SMC is conjugated with our peptide in order to get PEG-PEPTIDE-PEG. So, we expect to obtain three peaks representing the completely conjugated product: PEG-PEPIDE-PEG, incompletely conjugated product: PEG-PEPTIDE and unconjugated product: PEG-SMC (Figure 12).

We have run GPC tests on it and the results

a. Optimize and develop a hydrogel that can be specifically degraded by osteoclasts.

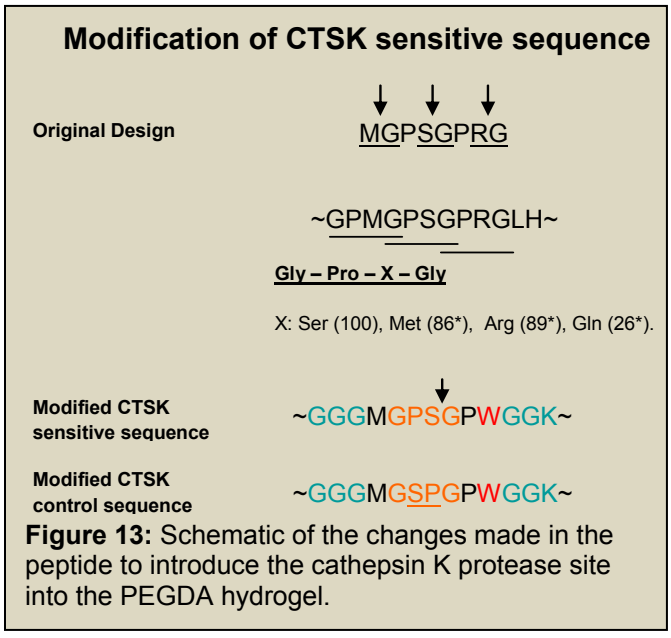

Figure 13: Schematic of the changes made in the peptide to introduce the cathepsin K protease site into the PEGDA hydrogel.

indicate that there is still unconjugated PEG, ie: we have PEG-Peptide or free PEG in the preparations. We have tried changing the ratio of peptide to PEG, changing the length of conjugation time, increasing the pore size of the dialysis membrane and changing the length we dialyze the conjugation products. These have led to a higher concentration of PEG-PEPTIDE-PEG as indicated by the GPC results (Figure 13). We have cathepsin K (Calbiochem; Cathepsin K, His•Tag®, Human, Recombinant, *E. coli*). Degradation tests have found that the material did not degrade as expected. Analysis of the materials suggested that the protease site may be too confined to actually bind enzyme for digestion, thus, the protease site was redesigned to have a longer amino acid sequence linker to allow for better digestion. Thus the modified peptide sequence is GGGMGPSGPWGGK, see figure 13.

We next examined the ability of the cathepsin K sensitive hydrogels to degrade in the presence of the enzyme. The hydrogels with the cathepsin K sensitive peptide GGGMGPSGPWGGK were designed to carry a cathepsin K sensitive cleavage site between serine and proline. Proteinase K was used as a positive control. While the gel degrades, the peptide that was incorporated into the hydrogel structure will be cleaved by enzymes and gradually release into solution. The degradation profiles of GPSG hydrogels were measured by monitoring the concentration change of tryptophan in solution at UV absorbance of 280 nm. Crosslinkable GPSG hydrogels were polymerized in microcuvettes and incubated with enzyme solutions. After equilibrium swelling in TBS overnight, hydrogels were treated with different enzymes to evaluate the degradation profiles (Figure 14). After incubation with different enzyme solutions for 24 hours, hydrogels in cathepsin K and proteinase K solutions has similar degradation profiles, both indicating a rapid tryptophan concentration increase within the first hour and reaching about 80% release of total tryptophan at 24 hours. No degradation was observed when hydrogels were incubated in TBS buffer, NaOAc buffer, and plasmin. Hydrogels incubated in nonspecific collagenase I and collagenase III solutions also released 40% of incorporated tryptophan after a 24 hour incubation (figure 7). ***This work has recently been accepted for publication in Journal Biomaterials Research (Chih-Wei Hsu, Ronke M. Olabisi, Elizabeth A. Olmsted-Davis, Alan R. Davis, Jennifer L. West Cathepsin-K sensitive poly(ethylene Glycol) hydrogels for degradation in response to bone formation. This subaim is completed.***

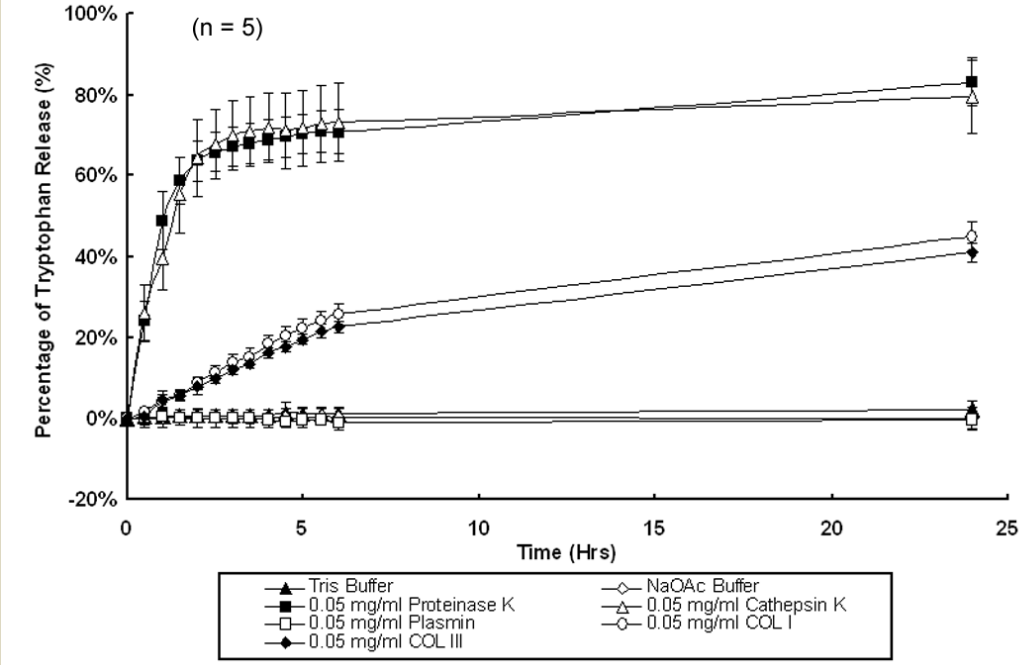

Figure 14: Degradation profiles of cathepsin K-sensitive GPSG hydrogels. Hydrogel droplets (3 µl) were polymerized in each micro-cuvette and swelled overnight with 250 µl of TBS buffer. Each hydrogel was incubated in buffer or enzyme solution at 0.05 mg/ml at 37^{O}C. UV absorbance at 280 nm was measured over 24 hours to monitor tryptophan release corresponding to the degradation of the GPSP hydrogels.

b. Engineer cellular binding sights within the hydrogel to determine if this improves, cell viability of the transduced cells, and in turn BMP2 expression, and to tentatively enhance the migration of mesenchmyal stem cells to the sight of bone formation. **(Months 0-24)**

We have introduced RGD binding sites within and throughout the hydrogel to enhance binding of the osteoclasts (see above section) as well as other cell migration. This has been very effective in allowing cells to bind to the material, during bone formation. Additionally, inclusion of the RGD binding sites within the material has appeared to greatly enhance cell viability, allowing for the cells to remain viable. However, the most optimal improvement for BMP2 expression and cell viability has come from altering the structures to be

microspheres, rather than larger beads (Bikram *et al*). Comparison of the BMP2 secretion from larger hydrogel structures to the microbead structures, showed a significant improvement. Figure 15 shows the BMP2 expression from larger bead structures, in comparison to the cells which were not encapsulated (Plated cells).

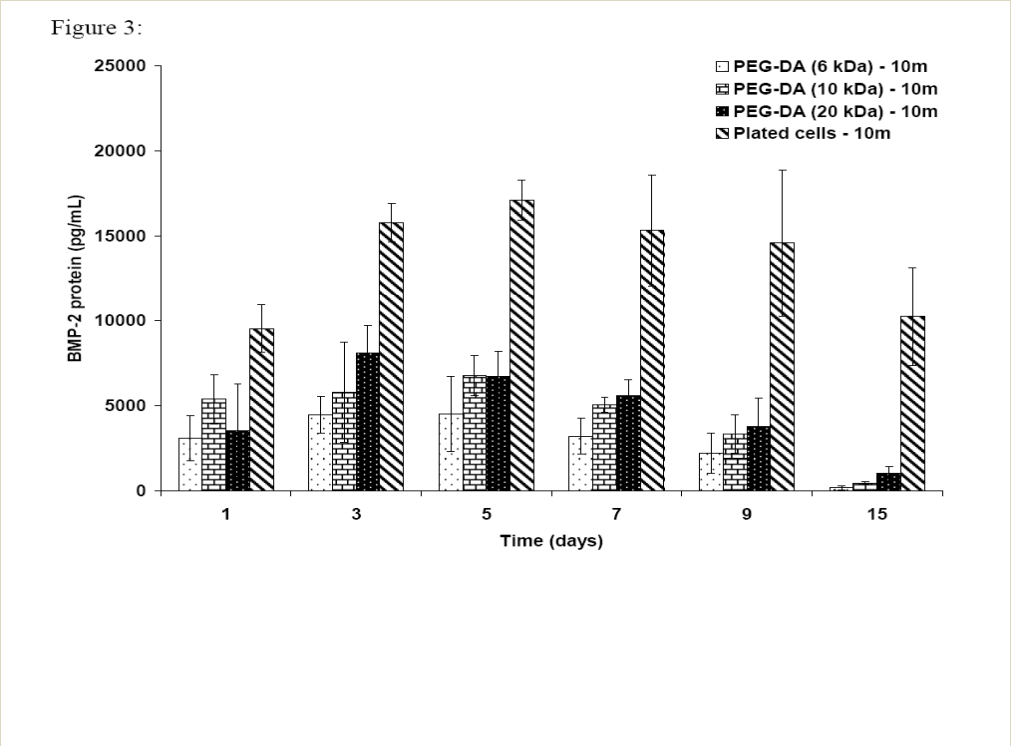

Figure 15: Western blot analysis for the detection of secreted BMP-2 protein. (a) Human recombinant BMP2 (lane 1), conditioned medium from PEG-DA (10 kDa) hydrogels only (lane 2), conditioned medium from 10 million MRC-5 cells encapsulated within PEGDA (10 kDa) hydrogels (lanes 3 and 4), conditioned medium from 10 million transduced fibroblasts control (lanes 5–8), human recombinant BMP-2 (lane 9), conditioned medium containing secreted BMP-2 protein from 10 million transduced fibroblasts encapsulated within PEG-DA (10 kDa) hydrogels (lanes 10–17). (b) Alkaline phosphatase activity in W20-17 cells without the addition of conditioned medium (W20-17) and after addition of conditioned media from PEG-DA (10 kDa) hydrogels with 10 million transduced fibroblasts and control plated transduced fibroblasts (Days 1–15). Data reported as mean ± SD, n = 5.

As seen in Figure 15, the BMP2 expression is reduced by 50% in culture supernatants isolated from the encapsulated cells within the bead structures, as compared to the plated cells.

We chose to next re-engineer the encapsulated structures, into microspheres, which hold between 0-100 cells. As seen in figure 16, within the microspheres, live cells converted the non-fluorescent calcein AM into green fluorescent calcein while ethidium homodimer freely passed through the permeable membranes of dead cells to bind the DNA and fluoresce red. Encapsulated cells showed high viability 95 ± 0.5 %, suggesting that they were not adversely affected by the microencapsulation process.

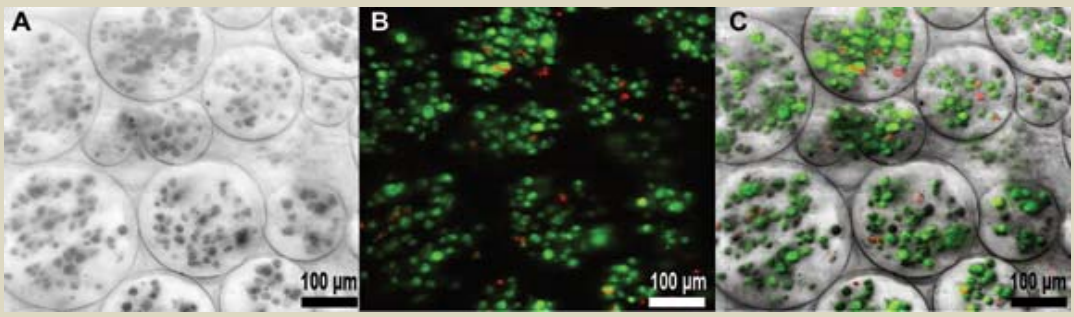

Figure 16: Viability of AdBMP2-transduced cells (2500 vp/cell) within microspheres was assessed at day 7 using a LIVE/DEAD® Viability/Cytotoxicity Kit for mammalian cells (Invitrogen, Molecular Probes, Eugene, OR). **A.** Minimum intensity projection of a differential interference contrast (DIC) Z-stack. **B.** Maximum intensity projection of fluorescent Z-stack merge of red and green channels. The red channel was thresholded to eliminate diffuse virus staining. Dead cells appear red and live cells appear green. **C.** Overlay of panels A and B. Living cells accounted for 95.08% ± 0.47% of total cells encapsulated.

We also compared the level of BMP2 in culture supernatant taken from both cells directly plated and cells encapsulated in microspheres. BMP2 activity was quantified by measuring alkaline phosphatase (AP) activity in W20-17 cells exposed for 72 hours to the culture supernatants from AdBMP2-transduced cells directly plated or encapsulated in microspheres was significantly elevated over control cells but there was no difference between these groups, indicating the BMP-2 released is functionally active (Figure 17A). A 9 day time course of BMP-2 levels in culture supernatant was quantified by ELISA to be approximately 17,500 pg/ml and 15,000 pg/ml for directly plated and microencapsulated cells, respectively (Figure 17B). No BMP-2 was detected in either culture supernatant from AdEmpty cassette-transduced cells, or control cells. The results suggest that the smaller structures, may allow for both greater cell viability and diffusion of BMP2.

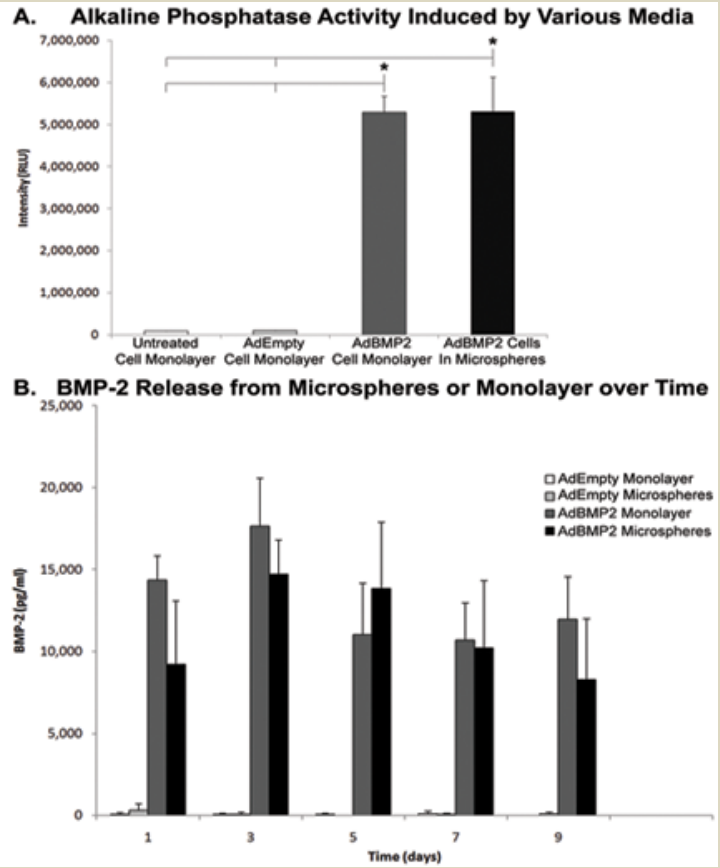

Figure 17: Comparison of BMP-2 expression, secretion and activity after PEGDA encapsulation. **A.** BMP-2 protein in culture supernatant taken from AdBMP2- or AdEmpty cassette-transduced cells (25000 vp/cell) (monolayer), or those encapsulated in PEGDA microspheres was quantified by sampling every other day for 9 days and evaluated using an ELISA. **B.** Alkaline phosphatase activity in W20-17 cells after addition of conditioned media from AdBMP2- or AdEmpty cassette-transduced cells (25000 vp/cell) (monolayer), or AdBMP2-transduced cells encapsulated in PEGDA microspheres. As a negative control, we also included culture supernatant from untransduced cells. Alkaline phosphatase activity is depicted as the average relative chemiluminescence units (RLU), where n=3. Error bars represent means ± SD for n=3. A Student t-Test was applied to demonstrate significance. AdBMP2-transduced monolayer and microsphere groups had significantly greater alkaline phosphatase activity and BMP-2 concentration levels ($p < 0.05$) when compared against other groups, but no differences when compared to each other. In other words, microencapsulation had no effect on BMP-2 release and function

MicroCT analysis of bone formation showed a significantly greater volume of heterotopic ossification in tissues receiving microspheres (Figure 18A, C) than those receiving directly injected cells (Figure 18B, D). Statistical power to detect differences between volumes formed in these groups was 72.5%. Cross-sectional microCT analysis of the newly formed bone revealed a similar architecture between the groups. Heterotopic bone formed by both the microencapsulated cells and directly injected cells had a pattern of dense bone surrounding a hollow interior (Figures 18C and D); however the circumference of bone within the directly injected cells was significantly smaller. Microencapsulated AdBMP2-transduced cells produced approximately twice the bone volume of unencapsulated cells (Figure 19B). Despite the volumetric increase, the bone tissue mineral content was statistically similar between these groups, although trending towards an elevation in samples that received the microspheres (Figure 19A). This corresponds with the change in tissue mineral density of the new bone surrounding the microspheres (Figure 19C). The newly formed bone appears to be slightly less dense, leading to the overall similarity in mass between the two groups. Statistical power to detect differences between bone densities in these groups was 76.7%.

From histological analysis, both groups had significant new bone formation within the muscle (Figure 20). In tissues that had received the direct injection of AdBMP2-transduced cells, there was a small compact piece of bone forming a ring-like structure encircling what appears to be blood and tentative stroma, and just exterior to this structure was significant adipose (Figure 20A). A similar structure was observed in tissues that had received microspheres (Figure 20B). Since the microspheres did not degrade, they appear histologically as gaps or holes within the matrix (Figure 20B). Thus, despite the presence of nondegradable microspheres, both structures were patterned to have a denser bone structure with a bone marrow-like cavity on the interior.

This work has been published in *Olabisi, R. et al, Tissue Engineering Part A. Dec 2010, 16(12):3727-36.*

This sub-aim is completed.

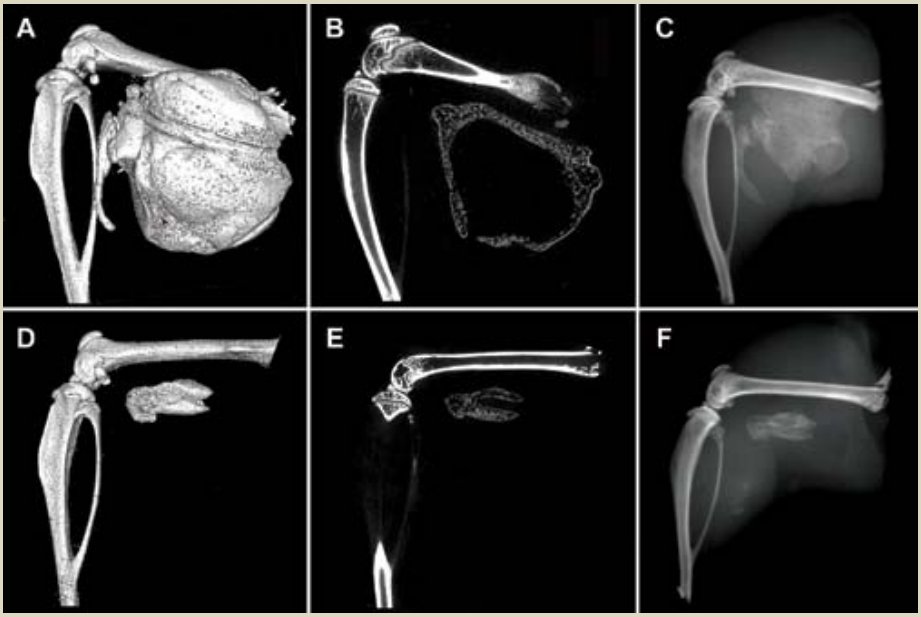

Figure 18: Micro computational analysis of the resultant heterotopic bone formation. Left images (**A, D**) are 3D surface renderings of the resultant heterotopic bone, while middle images (**B, E**) are cross-sectional slices through the new bone. Right images (C, F) show corresponding radiograms. Panels A - F show the resultant mineralization of the muscle tissues after injection of AdBMP2-transduced cells (2500 vp/cell) encapsulated into PEGDA microspheres (**A - C**) or direct injection of unencapsulated AdBMP2-transduced cells (**D - F**). Both have a denser rim of bone, with a hollow interior structure, suggesting that the biomaterial did not alter bone patterning.

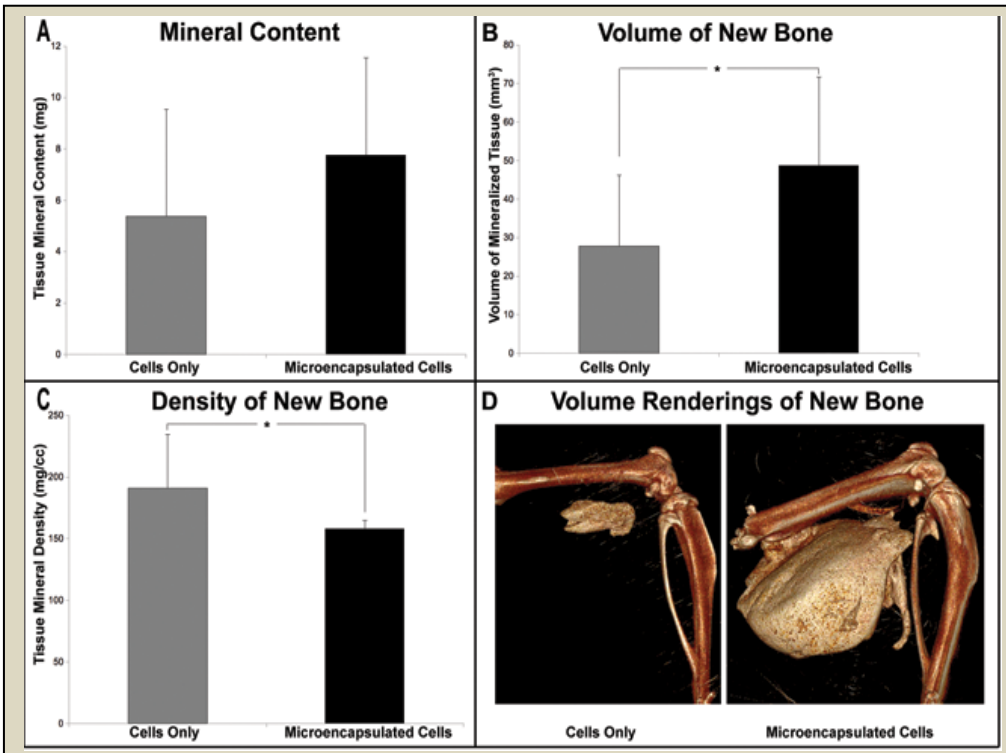

Figure 19: Quantification of the heterotopic ossification using microcomputational analysis. Cells were transduced with AdBMP2 and either directly injected or encapsulated into microspheres prior to injection, and the resultant heterotopic bone was analyzed two weeks later. Tissue parameters: **A.** bone tissue mineral content, **B.** bone volume of mineralized tissue, and **C.** bone tissue mineral density were calculated for the newly formed bone (n=6 per group). The means and standard deviations for each group were calculated and compared using a one-way analysis of variance. Results indicate that mineral content is statistically equivalent (p=0.2) between the groups, whereas the AdBMP2-transduced cells in microspheres had a significantly greater volume (p=0.038) than the AdBMP2-transduced cells directly injected. Alternatively, the bone tissue mineral density was significantly denser for the group receiving the cells directly as compared to those in microspheres (p=0.029). Panel **D.** shows a 3D volume rendering of new bone formed in cell only and microencapsulated cell groups, respectively.

c. Test addition of proteins that may enhance the BMP2 bone inductive response, such as VEGF-A or –D and compare enhancement of bone formation. (Months 24-36)

We have recently published the significant elevation in these VEGF proteins after expression of BMP2 in the local tissues (Fouletier-Dilling, et.al. J Bone Miner Res. 25(5):1147-56. 2010 PMID: 19839764). From this work, additional delivery of VEGFs does not enhance the reaction, or new vessel formation, most likely because this is maximally activated. ***Therefore this subaim is completed.***

d. Test these gels in vitro. (Months 12-36)

We next tested the degradable hydrogel to determine if it could be selectively degraded by osteoclasts. Raw 264.7 cells were differentiated in culture medium containing 30 ng/ml RANKL for 4 days. Cells collected through gradient centrifugation and placed in culture where they were enzymatically stained for tartrate acid phosphatase activity (TRAP). Multinucleated cells in the culture appeared to stain positive for TRAP suggesting that they had undergone osteoclast differentiation. The majority of cells at the bottom fraction of the gradient contained the TRAP+ dRAW 264.7 osteoclasts were then used for hydrogel degradation studies. To demonstrate the ability of the cells to

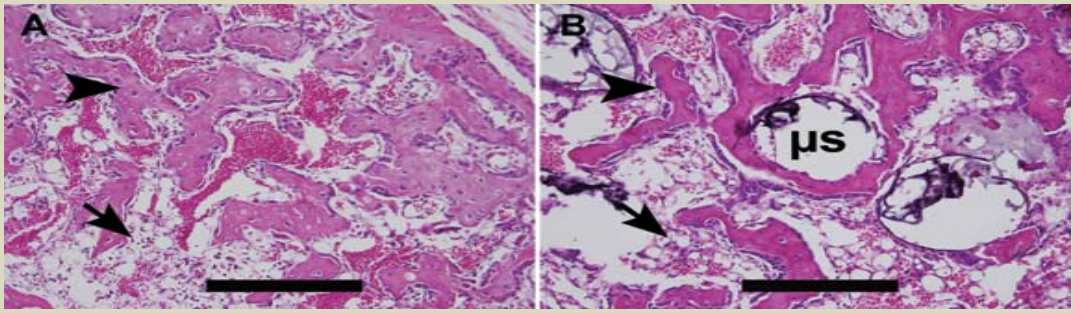

Figure 20: Photomicrographs of heterotopic ossification. Hematoxylin and eosin stains of new bone formation by: **A.** directly injected and **B.** microsphere (μs) encapsulated cells. Both groups show small compact pieces of bone (arrowheads) forming ring-like structures, encircling what appears to be blood and tentative stroma in the inner region, with significant adipose (arrows) just exterior to the new bone. Scale bars are 500 μm.

both adhere to the hydrogel material so a normal substrate for growth, as well as have the selectivity in degradation, we next plated both primary osteoblasts and the TRAP+ dRAW264.7 osteoclasts onto GPSG hydrogel sheets containing the RGD binding sites which were preformed, to provide a smooth surface to ensure they do not possess imperfections other than those introduced by degradation from the cell populations.

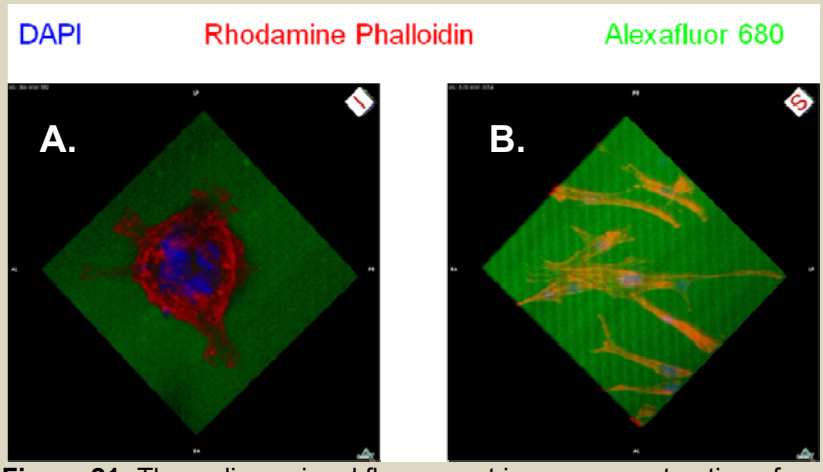

Figure 21: Three-dimensional fluorescent image reconstruction of an active osteoclast on the GPSG hydrogel surface. The GPSG hydrogel was labeled with Alexafluor 680 fluorophore (green), which is conjugated with the acryloyl-PEG-RGDS and incorporated into the hydrogel by photo-polymerization. The cells were fixed and permeabilized before staining the nuclei with DAPI (blue) and F-actin by rhodamine phalloidin (red) 48 hours after seeding. (A) Composed z-stack images of the osteoclast on hydrogel. (B) Composed z-stack images of osteoblasts on hydrogel. Osteoblasts did not appear to leave any pits.

As can be seen in figure 21, both cell types readily adhered to the material, and formed normal cell structures observed in tissue culture. The degradable or GPSG hydrogels possessing Alexafluor 680 (green color) were fixed and stained with DAPI (blue color) for nuclei and rhodamine (red color) phalloidin for F-actin in the cytoplasm. As can be seen in figure 21 and 22, observed on hydrogel surface were actual resorption pits generated by RAW264.7 osteoclasts which were absent on the GPSG hydrogels which had been seeded with osteoblasts. Hydrogels-osteoclasts interactions were examined under confocal microscopy at higher magnification. Multinuclear and polarized cells RAW264.7 osteoclasts were identified on the hydrogel surface, (Figure 22A). A sealing ring of F-actin and multiple nuclei were clearly observed (Figure 22B). On the hydrogel surface where the osteoclast was located, a decrease in the fluorescent signal was observed (Figure 22C). The z-stack images were then examined closely by three-dimensional reconstructions using a volume rendering method. Figure 22D is the side view, showing the osteoclast attached to the hydrogel. From the three-dimensional perspective of the image from the top (Figure 22E) and bottom (Figure 22F) of the hydrogel, the loss in fluorescent signal of the hydrogel reveals a hole in the hydrogel through which the cell can be seen. This signal loss is indicative of activity by the differentiated RAW264.7 osteoclasts, degrading the underlying hydrogel and creating a pit, resulting in the fluorescent intensity loss. No signal loss was observed on the gels seeded with dMC3T3-E1 cells. Therefore it appears that the osteoclasts may be selectively able to remodel the hydrogel material as predicted. ***This work has recently been accepted for publication in Journal Biomaterials Research (Chih-Wei Hsu, Ronke M. Olabisi, Elizabeth A. Olmsted-Davis, Alan R. Davis, Jennifer L. West Cathepsin-K sensitive poly(ethylene Glycol) hydrogels for degradation in response to bone formation.*** ***This subaim is completed.***

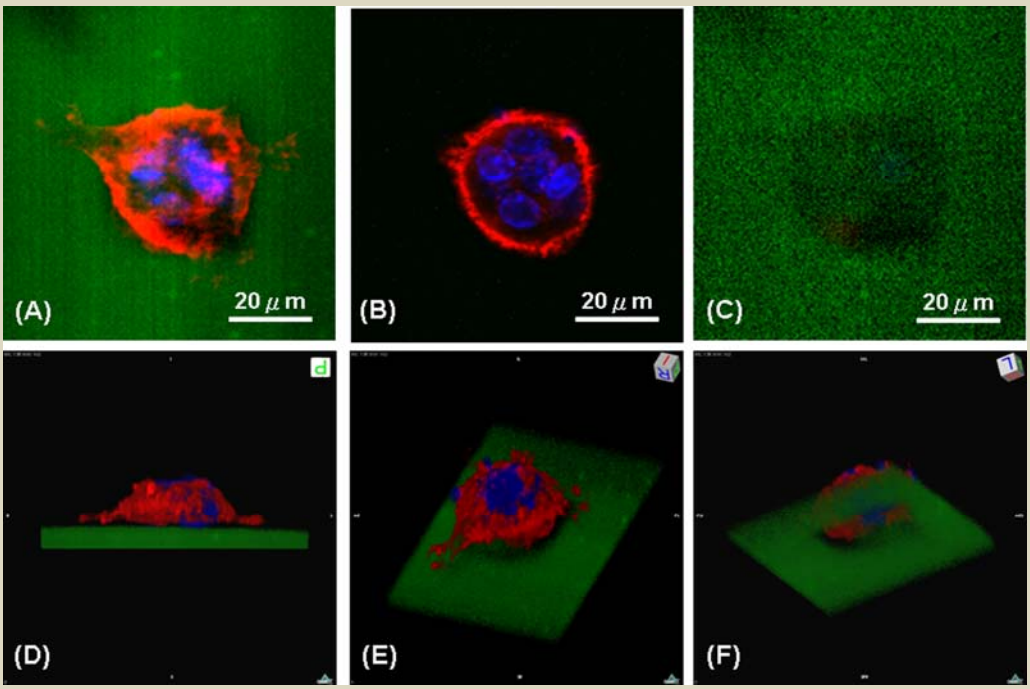

Figure 22: Three-dimensional fluorescent image reconstruction of an active osteoclast on the GPSG hydrogel surface. The GPSG hydrogel was labeled with Alexafluor 680 fluorophore (green), which is conjugated with the acryloyl-PEG-RGDS and incorporated into the hydrogel by photo-polymerization. The cells were fixed and permeabilized before staining the nuclei with DAPI (blue) and F-actin by rhodamine phalloidin (red) 48 hours after seeding. (A) Composed z-stack images of the osteoclast and hydrogel. (B) Sealing ring and multiple nuclei of the osteoclast. (C) GPSG hydrogel with fluorescent signal lost at middle. Z-stack Images were reconstructed using the volume renderings algorithm and presented from (D) side view, (E) orthogonal view from above, and (F) from bottom. The resorption site is located underneath the osteoclast, which was can be observed in the loss of the fluorescent intensity of Alexafluor 680. The resorption pit on the hydrogel surface can be clearly seen from different angles, suggesting that the GPSG hydrogel has been degraded by cathepsin K secreted by osteoclasts.

Test these gels in vivo. ***(Months 36-48)***
We next tested the material *in vivo* to determine if we observed degradation, and replacement of the microspheres with bone. We injected the microspheres, and then approximately 3 weeks after injection harvested the tissues, processed, and sectioned through the newly formed heterotopic ossification to detect the microspheres. Figure 23 shows a representative photomicrograph of a hematoxylin and eosin stained section of heterotopic bone and bone marrow. Intact microspheres can be detected within this section; however, there are also microspheres within the maturing bone that appear to be degrading. Further, the yellow rectangle encompasses a region which appears to be newly formed heterotopic bone, in the shape of a microsphere, suggesting that the removal of that material may be complete at this time. We are currently completing these in vivo experiments for publication. In these experiments, we have added an Alexafluor dye to the hydrogel material, and thus can localize the material through microscopy. In these studies, we will confirm or engineer a similar healing rate as obtained with the PEGDA hydrogel, but will eventually be removed from the tissues, thus allowing the bone to assume a normal shape, structure, and make up. *These studies should be completed within the next year.*

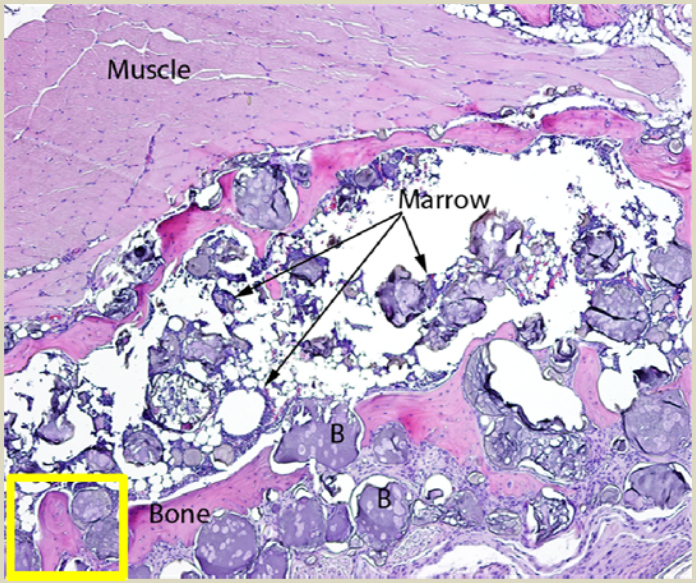

Figure 23: Photomicrograph of a hematoxylin and eosin stained tissue section depicting the degradation of the microbeads *in vivo*.

Conclusions: In this aim we have optimized the polymer to be able to bind cells such as osteoclasts through RGD binding; we have introduced cathepsin K protease recognition sites and shown *in vitro* osteoclast selective degradation over a number of different fibroblasts including osteoblasts. Finally we have early preliminary data in which we can observe the polymer removal *in vivo*. Further we have verified the expression of VEGFs within the local tissue environment and presence of rapid new vessels, and determined

that VEGF activity is maximally stimulated, and inclusion of additional on the polymer would likely not result in significant additional benefit. The studies in this aim have been published in three manuscripts.

Task 3: To achieve rapid bone formation by percutaneous injection of the encapsulated Ad5F35BMP2 transduced human bone marrow mesenchymal stem cells (hBM-MSCs) into the adjacent musculature of athymic rats in a model of nonunion.

a. Obtain approvals through the DOD institutional review board for approval to work with the human mesenchymal stem cells. (Months 0-12) We have approval to use human mesenchymal stem cells either encapsulated or unencapsulated for in two models for critical size defects in both Athymic as well as Wistar rats. The two models are the fibula which is fused to the tibia and therefore does not require additional fixation, as well as the femur model, which involves external fixation to maintain the defect and non-union. We have generated both rat MSCs and human MSCs but have found that skin fibroblasts appear to be more stable within the hydrogels and data shown below suggests that they are more reliable for achieving rapid bone formation *in vivo*. ***This subaim is completed***.

Figure 24: X-rays of bone healing in a rat fibula after injection of the GPSG hydrogels (selectively degradable through bone remodeling)**.**

b. Once the gels have been modified to offer optimal properties for bone formation and removal, we will test these in a rat model of a critical-size defect. We will demonstrate the ability to induce bone healing in the presence of tetracycline. (Months 24-40) We have completed the studies with the hydrogel and found that the optimal structure is to produce microbeads or microspheres which encapsulate 0-100 cells and provide high cell viability long term, and comparable BMP2 expression *in vitro* to those which are not encapsulated (See task 1 section). From these studies we next encapsulated the cells in the GPSG hydrogel (Cathepsin K degradable hydrogel) and injected the microspheres into the fibula model. We chose to test the material in both the fibula and femur defect models, because of the differences in mechanical forces and stability of the bone healing. In the fibula model, resorption is significantly increased, in the skeletal bone, and therefore would potentially remodel the material very quickly. Alternatively, the femur model has more rapid bone healing, and potentially less immediate remodeling and the potential kinetics of removal of the material will be different. Figure 24 shows preliminary data in the fibula model, using the degradable hydrogel. In these studies it appears that remodeling of the materials, as expected, is fairly rapid, and that the new bone is rapidly decreased. It is intriguing that a portion of the region appears to perhaps have remodeled too quickly, with an apparent hole found in the HO at 4 weeks. What is fascinating is that substantial remodeling has now occurred at 6 weeks, with the apparent hole now being in line with the fibula itself, causing a curved pattern, which was not obvious from the 4 week xray. We have a series of these animals now undergoing bone healing, and will continue to follow them either by longitudinal x-ray or through static time points histologically, and will compare to bone healing in the femur model using the same material. *These experiments are ongoing, and should be completed in the next 6 months.*

c. Analyze the modified injectable hydrogel for optimal volume, in vivo crosslinking, design, selective degradation, and inflammatory reaction using both live animal imaging and histology. (Months 24-48)
We have previously determined that crosslinking of the hydrogel *in vivo* leads to reduction in BMP2 expression from the cells, and also provides for a shape which is suboptimal for inducing bone formation. We have determined that the optimal structure for inducing targeted bone formation is to pre-form the hydrogel encapsulated cells into microspheres or beads, which are injectable, and can be placed within the tissue defect to recruit cells for *de novo* bone formation. We have induced heterotopic bone using these microspheres, and found that we observe normal looking bone, and no apparent inflammatory reaction to the hydrogel or allogenic cells, and thus bone formation can occur rapidly at the targeted site. *(See above sections).* ***This work has been published in Olabisi, R. et al, Tissue Engineering Part A. Dec 2010, 16(12):3727-36. This sub-aim is completed.***

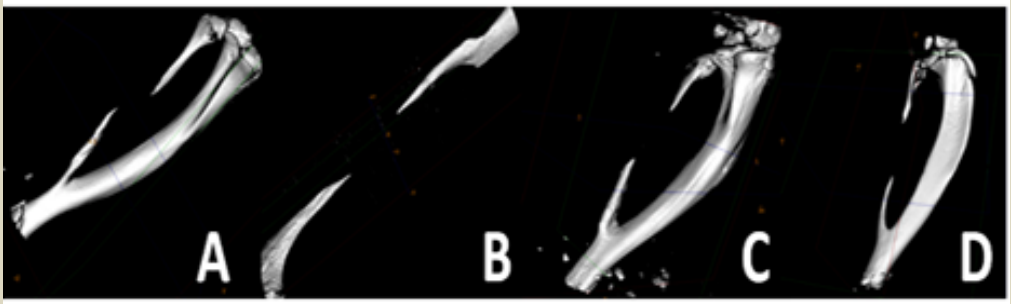

Figure 25: Representative three dimensional reconstructions of rat fibulas through microcomputational analysis. Varying sizes of defects (1 mm - 10 mm) were surgically introduced into rat fibulas and two weeks later analyzed for the presence of bone repair. The results depicted show an approximately 10 mm defect independent of the original defect size **(A)** 1 mm, **(B)** 2 mm, **(C)** 5 mm and **(D)** 10 mm.

d. Bone healing will be tested both biomechanically as well as radiologically using microCT to confirm the fusion. (Months 40-48)
Approvals have been obtained from Baylor College of Medicine and more recently from the Department of Defense for all the animal models. We next established a model of critical size defects in rat long bone. Varying sizes of bone were removed from the rat fibula starting with a simple fracture (1mm), and systematically increasing in one millimeter increments to a maximum of 10 mm. The rat fibula was selected over other potential bones because unlike in humans, in rodents this bone is uniquely fused to the adjacent tibia. Therefore, a critical defect can readily be introduced without need for additional fixation. After 2 weeks bone healing was radiologically evaluated using microcomputational tomography (μCT). Surprisingly, in all cases 1 mm, 2 mm, 5 mm, and 10 mm defects (Fig. 25A-D, respectively) we observed a similar size defect of approximately 10 mm or the maximum size introduced into the bone, and the bone ends appeared to be pointed, suggesting that the bone was undergoing significant resorption.

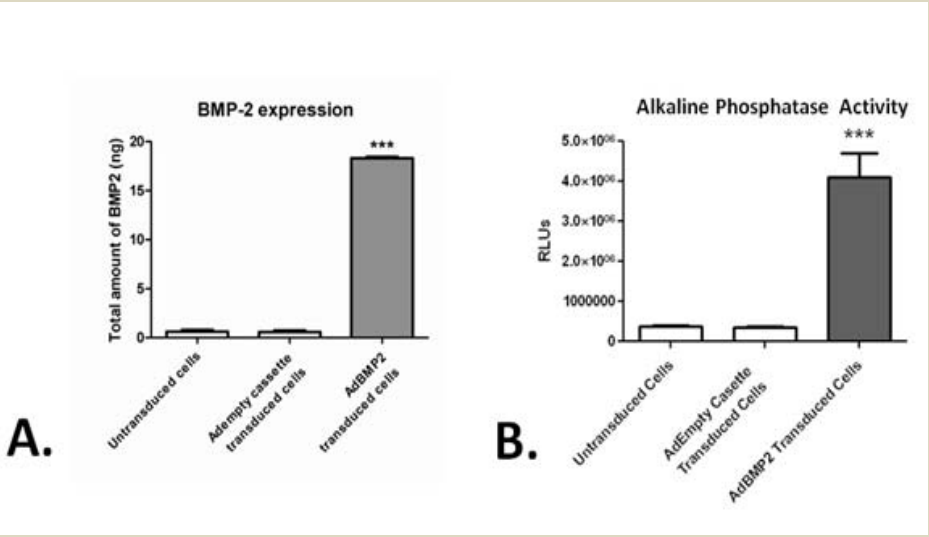

Figure 26: Quantification of BMP2 protein and activity from adenovirus transduced cells. **A.** BMP2 activity in culture supernatant collected 72 hours after transduction with AdBMP2- or AdEmpty cassette-transduced cells (25000vp/cell) was quantified using an ELISA. BMP2 protein is represented as total protein produced by 5 x 10^6 cells. Error bars represent means ± SD for n=5. A student t-Test was applied to demonstrate significance. **B.** Alkaline phosphatase activity in W20-17 cells after addition of conditioned media from AdBMP2- or AdEmpty cassette-transduced cells (25000 vp/cell). To demonstrate endogenous levels of alkaline phosphatase we included the cells alone. Alkaline phosphatase activity is depicted as the average relative chemiluminescence units (RLU), where n=3. Error bars represent means ± SD for n=3. A Student t-Test was applied to demonstrate significance.

We next defined the dose of AdBMP2 transduced cells required to provide optimal healing of the bone defect. Fibroblasts were transduced with AdBMP2 at 2500vp/cell and BMP2 protein as well as activity was quantified 72 hours later. Total BMP2 protein within the culture supernatant was approximately 18.6

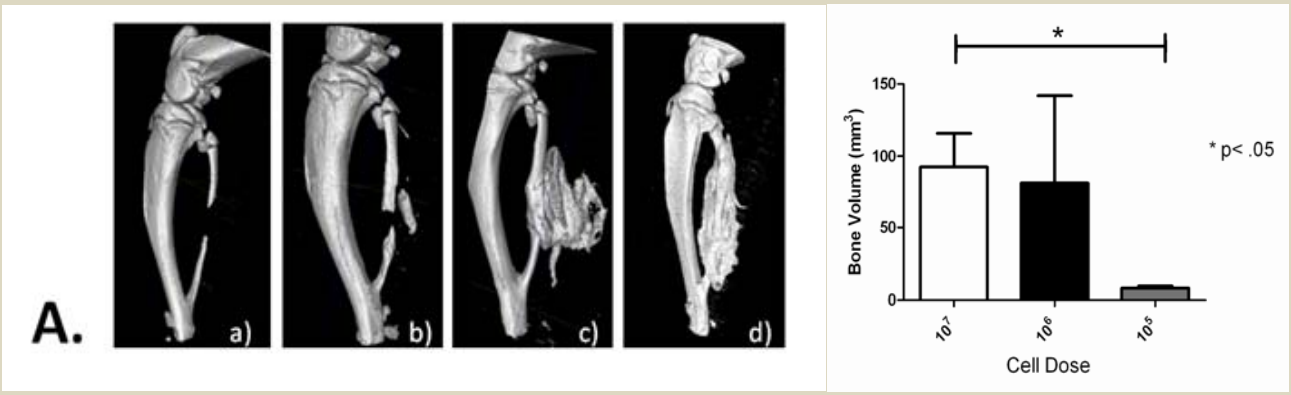

Figure 27: Resultant bone formation from the introduction of adenovirus transduced cells into the defect site. **A.** Representative three dimensional surface renderings obtained from micro computational analysis of the resultant bone repair two weeks after introduction of critical size defect in the rat fibula and delivery of varying numbers of AdBMP2 transduced cells; **(a)** 5 x 10^4 cells **(b)** 5 x 10^5 **(c)** 5 x 10^6 **(d)** 5 x 10^7. **B.** Quantification of the bone repair using microcomputational analysis. Bone volume of the newly forming bone as depicted in Figure 3A, was calculated for each cell dose (n=5 per group). The means and standard deviations for each group were calculated and compared using a one-way analysis of variance.

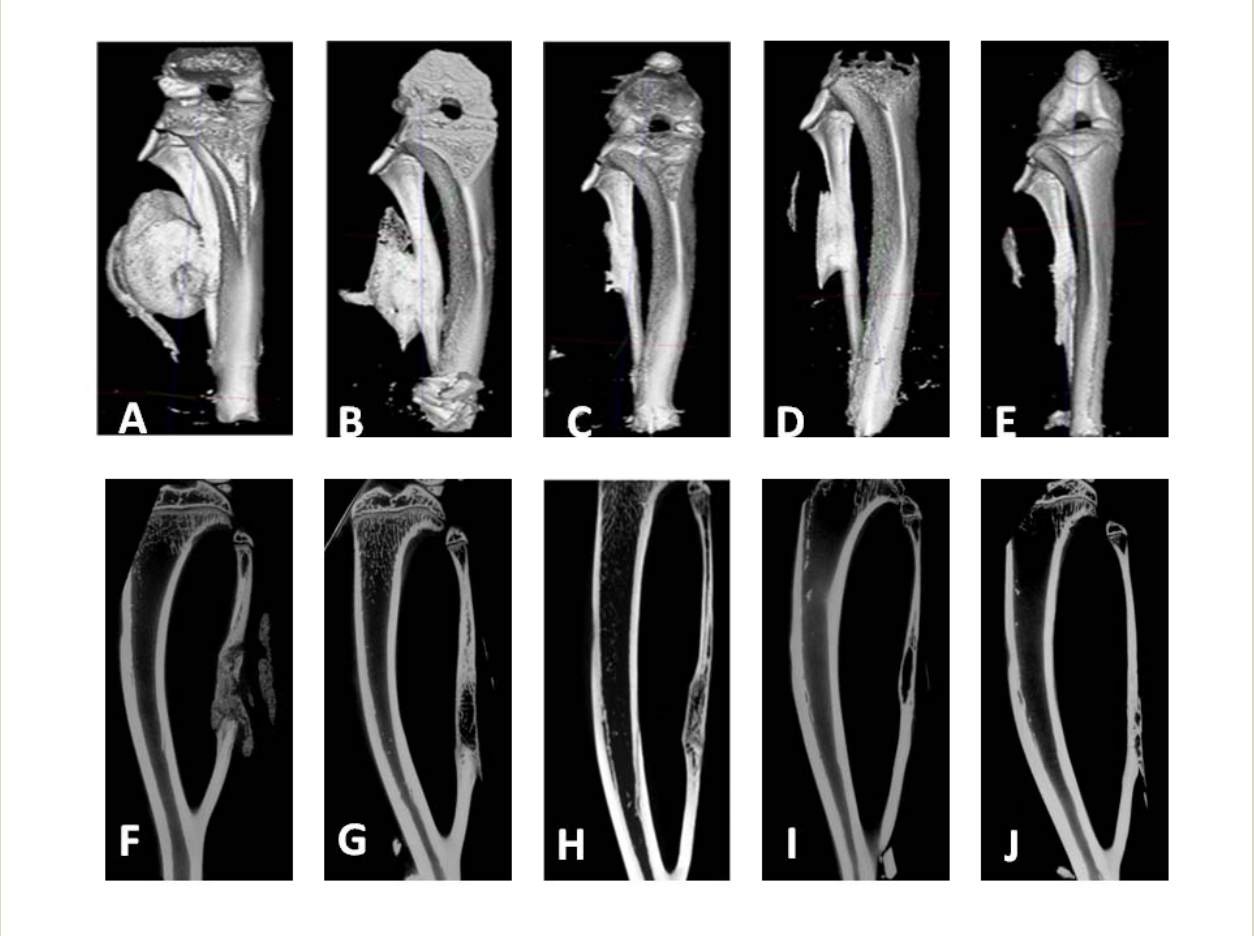

Figure 28: Micro-computational analysis of bone healing over time. Representative three dimensional surface renderings (A-E) or two dimensional reconstructions (F-J) of bone healing over time; **(A and F)** 2 weeks; **(B and G)** 4 weeks; **(C and H)** 6 weeks; **(D and I)** 9 weeks; and **(E and J)** 12 weeks after introduction of the AdBMP2 transduced cells in the fibula defect; n=9 per group.

nanograms per 1 x 10^6 cells (Fig 26A). Cells transduced with AdEmpty, as well as untransduced cells, did not produce BMP2. Interestingly, a standard dose of recombinant BMP2 protein used to induce bone formation in a rat critical size defect was approximately 12 ugs. Since 5 x 10^6 BMP2-producing cells is adequate to heal the bone completely (Fig. 27A), and we have determined that the transduced cells are present at a maximum of 5 days. This means that a maximum of 93 ng is sufficient to completely heal the bone in this model. This is 130 times less than the amount of protein used in other rat defect studies with recombinant BMP2 suggesting that the prolonged local generation of BMP2 is critical to success due to the short half life of the protein.

Further, BMP2 protein activity, as determined by the elevation in the BMP2 responsive protein alkaline phosphatase, showed that this BMP2 being made is active (Fig. 26B). At no time did we observe either BMP2 activity or protein in culture supernatant isolated from the AdEmpty cassette cells or cells alone. Various numbers of the AdBMP2 transduced cells were next injected simultaneously with the introduction of a 3 mm bone defect in the fibula. The cells were injected into the void region, and surrounding muscle tissues of the rats (n=5), and potential bone formation allowed to progress for two weeks. Representative images of the resulting new bone are shown in Figure 27. As seen in Figure 27A, the new bone formation varied drastically with cell numbers. At no time did we observe bone formation or healing in the samples receiving 5 x 10^4 cells, suggesting that there is a threshold amount of BMP2 required for inducing bone formation. Alternatively, there was no statistical difference between the two highest cell numbers or doses (27B), indicating that there is a maximum bone formation response that can be achieved with this system. No bone formation was observed in with the 5 x 10^4 cell dose, whereas there is a significant 10 fold change in bone volume between the 5 x 10^5 and 5 x 10^7 cell doses. There was significant difference between the highest doses 5 x 10^6 and 5 x 10^7 suggesting that there this may be a maximum response to BMP2. For that reason, we used this dose for all subsequent experiments.

We next determined the ability of the therapy to heal the critical size defect over 12 weeks. Figure 28 shows there is substantial bone formation at 2 weeks using this dose of cells, which appears to quickly resorb and by 4 weeks the new bone more closely resembles the fibula that it is replacing. However, as seen in the cross sectional μCT (Fig. 28F) new bone appears to be immature in nature. Although it spans the defect and is contiguous with the skeletal bone, it has not remodeled to have contiguous cortices, which suggests that this may not be well integrated at this stage. Alternatively, by 6-12 weeks a cortical bone structure begins to appear in the newly formed bone (Fig. 4H-J), suggesting that the bone is being remodeled and most likely fused. Bone healing and remodeling appears to be complete by 6 weeks (Fig. 4H) with little additional remodeling occurring at weeks 9 through 12. Interestingly, there appears to be additional bone attached to the skeletal bone (Fig. 28C-E), or actual residual heterotopic ossification that has not been resorbed. Additionally, some samples appeared to have a small amount of residual heterotopic ossification which was not attached to the fibula, but remained in the muscle between fibers.

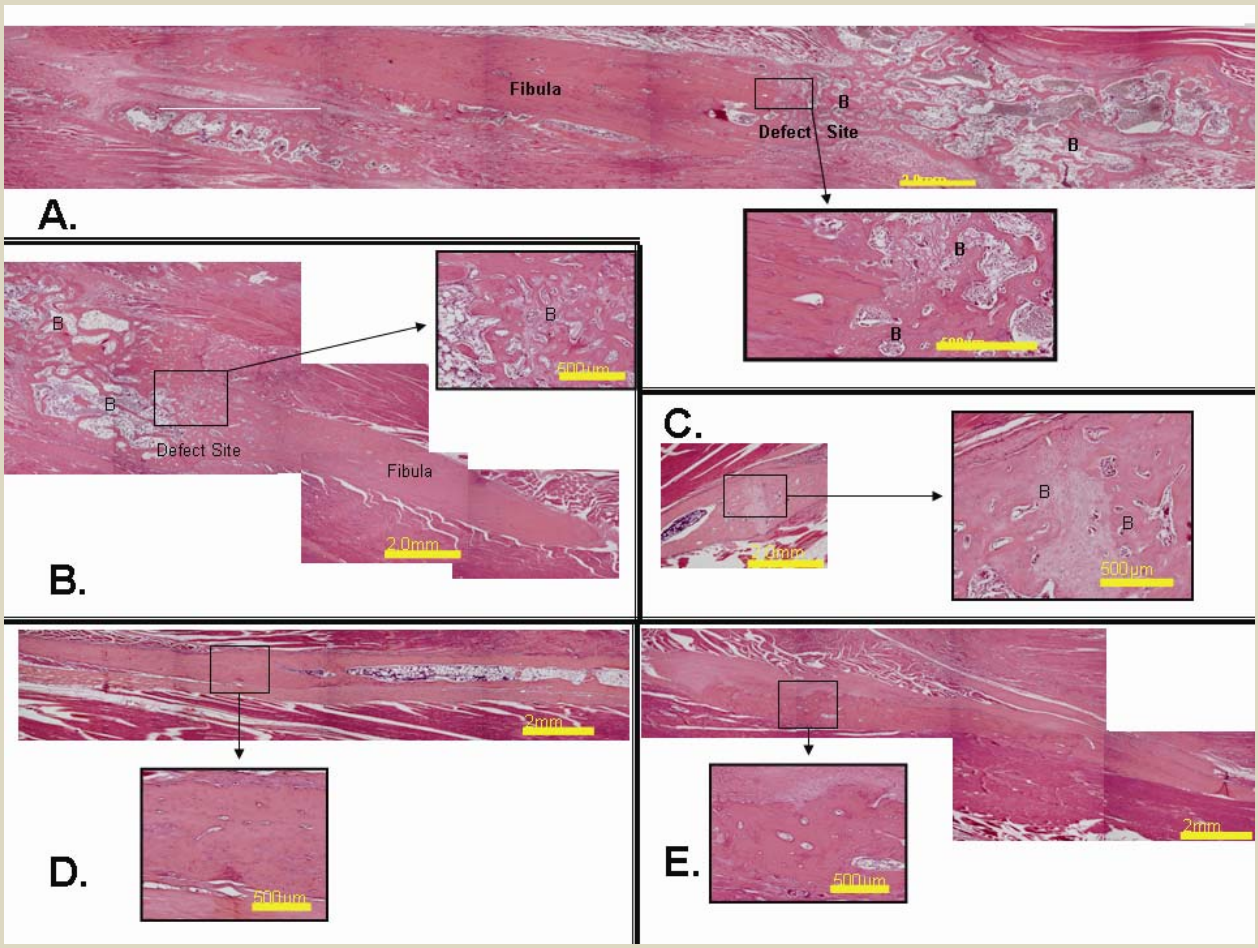

Figure 29: Representative photomicrographs of the fibula defect at various times after introduction of the AdBMP2 transduced cells. Tissues were formalin fixed decalcified, paraffin embedded and serial sectioned (5 µm) through the entire fibula region. Every fifth section was hematoxylin and eosin stained, and images taken which were representative of the defect region in particular the junction with the fibula at various times, **(A)** 2 weeks, **(B)** 4 weeks, **(C)** 6 weeks, **(D)** 9 weeks, and **(E)** 12 weeks. The appearance of bone is identified with [B].

We next looked at the bone architecture by analyzing cross-sectional cuts through the bone. The architecture appeared to change dramatically over the course of bone healing. Changes in bone architecture are a component of bone remodeling and aid in determining if the new bone has truly fused to the skeletal bone. Fusion at the defect site is a critical parameter in this system, because the majority of the new bone is made *de novo*, as heterotopic ossification, and it must fuse to the skeletal bone to complete healing. At 2 weeks the new bone is found throughout the skeletal defect (Fig. 28F); however, it appears to be immature bone, which has not remodeled or integrated into the adjacent skeletal bone. This is in contrast to the adjacent skeletal bone, which has well defined cortices and a hollow bone marrow cavity. Thus although there is new bone, it does not appear to be well fused into the skeletal bone, or healed to the point such that it is one contiguous remodeled structure. However, by 6 weeks portions of the new bone appear to be remodeled with defined cortical bone and the tentative fusion site are less apparent (Fig. 28H), suggesting that the bone is integrated and almost completely healed. By 9 to 12 weeks, we observed integrated structures with the only abnormality being the additional small amounts of bone on the outer cortex (Fig. 28I-J).

We next examined the bone healing through histological analysis to confirm the remodeling and fusion of the newly formed bone with the skeletal bone. This requires bone remodeling to replace the woven bone and lamellar bone junction with integrated remodeled bone. Photomicrographs from representative samples of the healing fibulas show substantial immature bone that completely fills and surrounds the defect (Fig. 29). Over time however, the bone remodels considerably and new cartilage is no longer present in the tissues (Fig. 29B). By 6 weeks, the bone appears to be considerably more mature, with thicker cortical area that are contiguous with the skeletal cortical bone (Fig. 29C). Interestingly, the adjacent cortical bone appears to have a significant gap, which may represent either an area where the bone is vascularized, as evidenced by the pooling of blood

or alternatively, a defect introduced during healing (Fig. 29C). However, this defect was not observed through radiograph analysis (Fig. 29C), suggesting that it comprises a relatively small region of the new bone. It is also of interest to note that in the serial sections where this cortex appears uniform and contiguous, the adjacent cortex now appears ruffled. This indicates that although it is healing, the new shape of the bone does not exactly mimic the original fibula. At 9 and 12 weeks, there is once more additional bone on the exterior of the fibula. However, the interior cortex appears uniform and similar to the normal fibula (figure 29D and E).

We next tested the ability of the hydrogel encapsulated AdBMP2 transduced cells to induce bone healing in a critical size defect in the rat femur. In this model, we introduce a 3-5 mm critical defect within wild type rat femurs. Using a model of external fixation, which can be removed without the need for further surgery, AdBMP2 or Adempty cassette transduced cells micro-encapsulated into PEGDA hydrogel microbeads or unencapsulated AdBMP2 transduced cells were directly injected into the defect prior to injection (figure 30Aand B respectively). New bone formation was assessed by x-ray at two weeks after initial induction. Unexpectedly, we saw no new bone formation within the group receiving cells directly, whereas recipients of microbeads had substantial bone formation. We propose that free cells are unable to persist at site or as viable cells or to otherwise function in the void, whereas cells encapsulated by the polymer structure were retained in situ in a functional stat and so were capable of filling the defect. Of note, polymer containing AdEmpty cassette transduced cells (figure 30C) failed to produce new bone or healing over the same period. We analyzed the new bone histologically (figure 30E), to determine if it was well integrated with the skeletal bone and could span the defect. As seen in figure 30E, there is substantial new bone, cartilage and adipose within the defect, with more mature bone on the edges, all of which was well integrated with the skeletal cortical bone. Amazingly, two independent bone pathologists reported complete healing, in these animals based on contiguous bone bridging the defect. The majority of the microbeads are outside the area of new bone, suggesting that this bone healing is assuming a fracture-callus like pattern of repair. We are now following bone healing in these animals longitudinally (Figure 31) and at fixed time points (2, 3, 6, 9, and 12 weeks) to confirm bone remodeling and for biomechanical testing, to confirm bone healing. Preliminary biomechanical studies (Stiffness and torsional strain-yield strength) suggest that by week 4 the bone is at least 60% that of the adjacent uninjured limb and by 9-18 weeks the bone is actually stronger than the adjacent limb. Further, the parameters do not change after 9 weeks suggesting that healing has reached the maximum strength.

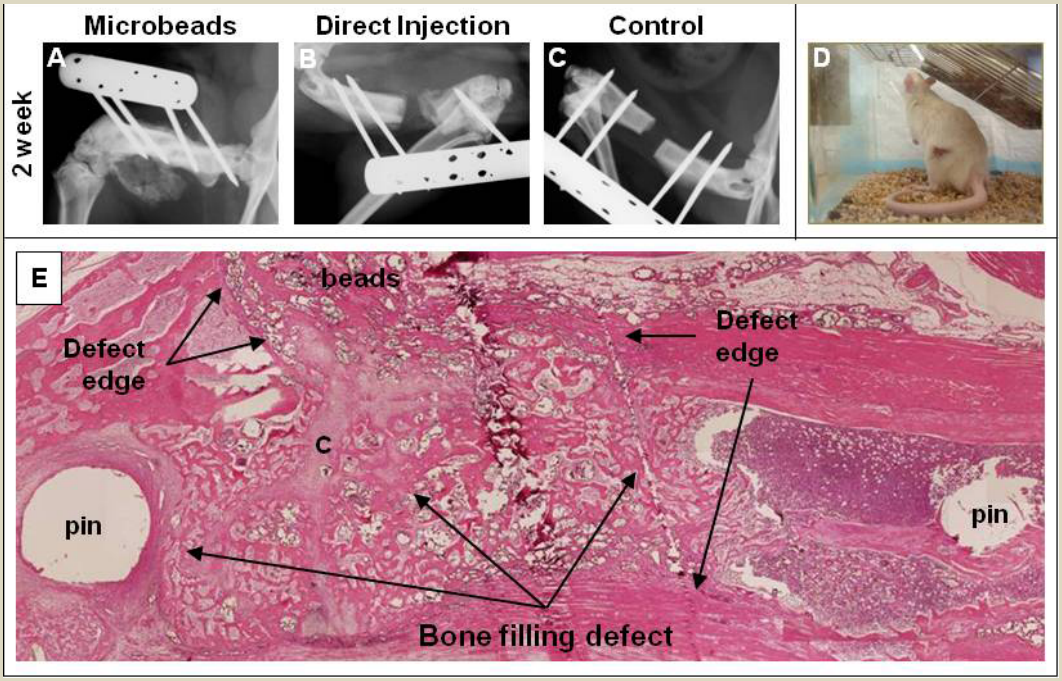

Figure 30: Radiological analysis of HO within the critical size defect in rat femurs, two weeks after injection of A.) AdBMP2 transduced cells encapsulated in microbeads, B.) directly injected AdBMP2 transduced cells, or C.) Adempty cassette transduced encapsulated cells (control). D Photo of a representative rat 3 weeks after receiving both the femoral defect and the osteoinductive microspheres. All additional fixation has been removed approximately one week prior to this photo. The rat shows no apparent lameness or distress. E. Photomicrograph of a hematoxylin and eosin stained tissue section, which shows obvious bone formation spanning the defect, with integration of the cortical bone, and showing the microbeads on the outside of the callus (c) stands for cartilage.

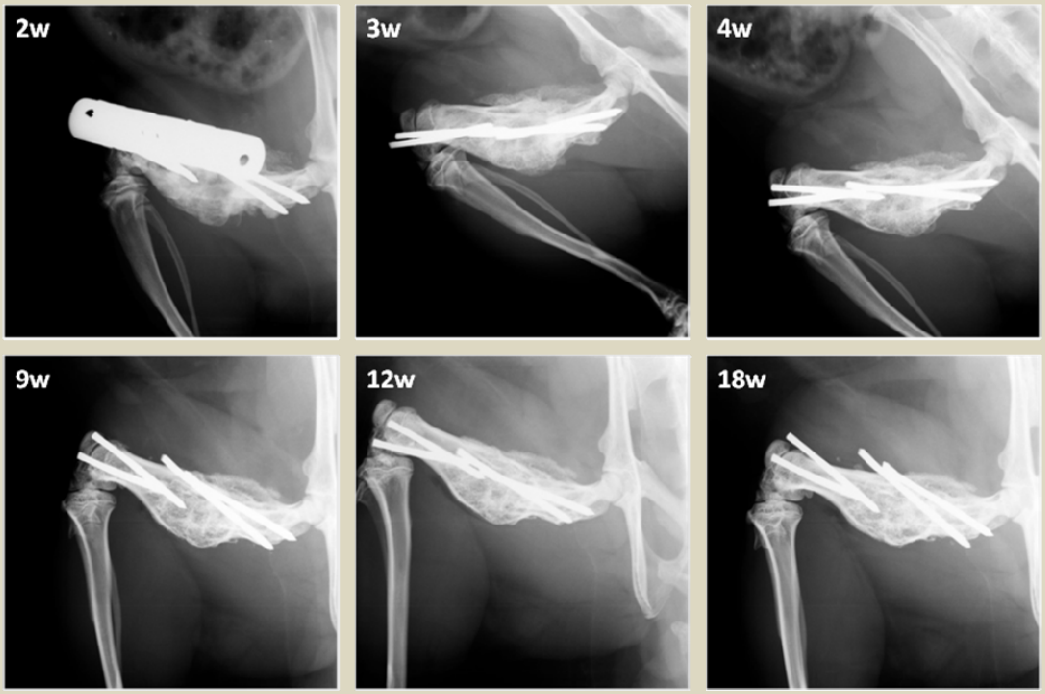

Figure 31: Representative longitudinal x-rays of bone healing in a critical size femoral defect of wild type (Wistar) rat. These images are representative of a larger group n=20.

We have confirmed the stability of the new bone, by removing the external fixator device and allowing the animal to assume normal activities. Although these are minor activities for laboratory rats, in no cases did we observe additional fracture, lameness or signs of pain or distress in the animals. Figure 30D shows a representative rat standing on treated hind limb, one week after removal of any fixation. Limb function and health has now persisted in this experimental group for more than 3 months, however additional biomechanical analysis is currently being performed, since previous studies suggest that bone only needs to achieve a fraction of the structural rigidity of a normal bone for it to support basic activities of daily living.

We have demonstrated complete bone healing with this gene therapy approach using two different models. In these models, we observe rapid bone healing by 3-6 weeks, as determined through radiological, histological and biomechanical analysis. We have demonstrated that the amount of bone produced can be scaled to the size and amount of material injected. Further, we have demonstrated that this injectable material will remain at the site of injection, even in a void region, and that it can rapidly enhance regenerative processes both in the soft tissue as well as the bone itself. The encapsulated material provides the ability to use allogenic cells without graft versus host inflammatory responses, and thus can be injected multiple times, depending on the initial bone shape and localization. In other words, bone may be shaped by multiple injections of the material without fear of immune rejection. This material is capable of being cryopreserved and we have currently started to provide samples to other investigators upon request and approved MTA. Finally we have demonstrated the ability to scale up from mice to rats and have preliminary data in dogs that suggests that the material is completely scalable, and the versatility that cryopreservation (without loss of efficacy) provides a method for easy manufacturing of the material. We have filed for a preliminary patent, and are hoping to obtain additional funding to complete the necessary canine studies to translate this into the clinic.

Key Accomplishments:

Task 1: To produce high levels of BMP2 from human mesenchymal stem cells transduced Ad5F35BMP2 adenovirus in the presence of tetracycline carrying a red luciferase reporter gene.

- We have determined that dsRED is the most sensitive of the reporter modalities for detecting the cells in the hydrogel material after introduction into the mouse muscle.
- We have published experiments which shows that encapsulation of the transduced cells in hydrogel can extend transgene expression within the tissues. We have demonstrated a 3 fold enhancement of the bone formation with hydrogel. However, most likely the enhanced bone formation is a result of the greater volume of tissue expressing the BMP2 rather than the extended expression of the BMP.
- The encapsulation of the cells into these microspheres, has been engineered to be an extremely rapid procedure, which is scalable and "self forming" so that minimal labor is required to produce these on a large scale. Therefore costs would not be prohibitive for manufacturing the material.
- We have examined the tissues to for the presence of phosphoSmad and identified cells within the nerve sheath that appear to be responding to the BMP2. We then looked at both characterizing the mechanism by which the BMP2 exposure leads to bone formation, and identified a novel neural crest stem cell population. Further, blocking expansion of this population appeared to significantly reduce bone formation.
- **Studies completed in this aim have been published in two peer-reviewed publications.**

Task 2: To design an optimal hydrogel material that will rapidly promote endochondral bone formation and be capable of removal through bone remodeling processes.

- We have optimized the hydrogel to be able to encapsulate the AdBMP2 transduced cells, and express the BMP2 at similar levels to the un-encapsulated cells.
- We have constructed the cathepsin K protease site, and introduced it into the hydrogel material.
- We have initially tested this material and found it to be selectively degraded by cathepsin K as compared to other proteases.
- We have shown that osteoclasts will adhere, form ruffled borders, and start to resorb the material, presumably by the production of cathepsin K.
- We have introduced RGD peptide binding sites to the hydrogel material to provide adhesion for the osteoclasts, as well as to extend the life span of the cells within the gel.
- We have demonstrated the rapid increase in VEGFD and VEGFA within the tissues within 48 hours after delivery of the AdBMP2 transduced cells. Further, we have demonstrated the formation of new vessels within 48 hours of delivery of the AdBMP2 transduced cells. This work was published, *Fouletier-Dilling CF, et al.,(2010) J Bone Miner Res. 25(5):1147-56. PMID: 19839764*
- We have engineered RANK ligand into the hydrogel material which can be bound by the osteoclast precursors to induce osteoclastogenesis, similar to skeletal remodeling. In normal bone remodeling RANKL is released by the osteoblasts to induced osteoclast differentiation, and resorption. Thus it will aid in allowing the biomaterial to function similar to normal bone matrix.
- We are finishing these *in vitro* experiments by demonstrating the inability of other fibroblasts to degrade the material. We have preliminary data that we are currently quantifying to demonstrate the amount of hydrogel degradation we observe in the presence of osteoclasts versus other osteoblasts or other fibroblast cells and have published this in a peer reviewed journal.
- **Studies completed in this aim have been published in three peer-reviewed publications.**

Task 3: To achieve rapid bone formation by percutaneous injection of the encapsulated Ad5F35BMP2 transduced human bone marrow mesenchymal stem cells (hBM-MSCs) into the adjacent musculature of athymic rats in a model of nonunion.

- We have established and set up a reproducible critical size defect model that due to the nature of the site is a tremendously challenging model of bone healing. In the fibula model, which is a non-weight bearing bone in the rat, even a simple fracture cannot heal the bone.
- In these experiments we have performed a dose curve and demonstrated that bone volume increased with delivery of more AdBMP2 transduced cells, and that there was a dose which provided maximal bone formation at which point addition of more AdBMP2 transduced cells did not result in greater bone formation. The results are presumably due to saturation of the BMP2 receptors within the area of bone formation.

- We have demonstrated the ability to transduce both the human cells to express high levels of BMP2, as well as the rat fibroblasts, which we believe to be genetically matched donors.
- We have demonstrated the ability of the AdBMP2 transduced cells to heal a large critical size defect in the fibula through generation of *de novo* bone formation within the muscle, and that the large volume of bone originally generated resorbs quickly leaving on the HO which has integrated with the fibula bone, and remodeled to heal the structure. Bone healing was complete in 6-9 weeks after delivery of the AdBMP2 transduced cells.
- We have established a model of critical size defect within the femur (3-5 mm) in wild type rats, through implementation of an external fixation device, which can be removed (non-surgically) from the animal during or at completion of bone healing. This model allows us to analyze the bone formation radiologically, without interference from the hardware, and to remove the hardware without risk of disrupting the fracture callus.
- We have tested the AdBMP2 or Adempty cassette transduced cells encapsulated in the PEGDA hydrogel material and found that new bone formation occurred rapidly within the defect site, and could span the defect within 2 weeks. Further, this bone was substantial enough to permit the animal to be weight bearing without the need for continued external fixation.
- Analysis of the bone, suggested that by three weeks the bone was well integrated, and structurally remodeled to be considered "healed" by two independent bone pathologists. Radiological assessment of the bone suggested that mineral content and volume was stable by 4 weeks in n=6 samples suggesting that the bone had maximal mineral content and defined cortexes within this period. Preliminary biomechanical studies suggest that the bone had stiffness and torsional (yield strength) of 60% that of the adjacent uninjured femur, at 4 weeks, and by 6-18 weeks had substantially more strength than the normal femur, but that by 6 weeks these parameters were stable with little change through week 18.
- We are currently assembling two publications from the femur studies.
- We have also worked out a protocol for cryopreserving the material so that large batches of allogenic cells can be transduced qualified, and then encapsulated, stored, and quality tested, for use in our studies, dissemination to other investigators, and eventually for clinical studies.
- We have filed a preliminary patent application with Rice University and Dr. West for this material.
- **Studies completed in this aim have been published in one peer-reviewed publication. Three other publications are at various stages of review and are projected to be published during this year.**

Reportable Outcomes in the past year:

Oral presentation:

- Olmsted-Davis E. A., Davis, A.R. and West, J. L. The Role of the Peripheral Nervous System in Heterotopic Ossification. Advances in Mineral Metabolism and John Haddad Young Investigators Meeting, Aspen, CO April 6-10.
- Ronke Olabisi, Corinne Sonnet, ZaWaunyka Lazard, Chartrisa Simpson, Alan Davis, Jennifer West, Elizabeth Olmsted-Davis, Hydrogel Microencapslation Permits Critical Size Defect Repair Via Gene Therapy. In Society For Biomaterials Annual Meeting and Exposition, Orlando, FL 13-16 April, 2011
- Sonnet C, Olabisi R, Sullivan K, LaShan Simpson C, Hipp J, Davis AR, West JL, and Olmsted-Davis EA. Induction of heterotopic ossification in rats requires skeletal bone. Texas Bone Disease Program of Texas. March 2011.

Poster presentation:

- Ronke Olabisi, Corinne Sonnet, ZaWaunyka Lazard, Chartrisa Simpson, Alan Davis, Jennifer West, Elizabeth Olmsted-Davis, Critical Size Defect Repair through a Single Injection. In 57th Annual Meeting of the Orthopaedic Research Society, Long Beach, CA, 13-16 January 2011.

- Ankit Rajgariah, Ronke Olabisi, Ph. D., Lashan Simpson, Corrine Sonnet, Alan R. Davis, Elizabeth Olmsted-Davis, Jennifer West, Determining The Number of Cells Encapsulated When Making PEG-DA Hydrogel Microspheres. In Biomedical Engineering Society Annual Meeting, Austin, TX 6-9 Oct 2010.

- Ronke M Olabisi, ZaWaunyka Lazard, Mary Hall, Eva Sevick, Alan R Davis, Elizabeth A Olmsted-Davis, Jennifer L West, Hydrogel microspheres increase cell survival and increase new bone volume in a gene therapy bone formation model. In Society for Biomaterials Annual Meeting and Exposition, Seattle, WA, 21 - 24 April 2010.

- Ronke M Olabisi, Chi-Wei Hsu, Alan R Davis, Elizabeth A Olmsted-Davis, Jennifer L West, Cathepsin-K and Osteoclast Sensitive Poly(ethylene) Glycol Hydrogels. In 56th Annual Meeting of the Orthopaedic Research Society, New Orleans, LA, 6 - 10 March 2010.

- Jennifer Mumaw, Erin Jordan, Corinne Sonnet, Ronke Olabisi, Elizabeth Davis, Alan Davis, Jennifer West, Steven Stice. Cryopreservation of encapsulated therapeutic cells in a model for bone regeneration. Petit Institute for Bioengineering and Bioscience Industrial Partners Symposium. Atlanta, GA 21-22 Oct 2010.

Manuscripts Published or in Press:

- Fouletier-Dilling CF, Wada A, Lazard Z, Salisbury E, Gannon F, Vadakkan T, Gao L, Hirschi K, Dickinson M, Davis AR, Olmsted-Davis E. (2010). J Bone Miner Res. 25(5):1147-56. PMID: 19839764

- Ronke M. Olabisi, ZaWaunyka Lazard, Elizabeth A. Olmsted-Davis, Alan R. Davis, Jennifer L. West. (2010). Comparison of endochondral bone formation after delivery of a cell based gene therapy system, with and without PEG-DA hydrogel encapsulation. Tissue Engineering Part A. 16(12):3727-36.

- Chih-Wei Hsu, Ronke M. Olabisi, Elizabeth A. Olmsted-Davis, Alan R. Davis, Jennifer L. West Cathepsin-K sensitive poly(ethylene Glycol) hydrogels for degradation in response to bone formation. (Journal Biomaterials Research, In Press)

- ZaWaunyka Lazard, Jerome Saltarrelli, Christian Clarke, Michael Heggeness, Jennifer West, Alan R. Davis, and Elizabeth Olmsted-Davis. Induction of targeted heterotopic ossification for healing traumatic bone injury. (Journal of Cellular Biochemistry, In Press).

- Elizabeth Salisbury, Eric Rodenberg , Corinne Sonnet, John Hipp, Francis Gannon, Tegy Vadakkan, Aya Wada, Mary Dickinson, Elizabeth A. Olmsted-Davis, and Alan R. Davis. Sensory Nerve Induced Inflammation Contributes to Heterotopic Ossification. (Am J Pathology, In Press).

Manuscripts in Review:

- Sonnet C, Olabisi R, Sullivan K, LaShan Simpson C, Lazard Z, Heggeness M, Gannon F, Fuentes A, Hipp J, Davis AR, West JL, Olmsted-Davis EA. Rat femoral critical size defect repair using BMP2-expressing microbeads.

- Sonnet C, Olabisi R, Sullivan K, LaShan Simpson C, Hipp J, Davis AR, West JL, and Olmsted-Davis EA. Induction of heterotopic ossification in rats requires skeletal bone.

- Jennifer Mumaw, Erin Jordan, Corinne Sonnet, Ronke Olabisi, Alan Davis, Jennifer West, Steven Stice, Elizabeth Olmsted-Davis. Cryopreservation of encapsulated therapeutic cells in a model for bone regeneration.

Conclusions:

We have completed 90 percent of the proposed studies in this application and published the findings in five separate peer-reviewed manuscripts. We have identified some of the earliest events in BMP2 induced bone formation, and including a novel stem cell population that with 24 hours appears to expand and migrate

towards the region of BMP2. Disruption of this process leads to reduction in bone formation. We have also developed a novel cell based gene therapy system which can produce bone formation at a targeted location. This system involves encapsulation of the transduced cells into microspheres, using PEGDA hydrogel. Each step within this system offers significant benefits for safety and efficacy.

First, this system offers significant benefits, in that the ex vivo transduction of the cells, and extensive washing removes any adenovirus, and thus the cells although expressing high levels of BMP2 are no longer are considered to be virus associated. Therefore, the risks associated with virus transduction of cells are no longer a clinical concern. This type of gene therapy approach has already been implemented extensively in the clinic for the treatment of cancers. Additionally this transduction process is non-integrating into the chromosome, which avoids risks associated with random integration within genes resulting in long term adverse reactions. The non-integration also provides the ability for multiple copies to be expressed within the cells, and therefore higher level of transgene expression from a single cell than the genetically modified cells that rely on chromosomal integration.

Second, encapsulation within the hydrogel, has been shown to sequester the cells to the target site, and avoids random bone formation or even diffusion of the cells which would reduce efficacy. Although injectable the microspheres are large enough that they cannot enter the vasculature, and therefore do not pose a risk for adverse reactions in other tissues. Finally the inclusion of the hydrogel not only allows the system to function in void regions of large defects to recruit cells for repair, but it also blocks inflammatory reactions against allogenic cells. The inert nature of the hydrogel provides the ability to re-inject additional material at any time during bone healing, to provide additional bone without risk of previous priming by the foreign cells. Finally the ability to remove the microspheres during bone remodeling, provides a biological method for removing the small microspheres from bone matrix, without implementing processes that are destructive to the new bone, and will allow for solid bone to replace the small amount of bone that appears to have microspheres, embedded.

Finally, the ability to use both allogenic cell lines, as well as cryopreservation greatly enhances the versatility of this system to be easily implemented clinically. We have shown that a human qualified cell line that can be readily expanded such as either mesenchymal stem cells, or skin fibroblasts, are readily transduced ex vivo with the adenovirus, and extremely hardy to encapsulation in our current formulations. Thus clinical manufacturing of this material is easily achieved by implementation of a GMP qualified cell line, currently available to us through our GMP cell processing facility within the CAGT, which can be ex vivo transduce with a GMP produced adenovirus, which is easily produced by our system facility which is a GMP based vector core (We are a GLP based core). The cells washed, and then encapsulated in GMP setting within the PEG hydrogel, which is already approved for use in the clinic. Further the West laboratory has already established a GMP facility for the production of clinical lots of PEGDA hydrogel. This can be done in large batches, provided a lot number and cryopreserved, efficacy tested; QA/QC'd, and then would be ready for distribution to clinical sites. We propose to initiate the first clinical trials at the complete of animal testing with our "first generation" PEGDA hydrogel encapsulated microspheres, or "osteospheres" and follow with the biodegradable formulation. Although we need to secure additional funding for large animal studies, we propose that translation will be much easier since we have already translated from mice, to out bred, wild type rats. We have also applied for a provisional patent to protect this area of our work.

These microspheres are injectable and are retained at the injection site where they rapidly produce new bone formation. When injected into a critical size defect new bone formation was rapidly induced, and substantial enough to span the defect and provide initial stabilization. The external fixation device which stabilized the femur ends, and prevents compression, was removed in 10 wild type rats, at 2 weeks, resulting in continued bone healing, without any additional fractures in the animals. Further, these animals ambulated normally, and with no apparent lameness or reduction in activity. We have followed the bone healing in a number of these rats to 18 weeks, and found that mineralization peaked at 4-6 weeks, and represented complete healing both histologically as well as radiologically. We are currently completing the biomechanical – torsional testing (stiffness, and yield strength) and assembling two manuscripts. We have also developed a formulation of the injectable microspheres, which can be remodeled through bone remodeling, which is recently published, and we are currently completing the testing of this material for "tuning" in vivo, to provide for similar bone healing, and eventual material remodeling.

With completion of this grant, we have completed all the proposed experiments and all necessary GLP efficacy data required by the FDA for small animal studies. We have developed the "first generation product" and production method which could easily be translated into a clinical GMP manufacturing facility and both cell culture and encapsulation procedures are scalable to produce large batches of the material for potential clinical

trials. Further, the protocols have been developed to provide for a manufacturing method that could readily implement on a large scale which are not labor intensive or highly costly.

Four manuscripts remain in preparation and/or review while five publications are already in press. The next phase or extension of this work is to rapidly test the material in a canine model which would complete the animal studies required prior to filing of an IND for translation into the clinic.

References:

1. Gowen, M., et al. (1999). Cathepsin K knockout mice develop osteopetrosis due to a deficit in matrix degradation but not demineralization. *J Bone Miner Res* 14: 1654-1663.
2. Hollberg, K., Nordahl, J., Hultenby, K., Mengarelli-Widholm, S., Andersson, G., and Reinholt, F. P. (2005). Polarization and secretion of cathepsin K precede tartrate-resistant acid phosphatase secretion to the ruffled border area during the activation of matrix-resorbing clasts. *J Bone Miner Metab* 23: 441-449.
3. Yang, F., Williams, C. G., Wang, D. A., Lee, H., Manson, P. N., and Elisseeff, J. (2005). The effect of incorporating RGD adhesive peptide in polyethylene glycol diacrylate hydrogel on osteogenesis of bone marrow stromal cells. *Biomaterials* 26: 5991-5998.
4. Fouletier-Dilling, CM. et al. (2005). Novel compound enables high-level adenovirus transduction in the absence of an adenovirus-specific receptor. *Hum Gene Ther* 16: 1287-1297.
5. Fouletier-Dilling CM, Gannon F, Olmsted-Davis EA, Lazard Z, Heggeness MH, Shafer JA, Hipp JA, and A.R. Davis. (2007) Efficient and Rapid Osteoinduction in an Immune Competent Host. Hum Gene Ther 18(8):733-45 (Fast Track publication and Cover).
6. Olmsted-Davis, EA, *et al.* (2002). Use of a chimeric adenovirus vector enhances BMP2 production and bone formation. *Hum Gene Ther* 13: 1337-1347.
7. Bikram M, Fouletier-Dilling CM, Hipp JA, Gannon F, Davis AR, Olmsted-Davis EA, and West JL (2007) Endochondral Bone Formation from Hydrogel Carriers Loaded with BMP2-Transduced Cells. Ann Biomed Eng. 35(5):796-807.
8. Olmsted, EA. *et al.* (2001). Adenovirus-mediated BMP2 expression in human bone marrow stromal cells. *J Cell Biochem* 82: 11-21.
9. Gugala, Z., Davis, A.R., Fouletier-Dilling, C, F. Gannon, Lindsey, R.W., Olmsted-Davis, EA (2007) Adenovirus BMP2-Induced Osteogenesis in combination with various collagen carriers. Biomaterials, 28(30):4469-79.

Appendix:

- Fouletier-Dilling CF, Wada A, Lazard Z, Salisbury E, Gannon F, Vadakkan T, Gao L, Hirschi K, Dickinson M, Davis AR, Olmsted-Davis E. (2010). J Bone Miner Res. 25(5):1147-56. PMID: 19839764

- Ronke M. Olabisi, ZaWaunyka Lazard, Elizabeth A. Olmsted-Davis, Alan R. Davis, Jennifer L. West. (2010). Comparison of endochondral bone formation after delivery of a cell based gene therapy system, with and without PEG-DA hydrogel encapsulation. Tissue Engineering Part A. 16(12):3727-36.

- Chih-Wei Hsu, Ronke M. Olabisi, Elizabeth A. Olmsted-Davis, Alan R. Davis, Jennifer L. West Cathepsin-K sensitive poly(ethylene Glycol) hydrogels for degradation in response to bone formation. (Journal Biomaterials Research, In Press)

- ZaWaunyka Lazard, Jerome Saltarrelli, Christian Clarke, Michael Heggeness, Jennifer West, Alan R. Davis, and Elizabeth Olmsted-Davis. Induction of targeted heterotopic ossification for healing traumatic bone injury. (Journal of Cellular Biochemistry, In Press).

- Elizabeth Salisbury, Eric Rodenberg , Corinne Sonnet, John Hipp, Francis Gannon, Tegy Vadakkan, Aya Wada, Mary Dickinson, Elizabeth A. Olmsted-Davis, and Alan R. Davis. Sensory Nerve Induced Inflammation Contributes to Heterotopic Ossification. (Am J Pathology, In Press).

Revised Manuscript

Vessel formation is induced prior to the appearance of cartilage in BMP2-mediated heterotopic ossification

C. Fouletier Dilling[1], A.M. Wada[2], Z.W. Lazard[1], E.A. Salisbury[1], F.H. Gannon[3], T. J. Vadakkan[2], L. Gao[2], K. Hirschi[1,4], M.E. Dickinson[2], A.R. Davis[1,5], E.A. Olmsted-Davis

[1]Center for Cell and Gene Therapy, Baylor College of Medicine, Houston, TX [2]Departments of Molecular Physiology and Biophysics, and Medicine, Baylor College of Medicine, Houston, TX [3]Department of Pathology, Baylor College of Medicine, Houston TX [4]Department of Pediatrics, Pediatrics-Nutrition, Baylor College of Medicine, Houston, TX [5]Department of Pediatrics, Hematology-Oncology, Baylor College of Medicine, Houston, TX

Funded in part by RO1EB005173-01, USMRMC 06135010 and USMRMC 06136005

Running title: Vessels form prior to cartilage

cdillingdk@yahoo.com, wada@bcm.tmc.edu, zwl@bcm.tmc.edu, salisbur@bcm.tmc.edu, fgannon@bcm.tmc.edu, vadakkan@bcm.tmc.edu, liangg@bcm.tmc.edu, mdickins@bcm.tmc.edu, khirschi@bcm.tmc.edu ardavis@bcm.tmc.edu, edavis@bcm.tmc.edu

Corresponding Author Alan R. Davis Center for Cell and Gene Therapy One Baylor Plaza Houston, TX 77030 Ph 713-798-1237 Fax 713-798-1230 ardavis@bcm.tmc.edu ar

Word count: Number of figures Abstract: 249
Black and White: 1 Manuscript: 6754 Color: 5

All authors have no conflicts of interest

Abstract

Heterotopic ossification (HO) or endochondral bone formation at non-skeletal sites, often results from traumatic injury, and can lead to devastating consequences. Alternatively the ability to harness this phenomenon would greatly enhance current orthopedic tools for treating segmental bone defects. Thus understanding the earliest events in this process would potentially allow us to design more targeted therapies to either block or enhance this process. Using a murine model of HO induced by delivery of adenovirus transduced cells expressing bone morphogenetic protein 2, BMP2, we show here that one of the earliest stages in this process is the establishment of new vessels prior to the appearance of cartilage. As early as 48 hours after induction of HO, we observed the appearance of brown adipocytes expressing VEGFs, simultaneous with endothelial progenitor replication. This was determined by using a murine model, which possesses the VEGF receptor 2 (flk-1) promoter containing an endothelial cell enhancer, driving the expression of nuclear-localized yellow fluorescent protein (YFP). Expression of this marker has previously been shown to correlate with the establishment of new vasculature (1) and the nuclear localization of YFP expression allowed us to quantify changes in endothelial cell numbers. We found a significant increase in Flk1-H2B::YFP cells in BMP2-treated animals as compared to controls. The increase in endothelial progenitors occurred three days prior to the appearance of early cartilage. The data collectively suggests that vascular remodeling and growth may be essential to modify the microenvironment and enable engraftment of the necessary progenitors to form endochondral bone.

Keywords: Bone morphogentic protein type2; heterotopic ossification; vessel formation

Introduction

Endochondral bone formation is thought to proceed through an ordered series of events, starting with the proliferation and “condensation” of presumptive mesenchymal cells to form avascular cartilage. Hence it is presumed that the lack of vasculature and associated cellular replication creates the hypoxic environment necessary for chondrogenic differentiation. However, recent data from our laboratory using a model of heterotopic ossification, suggests that vessels may play an essential role in the induction of chondrogenesis (2).

It has been well established that vessel formation plays a key role in late events during the process of bone formation. Vessels invade the perichondrium and hypertrophic zone and are required for the replacement of cartilage by bone (3). The angiogenic factor, vascular endothelial growth factor (VEGF) promotes vascular invasion via specific receptors, including Flk1 (VEGF-receptor 2) expressed in endothelial cells, in the perichondrium or surrounding tissue (4) (5). These events of cartilage matrix remodeling and vascular invasion are necessary for the migration and differentiation of osteoblasts and osteoclasts which remove mineralized cartilage matrix and replace it with bone. However, much less is known about the role of vessel formation prior to the appearance of the pre-cartilage tissue.

During normal wound repair, a series of cell signaling events are induced by the hypoxic state of the tissues, resulting in up-regulation of hypoxia inducible factor (HIF1) that in turn up-regulates a series of factors including several VEGFs (A, B, and D), leading to vessel formation. Hypoxia-induced angiogenesis has been proposed to be necessary for creating specialized vessels that facilitate progenitor homing and engraftment into damaged

tissues (6). Little is known as to whether such a process plays a key role in the repair of bone. Using a model of *de novo* bone formation to identify the earliest events in this process, we have demonstrated that myelo-mesenchymal stem cells are recruited to the tissues to form the early cartilage (7). One of the earliest events in this model is the appearance of brown adipocytes. These cells are capable of utilizing their uncoupled aerobic respiration to reduce localized oxygen tension and effectively pattern the newly forming cartilage condensations (8). This is consistent with *in vitro* data where bone marrow derived mesenchymal stem cells can undergo chondrogenesis in the presence of bone morphogenetic protein 2 (BMP2) and low oxygen (9). We also observed the appearance of vessels lining the edges of the perichondrial region, separated only by brown adipose, suggesting that perhaps the reduction in oxygen tension coordinately activates new vessel formation in the region (8). Thus, these progenitors may indeed be recruited to the site of new bone formation through the vasculature. In this study we focused on defining this tentative early vessel formation.

To determine this, we chose to employ a transgenic mouse model which expresses the fusion protein, human histone H2B with enhanced yellow fluorescent protein (EYFP) (H2B:YFP) in endothelial cells under the regulation of a Flk1 promoter/enhancer fragment (Flk1-H2B::YFP) (1). Recent improvements in genetically encoded fluorescent protein expression in animal models along with advances in optical imaging and image analysis software have enabled the analysis of many aspects of tissue development at a cellular level (10). Previous studies using this transgenic animal indicates that Flk1-H2B::YFP expression is restricted to endothelial cells of smaller and/or newly forming vessels (8), thus providing a mechanism for quantification of new vessels.

Here we demonstrate new vessel formation within the tissues prior to the appearance of the presumptive cartilage. Quantification of the number of endothelial cells shows that one of the first steps of bone formation is to induce additional endothelial cell proliferation. Histological analysis shows that increases in endothelial cell numbers are evident, just prior to the influx of chondrocytic progenitors. Immunohistochemical analysis of the tissues prior to the mesenchymal condensations, revealed a rapid and transient expression of VEGFA and D from the brown adipocytes. The data collectively, suggests that the brown adipocytes may play a key role in establishing patterning of the cartilage through regulation of oxygen tension within the tissues, through induction of both aerobic respiration, as well as early angiogenesis.

MATERIALS AND METHODS

Cell culture: A murine C57BL/6 derived cell line (MC3T3-E1) was obtained from American Type Culture Collection, propagated in αMEM supplemented with 10% fetal bovine serum (Hyclone, Logan, UT), 100 units/ml penicillin, 100 µg/ml streptomycin, and 0.25 µg/ml amphotericin B (Life Technologies Inc., Gaithersburg, MD). Briefly, the cells were grown in DMEM supplemented as described above and cultured at a subconfluent density in order to maintain the phenotype. All cell types were grown at 37□C and 5% CO_2 in humidified air.

Transduction of cells with adenovirus in the presence of GeneJammer®

***Adenoviruses*:** Replication defective first generation human type 5 adenovirus (Ad5) deleted in regions E1 and E3 was constructed to contain the cDNA for BMP2 in the E1 region of the viral genome (11). The virus particles (vp) to plaque forming unit (pfu) ratios

were: 55 and 200 for Ad5BMP2 and Ad5-empty respectively, and all viruses were shown to be negative for replication competent adenovirus.

The C57BL/6 cell line or MC3T3-E1 (1×10^6), were transduced with Ad5BMP2 or Adempty cassette control virus at a concentration of 5000 vp/cell with 1.2% GeneJammer® as previously described (12).

Heterotopic bone assay: The transduced cells were resuspended at a concentration of 5×10^6 cells/100 µl PBS, and then delivered through intramuscular injection into the hind limb quadriceps muscle of Flk1 mice. Animals were euthanized at daily intervals and hind limbs were harvested, embedded and placed at -80°C. All animal studies were performed in accordance with standards of the Baylor College of Medicine, Department of Comparative Medicine after review and approval of the protocol by the Institutional Animal Care and Use Committee (IACUC).

Histological analysis and staining analysis:

Soft tissues encompassing the site of new bone formation were isolated from the rear hind limb of the mice. Both the skin and skeletal bone were removed from the tissues prior to freezing. Serial sections (15 µm) were prepared that encompassed the entire tissues (approximately 50 sections per tissue specimen). We then performed Hematoxylin and Eosin staining on every 5^{th} slide which allowed us to locate the region containing either our delivery cells or the newly forming endochondral bone. Serial unstained slides were used for immunohistochemical staining (either single or double-antibody labeling). For double antibody labeling, samples were treated with both primary antibodies simultaneously

followed by washing and incubation with respective secondary antibodies, used at 1:500 dilution to which Alexa Fluor 488, 594, or 647 were conjugated. Primary antibodies were used as follows: SMA mouse monoclonal used at 1:200 dilution; Sigma Chem Co, St Louis, MO), CD31 (rat monoclonal used at 1:75 dilution; BD Pharmingen, San Diego, CA), Flk1 (goat polyclonal used at 1:100 dilution; R&D systems, Minneapolis, MN), Ki67 (rat monoclonal used at 1:100, Dako, Carpinteria, CA), VEGF-D (goat polyclonal used at 1:100 dilution, Santa Cruz Biotechnology, INC, Santa Cruz, CA). Stained tissue sections were examined by confocal microscopy (Zeiss Inc, Thornwood, NY, LSM 510 META) using a 20x/0.75NA objective lens.

Flk1 positive cell quantification in BMP -induced tissues: To quantify the increase in YFP positive cells in the BMP-induced tissues, frozen sections across these tissues were counterstain with DAPI and the YFP expression was compared to that obtained in the control tissues. First, a series of low magnification (5.4x and 12x) bright field images of a tissue section were taken and overlapped to reconstruct the tissue section using Adobe Photoshop CS3. The reconstructed montage image was used to measure the area of the tissue section using a manual contour tracing method (Zeiss Axiovision). The area of each of the frozen sections was calculated in a similar manner. Area measurements are used to determine the density of labeled cells as indicated below.

High resolution (10X/NA0.45, 1024x1024 pixels), dual channel images of tissue sections nuclear stained with DAPI were taken using a confocal microscope (Zeiss LSM 510 META). In each image, the number of nuclei in the DAPI and YFP channels was counted using a modified watershed segmentation algorithm (FARSIGHT, RPI) which makes use of both intensity and volume thresholds to distinguish two nuclei as separate. All

the nuclei counted using the software were DAPI positive. The fraction of DAPI stained nuclei marked by YFP were counted as YFP positive. The density of YFP positive cells in a tissue section was defined as the ratio of the number of YFP positive nuclei in the tissue section measured from the high magnification images to the area of the tissue section measured from the low magnification images. The density of the YFP positive nuclei was calculated for a number of control and BMP treated tissues at 2 and 4 days after injection. The ratios were then averaged over the various control and BMP2-treated tissues. The p-values were calculated using a Student's t-test.

Flk1-YFP positive cell association analysis:

To characterize the cell type(s) that express YFP in the adult muscle tissue, we performed immunoflourescent studies using endothelial cell marker CD31 and Flk1 antibodies; for vascular smooth muscle cells -smooth α actin (SMA). Association of cells expressing YFP with immuno-labeled cells was analyzed using (FARSIGHT, RPI, NY) and a custom program written in MATLAB (MathWorks, Natick, MA). After identification of each nucleus by DAPI staining, YFP positive and negative cells were then analyzed for association with fluorescent signals of each antibody. An intensity threshold was applied to the red channel in each image to identify a cell positive or negative for the immunofluorescent signal. Each identified nucleus and overlapping red channel were counted as CD31, Flk1, or SMA positive and then as either YFP negative and positive. Co-localization percentages are shown in the supplemental data section (Table S-1) and describe in detail the YFP positive cell types. The number of YFP+/Ki67+ nuclei in an area of the tissue was calculated by adding the YFP+/Ki67+ in each of the confocal images taken within the area. The area

fraction of YFP+/Ki67+ was defined as the total number of YFP+/Ki67+ in the images taken within the area divided by the number of images. The area fraction was measured for five different areas and the average area fraction was calculated for control and BMP treated tissues for every 5th slide sectioned throughout the entire hindlimb. The area fractions of YFP+/Ki67+ nuclei in the control and the BMP treated tissues on day 2 were 3.97 ± 2.96 and 6.11 ± 1.76 respectively. The area fractions for day 4 were 5.04 ± 0.72 and 6.41 ± 1.41 in the control and the BMP treated tissues. Based on the Student's t-test, the p value for the day 2 data was 0.21 and that for the day 4 data was 0.10. Taken together, the data supports the trend that YFP+/Ki67+ population increases on day 2 and day 4 after the BMP treatment.

Q-RT-PCR: Non-skeletal tissues (n=4 per group) surrounding the site of injection of the AdBMP2 or Adcontrol transduced cells were isolated at daily intervals for 7 days and prepared as total RNA using a Trizol reagent (Life Technologies, Carlsbad, CA) in accordance with the manufacturer's specifications. The two groups of RNAs were subjected to Q-RT-PCR analysis in parallel and the Ct values obtained normalized to both internal 18S ribosomal RNA used in multiplexing, and to each other to remove changes in gene expression common to both the BMP2 and control tissues by using the ® method of ΔΔCt along with Taqmanprimers and probes (Applied Biosystems, Carlsbad, CA) as previously described (8).

RESULTS

Upregulation of vessel markers prior to the onset of chondrogenesis:

We have previously described a model of rapid endochondral bone formation (13) in which mineralized bone is observed 7 days after the initial induction with BMP2. Observation of vessels lining the newly forming perichondrium suggests that vessels may undergo replication prior to chondrogenesis. To confirm this hypothesis, we examined tissues, at 24 hour intervals over the period leading up to chondrogenesis (day 5), for the presence or absence of endothelial cell replication. Figure 1 shows the co-expression of the endothelial cell specific factor, von Willibrand factor (VWF) (red) and Ki67 (green), a marker of cellular replication (14) in the vessels from tissues that received AdBMP2 transduced cells, starting 24 hours to 5 days (panels A-E, respectively). As can be seen in Figure 1, panel B, we did observe overlap of these two markers (yellow color), in tissues receiving the AdBMP2 transduced cellswhereas no replicating endothelial cells were observed in the control tissues (Panel F). We did not attempt to quantify the amount and apparent timing of replication using this method, because VWF is an extracellular matrix protein. Instead we employed the Flk1H2B::YFP model for quantifying endothelial progenitor replication over the course of early bone formation.

Flk1-H2B::YFP in vessels:

We next determined if there was a significant increase in the number of Flk1+ endothelial progenitors during bone induction, consistent with new vessel formation, prior to chondrogenesis. We chose to utilize the Flk1-H2B::YFP mouse model (1), in which new vessel formation could be readily quantified within the muscle tissues. Flk1 is a VEGF

receptor transiently expressed on endothelial cells, and is presumably thought to contribute to VEGF induced endothelial cell replication (15). Therefore quantification of the nuclear YFP expression within tissues from animalsreceiving either AdBMP2 or Adempty transduced cells allowed us to to quantify increases in the number of endothelial progenitors within the muscle prior to cartilage formation. We previously quantified the association of Flk1-H2B::YFP with other endothelial cells markers such as CD31, and found them to be 95% overlapping (supplemental data). Frozen sections were prepared by serial sectioning from Flk1-H2B::YFP adult hind limb soft tissue (n=4 per group) consisting of three groups, those receiving: (1) cells transduced with Ad5BMP2, (2) cells transduced with Ad5empty cassette control virus, and (3) normal mouse muscle. To ensure uniform quantification and adequate sampling, the entire region of soft tissues in the hind limb was sectioned and approximatelyever fifth section was for analyzed for YFP expression.

To quantify differences in the number of endothelial progenitors, the number of YFP+ cells per the total number of DAPI+ cells was determined using automated segmentation methods (see Materials and Methods). The total YFP+ cells was also quantified per total area of the tissue section to ensure there was no bias in the fields of view chosen for image analysis (see Materials and Methods). The total area of each tissue section was determined using a montage of images that were collected using wide-field microscopy (panels A and F) (figure 2). As can be seen in Figure 2, we found Flk1-H2B::YFP positive cells in both tissues receiving Adempty transduced cells (panels B-E) and AdBMP2 transduced cells (panels G-O). These panels are higher magnification confocal images of the region within the corresponding white box on the lower magnification high resolution wide-field montage of the entire tissues (panels A;

control and F; BMP2). The results of the quantification, (figure 3), shows the average number of Flk1H2B::YFP+ cells on day 2 and day 4. Analysis of the entire soft tissue within several mice showed a significant elevation in tissues receiving the AdBMP2 transduced cells ($p=0.017$, day 2 (Fig 3A) and $p=0.006$, day 4 (Fig 3B) as compared to the control, on both days 2 and 4. The peak was approximately 2 days after induction of bone formation with no statistically significant difference between these results and those obtained in tissue sections isolated 4 days after induction.

Endothelial progenitors undergo replication in tissues receiving AdBMP2 transduced cells: In the tissues receiving cells transduced with a control adenoviral vector, we observed randomly scattered YFP+ cells along the vessel structures, while in the tissues receiving AdBMP2 transduced cells we see clustering of the YFP+ cells (Figure 2). This prompted us to question whether the Flk1-H2B::YFP progenitors could be replicating, so we next quantified the number of Flk-H2B::YFP positive cells in these tissues. Representative images used for quantification of YFP positive cell proliferation activity are shown in Figure 4. Replicating endothelial progenitors were defined as nuclei positive for both Flk1-H2B::YFP (yellow) and the cell proliferation marker, Ki67 (red; figure 4). In both control and treated animals, we also observed proliferating cells, positive for Ki67, that did not overlap with Flk1-H2B::YFP. Quantification of cells positive for both Flk1-H2B::YFP and Ki67 (figure 4) indicates a large number of replicating endothelial progenitors in both control and BMP2 treated tissues at two days after induction. Therefore the percentage of dual positive cells was not significant at this early time point as compared to the control. However, by four days after induction with BMP2, we observed much fewer replicating Flk1-H2B::YFP cells in the control and significantly more in the experimental group (figure

4). This difference was found to be statistically signifcant.

Vascular Endothelial Growth Factor (VEGF) mRNA expression:

Endothelial progenitor replication appeared to start within 48 hours of induction with BMP2. This correlated with a significant elevation in the vascular endothelial growth factor, VEGF-D (also termed fos-induced growth factor, FIGF) and VEGFA, RNA expression (figure 5). Figure 5 show the changes in VEGF mRNA expression from day 1 after injection of AdBMP2-transduced cells until day 6 as determined by real time reverse transcription PCR (Q-RT-PCR). Both VEGF-A and VEGF-D mRNA expression was significantly increased on days 2 and 4 after induction of bone formation. VEFG-B and VEGF-C however, remained on the same level throughout the time course. Although the data cannot differentiate between expansion of cells expressing VEGF-A and -D elevated transcription within cells residing in the area, the results suggest that these potent endothelial growth factors are rapidly and transiently increased within the site of new bone formation prior to the onset of cartilage.

Role of brown adipose in vessel formation:

The data collectively suggests that vessel replication is occurring simultaneously with elevated expression of VEGFs within the tissues. Since one of the earliest events observed in our model, is the recruitment and expansion of brown adipocytes (8) we next chose to determine if these cells might be expressing the VEGFs.

Immunohistochemical analysis of Flk1-H2B::YFP tissues that received either

AdBMP2 or Adempty transduced cells, showed co-localization of VEGF-D (green; fig 6, panel c) and the brown adipocyte specific marker uncoupling protein 1 (UCP1; red; fig 6, panel d) (day 2). As can be seen in figure 6, panel e, the expression of UCP1 overlaps expression of VEGF-D, in cells which are adjacent to the Flk1-H2B::YFP+ endothelial progenitors, suggesting that the brown adipocytes may be contributing to the new vessel formation. We observed additional fluorescence within the surrounding muscle, which appears to be punctate, and not cell associated. This staining may represent secreted VEGF-D protein, in the tissues. To confirm the cell specific expression of VEGF-D in the brown adipocytes, we performed additional immunostaining, (Figure 6f). Positive expression of VEGF-D (brown staining) was observed only in the brown adipocytes, again suggesting that these cells may play a role in the regulation of new vessels.

Discussion

Similar physiological steps lead to bone formation during embryonic development and in adult organisms, for instance in fracture repair or heterotopic ossification. In both cases, bone formation begins with mesenchymal condensations and ends with maturation of the growth plate, recruitment of osteoblasts and the production of bone. Vascularization has been shown to play a critical role in this process, through the infiltration into cartilage to form vascularized bone (16). Here we present data that show that vessels play a much earlier role in patterning of the cartilage and bone. The results show the presence of new vessel formation prior to the onset of mesenchymal condensations and cartilage.

We have previously reported the presence of brown adipocytes within the tissues, two days after the initial induction. We have also shown that these cells regulate localized

oxygen tension through their unique metabolism (8). In this study we extend our knowledge of the functional role of brown adipocytes, to include their rapid and transient expression of the potent angiogenic factors VEGFA and D. Interestingly a similar rapid and transient expression of VEGFD has also been demonstrated in limb development and shown to be critical for patterning (17). We observed a biphasic expression pattern for VEGF-A and -D, suggesting multiple roles for this factor in bone formation. The second peak of expression correlates nicely with the transition of cartilage to bone formation which has been highly documented (16,18) However the first phase is less well studied, and in our model and appears to correlate with the establishment of new vessels just prior to the onset of chondrogenesis. Zelzer, *et al*, also reported a similar biphasic expression of VEGF-A during embryonic bone formation (19). In these studies, they showed two functional roles for VEGFA one prior to cartilage and one during the transition of cartilage to bone similar to our own observation in our model. The data collectively, suggests that the brown adipocytes may induce the synthesis of new vessels, as a component for patterning the newly forming cartilage. In the proposed model, the brown adipocytes induce new vessels, facilitating the recruitment of chondrogenic precursors, while at the same time lowering localized oxygen tension to allow for chondrogenic differentiation. In support of this mechanism, we show in this study, the presence of brown adipocytes, expressing VEGF-D only in areas adjacent to our newly expanding vessels as marked by Flk1H2B::YFP.

Using a model of rapid endochondral bone formation, we show the immediate expansion of vessels within the tissues in response to delivery of BMP2. Although BMP2/4 play a critical role in the patterning of cartilage and bone in the embryo (20), much evidence now links the bone morphogenetic proteins to a host of other earlier physiological functions

including vascularization of the early embryo (21) Thus it may not be surprising that the earliest stage of bone formation in our model is the induction of new vessel formation.

Upon BMP2 stimulation, the Flk-1-H2B::YFP endothelial progenitors expand, as the total number of positive cells per tissue area increases. The Flk1-H2B::YFP positive cells are clustered along individual vessels suggesting that these vessels are extending or remodeling in response to BMP2. At this point we can not determine whether this increase occurs via replication of tissue resident endothelial progenitors or the recruitment of progenitors to the site of new bone formation. Our data suggests that the expansion of these progenitors, at least in part, is due to the replication, since we observed an increase in the area of replicating endothelial cells within the tissues receiving AdBMP2 transduced cells on day 4 as compared to the control tissues. However, we can not rule out the possibility that at least some of these cells are recruited from either the circulation of surrounding tissues. Interestingly, their were significant clusters of replicating Flk1-H2B::YFP cells on day 2 in both tissue receiving the AdBMP2 and Adempty cassette transduced cells, suggesting that perhaps the initial inflammatory reponse may be somewhat masking the significance of the replication at this early time point. Alternatively, the increase in replication of the Flk1-H2B::YFP cell population at four days after induction of bone formation may represent the need for vascularization to recruit new chondro-osseous progenitors, since this coincides with the appearance of these cells within the tissues (22). However, recruitment from the surrounding tissue is equally likely, since recently, Kaplan *et al* (34) showed local stem and progenitor contribution to heterotopic bone formation in a murine model of stem cell transplantation, and this process may require new vessel formation for establishment of these cells.

Vascular endothelial growth factors (VEGFs) have been shown to be essential to expansion of both endothelial cells as well as vascular smooth muscle cells which assemble to form the vessel structure. Although VEGFA has been most commonly shown to be responsible for angiogenesis in most systems, recent studies in murine muscle, have found VEGF-D to be an extremely potent angiogenic factor (23). This family member is better known for its critical role in the expansion of lymphatic vasculature (23). In our model we see both factors highly expressed in the tissues receiving the BMP2 transduced cells, as compared to those receiving control cells. Again the rapid but transient elevation in VEGF expression suggests that these factors may be driving the endothelial cell replication. Knockout studies have confirmed that BMPs regulate vasculogenesis during embryonic development (24). Functional deletion of BMP-4 and the BMP I receptor in mice leads to impaired mesoderm precursors required for vascular development (25) (26). It has also been shown that addition of BMP neutralizing antibodies or noggin suppresses endothelial cell formation during development while addition of rhBMP4 promotes it (27).

We and others have recently shown the chondrocyte to be of myeloid original, which circulates to the site of new bone formation (28) (22). These cells must then recruit and pass from the vessels into the tissues, through a process known as extravasation (29) This process has been shown to require small vasculature, which has a reduced blood flow (29) Thus it is conceivable that brown adipocytes express the VEGFs to form new vessels, capable of permitting recruitment of chondrocytic progenitors to the correct location for endochondral bone formation. Since vascular invasion of the growth plate has been well documented to precede the recruitment of osteoblast progenitors to form the new bone (16,18,29,30), it would not be surprising to have an earlier phase of this process that

recruited the chondrocytic progenitors. We have previously shown that the brown adipocytes are capable of inducing hypoxia in the local environment which in the presence of BMP2 has been shown to induce chondrogenesis (8). Thus we propose that the brown adipocytes are capable of patterning the newly forming cartilage by inducing new vessel formation, while simultaneously removing oxygen through uncoupled aerobic respiration. Once the progenitors differentiate into chondrocytes, they then express a number of anti-angiogenic proteins, to prevent in growth of new vessels, thus momentarily attenuating this early wave of angiogenesis (31) (32) (33) (35). Thus the results presented in this study extend our knowledge about the critical nature vascularization plays not only in bone formation but in cartilage as well. The data collectively shows a novel process for patterning of new endochondral bone, in adult organisms. Further, this is one of the first studies that attempt to understand the biology of tissue engineering of cartilage. Surprisingly one of the critical components we have identified is contradictory to our current dogma, that cartilage does not require vessels. The study suggests that brown adipose may play a pivotal role in establishing new vessels, essential for recruitment of chondrogenic progenitors, and patterning of the tissues. These findings may ultimately play an important role in our efforts to replace damaged cartilage through tissue engineering.

Figure Legends:

Figure 1: Immunohistochemical analysis of endothelial cell replication in tissues isolated at daily intervals after induction of bone formation with cells expressing BMP2. (A-E) days 1, 2, 3 , 4, and 5 respectively, after injection of BMP2-producing cells, paraffin sections were prepared and stained with an antibody against Ki-67 followed by as secondary antibody conjugated to Alexa fluor 488 (green) mixed with an anti-Von Willibrand Factor (VWF) antibody followed by a secondary antibody conjugated to Alexa fluor 547 (red). **Panel F** shows a representative image, similar staining, taken from tissues isolated from mice injected with cells transduced with a control vector (Adempty).

Figure 2: Wide-field and confocal images of whole tissue sections and quantification of Flk1-H2B::YFP cells. (A,F) Representative montages of low magnification grayscale images (1 pixel = 0.003mm) used for calculating total area for tissue sections. A single representative tissue section is depicted after the entire hind limb muscles which encompassed the injection site were isolated 2 after receiving an intramuscular injection of cells transduced with either Ad empty control vector **(panel A)** or AdBMP2 **(panel B)** and sectioned at 15 uM thickness. Although every 5th section across the entire tissue was analyzed, we show only a single representative image of each type. The corresponding regions with positive YFP signal, shown by the boxed areas, were imaged by confocal microscopy (panels B-E, G-O) for counting the YFP positive cell numbers.

Figure 3: Increase in Flk-H2B::YFP positive cells in BMP2-induced tissue at Day 2 and 4. Quantification of Flk1-H2B::YFP cells within the tissues, two and four days afterinduction with AdBMP2 transduced or control cells. YFP nuclei were counted and reported as ratio of the total area of the tissue section determined using the wide-field montage. Flk-H2B::YFP positive cells were significantly elevated in the tissues receiving BMP2 as compared to the controls. The graph depicts the average number of Flk-H2B::YFP positive cells in 5 sections for Day 2 control, 7 sections for Day 2 BMP, 8 sections for Day 4 control, and 6 sections for Day 4 BMP. The number of images taken in each section ranged from 4 through 22.* denotes a significant difference as determined by the Student's t-test.

Figure 4: Quantification of YFP positive cell proliferation. Representative images of Flk1-H2B::YFP and the cell proliferation marker Ki-67. Co-localization of Flk1H2B::YFP (yellow) and Ki-67 (red), was detected in BMP2-treated and control tissues. Graphs show the total number of YFP+/Ki67+ in the images taken within the area divided by the number of images analyzed. The area fraction was measured for nine at day 2, five at day 4 BMP and eight at day 2, four at day 4 control different areas and the average area fraction was calculated for control and BMP treated tissues. The area fractions of YFP+/Ki67+ nuclei in the control and the BMP treated tissues on day 2 were 7.32 ± 3.26 and 10.20 ± 6.95 respectively. The area fractions for day 4 were 6.97 ± 2.32 and 11.26 ± 2.58 in the control and the BMP treated tissues. Based on the Student's t-test, the p value for the day 2 data was 0.29 and that for the day 4 data was 0.035. Taken together, the data showed that significant YFP+/Ki67+ population increases by day 4 after the BMP treatment, however, at day 2, there are no significant differences in dividing YFP cell population between control and BMP treated tissues.

Figure 5: Expression of VEGF-D during the early stages of endochondral bone formation. Results of real time quantitative RT-PCR analysis of *VEGF-A,-B,-C, and -D* mRNA levels in tissues surrounding the lesional site that received either the AdBMP2or Adempty cassette-transduced cells isolated at daily intervals for up to 7 days after initial injection. Four biological replicates were run in triplicate and the averages normalized against an internal standard (ribosomal RNA). The samples receiving AdBMP2 transduced cells were then compared to those obtained from the tissues receiving cells transduced with Adempty cassette virus. Therefore the graph depicts the fold changes in VEGF RNAs in the BMP2 samples over time as compared to the control tissues. Error bars depict ± one standard deviation unit. * denotes samples that had a statistically significant ($p < 0.05$) difference from all other samples by the ANOVA test.

Figure 6: Immunohistochemical staining for brown adipocytes expressing VEGFD (green color, c) in tissues isolated from the Flk1-H2B::YFP mice 4 days after receiving MC3T3 cells transduced with Ad5BMP2. Brown adipocytes were identified as cells expressing uncoupling protein 1 (UCP 1; **d,** red color) and the yellow color (**b**) represents the Flk-yfp+ endothelial cells within the muscle. The tissues were also stained with VEGFD antibodies (**c**) and counterstained with dapi (blue color, **a**) that stains the nucleus of cells. A merger of these stains (UCP-1, VEGF-D, and YFP) is shown in panel **e**. In panel **f** a paraffin section taken 4 days after injection of BMP2producing cells, was stained with an antibody against UCP1 and staining was visualized using 3,3'-Diaminobenzidine (DAB) as previously described (8). No staining was observed on a paraffin section taken 4 days after injection of cells transduced with the empty control vector Ad5HM4 (data not shown).

REFERENCES

1. Fraser ST, Hadjantonakis AK, Sahr KE, Willey S, Kelly OG, Jones EA, Dickinson ME, Baron MH 2005 Using a histone yellow fluorescent protein fusion for tagging and tracking endothelial cells in ES cells and mice. Genesis **42**(3)**:**162-71.
2. Shafer J, Davis AR, Gannon FH, Fouletier-Dilling CM, Lazard Z, Moran K, Gugala Z, Ozen M, Ittmann M, Heggeness MH, Olmsted-Davis E 2007 Oxygen tension directs chondrogenic differentiation of myelo-monocytic progenitors during endochondral bone formation. Tissue Eng **13**(8)**:**2011-9.
3. Colnot C, Lu C, Hu D, Helms JA 2004 Distinguishing the contributions of the perichondrium, cartilage, and vascular endothelium to skeletal development. Dev Biol **269**(1)**:**55-69.
4. Maes C, Stockmans I, Moermans K, Van Looveren R, Smets N, Carmeliet P, Bouillon R, Carmeliet G 2004 Soluble VEGF isoforms are essential for establishing epiphyseal vascularization and regulating chondrocyte development and survival. J Clin Invest **113**(2)**:**188-99.
5. Gerber HP, Vu TH, Ryan AM, Kowalski J, Werb Z, Ferrara N 1999 VEGF couples hypertrophic cartilage remodeling, ossification and angiogenesis during endochondral bone formation. Nat Med **5**(6)**:**623-8.
6. Li J, Zhang YP, Kirsner RS 2003 Angiogenesis in wound repair: angiogenic growth factors and the extracellular matrix. Microsc Res Tech **60**(1)**:**107-14.
7. Fouletier-Dilling CM, Gannon FH, Olmsted-Davis EA, Lazard Z, Heggeness MH, Shafer JA, Hipp JA, Davis AR 2007 Efficient and rapid osteoinduction in an immune-competent

host. Hum Gene Ther **18**(8)**:**733-45.
8. Olmsted-Davis E, Gannon FH, Ozen M, Ittmann MM, Gugala Z, Hipp JA, Moran KM, Fouletier-Dilling CM, Schumara-Martin S, Lindsey RW, Heggeness MH, Brenner MK, Davis AR 2007 Hypoxic adipocytes pattern early heterotopic bone formation. Am J Pathol **170**(2)**:**620-32.
9. Shen M, Yoshida E, Yan W, Kawamoto T, Suardita K, Koyano Y, Fujimoto K, Noshiro M, Kato Y 2002 Basic helix-loop-helix protein DEC1 promotes chondrocyte differentiation at the early and terminal stages. J Biol Chem **277**(51)**:**50112-20.
10. Hadjantonakis AK, Dickinson ME, Fraser SE, Papaioannou VE 2003 Technicolour transgenics: imaging tools for functional genomics in the mouse. Nat Rev Genet **4**(8)**:**613-25.
11. Olmsted EA, Blum JS, Rill D, Yotnda P, Gugala Z, Lindsey RW, Davis AR 2001 Adenovirus-mediated BMP2 expression in human bone marrow stromal cells. J Cell Biochem **82**(1)**:**11-21.
12. Fouletier-Dilling CM, Bosch P, Davis AR, Shafer JA, Stice SL, Gugala Z, Gannon FH, Olmsted-Davis EA 2005 Novel compound enables high-level adenovirus transduction in the absence of an adenovirus-specific receptor. Hum Gene Ther **16**(11)**:**1287-97.
13. Olmsted-Davis EA, Gugala Z, Gannon FH, Yotnda P, McAlhany RE, Lindsey RW, Davis AR 2002 Use of a chimeric adenovirus vector enhances BMP2 production and bone formation. Hum Gene Ther **13**(11)**:**1337-47.
14. Gerdes J, Schwab U, Lemke H, Stein H 1983 Production of a mouse monoclonal antibody reactive with a human nuclear antigen associated with cell proliferation. Int J Cancer **31**(1)**:**13-20.
15. Sato Y, Kanno S, Oda N, Abe M, Ito M, Shitara K, Shibuya M 2000 Properties of two VEGF receptors, Flt-1 and KDR, in signal transduction. Ann N Y Acad Sci **902:**201-5; discussion 205-7.
16. Reddi AH 1994 Bone and cartilage differentiation. Curr Opin Genet Dev **4**(5)**:**737-44.
17. Trelles RD, Leon JR, Kawakami Y, Simoes S, Belmonte JC 2002 Expression of the chick vascular endothelial growth factor D gene during limb development. Mech Dev **116**(1-2)**:**239-42.
18. Reddi AH 1992 Regulation of cartilage and bone differentiation by bone morphogenetic proteins. Curr Opin Cell Biol **4**(5)**:**850-5.
19. Zelzer E, McLean W, Ng YS, Fukai N, Reginato AM, Lovejoy S, D'Amore PA, Olsen BR 2002 Skeletal defects in VEGF(120/120) mice reveal multiple roles for VEGF in skeletogenesis. Development **129**(8)**:**1893-904.
20. Li X, Cao X 2006 BMP signaling and skeletogenesis. Ann N Y Acad Sci **1068:**2640.
21. Hogan BL 1996 Bone morphogenetic proteins in development. Curr Opin Genet Dev **6**(4)**:**432-8.
22. Shafer J DA, Gannon FH, Fouletier-Dilling CM, Lazard Z, Moran K, Gugala Z, Ozen M, Ittmann M, Heggeness MH, Olmsted-Davis E 2007 Oxygen tension directs chondrogenic differentiation of myelo-monocytic progenitors during endochondral bone formation. Tissue Eng **13**(8)**:**2011-9.
23. Rissanen TT, Markkanen JE, Gruchala M, Heikura T, Puranen A, Kettunen MI, Kholova I, Kauppinen RA, Achen MG, Stacker SA, Alitalo K, Yla-Herttuala S 2003 VEGF-D is the strongest angiogenic and lymphangiogenic effector among VEGFs delivered into skeletal muscle via adenoviruses. Circ Res **92**(10)**:**1098106.
24. Moser M, Binder O, Wu Y, Aitsebaomo J, Ren R, Bode C, Bautch VL, Conlon FL,

Patterson C 2003 BMPER, a novel endothelial cell precursor-derived protein, antagonizes bone morphogenetic protein signaling and endothelial cell differentiation. Mol Cell Biol **23**(16)**:**5664-79.
25. Mishina Y, Suzuki A, Gilbert DJ, Copeland NG, Jenkins NA, Ueno N, Behringer RR 1995 Genomic organization and chromosomal location of the mouse type I BMP-2/4 receptor. Biochem Biophys Res Commun **206**(1)**:**310-7.
26. Winnier G, Blessing M, Labosky PA, Hogan BL 1995 Bone morphogenetic protein-4 is required for mesoderm formation and patterning in the mouse. Genes Dev **9**(17)**:**2105-16.
27. Kelly MA, Hirschi KK 2009 Signaling Hierarchy Regulating Human Endothelial Cell Development. Arterioscler Thromb Vasc Biol.
28. Zhao Y, Glesne D, Huberman E 2003 A human peripheral blood monocyte-derived subset acts as pluripotent stem cells. Proc Natl Acad Sci U S A **100**(5)**:**2426-31.
29. Ruster B, Gottig S, Ludwig RJ, Bistrian R, Muller S, Seifried E, Gille J, Henschler R 2006 Mesenchymal stem cells display coordinated rolling and adhesion behavior on endothelial cells. Blood **108**(12)**:**3938-44.
30. Otsuru S, Tamai K, Yamazaki T, Yoshikawa H, Kaneda Y 2007 Bone marrow-derived osteoblast progenitor cells in circulating blood contribute to ectopic bone formation in mice. Biochem Biophys Res Commun **354**(2)**:**453-8.
31. Pufe T, Petersen WJ, Miosge N, Goldring MB, Mentlein R, Varoga DJ, Tillmann BN 2004 Endostatin/collagen XVIII--an inhibitor of angiogenesis--is expressed in cartilage and fibrocartilage. Matrix Biol **23**(5)**:**267-76.
32. Oshima Y, Sato K, Tashiro F, Miyazaki J, Nishida K, Hiraki Y, Tano Y, Shukunami C 2004 Anti-angiogenic action of the C-terminal domain of tenomodulin that shares homology with chondromodulin-I. J Cell Sci **117**(Pt 13)**:**2731-44.
33. Hayami T, Funaki H, Yaoeda K, Mitui K, Yamagiwa H, Tokunaga K, Hatano H, Kondo J, Hiraki Y, Yamamoto T, Duong le T, Endo N 2003 Expression of the cartilage derived anti-angiogenic factor chondromodulin-I decreases in the early stage of experimental osteoarthritis. J Rheumatol **30**(10)**:**2207-17.
34. Kaplan FS, Glaser DL, Shore EM, Pignolo RJ, Xu M, Zhang Y, Senitzer D, Forman SJ, Emerson SG 2007 Hematopoietic stem-cell contribution to ectopic skeletogenesis. J Bone Joint Surg Am **89**(2)**:**347-57.
35. Shukunami C, Iyama K, Inoue H, Hiraki Y 1999 Spatiotemporal pattern of the mouse chondromodulin-I gene expression and its regulatory role in vascular invasion into cartilage during endochondral bone formation. Int J Dev Biol **43**(1)**:**39-49.

Supplemental data:

To verify that the Flk-H2B::EYFP was restricted to endothelial cells, we first analyzed the normal adult muscle to examine that the Flk-1-H2B::EYFP expressed in the endothelial cells. YFP positive cells appeared to be association with the endothelial cells labeled by antibodies against CD31 and Flk1 (figure1). When endogenous Flk1 positive cells are immunolabled, smaller vessels showed co-localization of YFP and Flk1 positive cells,

however, not all the Flk1 positive vessels contained YFP positive cells. Since vascular smooth muscle actin (SMA) is also expressed by cell surrounding vascular endothelial cells, we examined whether the YFP expression is associated with the smooth muscle cells using SMA antibody for immuostaining, and we do see the YFP expression in smooth muscle positive vasculature (figure. 1). From our immunolocalization analysis, the endothelial marker VE-cadherin (data not shown) and CD31 marker also exhibit a similar localization pattern with YFP positive cells (figure. 1, table 1).

Using image analysis software, FARSIGHT (RPI, New York), we performed segmentation analysis on RGB images, where we associated immunostaining signals to the red channel, YFP to the green channel, and DAPI to the blue channel. First, DAPI stained nuclei in the blue channels were segmented using FARSIGHT. The total number of segmented nuclei was defined as the total number of cells. Similarly, YFP positive nuclei in the green channels were segmented and counted as YFP positive cells (figure. 1). The fraction of cells that were immumostaining positive was counted by taking the ratio of DAPI stained nuclei that were immumostaining positive (red channel) to the total number of DAPI stained nuclei. Then, the immuno-stained positive cells were classified as YFP positive cells and YFP negative cells. Data sets were quantified and described in the table 1. From this analysis, we demonstrated that adult muscle tissue express H2B::EYFP in the endothelial cells, however, they represents a subset of endothelial cells.

CD31 (8 pictures)	CD31+/DAPI+	YFP+ CD31+/YFP+	YFP+ CD31+/CD31+
Mean	84.56%	100.00%	20.74%
Stv	10.87%	†	16.95%
Confident Interval (95%)	7.10%	†	11.07%

Figure.1

Table.1

All nucleus → DAPI+ DAPI with CD31+ and YFP-→CD31+ DAPI with CD31-and YFP+ →YFP+

CD31 (8 pictures)	CD31+/DAPI+	YFP+ CD31+/YFP+	YFP+ CD31+/CD31+
Mean	84.56%	100.00%	20.74%
Stv	10.87%	†	16.95%
Confident Interval (95%)	7.10%	†	11.07%
VE-Cad (6 pictures)	**VE-Cad+/DAPI+**	**YFP+ VE-Cad +/YFP+**	**YFP+VE-Cad +/VE-Cad +**
Mean	87.67%	100.00%	8.61%
Stv	6.59%	†	3.67%
Confident Interval (95%)	4.31%	†	2.40%
FLK1 (6 pictures)	**FLK1+/DAPI+**	**YFP+ FLK1 +/YFP+**	**YFP+ FLK1 +/FLK1 +**
Mean	94.93%	100.00%	16.94%
Stv	5.22%	†	7.02%
Confident Interval (95%)	4.18%	†	5.61%
SMA (12 pictures)	**SMA +/DAPI+**	**YFP+ SMA +/YFP+**	**YFP+ SMA +/ SMA +**
Mean	62.64%	93.31%	23.53%
Stv	16.71%	10.04%	14.14%

CD31 (8 pictures)	CD31+/DAPI+	YFP+ CD31+/YFP+	YFP+ CD31+/CD31+
Mean	84.56%	100.00%	20.74%
Stv	10.87%	†	16.95%
Confident Interval (95%)	7.10%	†	11.07%
VE-Cad (6 pictures)	**VE-Cad+/DAPI+**	**YFP+ VE-Cad +/YFP+**	**YFP+VE-Cad +/VE-Cad +**
Mean	87.67%	100.00%	8.61%
Stv	6.59%	†	3.67%

DAPI with CD31+ and YFP+ →CD31+YFP+

Figure 1

Click here to download high resolution image

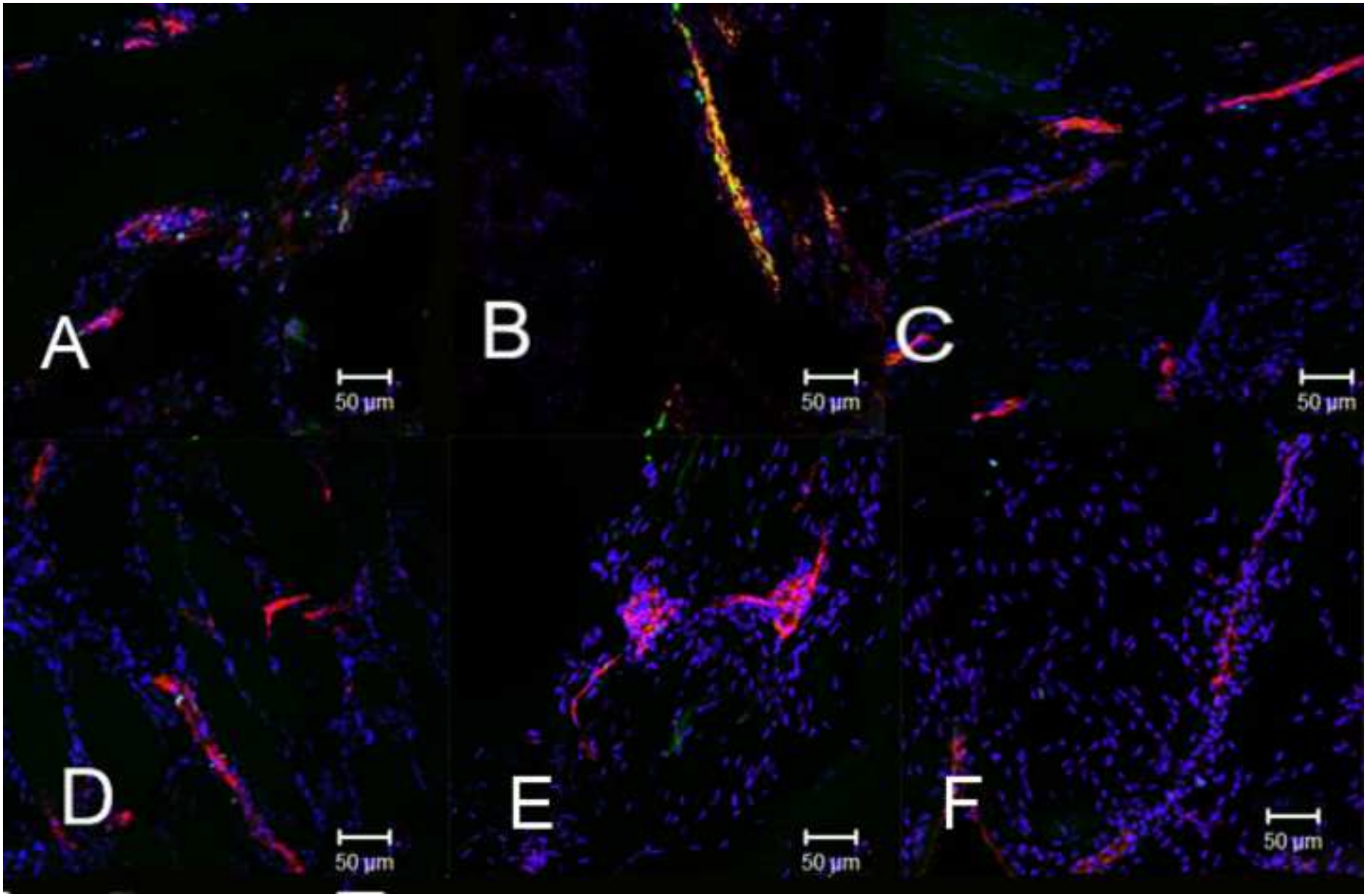

Figure 2

Click here to download high resolution image

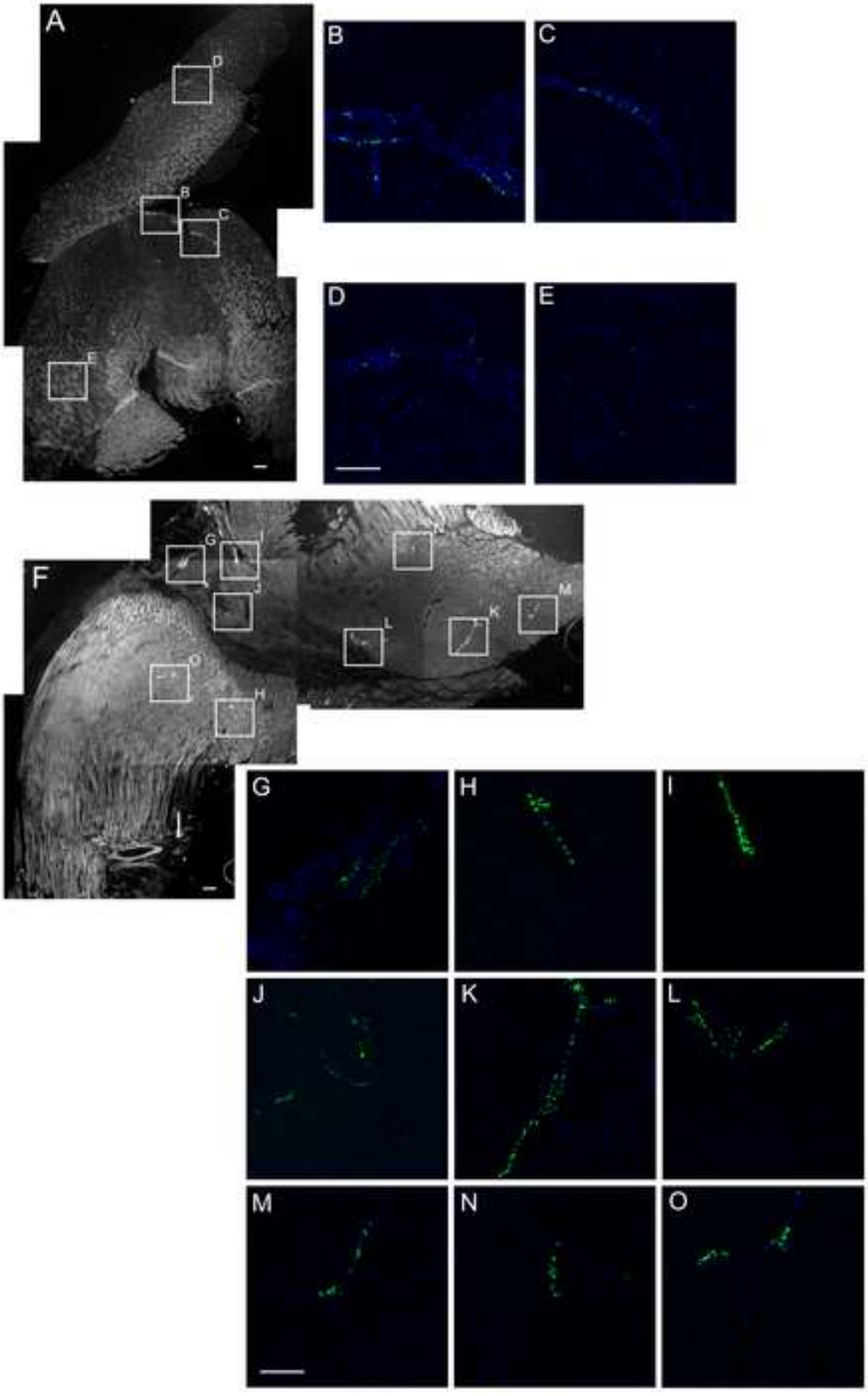

Figure 3

Click here to download high resolution image

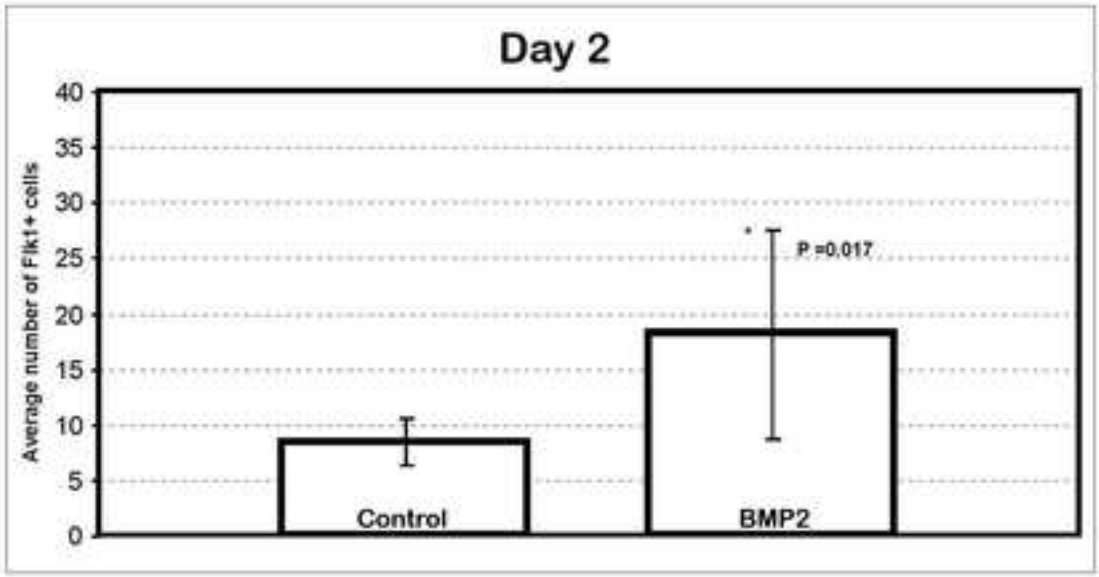

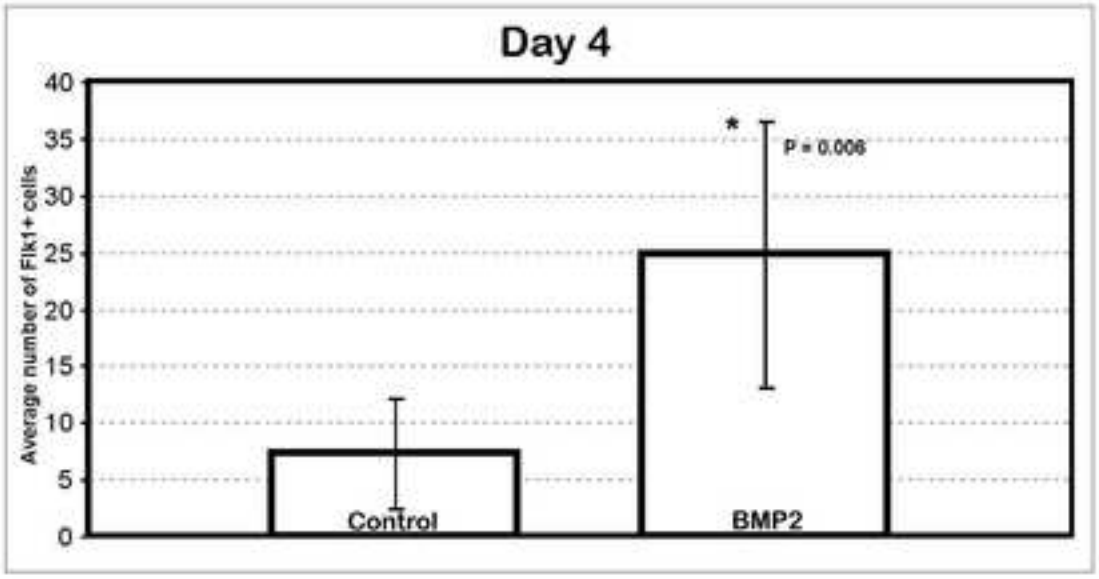

Figure 4

Click here to download high resolution image

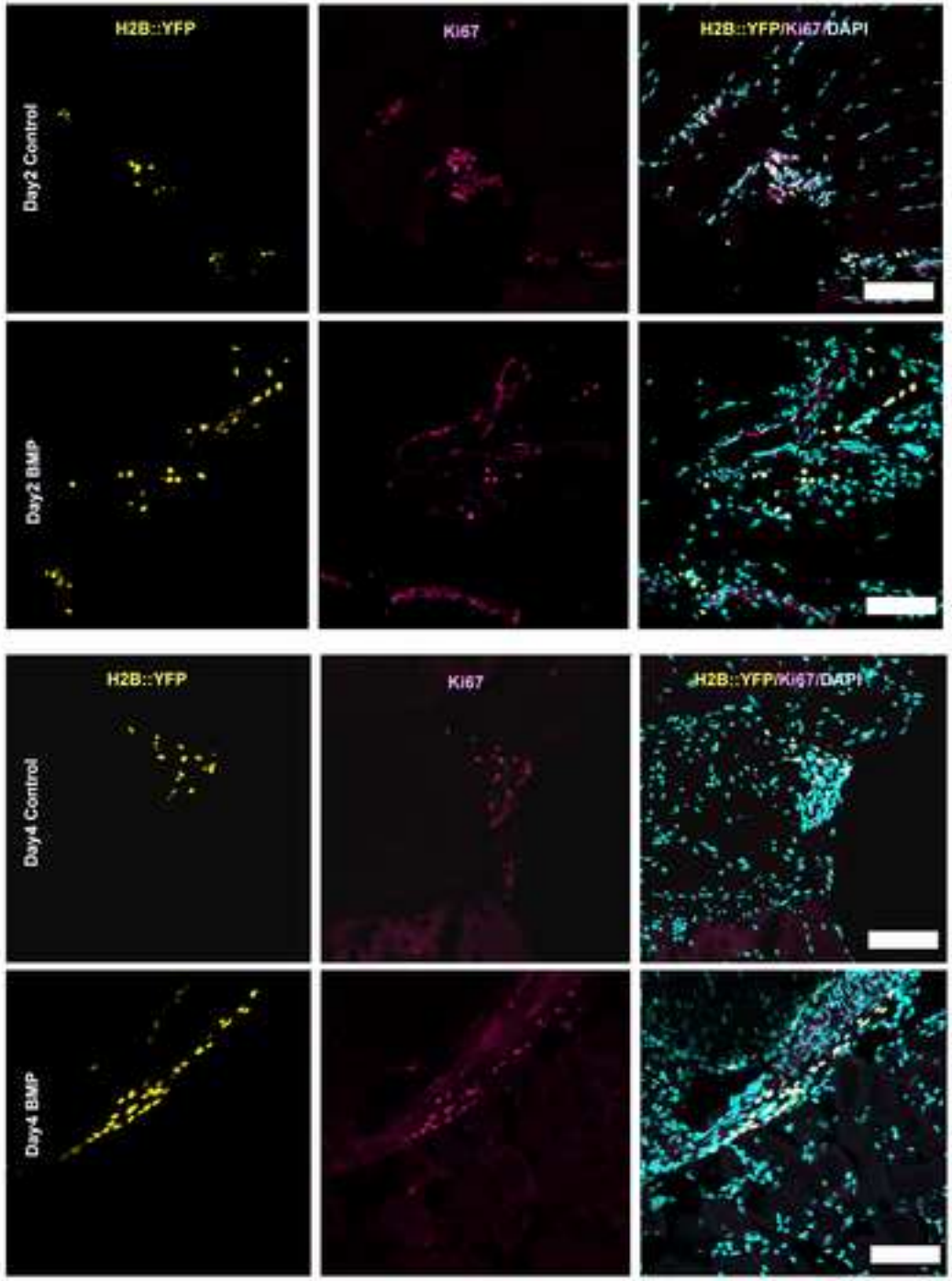

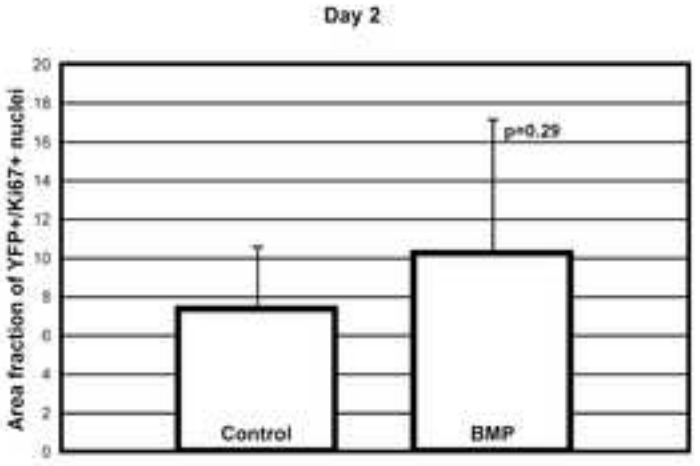

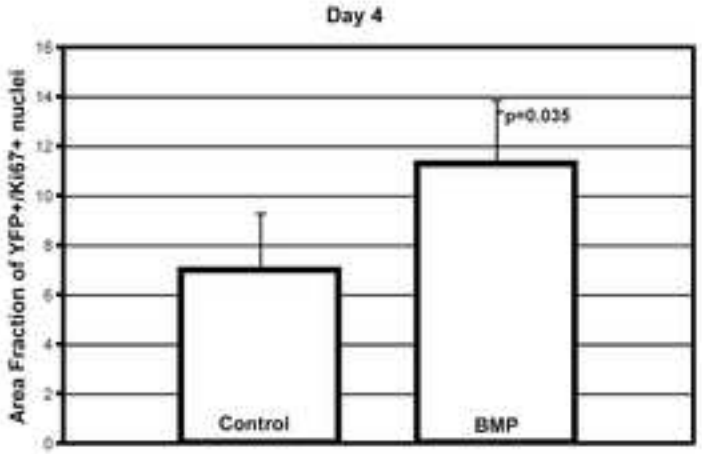

Figure 5

Click here to download high resolution image

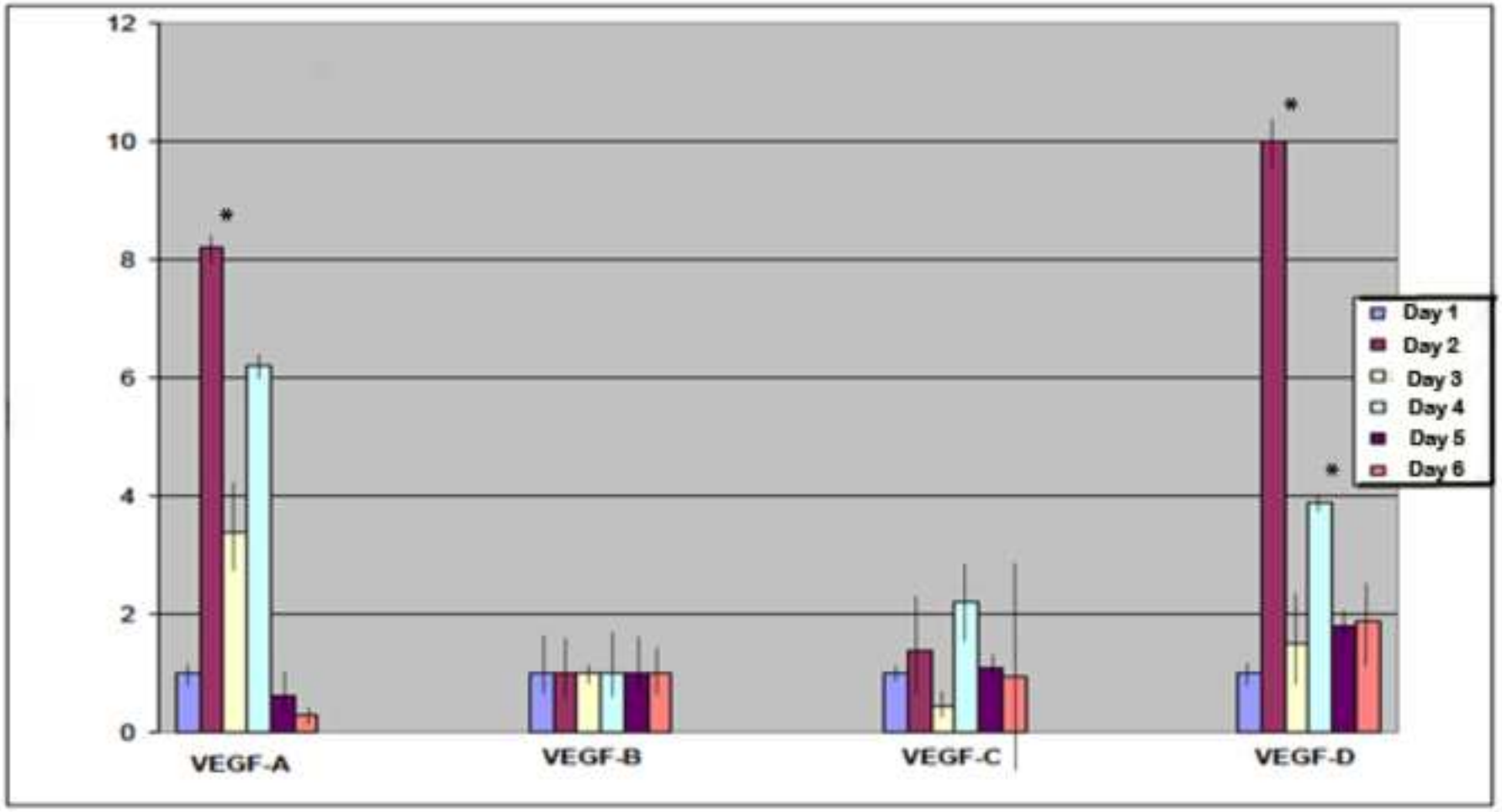

Figure 6

Click here to download high resolution image

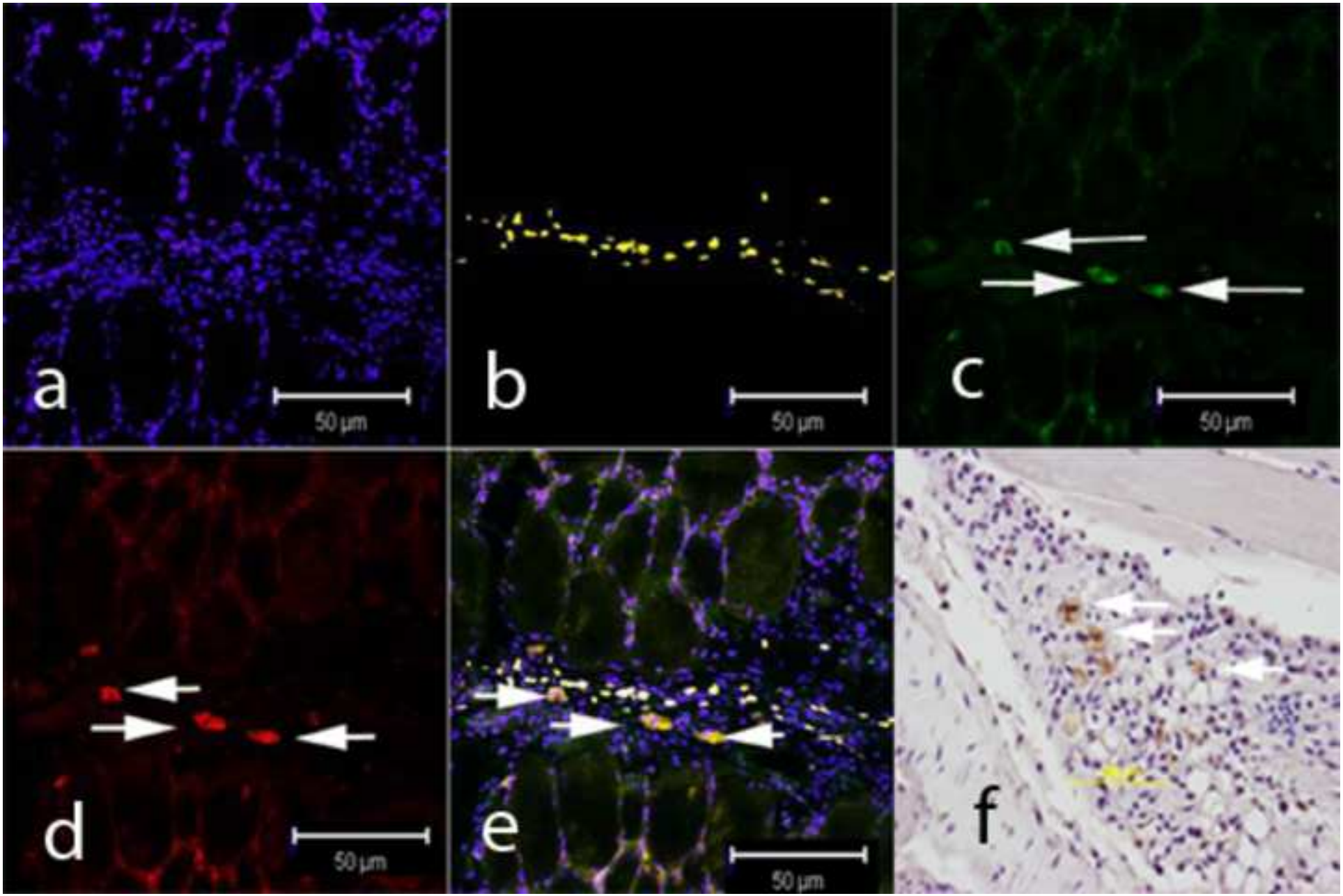

TEA-2010-0234-ver9-Olabisi_1P
Type: research-article

TISSUE ENGINEERING: Part A
Volume 00, Number 00, 2010

DOI: 10.1089/ten.tea.2010.0234

Original Article

Hydrogel Microsphere Encapsulation of a Cell-Based Gene Therapy System Increases Cell Survival of Injected Cells, Transgene Expression, and Bone Volume in a Model of Heterotopic Ossification

Ronke M. Olabisi, Ph.D.,[1] ZaWaunyka W. Lazard, B.S.,[2] Christy L. Franco, B.S.,[1] Mary A. Hall, Ph.D.,[3] Sun Kuk Kwon, Ph.D.,[3] Eva M. Sevick, Ph.D.,[3] John A. Hipp, Ph.D.,[4] Alan R. Davis, Ph.D.,[2] Elizabeth A. Olmsted-Davis, Ph.D.,[2] and Jennifer L. West, Ph.D.[1]

Bone morphogenetic proteins (BMPs) are well known for their osteoinductive activity, yet harnessing this capacity remains a high-priority research focus. We present a novel technology that delivers high BMP-2 levels at targeted locations for rapid endochondral bone formation, enhancing our preexisting cell-based gene therapy system by microencapsulating adenovirus-transduced cells in nondegradable poly(ethylene glycol) diacrylate (PEGDA) hydrogels before intramuscular delivery. This study evaluates the *in vitro* and *in vivo* viability, gene expression, and bone formation from transgenic fibroblasts encapsulated in PEGDA microspheres. Fluorescent viability and cytotoxicity assays demonstrated >95% viability in microencapsulated cells. ELISA and alkaline phosphatase assays established that BMP-2 secretion and specific activity from microencapsulated AdBMP2-transduced fibroblasts were not statistically different from monolayer. Longitudinal transgene expression studies of Ad5dsRED-transduced fibroblasts, followed through live animal optical fluorescent imaging, showed that microencapsulated cells expressed longer than unencapsulated cells. When comparable numbers of microencapsulated AdBMP2-transduced cells were intramuscularly injected into mice, microcomputed tomography evaluation demonstrated that the resultant heterotopic bone formation was approximately twice the volume of unencapsulated cells. The data suggest that microencapsulation protects cells and prolongs and spatially distributes transgene expression. Thus, incorporation of PEGDA hydrogels significantly advances current gene therapy bone repair approaches.

Introduction

Although bone possesses the capacity to repair, major insults often require surgical intervention and bone grafting.[1] In the United States, ~550,000 fractures require bone grafting annually,[2] as do millions of total joint arthroplasties, spinal arthrodeses, maxillofacial surgeries, and implant fixations.[3] In an effort to circumvent the obstacles associated with grafts, researchers have used osteoinductive growth factors, such as bone morphogenetic proteins (BMPs).[4,5] BMP-2 possesses the ability to induce *de novo* bone formation at targeted locations and is FDA approved.

Nevertheless, many clinicians have found recombinant BMP-2 to have inconsistent efficacy, especially in complex clinical scenarios such as traumatic injury,[6,7] These findings have led to a renewed emphasis to develop better methods of delivering BMP-2.[8] BMPs are rapidly cleared when administered in solution,[5] necessitating a carrier, like collagen, that can retain and sequester BMPs.[4,5] BMPs have natural affinity for collagen.[2,5,8] Unfortunately, collagen can elicit an immune response,[5,9] presents handling difficulties, and does not maintain a stable form, and use of a collagen sponge reduces the bioavailability of BMP to such a degree that large amounts are necessary for a therapeutic response.[4,5,9] Given these drawbacks, the search for alternative carrier materials that are biocompatible, biodegradable, osteoinductive, and osteoconductive is of the utmost importance.[5,10]

Poly(ethylene glycol) diacrylate (PEGDA) hydrogels are widely used in tissue engineering applications because they are bioinert and mimic many physical properties of soft

[1]Department of Bioengineering, Rice University, Houston, Texas.
[2]Center for Cell and Gene Therapy, Baylor College of Medicine, Houston, Texas.
[3]Center for Molecular Imaging, The University of Texas Health Science Center, Houston, Texas.
[4]Department of Orthopaedic Surgery, Baylor College of Medicine, Houston, Texas.

tissues.[4,11] Because of the immunoprotection they can provide, hydrogels are also used for cell encapsulation.[4,11] PEGDA hydrogels have demonstrated immunoprotection of porcine islets while permitting the diffusional release of insulin, returning diabetic mice to normoglycemia.[12] Here we present the use of PEGDA hydrogels to microencapsulate cells that produce and secrete high levels of BMP-2. Previous attempts to encapsulate our cell-based gene therapy system into a macroscopic hydrogel resulted in a significant decrease in BMP-2 release and resultant bone formation as compared to unencapsulated cells.[4] Here we hypothesize that microencapsulation will permit greater BMP-2 release than macroscopic hydrogels, and that the hydrogel microspheres will protect these cells from clearance and thereby prolong their transgene expression. We first evaluate the fate of the microencapsulated cells both *in vitro* and *in vivo* through measures of viability and transgene expression. Then, we determine the microencapsulated cells efficacy in forming bone. In this study, we utilize a nonobese diabetic/severely compromised immunodeficient mouse model to evaluate our transgenic cells *in vivo* without the confounding effects of an immune system.

Materials and Methods

Cell culture

Human diploid fetal lung fibroblasts (MRC-5) were obtained from American Type Culture Collection (ATCC, Manassas, VA) and propagated in a humidified incubator at 37°C/5% CO_2 in Dulbecco's modified Eagle's medium (Sigma, St. Louis, MO) supplemented with 10% fetal bovine serum (HyClone, Logan, UT), 1000 U/L penicillin, 100 mg/L streptomycin, and 0.25 μg/mL amphotericin B (Invitrogen Life Technologies, Gaithersburg, MD).[13] Murine bone marrow stromal cells (W20-17; a gift from Genetics Institute, Cambridge, MA) were propagated as previously described.[14]

Adenoviruses and cell transduction

Replication-defective human adenovirus type 35 fiber (Ad5F35) and E1-E3 deleted first-generation human type 5 adenovirus (Ad5) were constructed to contain cDNAs for BMP-2 in the E1 region of the virus.[15] For the viruses Ad5BMP2, Ad5dsRED, and Ad5empty cassette, the viral particle (VP)-to-plaque-forming unit ratio was 1:83, 1:2, and 1:111, respectively, and all viruses were confirmed to be negative for replication-competent adenovirus. MRC-5 cells were transduced as previously described with Ad5BMP2, Ad5dsRED, or Ad5empty cassette at a viral concentration of 2500 VP/cell.[15,16] Briefly, virus was added to fresh supplemented Dulbecco's modified Eagle's medium and incubated with cells at 37°C overnight.

Synthesis of PEGDA

PEGDA was prepared by combining 0.4 mmol/mL acryloyl chloride, 0.2 mmol/mL triethylamine, and 0.1 mmol/mL dry PEG (6000 Da; Fluka, Milwaukee, WI) in anhydrous dichloromethane under argon overnight. The resulting PEGDA was then precipitated with ether, filtered, lyophilized, and stored under argon at −20°C. PEGDA was analyzed by proton NMR (Avance 400 MHz; Bruker, Billerica, MA; solvent, *N*,*N*-dimethylformamide-d7) and only materials with a degree of acrylation >85% were used.

Microencapsulation

Hydrogel precursor solutions were formed by combining 0.1 g/mL 10 kDa PEGDA (10% w/v) with 1.5% (v/v) triethanolamine/HEPES-buffered saline (pH 7.4), 37 mM 1-vinyl-2-pyrrolidinone, 0.1 mM eosin Y, and transduced MRC-5 cells for a final concentration of 6×10^4 cells/μL. A hydrophobic photoinitiator solution (2,2-dimethoxy-2-phenyl acetophenone in 1-vinyl-2-pyrrolidinone; 300 mg/mL) was combined in mineral oil (3 μL/mL, embryo tested, sterile filtered; Sigma-Aldrich, St. Louis, MO). The microspheres were formed after adding the hydrogel precursor solution into the mineral oil, emulsifying by vortex for 2 s while exposing to white light for an additional 20 s. Microspheres were isolated by two medium washes followed by 5 min centrifugation at 1350 rpm. Cells and microspheres were quantified by measuring the amount of soluble formazan produced by cellular reduction of the tetrazolium compound [3-(4,5-dimethylthiazol-2-yl)-5-(3-carboxymethoxyphenyl)-2-(4-sulfophenyl)-2H-tetrazolium, inner salt; MTS]. Briefly, cells were counted with a Coulter Counter and a serial dilution was used as a standard curve. Microsphere and cell samples were placed in the Transwells (0.4 μm pore polycarbonate membrane Transwell inserts; Corning, Inc., Lowell, MA) in a 24-well plate with 1 mL of culture medium, and 200 μL of CellTiter 96® AQueous One Solution Reagent was added into each well. The plate was incubated for 1 h at 37°C in a humidified, 5% CO_2 atmosphere, and then the transwells were removed and the absorbance of the medium was recorded at 490 nm. To ensure proper comparisons between the microspheres and the monolayer cells, we measured the loss of cells following the encapsulation procedure and loss in the injection needle, and then accounted for and equalized cell numbers between groups before injection.

Preparation of cells for intramuscular injection

Cells transduced with Ad5BMP2, Ad5dsRED, or Ad5empty cassette were removed with trypsin, and separated into two groups: direct injection and microencapsulation. Cells directly injected were suspended at a concentration of 5×10^6 cells per 100 μL of phosphate-buffered saline and aspirated into a syringe with a 22-gauge needle. Microencapsulated cells were encapsulated at a concentration of 5×10^6 cells per 300 μL of microspheres, which were in turn suspended in 1 mL of phosphate-buffered saline and aspirated into a syringe with an 18-gauge needle.

Viability assays

MRC-5 cells were transduced with Ad5F35BMP2, harvested, and encapsulated in microspheres as described. Microspheres were maintained in culture for 1 week post-microencapsulation, and then incubated with media and 2 μM calcein acetoxymethyl ester and 4 μM ethidium homodimer (LIVE/DEAD® Viability/Cytotoxicity Kit for mammalian cells; Invitrogen, Molecular Probes, Eugene, OR) for 20 min at 37°C in a humidified, 5% CO_2 incubator. Microspheres were imaged under a confocal microscope (ex/em ~495 nm/~515 nm). Fluorescent and differential interference

contrast projections of Z-stacks were created. The red channel was thresholded to eliminate diffuse virus staining but retain nuclear stains. Total cells were counted from differential interference contrast images, live cells from green fluorescent images, and dead cells from red fluorescent images to obtain a measure of viability.

BMP-2 quantification

BMP-2 expression was evaluated for MRC-5 cells transduced with Ad5F35BMP2 or Ad5F35HM4 using ELISA and alkaline phosphatase (AP) assays. ELISAs were performed with a BMP-2 Quantikine ELISA kit from R&D Systems (Minneapolis, MN) using culture supernatant collected 72 h after adenovirus transduction. Transduced cells were microencapsulated or plated directly in 0.4 μm pore polycarbonate membrane Transwell inserts (Corning, Inc.) and W20-17 cells were cultured in the wells. After 72 h, W20-17 cells were assayed for AP activity.[15] Cellular AP was extracted by conducting three freeze–thaw cycles on the W20-17 cells in a 100 $\mu M/cm^2$ concentration of 25 mM Tris-HCl (pH 8.0) and 0.5% Triton X-100. A chemiluminescent disodium 3-(4-methoxyspiroy distributes-4-yl) phenyl phosphate (CSPD) substrate with Sapphire-II enhancer (Tropix; Applied Biosystems, Foster City, CA) was added to the samples for enhanced AP sensitivity. The light output after a 2 s delay was integrated from each sample for 10 s with a luminometer (TD-20/20; Turner BioSystems, Sunnyvale, CA). AP levels were recorded in relative luminescence units. These AP levels were then normalized to protein content with the bicinchoninic acid assay. Data are presented as percent AP induction relative to that of basal control cells not exposed to BMP-2.

Animal studies

All animal studies were performed in accordance with an Institutional Animal Care and Use Committee (IACUC)–approved protocol. Microencapsulated or unencapsulated transduced cells were delivered by intramuscular injection into the hind limb quadriceps muscle of nonobese diabetic/severely compromised immunodeficient female mice (8–12 weeks old; Charles River Laboratories, Wilmington, MA) ($n = 12$).

Live animal optical fluorescence imaging

The hind limbs ($n = 12$) of six mice were imaged longitudinally for 34 days following injection of fibroblasts (±microencapsulation) transduced with Ad5dsRED (2500 VP/cell). Fluorescent imaging was performed at excitation and emission wavelengths of 568 nm and 610 ± 30 nm, respectively. The excitation light was supplied by a 200 mW Argon/Krypton laser (Model No. 643R-AP-A01; Melles Griot Laser Group, Carlsbad, CA), and the emission light was collected after it passed through holographic (SuperNotch-Plus™ 568 nm; Kaiser Optical Systems Inc., Ann Arbor, MI) and bandpass (HQ610/60m; Chroma Technology Corporation, Bellows Falls, VT) filters and was focused onto an electron-multiplying charge-coupled device (EMCCD) camera (Photon Max 512; Princeton Instruments, Trenton, NJ) using a Nikon camera lens (Nikkor 28 mm; Nikon, Inc., Melville, NY). Exposure times were ~200 ms. Image analysis was performed using ImageJ. Fluorescence intensity (FI) was measured and recorded for a region of interest (ROI) for each site of the animal injected with cells. The ROI dimensions were constant for every site imaged and each ROI was chosen to include the optimal fluorescent signal for the given site. A target to background ratio (TBR) of FI was calculated for each site by subtracting a background (B) ROI from the target (T) ROI, and then dividing the result by the background (B) ROI; TBR = (T − B)/B. The TBR value was plotted versus time (i.e., day postinjection of cells). Results represent the mean TBR of FI for unencapsulated and/or encapsulated Ad5dsRed or AdEmpty cassette transduced cells ($n = 4$ per group).

Heterotopic bone assay

Microencapsulated or unencapsulated AdBMP2-transduced cells were injected into the hind limb quadriceps muscles ($n = 12$) of six mice. Animals were euthanized 2 weeks after injection of the transduced cells.

Histological analysis

Mouse hind limbs were harvested, fixed in formalin, and decalcified. Hind limbs were then divided longitudinally and sectioned from the inner surface outward. Serial sections (5 μm) encompassing the entire hind limb reactive site were prepared. Every fifth slide was stained with hematoxylin and eosin. All sections were analyzed by light microscopy.

4C ▶

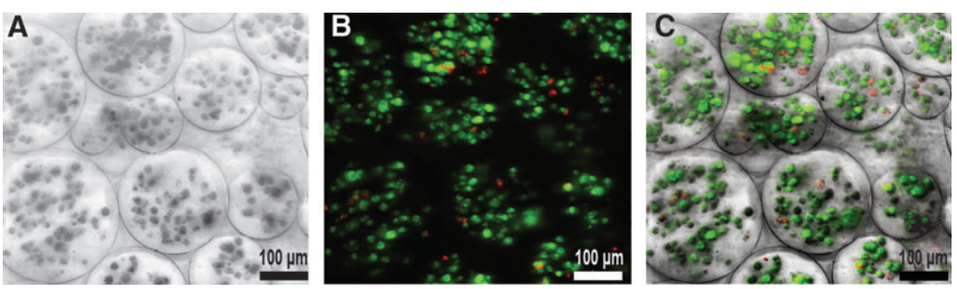

FIG. 1. Viability of AdBMP2-transduced cells (2500 VP/cell) within microspheres was assessed at day 7 using a LIVE/DEAD® Viability/Cytotoxicity Kit for mammalian cells (Invitrogen, Molecular Probes, Eugene, OR). (**A**) Minimum intensity projection of a differential interference contrast Z-stack. (**B**) Maximum intensity projection of fluorescent Z-stack merge of red and green channels. The red channel was thresholded to eliminate diffuse virus staining. Dead cells appear red and live cells appear green. (**C**) Overlay of panels (**A**) and (**B**). Living cells accounted for 95.08% ± 0.47% of total cells encapsulated. BMP, bone morphogenetic protein; VP, viral particle.

Microcomputed tomography

Microcomputed tomography (micro-CT) examinations were obtained of both legs at 15 μm resolution (eXplore Locus SP; GE Healthcare, London, ON, Canada). A hydroxyapatite phantom was scanned alongside each specimen and was used to convert the scan data from arbitrary units to units of equivalent bone density. A 3D ROI was defined for each specimen to isolate the new mineralized tissue from the normal skeletal structures (femur, tibia, and patella). The scans were thresholded to exclude any tissue with a density <100 mg/cc, and the tissue volume within the ROI was calculated as a measure of the total amount of mineralized tissue. The tissue mineral content was measured as an estimate of the total mineral in the region and the tissue density was calculated to quantify the density of the mineralized tissue. The resulting data were analyzed by one-way analysis of variance.

Statistical analysis

For BMP-2 ELISAs and AP assays, all data were taken in triplicate and reported as mean and standard deviation. Values for optical fluorescence and bone mineralization data were obtained as described and also reported as mean and standard deviation. A Student's *t*-test was performed for all measurements between controls and each experimental condition. *Post hoc* power analyses were conducted for data from *in vivo* assays to estimate the power to detect changes in gene expression and bone properties.

Results

Validation of the microspheres containing AdBMP2-transduced cells

Within the microspheres, live cells converted the nonfluorescent calcein AM into green fluorescent calcein, while ethi-

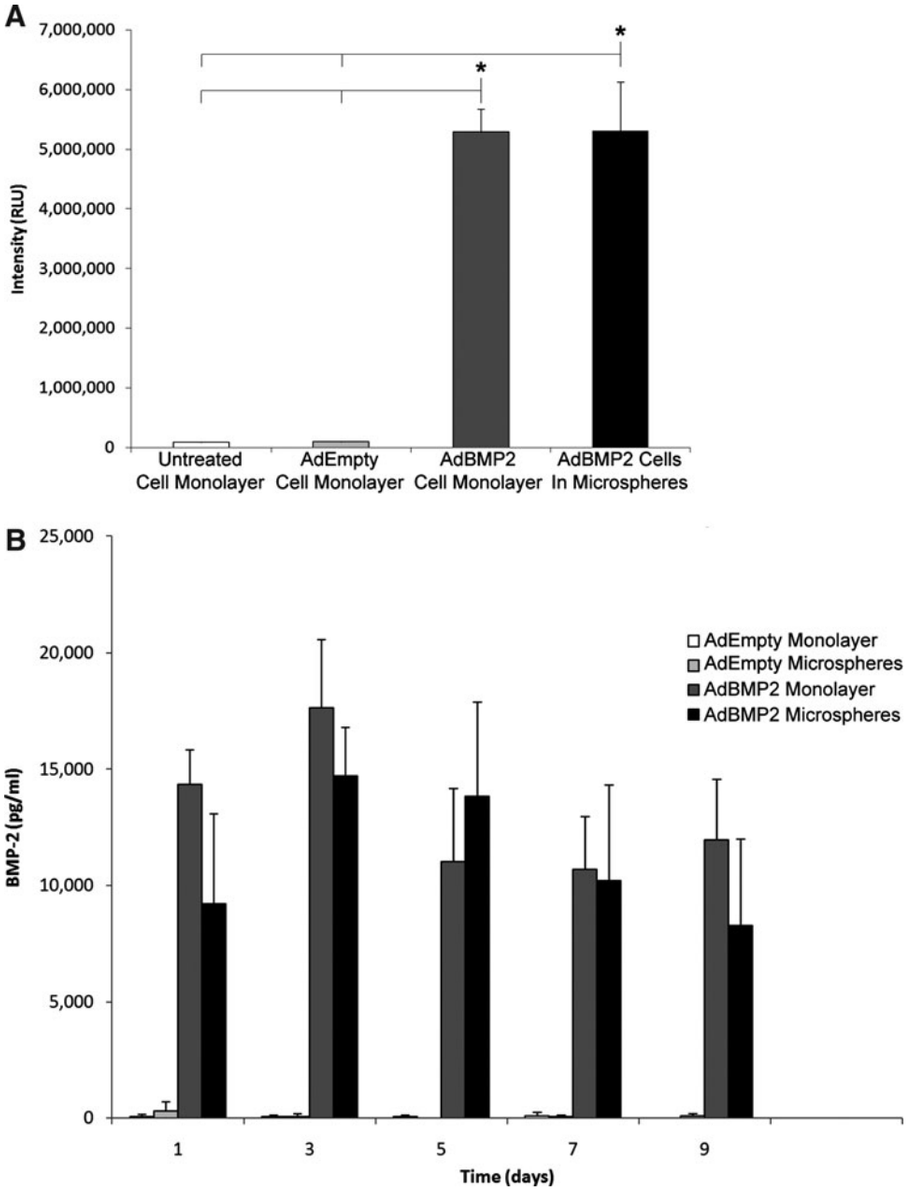

FIG. 2. Comparison of BMP-2 expression, secretion, and activity after PEGDA encapsulation. (**A**) BMP-2 protein in culture supernatant taken from AdBMP2- or AdEmpty cassette-transduced cells (25000 VP/cell) (monolayer), or those encapsulated in PEGDA microspheres were quantified by sampling every other day for 9 days and evaluated using an ELISA. (**B**) AP activity in W20-17 cells after addition of conditioned media from AdBMP2- or AdEmpty cassette-transduced cells (25000 VP/cell) (monolayer), or AdBMP2-transduced cells encapsulated in PEGDA microspheres. As a negative control, we also included culture supernatant from untransduced cells. AP activity is depicted as the average RLU, where $n=3$. Error bars represent means $\pm$ SD for $n=3$. A Student's *t*-test was applied to demonstrate significance. AdBMP2-transduced monolayer and microsphere groups had significantly greater AP activity and BMP-2 concentration levels ($p<0.05$) when compared against other groups, but no differences when compared to each other. In other words, microencapsulation had no effect on BMP-2 release and function. AP, alkaline phosphatase; PEGDA, poly(ethylene glycol) diacrylate; RLU, relative chemiluminescence units.

AU3 ▶

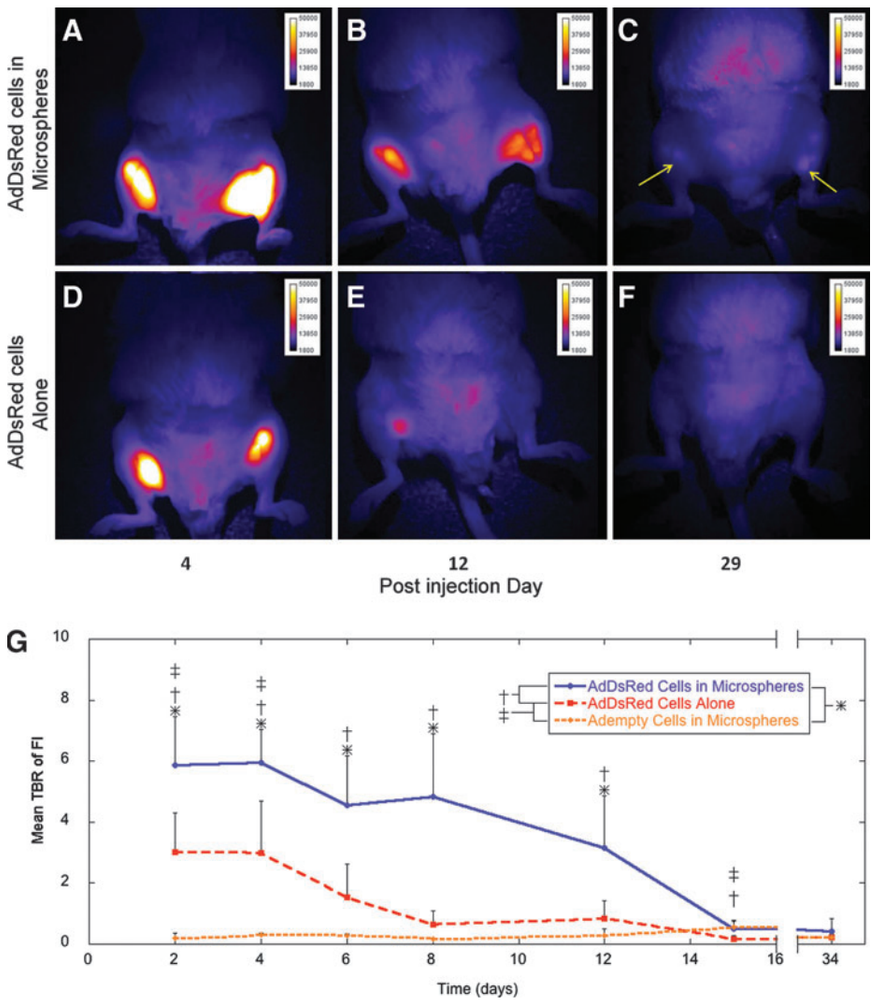

FIG. 3. Optical fluorescence imaging of mice injected with cells expressing dsRed. (**A–C**) Images of a representative mouse ($n = 4$) injected with dsRed-expressing cells encapsulated in microspheres. (**D–F**) Images of a mouse injected with dsRed-expressing cells directly, without microspheres. The images were taken at day 4, 12, and 29 postinjection of cells. By day 29, the fluorescent signal is at background levels or undetectable for the mouse given dsRed-expressing cells without microspheres (**F**). Whereas, the signal remains detectable in the mouse given dsRed-expressing cells encapsulated in microspheres (**C**). (**G**) Mean TBR of FI in mice given unencapsulated dsRed cells, microencapsulated dsRed cells, or microencapsulated control cells. $^{*}p \leq 0.05$ for microencapsulated dsRed cells versus microencapsulated control cells; $^{\dagger}p \leq 0.05$ for microencapsulated dsRed cells versus unencapsulated dsRed cells; $^{\ddagger}p \leq 0.05$ for unencapsulated dsRed cells versus microencapsulated control cells. FI, fluorescence intensity; TBR, target-to-background ratio.

dium homodimer freely passed through the permeable membranes of dead cells to bind the DNA and fluoresce red (Fig. 1). Encapsulated cells showed high viability 95% ± 0.5%, suggesting that they were not adversely affected by the microencapsulation process. The AP activity of W20-17 cells exposed for 72 h to the culture supernatants from AdBMP2-transduced cells directly plated or encapsulated in microspheres was significantly elevated over control cells, but there was no difference between these groups, indicating that the BMP-2 released is functionally active (Fig. 2A). A 9 day time course of BMP-2 levels in culture supernatant was quantified by ELISA to be ~17,500 and 15,000 pg/mL for directly plated and microencapsulated cells, respectively (Fig. 2B). No BMP-2 was detected in either culture supernatant from AdEmpty cassette-transduced cells, or control cells.

In vivo *comparison of transgene expression with and without encapsulation in PEGDA hydrogel*

Two days after the initial injection of cells, dsRED expression was readily detected whether cells were encapsulated or not, and in no cases were cells or microspheres detected migrating from the injection site (Fig. 3A). The dsRED expression, as measured by FI at 590 ± 10 nm, was significantly elevated in microencapsulated Ad5dsRED-transduced cells compared to other groups (Fig. 3B). Microencapsulated control cells transduced with AdEmpty cassette had no fluorescent signal at 590 ± 10 nm, demonstrating that neither the cells nor the PEGDA were autofluorescing. FI in animals receiving Ad5dsRED-transduced cells directly injected was substantially reduced after 7 days and was indistinguishable from control. In microencapsulated Ad5dsRED-transduced cells, this 590 ± 10 nm dsRED fluorescent signal was significantly elevated over that of microencapsulated control cells for 15 days (Fig. 3B). After 15 days, these levels dropped; however, signal was still detectable (Fig. 3A, arrows) in some animals, suggesting that the microencapsulated cells remained viable to express the dsRED transgene. Statistical power to detect intensity over control ranged from 100% in microencapsulated cells to 99.7% in directly injected cells, and power to detect the difference between microencapsulated and unencapsulated cells was 88%.

In vivo *bone formation with and without microencapsulation in PEGDA hydrogels*

Micro-CT analysis of bone formation showed a significantly greater volume of heterotopic ossification in tissues

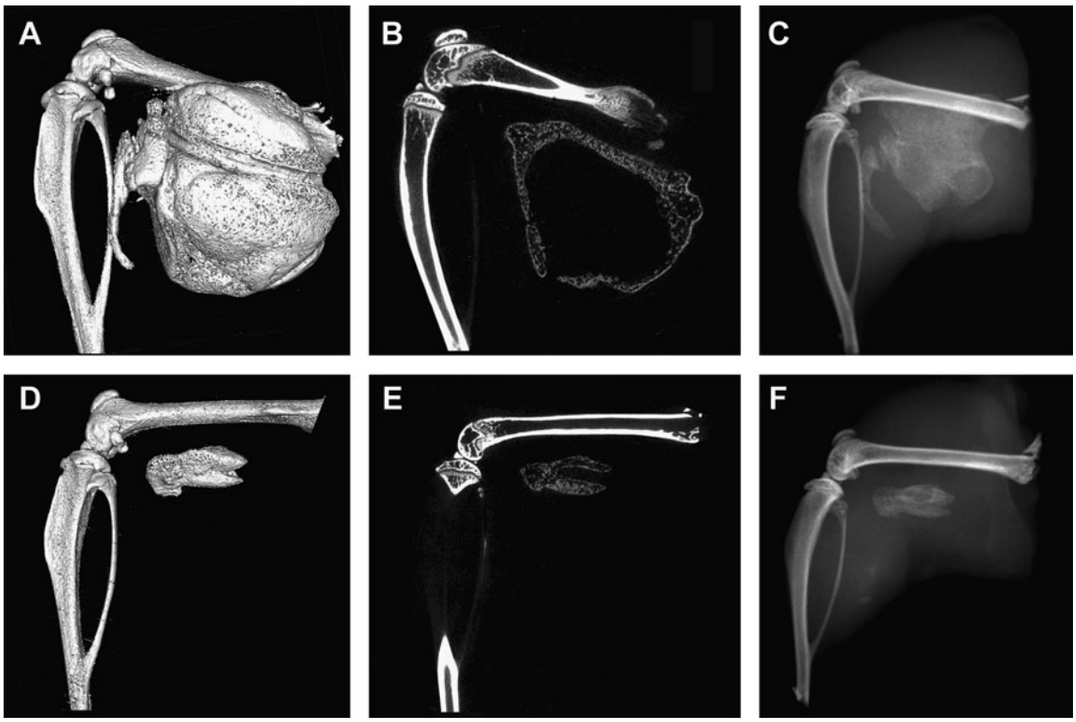

FIG. 4. Microcomputational analysis of the resultant heterotopic bone formation. (**A, D**) Three-dimensional surface renderings of the resultant heterotopic bone. (**B, E**) Cross-sectional slices through the new bone. (**C, F**) Corresponding radiograms. (**A–F**) The resultant mineralization of the muscle tissues after injection of AdBMP2-transduced cells (2500 VP/cell) encapsulated into PEGDA microspheres (**A–C**) or direct injection of unencapsulated AdBMP2-transduced cells (**D–F**). Both have a denser rim of bone, with a hollow interior structure, suggesting that the biomaterial did not alter bone patterning.

F4 ▶ receiving microspheres (Fig. 4A, C) than those receiving directly injected cells (Fig. 4B, D). Statistical power to detect differences between volume formed in these groups was 72.5%. Cross-sectional micro-CT analysis of the newly formed bone revealed a similar architecture between the groups. Heterotopic bone formed by both the microencapsulated cells and directly injected cells had a pattern of dense bone surrounding a hollow interior (Fig. 4C, D); however, the circumference of bone within the directly injected cells was significantly smaller. Microencapsulated AdBMP2-transduced cells produced approximately twice the

F5 ▶ bone volume of unencapsulated cells (Fig. 5B). Despite the volumetric increase, the bone tissue mineral content was statistically similar between these groups, although trending toward an elevation in samples that received the microspheres (Fig. 5A). This corresponds with the change in tissue mineral density of the new bone surrounding the microspheres (Fig. 5C). The newly formed bone appears to be slightly less dense, leading to the overall similarity in mass between the two groups. Statistical power to detect differences between bone density in these groups was 76.7%.

From histological analysis, both groups had significant

F6 ▶ new bone formation within the muscle (Fig. 6). In tissues that had received the direct injection of AdBMP2-transduced cells, there was a small compact piece of bone forming a ring-like structure encircling what appears to be blood and tentative stroma, and just exterior to this structure was significant adipose (Fig. 6A). A similar structure was observed in tissues that had received microspheres (Fig. 6B). Since the microspheres did not degrade, they appear histologically as gaps or holes within the matrix (Fig. 6B). Thus, despite the presence of nondegradable microspheres, both structures were patterned to have a denser bone structure with a bone marrow-like cavity on the interior.

Discussion

Here we present a novel system for the sustained production and release of BMP-2 in a targeted manner. This approach expands on our previously reported cell-based gene therapy system, which successfully employs adenovirus transduction of fibroblasts to express high levels of BMP-2 at a targeted location.[4,13,17] High levels of BMP-2 can lead to rapid heterotopic ossification.[6,13] We previously demonstrated rapid clearance of AdBMP2-transduced cells,[13,17] thus limiting both the levels and duration of BMP-2 that can be achieved locally. Thus, we encapsulated the transduced cells within PEGDA hydrogel microspheres. Careful manipulation of their tunable physical characteristics enable PEGDA hydrogels to better approximate a tissue of interest, to regulate nutrient/waste diffusion, or to prevent interaction with immune cells.[4,11] Current carriers in clinical use, such as collagen sponges, do not retain BMP-2 efficiently, require large amounts of recombinant BMP-2 for a therapeutic effect, and are often plagued with variability,

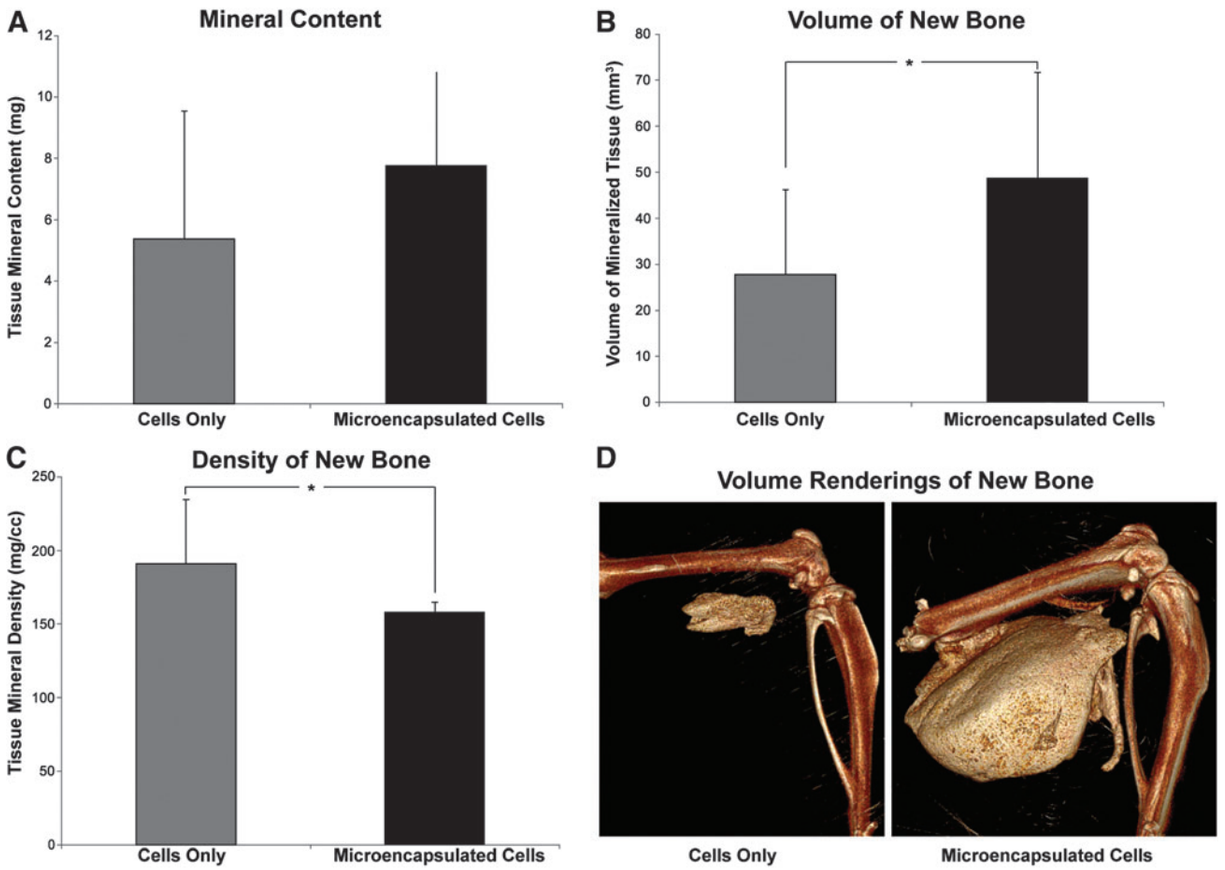

4C ▶

FIG. 5. Quantification of the heterotopic ossification using microcomputational analysis. Cells were transduced with AdBMP2 and either directly injected or encapsulated into microspheres prior to injection, and the resultant heterotopic bone was analyzed 2 weeks later. Tissue parameters: (**A**) bone tissue mineral content, (**B**) bone volume of mineralized tissue, and (**C**) bone tissue mineral density were calculated for the newly formed bone ($n = 6$ per group). The means and standard deviations for each group were calculated and compared using a one-way analysis of variance. Results indicate that mineral content is statistically equivalent ($p = 0.2$) between the groups, whereas the AdBMP2-transduced cells in microspheres had a significantly greater volume ($p = 0.038$) than the AdBMP2-transduced cells directly injected. Alternatively, the bone tissue mineral density was significantly denser for the group receiving the cells directly as compared to those in microspheres ($p = 0.029$). (**D**) A 3D volume rendering of new bone formed in cell only and microencapsulated cell groups, respectively. ◀ AU3

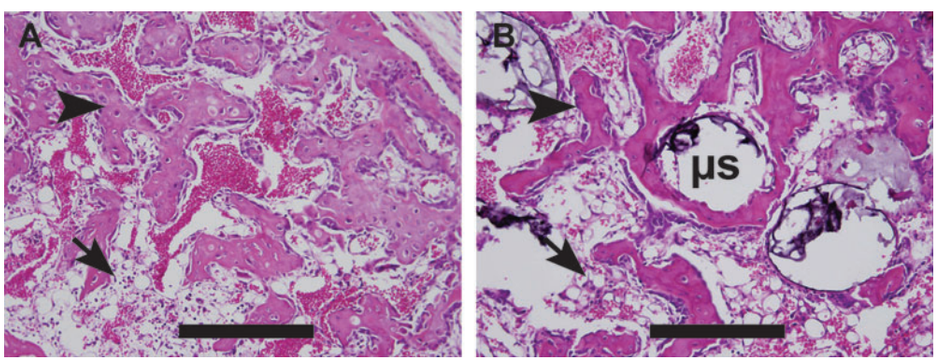

4C ▶

FIG. 6. Photomicrographs of heterotopic ossification. Hematoxylin and eosin stains of new bone formation by (**A**) directly injected and (**B**) microsphere (μs) encapsulated cells. Both groups show small compact pieces of bone (arrowheads) forming ring-like structures, encircling what appears to be blood and tentative stroma in the inner region, with significant adipose (arrows) just exterior to the new bone. Scale bars are 500 μm.

such as differences in handling, material properties, and, in some cases, triggering immunogenic responses.[4,5,9] Further, because collagen can bind BMP-2, our previous studies suggest that it reduced the efficacy of BMP-2 in general.[18] Additionally, the inflammation associated with the collagen sponge can also reduce the ability to produce targeted bone formation.

Our approach avoids these issues because we use a biocompatible synthetic carrier, which minimizes immune response and does not bind BMP-2. In addition, our approach is independent of cell line, permitting the transduction of any type of cell,[19] and with efficient transduction can deliver functional BMP-2 continually to the target site over several days. Further, we are able to get high transduction efficiencies, requiring a modest quantity of cells and microspheres for a therapeutic effect. We previously implanted AdBMP2-transduced cells that were macroencapsulated in larger hydrogels to demonstrate that encapsulated cells could continue to produce bone.[4] In the current study, we demonstrate that microencapsulated cells express and release high levels of BMP-2 and produce more bone volume than unencapsulated cells. Microencapsulation permits delivery via injection, avoiding surgery.

Viability and cytotoxicity assays confirmed cell survival of the microencapsulation process, while assays to determine BMP-2 activity and release from the microspheres confirmed that the hydrogels did not impede the protein's release. The release of proteins from hydrogels is related both to diffusion distances and the hydrogel mesh size.[20] The hydrogels in the current study were formed with 10% 10 kDa PEGDA, which has been estimated to have a mesh size of 280 Å.[21] Proteins having radii smaller than the hydrogel mesh size enjoy relatively free diffusion through the polymer.[22] Mature BMP-2 is a small protein ($\sim$16 kDa), and it has been suggested that it dimerizes immediately after synthesis. The biologically active form of BMP-2 is a homodimer whose dimensions are $70\times35\times30$ Å.[23] Thus, according to the literature, our hydrogel microspheres should have released the BMP-2, which our data confirmed. ELISAs performed demonstrate equivalent BMP-2 levels from AdBMP2-transduced cells in microspheres and monolayers. The murine bone marrow stromal cell line, W20-17 cells, have been shown to respond to functional BMP-2 by undergoing osteogenesis with a rapid increase in AP.[14] AP assays using these cells showed no difference between microencapsulated and unencapsulated AdBMP2-transduced cells, demonstrating that the protein that diffused through the PEGDA hydrogel possessed similar activity as BMP-2 in culture supernatant from cells directly plated.

The millimeter-scale hydrogels employed in our previous study were a proof of concept and well exceeded the diffusion limit of oxygen.[24] The radii of the microspheres in this study were roughly in the 50–150 μm range, providing excellent cell survival. Given the same volume of PEGDA carrier, when cells were (1) encapsulated in a single hydrogel,[4] (2) equally divided into four hydrogels,[4] or (3) microencapsulated, the greatest amount of detectable BMP-2 in the culture supernatant came from the microspheres, which released identical levels as the monolayer. Our current data confirm our hypothesis that optimal BMP-2 secretion is achieved when cells are encapsulated into the smaller microsphere structures. Further, the data show that the PEGDA hydrogel material is not affecting the production, secretion, or diffusion of BMP-2 within the microspheres.

Transduction with dsRED enabled the evaluation of *in vivo* gene expression. Because solution spread is a function of injection volume,[25,26] dsRED expression in the tissues receiving the microspheres encompasses a larger volume than the unencapsulated counterpart. Although the increased volume can be explained by the difference in injection volume, the magnitude of expression should not be affected by injection volume. Nevertheless, our results demonstrate an increase in FI of microencapsulated cells for 15 days over unencapsulated cells. Since this result cannot be explained by volume difference, it suggests that the elevated intensity is a result of the microencapsulation, likely protecting these cells from clearance. This result was similar to our previous findings where the delivered cells are rapidly cleared.[13] Collectively, the data suggest that microencapsulation prolongs transgene expression within the tissues, confirming our hypothesis.

Further, *in vivo* results confirm that microencapsulation does not interfere with expression of the BMP-2 transgene. Since bone formation occurred immediately surrounding the microspheres, the volume of new bone formation corresponded to the volume of material delivered. Despite the increased volume, the mass of new bone formed was equivalent between groups. The initial bone formation response may be directly related to cell number initially injected, which was equivalent in microencapsulated and unencapsulated groups. Previous work has demonstrated that bone is formed in as little as 1 week postinjection.[13] It is possible that our 2 week time point was too early to observe a maximal result. The bone formation immediately adjacent to the microspheres could potentially be exploited since the microspheres can be drained and applied as a paste. Thus, exact spatial placement of the transduced cells and resultant bone formation via microspheres delivery could produce bone in a desired location of a specified shape and size. This is a critical parameter for application of the therapy to traumatic bone injury.

Surprisingly, marrow-like structures formed in both cases with similar patterning to the normal skeleton. This indicates that despite the hydrogel's capacity to dictate the shape of the newly forming bone, it does not interfere with the structural patterning that is part of the biology of bone formation.

The microspheres demonstrated their capacity to form equivalent amounts of bone to unencapsulated cells. The current study was conducted in an immune-deficient animal model to demonstrate the best bone formation results. With nonautologous cells in immune-competent animals, bone formation does not proceed. Before examining the bone-forming capacity of these cells in an immune competent animal, it was necessary to demonstrate that microsphere encapsulation did not decrease the amount of bone formed. The decreased density of the bone formed by the microspheres does not indicate poorer quality bone, but simply reflects the larger volume of bone formed: recall, density is mass/volume. When this relation is applied to our bone formation results, the calculated density corresponds well to the measured density. Moreover, the decrease in bone density is only by 17%. As aforementioned, it is possible that later time points will reveal that the microspheres' bone

density eventually reaches that of the directly injected cells. Or alternately, this 17% difference may not matter—current clinical measures of bone mineral density mark normal as ±1 standard deviation from peak bone mineral density—a measure that corresponds to bone mineral density differences of 30%.[27]

Summary and Conclusions

In this study the effect of microencapsulating AdBMP2-transduced fibroblasts before injection was evaluated. The microsphere structures were evaluated *in vitro* for viability and BMP-2 activity and secretion, and then examined *in vivo* for transgene expression and viability. Although our measures established prolonged *in vivo* expression, they did not capture a prolonged *in vivo* response, and further studies at later time points would be necessary to confirm that prolonged BMP-2 expression would lead to an increased bone formation response. Nevertheless, the hydrogel microspheres produced equivalent amounts of bone in an equivalent amount of time. This is significant because PEGDA hydrogels have demonstrated immunoprotection of xenogeneic donor cells, preserving their function.[12] This is the first step toward bone formation using nonautologous cells in an immune-competent model. Our system is the first of its kind to induce bone formation and may impact gene therapy approaches to come.

Acknowledgments

Grant support: Defense Advanced Research Projects Agency W911NF-09-1-0040 and Department of Defense W81XWH-07-0281 and W81XWH-07-1-025. The authors thank Rita Nistal for performing the histology.

Disclosure Statement

No competing financial interests exist.

References

1. Murugan, R., and Ramakrishna, S. Development of nanocomposites for bone grafting. Compos. Sci Technol **65,** 2385, 2005.
2. Mussano, F., Ciccone, G., Ceccarelli, M., Baldi, I., and Bassi, F. Bone morphogenetic proteins and bone defects: a systematic review. Spine **32,** 824, 2007.
3. Mistry, A., and Mikos, A. Tissue engineering strategies for bone regeneration. Adv Biochem Eng Biotechnol **94,** 1, 2005.
4. Bikram, M., Fouletier-Dilling, C., Hipp, J., Gannon, F., Davis, A., Olmsted-Davis, E., and West, J. Endochondral bone formation from hydrogel carriers loaded with BMP2-transduced cells. Ann Biomed Eng **35,** 796, 2007.
5. Lutolf, M., Weber, F., Schmoekel, H., Schense, J., Kohler, T., Müller, R., and Hubbell, J. Repair of bone defects using synthetic mimetics of collagenous extracellular matrices. Nat Biotechnol **21,** 513, 2003.
6. Bishop, G.B., and Einhorn, T.A. Current and future clinical applications of bone morphogenetic proteins in orthopaedic trauma surgery. Int Orthop **31,** 721, 2007.
7. Cahill, K.S., Chi, J.H., Day, A., and Claus, E.B. Prevalence, complications, and hospital charges associated with use of bone-morphogenetic proteins in spinal fusion procedures. JAMA **302,** 58, 2009.
8. Liu, Y., Hunziker, E., Vaal, C., and Groot, K. Biomimetic Coatings vs. Collagen sponges as a carrier for BMP-2: a comparison of the osteogenic responses triggered *in vivo* using an ectopic rat model. Key Eng Mater **254,** 619, 2004.
9. Schmoekel, H., Weber, F., Schense, J., Graetz, K., Schawalder, P., and Hubbell, J. Bone repair with a form of BMP-2 engineered for incorporation into fibrin cell ingrowth matrices. Biotechnol Bioeng **89,** 253, 2005.
10. Halstenberg, S., Panitch, A., Rizzi, S., Hall, H., and Hubbell, J. Biologically engineered protein-graft-poly (ethylene glycol) hydrogels: a cell adhesive and plasmin-degradable biosynthetic material for tissue repair. Biomacromolecules **3,** 710, 2002.
11. Peppas, N.A. Hydrogels. In: Ratner, B.D., A.S.H., Schoen, F.J., and Lemons, J.E., eds. Biomaterials Science: An Introduction to Materials in Medicine. San Diego: Elsevier Academic Press, 2004, pp. 100–107. ◀AU2
12. Cruise, G.M., Hegre, O.D., Lamberti, F.V., Hager, S.R., Hill, R., Scharp, D.S., and Hubbell, J.A. *In vitro* and *in vivo* performance of porcine islets encapsulated in interfacially photopolymerized poly (ethylene glycol) diacrylate membranes. Cell Transplant **8,** 293, 1999.
13. Fouletier-Dilling, C., Gannon, F., Olmsted-Davis, E., Lazard, Z., Heggeness, M., Shafer, J., Hipp, J., and Davis, A. Efficient and rapid osteoinduction in an immune-competent host. Hum Gene Ther **18,** 733, 2007.
14. Thies, R. Recombinant human bone morphogenetic protein-2 induces osteoblastic differentiation in W-20-17 stromal cells. Endocrinology **130,** 1318, 1992.
15. Olmsted, E., Blum, J., Rill, D., Yotnda, P., Gugala, Z., Lindsey, R., and Davis, A. Adenovirus-mediated BMP2 expression in human bone marrow stromal cells. J Cell Biochem **82,** 11, 2001.
16. Davis, A., Wivel, N., Palladino, J., Tao, L., and Wilson, J. Construction of adenoviral vectors. Mol Biotechnol **18,** 63, 2001.
17. Fouletier-Dilling, C., Bosch, P., Davis, A., Shafer, J., Stice, S., Gugala, Z., Gannon, F., and Olmsted-Davis, E. Novel compound enables high-level adenovirus transduction in the absence of an adenovirus-specific receptor. Hum Gene Ther **16,** 1287, 2005.
18. Gugala, Z., Davis, A., Fouletier-Dilling, C., Gannon, F., Lindsey, R., and Olmsted-Davis, E. Adenovirus BMP2-induced osteogenesis in combination with collagen carriers. Biomaterials **28,** 4469, 2007.
19. Gugala, Z., Olmsted-Davis, E., Gannon, F., Lindsey, R., and Davis, A. Osteoinduction by *ex vivo* adenovirus-mediated BMP2 delivery is independent of cell type. Gene Ther **10,** 1289, 2003.
20. van Dijk-Wolthuis, W.N.E., Hoogeboom, J.A.M., Van Steenbergen, M.J., Tsang, S.K.Y., and Hennink, W.E. Degradation and release behavior of dextran-based hydrogels. Macromolecules **30,** 4639, 1997.
21. Liao, H., Munoz-Pinto, D., Qu, X., Hou, Y., Grunlan, M.A., and Hahn, M.S. Influence of hydrogel mechanical properties and mesh size on vocal fold fibroblast extracellular matrix production and phenotype. Acta Biomater **4,** 1161, 2008.
22. Elbert, D.L., Pratt, A.B., Lutolf, M.P., Halstenberg, S., and Hubbell, J.A. Protein delivery from materials formed by self-selective conjugate addition reactions. J Controlled Release **76,** 11, 2001.
23. Scheufler, C., Sebald, W., and Hulsmeyer, M. Crystal structure of human bone morphogenetic protein-2 at 2.7 A resolution. J Mol Biol **287,** 103, 1999.
24. Carmeliet, P., and Jain, R.K. Angiogenesis in cancer and other diseases. Nature **407,** 249, 2000.

Journal of Biomedical Materials Research Part A

Cathepsin K sensitive poly(ethylene glycol) hydrogels for degradation in response to bone resorption

Journal:	*Journal of Biomedical Materials Research: Part A*
Manuscript ID:	JBMR-A-10-0597.R1
Wiley - Manuscript type:	Original Article
Date Submitted by the Author:	10-Jan-2011
Complete List of Authors:	Hsu, Chih-Wei; Rice University, Bioengineering Olabisi, Ronke; Rice University, Bioengineering Olmstead-Davis, Elizabeth; Baylor College of Medicine, Center for Cell and Gene Therapy Davis, Alan; Baylor College of Medicine, Center for Cell and Gene Therapy West, Jennifer; Rice University, Bioengineering
Keywords:	Hydrogel, Biodegradation, Bone remodeling, Osteoclast

Cathepsin K sensitive poly(ethylene glycol) hydrogels for degradation in response to bone resorption[a]

Chih-Wei Hsu,[1,*] Ronke M. Olabisi,[1,*] Elizabeth A. Olmstead-Davis,[2] Alan R. Davis,[2] Jennifer L. West[1]

[a] No benefit of any kind will be received either directly or indirectly by the author(s).

[1] Department of Bioengineering, Rice University, 6100 Main St., Houston, TX 77005, USA

[2] Center for Cell and Gene Therapy, Baylor College of Medicine, One Baylor Plaza, Houston, TX 77030, USA

[*] Both authors contributed equally to this work.

Corresponding author:
Professor Jennifer L. West, Ph.D.
Bioengineering Department
Rice University
6100 Main St., MS142
Houston, TX 77005
Tel: 713-348-5955
Fax: 713-348-5877
Email: jwest@rice.edu

Abstract

We propose a new strategy of biomaterial design to achieve selective cellular degradation by the incorporation of cathepsin K-degradable peptide sequences into a scaffold structure so that scaffold biodegradation can be induced at the end of the bone formation process. Poly(ethylene glycol) diacrylate (PEGDA) hydrogels were used as a model biomaterial system in this study. A cathepsin K-sensitive peptide, GGGMGPSGPWGGK (GPSG), was synthesized and modified with acryloyl-PEG-succinimidyl carbonate to produce a cross-linkable cathepsin K-sensitive polymer that can be used to form a hydrogel. Specificity of degradation of the GPSG hydrogels was tested with cathepsin K and proteinase K as a positive control, with both resulting in significant degradation compared to incubation with nonspecific collagenases over a 24 hour time period. No degradation was observed when the hydrogels were incubated with plasmin or control buffers. Cell-induced degradation was evaluated by seeding differentiated MC3T3-E1 osteoblasts and RAW264.7 osteoclasts on GPSG hydrogels that were also modified with the cell adhesion peptide RGDS. Resulting surface features and resorption pits were analyzed by differential interference contrast (DIC) and fluorescent images obtained with confocal microscopy. Results from both analyses demonstrated that GPSG hydrogels can be degraded specifically in response to osteoclast attachment but not in response to osteoblasts. In summary, we have demonstrated that by incorporating a cathepsin K-sensitive peptide into a synthetic

polymer structure, we can generate biomaterials that specifically respond to cues from the natural process of bone remodeling.

Key words: Hydrogel; Biodegradation; Bone remodeling; Osteoclast

Introduction

Autologous bone grafts are considered the gold standard treatment in orthopedic surgery, where the biological properties of the grafts can undergo balanced bone formation and bone resorption at the implanted sites. These grafts have been commonly used in spinal fusion, revision total hip arthroplasty, maxillofacial reconstruction, and repair of segmental skeletal defects.[1-4] Despite being the standard of care, autografts are limited by donor-site morbidity and availability. As an alternative to the bone graft, three main classes of biomaterial have been designed and used extensively for different orthopedic applications: metals, ceramics, and polymers.[5] Although each class of biomaterial has its own advantages, poor degradation properties are a major drawback common to all. At best, these materials undergo non-specific degradation, and at worst, they are essentially non-degradable.

The ideal biomaterial for orthopedic applications should be osteoconductive, osteoinductive, osteogenic, and also bioresorbable. An important aspect of designing a degradable biomaterial

for orthopedic applications is the ability to synchronize the degradation of the material with cellular responses that occur during bone remodeling - a dynamic process consisting of both bone formation and resorption.[6] Bone formation is accomplished following mineralization by matrix producing osteoblasts, whereas bone resorption is carried out by osteoclasts. When the resorption cycle starts, osteoclasts migrate and attach to resorption sites. Attached osteoclasts then polarize and the apex membrane forms a functional secretory domain. Polarized osteoclasts secrete hydrochloric acid to dissolve hydroxyapatite and proteases to degrade the type I collagen-rich organic matrix. One such protease is cathepsin K, which is predominantly expressed in osteoclasts during bone resorption.[7-8] In the current study, by incorporating a collagen I (α-1) peptide fragment, we have developed a synthetic polymer with high sensitivity and specificity for cathepsin K.

Herein we describe such a biomaterial that was designed using our new strategy for creating biodegradable materials that degrade in response to specific cellular events. With poly(ethylene glycol) diacrylate (PEGDA) hydrogels as a model system, we demonstrate that we can fabricate the hydrogel scaffold to be gradually degraded and specifically targeted by bone resorption processes. The degradable hydrogel is designed by incorporating a short peptide fragment of type I collagen (α-1) (160-163), Gly-Pro-Ser-Gly (GPSG) , which was found to be highly cleavable between serine and glycine by cathepsin K.[9] After inserting this peptide into a PEGDA backbone,

we evaluated the degradation profiles of the cathepsin K-sensitive GPSG hydrogel in the presence of select enzymes. We also examined the hydrogel's capacity for degradation by osteoclasts and osteoblasts.

Materials and Methods

Specificity of degradation of the cathepsin K-sensitive peptide

The cathepsin K-sensitive peptide sequence, GPMGPSGPWGK, and a scrambled sequence, GMPSGGPPWGK, were synthesized on an APEX 396 peptide synthesizer (Aapptec, Louisville, KY). After synthesis, the peptides were cleaved from the polystyrene resin (95 % trifluoroacetic acid, 2.5 % water, and 2.5 % triisopropylsilane), precipitated in ethyl ether, and purified by dialysis. Following purification, the peptide molecular weights were confirmed with matrix-assisted laser desorption ionization time of flight mass spectrometry (MALDI-ToF; Bruker Daltonics, Billerica, MA).

Degradation products of these peptides were evaluated by MALDI-ToF after incubation with cathepsin K or a control solution. Procathepsin K (Enzo Life Science, Plymouth Meeting, PA) was first activated in 35 mM sodium acetate (pH 3.5) for 2 h at room temperature. Activated cathepsin K was then adjusted to 0.05 mg/ml in 50 mM sodium acetate buffer (NaOAc; pH 5.5, 2.5 mM EDTA, 1 mM DTT, 0.01 % Triton X-100, 0.2 mg/ml sodium azide). NaOAc buffer

without enzyme was used as a negative control and the reactions were allowed to proceed for 4 hours at 37 ^{O}C. The molecular weights of the degradation products were determined with MALDI-ToF mass spectrometry.

Synthesis and characterization of acryloyl-PEG-succinimidyl carbonate (acrylol-PEG-SMC)

All reagents were obtained from Sigma unless otherwise noted. Monoacrylation of poly(ethylene glycol) (PEG) was undertaken by reacting the PEG with a stoichiometric amount of acryloyl chloride in the presence of silver(I) oxide and a catalytic amount of potassium iodide, a process shown to selectively monofunctionalize PEG in high yields due to intramolecular hydrogen bonding between the two hydroxyl groups, which differ in acidity.[10] After reacting PEG (50 mM; 3,400 Da; Fluka, Milwaukee, WI) with 1.5 molar equivalent silver(I) oxide (75 mM), 1.1 molar equivalent acryloyl chloride (55 mM) and potassium iodide (30 mM) in anhydrous dichloromethane (DCM) overnight at 4 ^{O}C, the mixture was purified. Silver(I) oxide was first removed from the acryloyl-PEG-OH solution by filtering the mixture through a Celite 521 pad (Spectrum Chemical Manufacturing Corp, Gardena, CA). For further purification, the filtrate was dried using a Rotovap, re-dissolved in de-ionized water, and adjusted to pH 3 with 6 N HCl. After heating to 35 ^{O}C and venting to air for 1 h, activated charcoal (Fisher Scientific, Pittsburgh, PA) was added to the mixture and stirred overnight to absorb iodine. The charcoal

was then removed via filtration. Sodium chloride (25 % w/v) was dissolved in the aqueous filtrate followed by DCM extraction. The organic phase was collected and extracted again with 2 M potassium bicarbonate to remove chloride ions. Acryloyl-PEG-OH was recovered by precipitation in cold ethyl ether, filtered, dried under vacuum overnight, and lyophilized until completely dry. To proceed with the succinimidyl carbonate conjugation, acryloyl-PEG-OH (25 mM) was mixed with pyridine (75 mM) and N,N'-disuccinimidyl carbonate (100 mM) in anhydrous acetonitrile. After reacting under argon overnight, pyridine and acetonitrile were removed with a Rotovap. The mixture was re-dissolved in anhydrous DCM and filtered to remove unreacted N,N'-disuccinimidyl carbonate. Acetate buffer (0.1 M, pH 4.5, 15% NaCl) was then used for phase extraction. The organic layer was collected and dried with anhydrous magnesium sulfate. Acryloyl-PEG-SMC (Figure 1A) was recovered following precipitation in cold ethyl ether, filtered, and dried under vacuum overnight. The products were analyzed by ^{1}H-NMR (Advance 400, Bruker, Germany) and MALDI-ToF and stored at -80 ^{O}C under argon.

Synthesis and characterization of acryloyl-PEG-GPSG-PEG-acryloyl, acryloyl-PEG-RGDS, and fluorescently-labeled acryloyl-PEG-RGDS conjugates

The cathepsin K-sensitive peptide sequence GGGMGPSGPWGGK (GPSG) was synthesized on an APEX 396 peptide synthesizer and purified as previously described. The

glycine spacers sandwiching the peptide were included to avoid steric hindrance with cathepsin K following conjugation to PEG. Lysine, with a free amine on its side chain, enabled reaction with the active esters in the heterobifunctional acryloyl-PEG-SMC. The tryptophan residue allows the tracking of *in vitro* degradation by monitoring UV absorbance at 280 nm as the cleaved amino acid is released to solution.

The crosslinkable cathepsin K-sensitive acryloyl-PEG-GGGMGPSGPWGGK-PEG-acryloyl (acryloyl-PEG-GPSG-PEG-acryloyl) polymer was synthesized by reacting GPSG peptide with acryloyl-PEG-SMC in a 2.1:1 (PEG:peptide) molar ratio in a 50 mM sodium bicarbonate buffer (pH 8.5) at room temperature overnight (Figure 1B). The resulting product was dialyzed, lyophilized, and stored under argon at -20 ^{O}C until use. Similarly, the cell adhesive peptide Arg-Gly-Asp-Ser (RGDS, American Peptide, Sunnyvale, CA) was reacted with acryloyl-PEG-SMC in a 1.1:1 molar ratio to obtain acryloyl-PEG-RGDS. Conjugation products were analyzed by ^{1}H-NMR, gel permeation chromatography (GPC; Polymer Laboratories, Amherst, MA), UV/Vis and evaporative light scattering detectors.

Fluorescently labeled acryloyl-PEG-RGDS was synthesized as previously described.[11] In brief, purified acryloyl-PEG-RGDS was mixed with Alexa Fluor 680 carboxylic acid (Invitrogen, Carlsbad, CA) in 50 mM sodium bicarbonate buffer in a 1:10 (acryloyl-PEG-RGDS:dye) molar ratio and allowed to react for 1 h at room temperature. The desired products were then purified

by a Sephadex G-25 fine chromatography column (Amersham Bioscience, Uppsala, Sweden) followed by dialysis and lyophilization. Recovered products were stored under argon at -20 ^{O}C until use.

In vitro degradation profile of the PEG-GPSG-PEG hydrogel

For evaluation of PEG-GPSG-PEG hydrogel degradation, a pre-polymer solution was prepared by combining 0.1 g/ml crosslinkable acryloyl-PEG-GPSG-PEG-acryloyl with 1.5 % (v/v) triethanolamine, 37 mM 1-vinyl-2-pyrrolidinone, and 1 % (v/v) of 1.0 mM eosin Y in tris buffered saline (TBS; pH 7.5, 10 mM $CaCl_2$, 0.1 % Tween 20, 0.2 mg/ml sodium azide). The precursor solution was sterilized by filtration using a 0.22 µm filter (Millpore Corporation Bedford, MA). For *in vitro* enzyme degradation tests, 3 µl of pre-polymer solution was transferred to the bottom corner of a micro-cuvette (Brandtech, Essex, CT) and polymerized by exposing to visible light for 2 min. The power of the light source (Fiber Lite; Dolan Jenner Industries, Boxborough, MA) is 408 mW/cm^2 when measured at 490 nm, which is the excitation wavelength for Eosin Y. The spot temperature was measured to change in 2 min from 22ºC to 29ºC, well under the 37ºC of the incubator. Following equilibrium swelling overnight in 250 µl TBS, each hydrogel was incubated with 250 µl enzyme solution at 37 ^{O}C for 24 h. Proteinase K (Invitrogen), plasmin, type I and type III collagenase (COL I and COL III; Worthington,

Lakewood, NJ) were prepared in TBS to a final concentration of 0.05 mg/ml. Hydrogels were also incubated in TBS and NaOAc buffer as negative controls. Hydrogel degradation was evaluated by monitoring the release of tryptophan over time by measuring the absorbance change of test solutions with a UV/Vis spectrophotometer (Carey 50, Varian, Palo Alto, CA) at 280 nm. The percentage released was calculated by comparing hydrogel degradation against an equivalent volume of uncrosslinked pre-polymer solution after incubation with each respective enzyme. This control solution corresponds to 100 % degradation.

Cell maintenance of MC3T3-E1 and RAW 264.7 cells

Murine pre-osteoblast cells MC3T3-E1 subclone 4 and macrophage cells RAW 264.7 (ATCC, Manassas, VA, USA) were cultured in alpha-MEM medium (Gibco BRL, Canada) and DMEM (ATCC), respectively. Culture media were supplemented with 10% fetal bovine serum (FBS; Atlanta Biologicals, Lawrenceville, GA), 100 U/ml penicillin, and 100 mg/ml streptomycin (Gibco BRL, Canada). Cells were incubated at 37 ^{O}C with 5% CO_2. The media were refreshed every 2–3 d and confluent cells were subcultured through trypsinization for MC3T3-E1 and scraping for RAW 264.7. All experiments were conducted using cells between passages 4-10. MC3T3-E1 cells were differentiated into osteoblasts via supplied 50 µg/ml ascorbic acid and 10 mM b-glycerophosphate to the growth medium. Differentiation medium

was subsequently replaced every 2-3 d. To differentiate cells to multinuclear osteoclasts, RAW 264.7 were seeded at a density of 1.5 x 10^5 cells/cm^2 and allowed to adhere for 4 h. Culture media was then supplemented with 30 ng/ml of receptor activator of nuclear factor kappa B ligand (RANKL; R&D Systems Inc., Minneapolis, MN) and replaced every 2 d. The cells were cultured for an additional 4 d before further use.[12]

Serum gradient purification of differentiated multinuclear RAW264.7

Differentiated multinuclear RAW264.7 (dRAW264.7) were purified by a serum gradient.[12] After differentiation in culture medium supplemented with 30 ng/ml RANKL for 4 d, dRAW264.7 cells were trypsinized and resuspended in 15 ml of Moscona's high carbonate (MHB; pH 7.2, 137 mM NaCl, 2.7 mM KCl, 0.4 mM NaH_2PO_4, 12 mM $NaHCO_3$, and 11 mM dextrose) solution. A serum gradient was prepared by placing a layer of 15 ml 70% FBS solution in MHB at the bottom of a 50 ml conical tube, and slowly overlaying with a second layer of 15 ml 40% FBS solution. Fifteen ml of cell suspension was then slowly added to the top without disturbing the layers. The tube was capped and held undisturbed at room temperature for 30 min to permit cells to separate based on size. The top 17 ml layer, middle 16 ml layer, and bottom 12 ml layer were collected separately. Cells in each layer were centrifuged at 500 x g for 5 min, resuspended in culture medium, and seeded in 12 well tissue culture plates at a density of 5,000

cells/cm^2 overnight.

In order to confirm the presence of differentiated osteoclasts, cells were stained for the activity of tartrate-resistant acid phosphatase (TRAP) as previously described.[12] Briefly, after fixing cells in 4% formaldehyde, TRAP staining solution was prepared containing 0.125 mg/ml Naphthol AS-BI Phosphate, 0.1 M acetate buffer, 6.7 mM L(+)-tartrate, 1 mM sodium nitrite, and 0.07 mg/ml diazotized fast garnet GBC. Medium was aspirated and 1 ml of TRAP staining solution was added to each well. After staining at 37 ^{O}C for 1 h, each well was rinsed three times with deionized water and allowed to air dry before imaging.

Surface degradation of differentiated RAW 264.7 and MC3T3-E1 on PEG-GPSG-PEG hydrogels or bone

Flat hydrogel sheets for surface degradation studies were formed by adding 10 mM acryloyl-PEG-RGDS and 1 mM Alexaflour 680 labeled acryloyl-PEG-RGDS to the PEG-GPSG-PEG pre-polymer mixture (0.1 g/ml acryloyl-PEG-GPSG-PEG-acryloyl with 1.5 % (v/v) triethanolamine, 37 mM 1-vinyl-2-pyrrolidinone, and 1 % (v/v) of 1.0 mM eosin Y in TBS) and polymerizing between a mica sheet (Ted Pella, Inc., Redding, CA) and glass slide separated by a 1 mm Teflon spacer. The atomically smooth surface of the mica sheet permitted the formation of hydrogels with smooth surfaces that displayed no flaws even under high

magnification. Both MC3T3-E1 and RAW 264.7 cells were differentiated for 4 d in differentiation media in tissue culture plates. dRAW264.7 cells were removed by scraping and reseeded at a density of 5 x 10^4 cells/cm^2 on both PEG-GPSG-PEG hydrogels and porcine cortical bone slices, which served as control. Differentiated MC3T3-E1 (dMC3T3-E1) and multinuclear RAW264.7 osteoclasts collected at the bottom layer of the serum gradient were also seeded on the mica-molded hydrogel surfaces at the same density. Hydrogels seeded with either osteoblasts or osteoclasts and bone slices seeded with osteoclasts were then cultured in differentiation medium for 48 h before further analysis.

Confocal microscopy of pit formation on cathepsin K sensitive PEG hydrogel and bone surfaces

Following 48 hours of incubation, hydrogel surfaces were imaged after cells were either removed by 20 mM EDTA, or fixed and stained with 4',6-diamidino-2-phenylindole (DAPI; Invitrogen) and rhodamine phalloidin (Invitrogen). Similarly, bone slices were imaged following the removal of adherent dRAW264.7 cells. Differential interference contrast (DIC) or fluorescence images were taken by LSM-5 LIVE microscope systems (Carl Zeiss Inc., German). Z-stack images were acquired with a 20X objective. The z distance between each step was 0.253 µm. Images were all processed with ImageJ 142 (NIH, Bethesda, MD). Three dimensional image

reconstructions were processed using OsiriX Medical Imaging software (version 3.0.2; the OsiriX Foundation, Geneva, Switzerland). The areas of resorption lacunae on hydrogel and bone surfaces were measured using ImageJ.

Results

Characterization of synthesized materials

^{1}H-NMR analysis demonstrated that acryloyl-PEG-SCM was successfully synthesized and conjugated to GGGMGPSGPWGGK and RGDS. After purification, the acryloyl-PEG-SCM showed the methylene protons of PEG as a triplet at 3.6–3.7 ppm, the succinimidyl carbonate protons at 2.6 ppm, as well as the acrylate protons at 5.9–6.4 ppm. After conjugation to GGGMGPSGPWGGK and RGDS, the peak for the succinimidyl carbonate protons disappeared, but peaks for the methylene protons of PEG and acrylate protons remained indicating successful conjugation reactions. A shift in the molecular weights of conjugated products was also confirmed by GPC, demonstrating an 81% conjugation of the PEG-GPSG-PEG.

In vitro degradation of peptides and PEG-GPSG-PEG hydrogels

Mass spectrometry (MALDI-ToF) following incubation of the peptides GPMGPSGPWGK and GMPSGGPPWGK in cathepsin K or buffer, revealed peaks at predicted molecular weights

(predicted: 1070.39 Da; actual: 1091.23 Da) when incubated in NaOAc buffer. When incubated in cathepsin K, the peak at 1091.23 Da disappeared for the sequence GPMGPSGPWGK and predicted degradation peaks appeared at 280.26, 324.38 and 379.39 Da. When the scrambled sequence GMPSGGPPWGK was incubated in cathepsin K, there was no change to the spectrum.

The tryptophan incorporated in the GGGMGPSGPWGGK peptide allowed detection of enzymatic cleavage of the PEG-GPSG-PEG hydrogels by monitoring the release of tryptophan into solution. After incubation in different enzyme solutions for 24 h, hydrogels in cathepsin K and proteinase K solutions had similar degradation profiles, both indicating a rapid tryptophan concentration increase within the first hour and reaching about 80% release of total tryptophan at 24 h (Figure 2). No degradation was observed when hydrogels were incubated in TBS buffer, NaOAc buffer, or plasmin. Hydrogels incubated in nonspecific collagenase I and collagenase III solutions also released 40% of incorporated tryptophan after a 24 h incubation.

Differentiation of RAW264.7

RAW264.7 cells stained for TRAP activity were all negative prior to incubation with RANKL and all positive afterwards. Although all RANKL exposed RAW264.7 cells stained TRAP positive, not all of these cells fused into multinuclear cells (Figure 3A). After separation by serum gradient, the top fraction of the gradient contained most of the mononuclear cells. The

middle fraction of the gradient contained mixed groups of mononuclear and multinuclear cells. The majority of cells in the bottom fraction were multinuclear, containing a very small portion of mononuclear cells (Figure 3B to D). The multinuclear cells collected in the bottom fraction also stained TRAP positive, which indicated that they were differentiated multinuclear osteoclasts.

Comparison of surface resorption pits on cathepsin K-sensitive hydrogels and bone slices

After incubating with differentiated RAW264.7 cells for 48 hours, the surfaces of both the hydrogels and bone slices revealed similar resorption pits (Figure 4). The resorption pits on the hydrogel were smaller and greater in number than those on the bone. Despite the differences in size and number, the morphology of the pits was indistinguishable. Both hydrogel and bone slice surfaces were resorbed at the same order of magnitude (18,497.94 ± 65.03 μm^2 and 25,495.12 ± 24.58 μm^2), with similar percentages of total resorbed areas of 9.56% ± 0.03% and 13.17% ± 0.01%, respectively.

DIC images of cathepsin K-sensitive hydrogel surfaces seeded with dMC3T3-E1 and dRAW264.7

No features were detected on hydrogel surfaces seeded with dMC3T3-E1 osteoblasts (Figure 5A). On hydrogel surfaces seeded with dRAW264.7 osteoclasts, several features were

observed after cells were detached (Figure 5B). The intensity profile of the DIC image (Figure 5D) suggests that the features on the hydrogels were depressions.

Three dimensional image reconstruction of dRAW264.7 cells on the surface of cathepsin K-sensitive hydrogels

dRAW264.7 cells stained with DAPI and rhodamine phalloidin showed multinuclear, polarized cells on the hydrogel surface (Figure 6A; Supplement A video). A sealing ring of F-actin and multiple nuclei was clearly observed (Figure 6B). Within the hydrogel surface beneath an osteoclast, a decrease in the hydrogel's fluorescent signal was observed (Figure 6C). Three dimensional volume reconstructions of z-stack images further illustrate this fluorescent signal loss by showing it as a hole in the hydrogel through which the cell can be visualized (Figure 6D-F). This signal loss is indicative of activity by the differentiated RAW264.7 osteoclasts, degrading the underlying hydrogel and creating a characteristic resorption pit, resulting in the fluorescent intensity loss. No signal loss was observed on the hydrogels seeded with dMC3T3-E1 cells (Figure 7).

Discussion

In order to design an osteoclast degradable material, a cathepsin K sensitive peptide derived

from a collagen (α-1) fragment[9] was examined for its capability to provide enzyme degradable cleavage sites within PEG hydrogels. During the synthesis of the cathepsin K sensitive PEG polymer, we employed a method shown to result in selectively high yields of the desired acryloyl-PEG-GPSG-PEG-acryloyl.[10] Though unconjugated peptides and double conjugation in the form of GPSG-PEG-GPSG are possible, Miller *et al.* previously demonstrated that such species, which are initially physically entrapped within hydrogel, diffuse out during equilibrium swelling because they are not covalently bound.[13] Successfully conjugated acryloyl-PEG-GPSG-PEG-acryloyl also generates a distinct molecular weight shift, which makes dialysis a valid option for purification. Our GPC results confirmed this shift, corresponding to a conjugation yield of 81%.

The sensitivity of our peptide to cathepsin K was first evaluated by incubating GPM↓GPS↓GPWGK (predicted: 1070.39 Da; actual: 1091.23 Da) with cathepsin K, with the reported cleavage sites indicated by arrows. Our MALDI-ToF results showed the molecular weights of GPM (predicted: 303.38 Da; actual: 324.38 Da) and GPS (predicted: 259.26 Da; actual: 283.05 Da), confirming these cleavage sites and demonstrating the peptide's sensitivity to cathepsin K. Furthermore, our MALDI-ToF results revealed the molecular weight of the peptide GPW (predicted: 358.39 Da; actual: 381.06 Da), indicating that in addition to the reported cleavage site between M - G and P - S, cathepsin K can also recognize and cleave the peptide

between tryptophan (W) and G. Hence our peptide contains three cathepsin K cleavage sites: GPM↓GPS↓GPW↓GK. A scrambled version of the peptide GMPSGGPPWGK, in which the cathepsin K recognition site G-P-X-G (X represents serine, methionine, arginine (R), glutamine (Q)[9] or tryptophan) was disturbed did not degrade in the presence of cathepsin K, indicating the specificity of the enzyme for our sequence.

After establishing the specificity of cathepsin K for our peptide, we altered the sequence to GGGMGPS↓GPW↓GGK in order to permit conjugation with acryloyl-PEG-SMC while avoiding steric hindrance with the enzyme. In order to evaluate the sensitivity of cathepsin K for our hydrogel, we incubated the hydrogel before and after polymerization with cathepsin K, proteinase K, collagenases and buffers. Proteinase K is a one of the most active endopeptidases reported. It is a nonspecific serine protease extracted from fungus *Tritirachium album*[14] and was selected as a positive control. Proteinase K does not exhibit pronounced cleavage specificity and its predominant cleavage sites are peptide bonds adjacent to carboxyl groups of aliphatic, aromatic or hydrophobic amino acids. Simply, it cleaves proteins and peptides at A↓B, where A is an aliphatic, aromatic or hydrophobic amino acid and B is any amino acid. According to the ExPASy proteomics PeptideCutter tool (Swiss Institute of Bioinformatics), proteinase K cleaves our peptide sequence at the carboxyl side of the tryptophan (GGGMGPSGPW↓GGK), which is a hydrophobic and aromatic residue. Our results showed that cathepsin K degraded the

PEG-GPSG-PEG hydrogel at the same rate and amount as proteinase K, indicating that cathepsin K had a high sensitivity for our polymer.

In order to demonstrate the specificity of our polymer for degradation by cathepsin K, we selected collagenases type I, type III, and plasmin as negative controls. These proteases are specific to other sequences and, as expected, did not degrade the hydrogel to the same degree as proteinase K or cathepsin K. The collagenases only showed a moderate effect on our collagen-derived GPSG sequence, while plasmin was unable to degrade the peptide at all. Plasmin is an important serine protease present in blood. It plays a significant role during wound healing processes and clot dissolution.[15] The fact that plasmin has no sensitivity for our GPSG hydrogel poses an important advantage for future clinical applications, ensuring the hydrogel will remain without undergoing nonspecific degradation mediated by wound healing processes.

After we established cathepsin K's sensitivity and specificity for our hydrogel, we demonstrated the capacity of our polymer to undergo osteoclast specific degradation. When degrading bone, osteoclasts release hydrochloric acid to degrade the mineral component and collagenases and cathepsins to degrade the collagenous bone matrix. After a cycle of resorption, the osteoclast undergoes apoptosis, thus normal degradation proceeds as a sustained series of pitting processes. Our results showed such pitting with differentiated RAW267.4 osteoclasts on both bone and our hydrogel. Although the hydrogel resorption pits were smaller and greater in

number than those on the bone, similar differences in osteoclast resorption pit number and size on various biomaterials were attributed to degradation-induced calcium release,[16] which is thought to regulate osteoclastic resorption.[17] Since our hydrogel does not contain calcium, it does not stimulate this response. Nevertheless, the identical morphology of the pits on both surfaces and the comparable area resorbed indicate that osteoclasts were indeed capable of resorbing our PEG-GPSG-PEG hydrogel.

In summary, results of this study demonstrate our ability to synthesize an osteoclast degradable hydrogel. By incorporating the collagen I (α-1) peptide fragment, we have developed a synthetic polymer with a high sensitivity and specificity for cathepsin K. Enzyme degradation experiments establish that both the peptide fragment and polymerized hydrogel are degradable by cathepsin K, whereas nonspecific collagenases only have a moderate effect. Cell culture experiments demonstrated that osteoclasts are capable of binding to and degrading an RGDS-modified version of this hydrogel. When seeded with osteoblasts or osteoclasts, these hydrogels showed evidence of degradation only on surfaces seeded with osteoclasts, which revealed characteristic resorption pits, further demonstrating that degradation of the polymer is both enzyme and cell specific. In particular, our hydrogel is specific to the enzymes and cells with key roles in bone resorption.

We have previously demonstrated success forming heterotopic bone using genetically

modified cells encapsulated in PEGDA hydrogels.[18] These cells were transduced with an adenoviral vector to express bone morphogenetic protein, type 2 (BMP-2). The encapsulation with PEGDA was an improvement over directly injecting these cells because it enables the use of nonautologous cells in immune competent animals.[19] Despite the success in bone formation, bone did not form where the hydrogel was present. Because the modified cells need immunoprotection only for the duration of bone formation, degradation of the hydrogel after the cells have served their purpose would be beneficial. Although there exist hydrolytically degradable hydrogel systems, our cathepsin K degradable polymer would be an improvement over such systems because degradation would be timed to the arrival of osteoclasts, and would proceed during the remodeling process of the newly formed bone. Hydrolytically degradable systems degrade at a set rate, purely dependent upon the water uptake. Because bone formation proceeds differently between each individual, a set rate that might be ideal in one animal or patient may not be appropriate for another. Thus, the rate of degradation should be set by the rate of bone remodeling. Cell mediated degradation is useful in any scenario where the presence of the hydrogel is needed until the host tissue has replaced it. When cell types other than osteoclasts are targeted for material degradation, one can easily change the peptide sequence in the polymer backbone to achieve sensitivity to other proteolytic enzymes. This approach could improve the design of tissue engineering scaffolds, wound dressings and other biomaterial devices.

Conclusions

In summary, we have successfully used PEG hydrogels as a model system to demonstrate a new strategy to initiate biomaterial degradation through specific cellular response. We developed a PEG hydrogel system with a cathepsin K-sensitive peptide sequence GPSG incorporated into the polymer backbone. This hydrogel system can be gradually degraded with cathepsin K secreted by osteoclasts during bone resorption processes. In the future, this strategy can be applied to different biomaterials to improve their performance in orthopedic applications.

Acknowledgments

The authors would like to acknowledge their funding source, the Department of Defense grant number W82XWH-04-1-0068 and Melissa McHale for her assistance in editing this work.

References

1. Price CT, Connolly JF, Carantzas AC, Ilyas I. Comparison of bone grafts for posterior spinal fusion in adolescent idiopathic scoliosis. Spine (Phila Pa 1976) 2003;28(8):793-8.
2. Goldberg VM. Selection of bone grafts for revision total hip arthroplasty. Clin Orthop Relat Res 2000(381):68-76.
3. Nishida J, Shimamura T. Methods of reconstruction for bone defect after tumor excision: a review of alternatives. Med Sci Monit 2008;14(8):RA107-13.
4. Malizos KN, Zalavras CG, Soucacos PN, Beris AE, Urbaniak JR. Free vascularized fibular grafts for reconstruction of skeletal defects. J Am Acad Orthop Surg 2004;12(5):360-9.
5. Cornell CN. Osteobiologics. Bull Hosp Jt Dis 2004;62(1-2):13-7.
6. Hill PA. Bone remodelling. Br J Orthod 1998;25(2):101-7.
7. Vaananen HK, Zhao H, Mulari M, Halleen JM. The cell biology of osteoclast function. J Cell Sci 2000;113 (Pt 3):377-81.
8. Lecaille F, Bromme D, Lalmanach G. Biochemical properties and regulation of cathepsin K activity. Biochimie 2008;90(2):208-26.
9. Nosaka AY, Kanaori K, Teno N, Togame H, Inaoka T, Takai M, Kokubo T. Conformational studies on the specific cleavage site of Type I collagen (alpha-1) fragment (157-192) by cathepsins K and L by proton NMR spectroscopy. Bioorg Med Chem 1999;7(2):375-9.
10. Bouzide A, Sauve G. Silver (I) oxide mediated highly selective monotosylation of symmetrical diols. Application to the synthesis of polysubstituted cyclic ethers. Org. Lett 2002;4(14):2329-2332.
11. Hahn MS, Taite LJ, Moon JJ, Rowland MC, Ruffino KA, West JL. Photolithographic patterning of polyethylene glycol hydrogels. Biomaterials 2006;27(12):2519-24.
12. Collin-Osdoby P, Yu X, Zheng H, Osdoby P. RANKL-mediated osteoclast formation from murine RAW 264.7 cells. Methods Mol Med 2003;80:153-66.
13. Miller JS, Shen CJ, Legant WR, Baranski JD, Blakely BL, Chen CS. Bioactive hydrogels made from step-growth derived PEG-peptide macromers. Biomaterials 2010;31(13):3736-43.
14. Ebeling W, Hennrich N, Klockow M, Metz H, Orth HD, Lang H. Proteinase K from Tritirachium album limber. European Journal of Biochemistry 1974;47(1):91-97.
15. Li WY, Chong SS, Huang EY, Tuan TL. Plasminogen activator/plasmin system: a major player in wound healing? Wound Repair Regen 2003;11(4):239-47.
16. Redey SA, Razzouk S, Rey C, Bernache-Assollant D, Leroy G, Nardin M, Cournot G. Osteoclast adhesion and activity on synthetic hydroxyapatite, carbonated hydroxyapatite,

and natural calcium carbonate: relationship to surface energies. Journal of Biomedical Materials Research Part A 1999;45(2):140-147.

17. Kameda T, Mano H, Yamada Y, Takai H, Amizuka N, Kobori M, Izumi N, Kawashima H, Ozawa H, Ikeda K. Calcium-sensing receptor in mature osteoclasts, which are bone resorbing cells. Biochemical and biophysical research communications 1998;245(2):419-422.

18. Bikram M, Fouletier-Dilling C, Hipp J, Gannon F, Davis A, Olmsted-Davis E, West J. Endochondral Bone Formation from Hydrogel Carriers Loaded with BMP2-transduced Cells. Annals of Biomedical Engineering 2007;35(5):796-807.

19. Cruise GM, Hegre OD, Lamberti FV, Hager SR, Hill R, Scharp DS, Hubbell JA. In vitro and in vivo performance of porcine islets encapsulated in interfacially photopolymerized poly (ethylene glycol) diacrylate membranes. Cell transplantation 1999;8:293-306.

Figure legends:

Figure 1. A. Synthesis of acryloyl-PEG-succinimidyl carbonate (acryloyl-PEG-SCM) and B. modification of PEG derivatives. 3,400 Da PEG was first proceeded with (1) monoacrylation to produce acryloyl-PEG-OH. Monoacrylated PEG was reacted with N,N'-disuccinimidyl carbonate to produce acryloyl-PEG-SCM (2). Acryloyl-PEG-SCM was then reacted with adhesive ligand RGDS to form acryloyl-PEG-RGDS (3) or reacted with cathepsin K-sensitive peptide GGGMGPSGPWGGK to form crosslinkable cathepsin K sensitive GPSG polymer (4).

Figure 2. Degradation profiles of cathepsin K-sensitive GPSG hydrogels. Hydrogel droplets (3 µl) were polymerized in micro-cuvettes and swelled overnight with 250 µl of TBS buffer. Each hydrogel was incubated in buffer or enzyme solution at 0.05 mg/ml at 37 ^{O}C. UV absorbance at 280 nm was measured over 24 h to monitor tryptophan release corresponding to the degradation of the GPSP hydrogels.

Figure 3. Isolated TRAP-positive dRAW264.7 osteoclasts by serum gradient. After differentiation in medium containing 30 ng/ml RANKL for 4 d, dRAW264.7 cells were combined with mono- and multi-nuclear cells (Figure 3A). After separation by serum gradient, the top fraction contained most of the mononuclear cells. The middle fraction of the gradient contained mixed groups of mononuclear and multinuclear cells. The majority of cells in the bottom fraction were multinuclear cells, which contained a very small portion of mononuclear cells (Figure 3B to 3D). The multinuclear cells collected in the bottom fraction were also stained TRAP positive, which indicated that they were activated osteoclasts. The bottom fraction of TRAP+ dRAW 264.7 osteoclasts was then used for hydrogel degradation studies.

Figure 4. Comparison of resorption pits on both (A) bone slices and (B) GPSG hydrogels seeded with dRAW264.7 osteoclasts. Cells were seeded and cultured for 48 h. Cells were detached with 20 mM EDTA and images of hydrogel and bone slice surfaces were obtained on a LSM LIVE 5 confocal microscope. Similar pit features were observed on both bone slices and hydrogels. Although the pits on the hydrogel are smaller and also outnumbered the pits on the bone slices, both hydrogels and bone slices have a similar percentage of total resorption area.

Figure 5. Differential interference contrast (DIC) images of GPSG hydrogel surfaces seeded with (A) dMC3T3-E1 osteoblasts and (B) dRAW264.7 osteoclasts. Cells were seeded on the hydrogels and cultured for 48 h. Cells were detached with 20 mM EDTA and DIC images were obtained on a LSM LIVE 5 confocal microscope. No features were observed on gel surfaces

seeded with osteoblasts (A). On the gel surface seeded with osteoclasts (B), several features can be identified after cells were detached. (C) and (D) show an enlarged image and an intensity profile of the feature, which suggests that the features on the surface were depressions.

Figure 6. Three-dimensional fluorescent image reconstruction of an active osteoclast on the GPSG hydrogel surface. The GPSG hydrogel was labeled with Alexafluor 680 fluorophore (green), which is conjugated to the acryloyl-PEG-RGDS and incorporated into the hydrogel by photo-polymerization. The cells were fixed and permeabilized before staining the nuclei with DAPI (blue) and F-actin by rhodamine phalloidin (red) 48 hours after seeding. (A) Composed z-stack images of the osteoclast and hydrogel. (B) Sealing ring and multiple nuclei of the osteoclast. (C) The reduced fluorescent signal in the GPSG hydrogel marks the site of an osteoclast resorption pit. These pits, or resorption lacunae, are an extracellular space between the osteoclast ruffled border membrane and the hydrogel, which is sealed from the extracellular fluid by the sealing zone. (D-F) Z-stack Images were reconstructed using a volume rendering algorithm. (D) Side view shows the dome shape of the cell sitting above its resorption lacuna, indicating the polarization of an active osteoclast. (E) Orthogonal view of active osteoclast shown from above. (F) The orthogonal view from below shows a view of the osteoclast through the hole it has degraded in the hydrogel. This resorption site is located beneath the osteoclast, which can be observed in the loss of the fluorescent intensity of Alexafluor 680. The resorption lacuna on the hydrogel surface can be clearly seen from different angles, suggesting that the GPSG hydrogel has been degraded by cathepsin K secreted by osteoclasts.

Figure 7. Three-dimensional fluorescent image reconstruction of osteoblasts on the GPSG hydrogel surface. The GPSG hydrogel was labeled with Alexafluor 680 fluorophore (green), which is conjugated with the acryloyl-PEG-RGDS and incorporated into the hydrogel by photo-polymerization. The cells were fixed and permeabilized before staining the nuclei with DAPI (blue) and F-actin by rhodamine phalloidin (red) 48 hours after seeding. (A) Composed z-stack images of the osteoblasts and hydrogel. (B) Osteoblasts shown without the hydrogel. (C) GPSG hydrogel shown without the osteoblasts shows no decrease in fluorescent signal beneath the osteoblasts. Z-stack Images were reconstructed using a volume renderings algorithm and presented from (D) side view, (E) orthogonal view from above, and (F) from below.

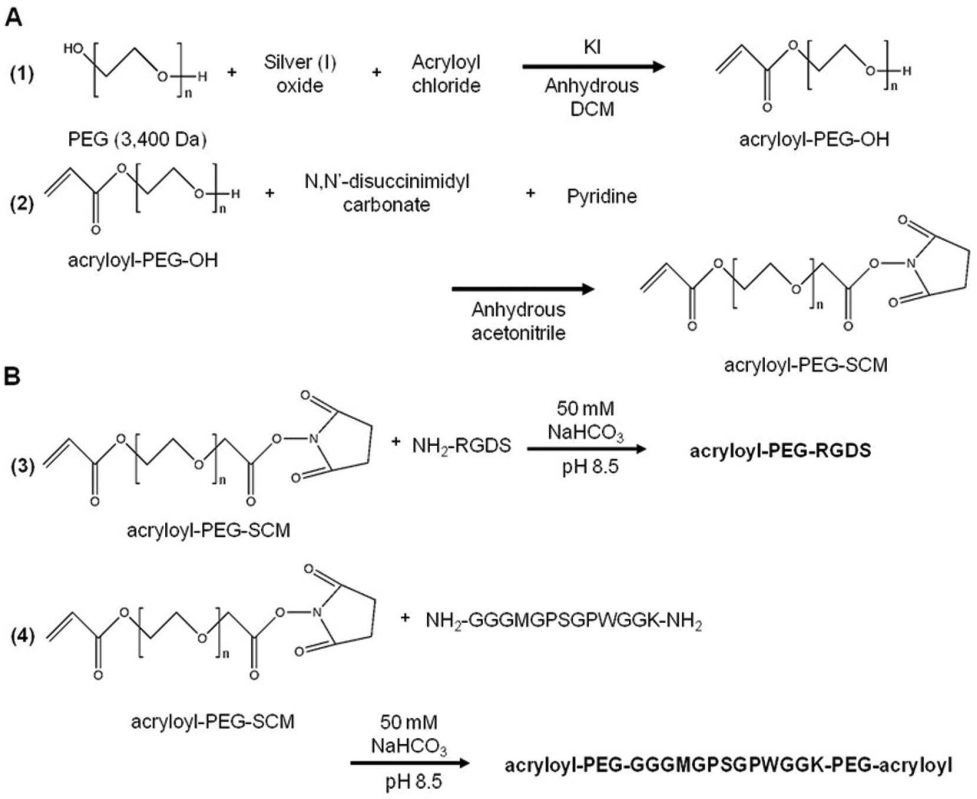

Figure 1. A. Synthesis of acryloyl-PEG-succinimidyl carbonate (acryloyl-PEG-SCM) and B. modification of PEG derivatives. 3,400 Da PEG was first proceeded with (1) monoacrylation to produce acryloyl-PEG-OH. Monoacrylated PEG was then reacted with N,N'-disuccinimidyl carbonate to produce acryloyl-PEG-SCM (2). Acryloyl-PEG-SCM was then reacted with adhesive ligand RGDS to form acryloyl-PEG-RGDS (3) or reacted with cathepsin K-sensitive peptide GGGMGPSGPWGGK to form crosslinkable cathepsin K sensitive GPSG polymer (4).
215x174mm (600 x 600 DPI)

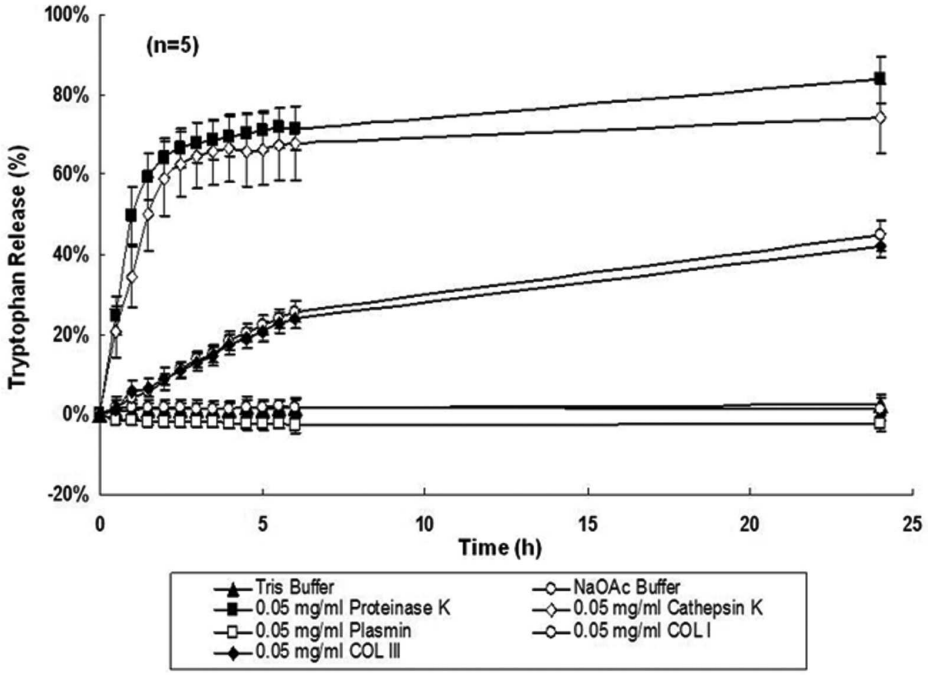

Figure 2. Degradation profiles of cathepsin K-sensitive GPSG hydrogels. Hydrogel droplets (3 µl) were polymerized in micro-cuvettes and swelled overnight with 250 µl of TBS buffer. Each hydrogel was incubated in buffer or enzyme solution at 0.05 mg/ml at 37OC. UV absorbance at 280 nm was measured over 24 h to monitor tryptophan release corresponding to the degradation of the GPSP hydrogels.
72x51mm (600 x 600 DPI)

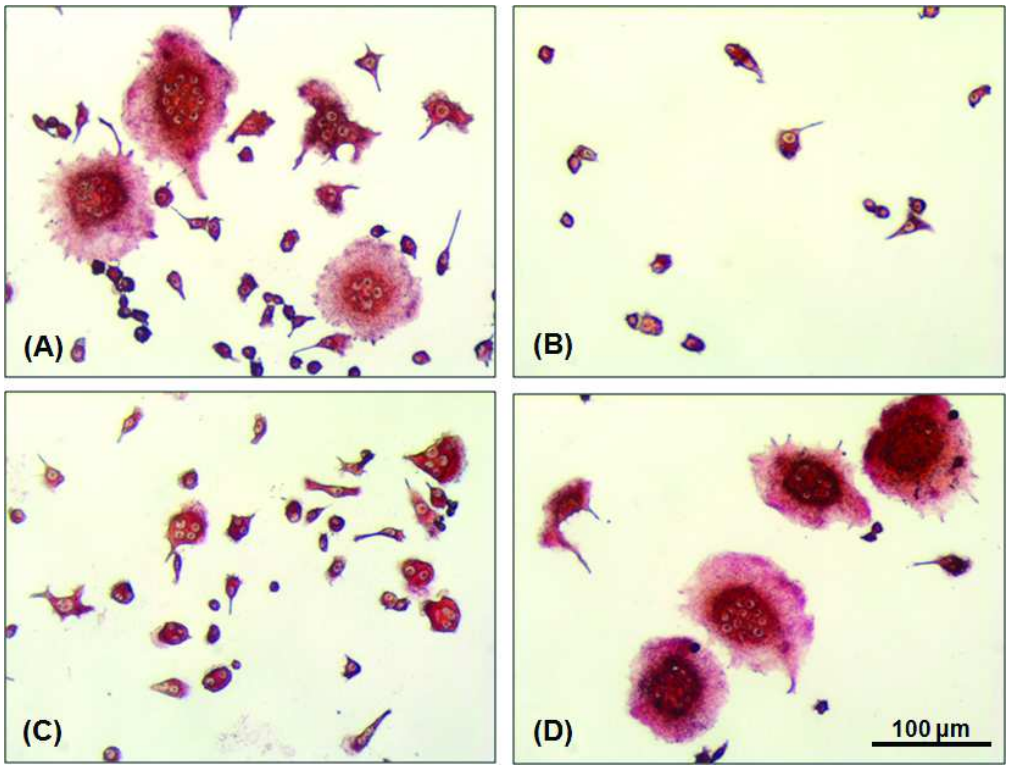

Figure 3. Isolated TRAP-positive dRAW264.7 osteoclasts by serum gradient. After differentiation in medium containing 30 ng/ml RANKL for 4 d, dRAW264.7 cells were combined with mono- and multi-nuclear cells (Figure 3A). After separation by serum gradient, the top fraction contained most of the mononuclear cells. The middle fraction of the gradient contained mixed groups of mononuclear and multinuclear cells. The majority of cells in the bottom fraction were multinuclear cells, which contained a very small portion of mononuclear cells (Figure 3B to 3D). The multinuclear cells collected in the bottom fraction were also stained TRAP positive, which indicated that they were activated osteoclasts. The bottom fraction of TRAP+ dRAW 264.7 osteoclasts was then used for hydrogel degradation studies.
69x52mm (300 x 300 DPI)

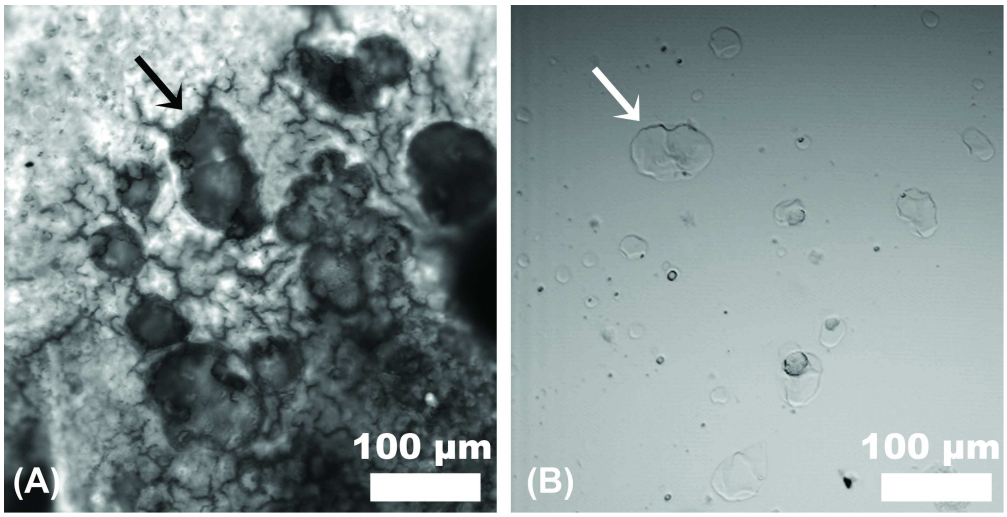

Figure 4. Comparison of resorption pits on both (A) bone slices and (B) GPSG hydrogels seeded with dRAW264.7 osteoclasts. Cells were seeded and cultured for 48 h. Cells were detached with 20 mM EDTA and images of hydrogel and bone slice surfaces were obtained on a LSM LIVE 5 confocal microscope. Similar pit features were observed on both bone slices and hydrogels. Although the pits on the hydrogel are smaller and also outnumbered the pits on the bone slices, both hydrogels and bone slices have a similar percentage of total resorption area.
240x121mm (300 x 300 DPI)

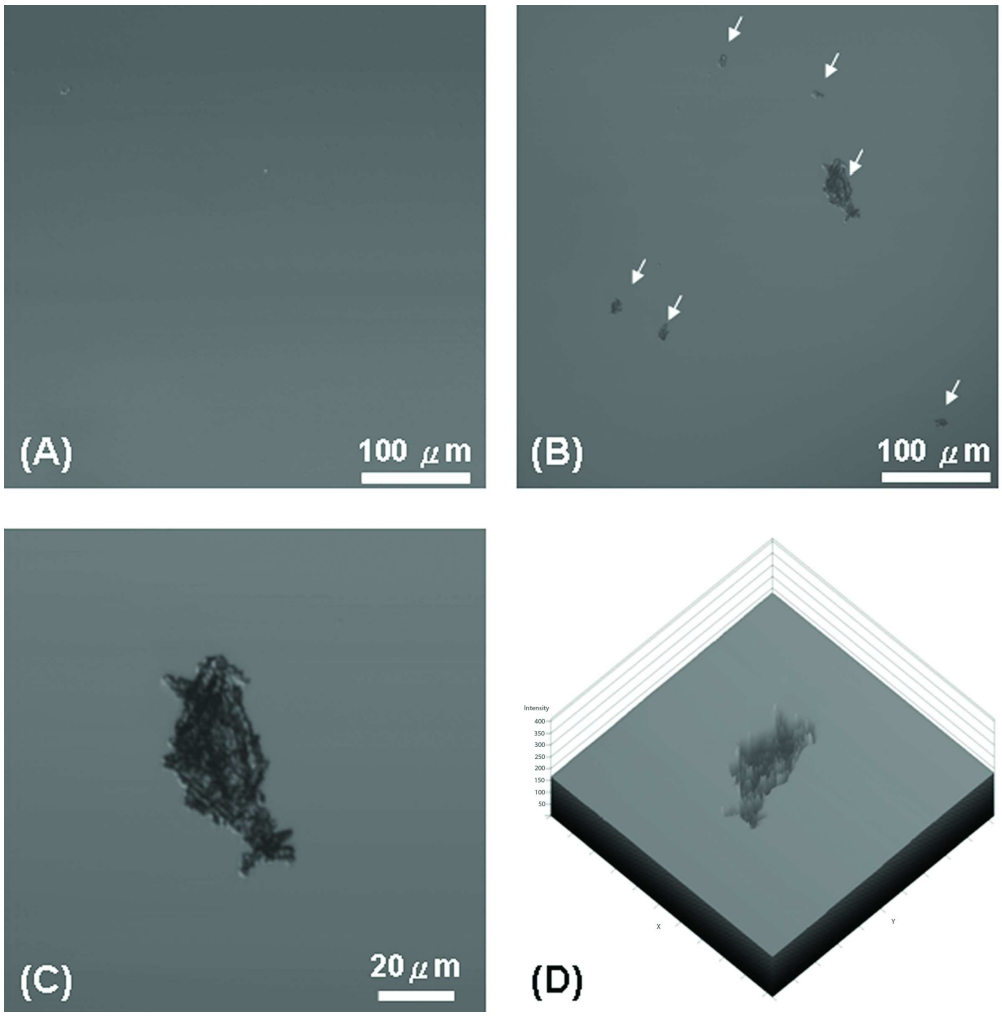

Figure 5. Differential interference contrast (DIC) images of GPSG hydrogel surfaces seeded with (A) dMC3T3-E1 osteoblasts and (B) dRAW264.7 osteoclasts. Cells were seeded on the hydrogels and cultured for 48 h. Cells were detached with 20 mM EDTA and DIC images were obtained on a LSM LIVE 5 confocal microscope. No features were observed on gel surfaces seeded with osteoblasts (A). On the gel surface seeded with osteoclasts (B), several features can be identified after cells were detached. (C) and (D) show an enlarged image and an intensity profile of the feature, which suggests that the features on the surface were depressions.
101x101mm (600 x 600 DPI)

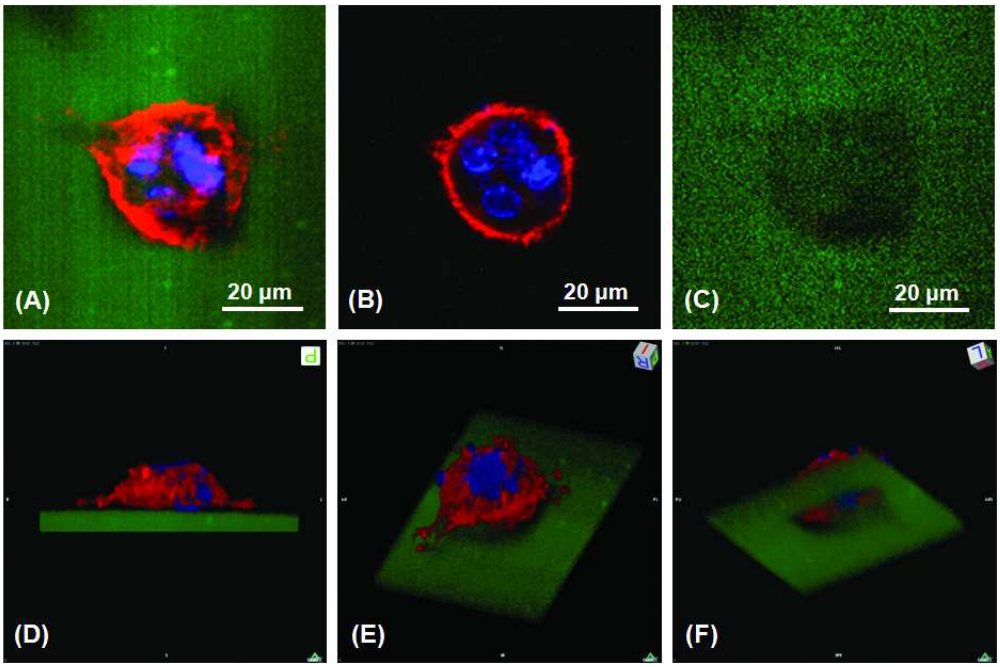

Figure 6. Three-dimensional fluorescent image reconstruction of an active osteoclast on the GPSG hydrogel surface. The GPSG hydrogel was labeled with Alexafluor 680 fluorophore (green), which is conjugated to the acryloyl-PEG-RGDS and incorporated into the hydrogel by photo-polymerization. The cells were fixed and permeabilized before staining the nuclei with DAPI (blue) and F-actin by rhodamine phalloidin (red) 48 hours after seeding. (A) Composed z-stack images of the osteoclast and hydrogel. (B) Sealing ring and multiple nuclei of the osteoclast. (C) The reduced fluorescent signal in the GPSG hydrogel marks the site of an osteoclast resorption pit. These pits, or resorption lacunae, are an extracellular space between the osteoclast ruffled border membrane and the hydrogel, which is sealed from the extracellular fluid by the sealing zone. (D-F) Z-stack Images were reconstructed using a volume rendering algorithm. (D) Side view shows the dome shape of the cell sitting above its resorption lacuna, indicating the polarization of an active osteoclast. (E) Orthogonal view of active osteoclast shown from above. (F) The orthogonal view from below shows a view of the osteoclast through the hole it has degraded in the hydrogel. This resorption site is located beneath the osteoclast, which can be observed in the loss of the fluorescent intensity of Alexafluor 680. The resorption lacuna on the hydrogel surface can be clearly seen from different angles, suggesting that the GPSG hydrogel has been degraded by cathepsin K secreted by osteoclasts.
79x52mm (300 x 300 DPI)

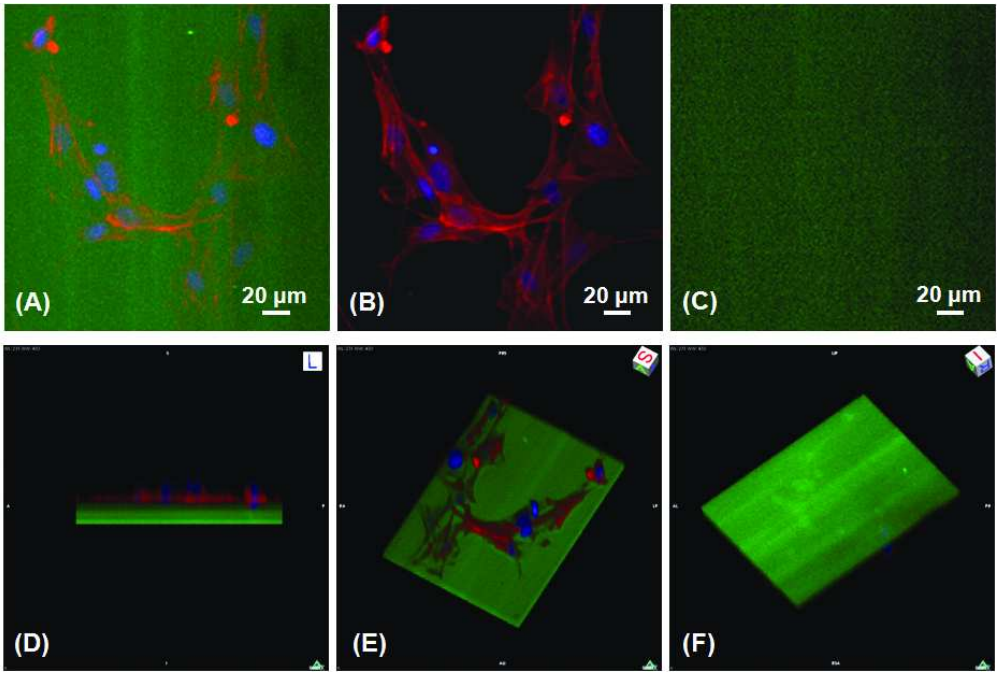

Figure 7. Three-dimensional fluorescent image reconstruction of osteoblasts on the GPSG hydrogel surface. The GPSG hydrogel was labeled with Alexafluor 680 fluorophore (green), which is conjugated with the acryloyl-PEG-RGDS and incorporated into the hydrogel by photo-polymerization. The cells were fixed and permeabilized before staining the nuclei with DAPI (blue) and F-actin by rhodamine phalloidin (red) 48 hours after seeding. (A) Composed z-stack images of the osteoblasts and hydrogel. (B) Osteoblasts shown without the hydrogel. (C) GPSG hydrogel shown without the osteoblasts shows no decrease in fluorescent signal beneath the osteoblasts. Z-stack Images were reconstructed using a volume renderings algorithm and presented from (D) side view, (E) orthogonal view from above, and (F) from below.
78x52mm (300 x 300 DPI)

Journal of Cellular Biochemistry

Cell Based Gene Therapy for Repair of Critical Size Defects in the Rat Fibula

Journal:	*Journal of Cellular Biochemistry*
Manuscript ID:	Draft
Wiley - Manuscript type:	Research Article
Date Submitted by the Author:	n/a
Complete List of Authors:	Lazard, ZaWaunyka; Baylor College of Medicine, Cell and Gene Therapy Heggeness, Michael; Baylor College of Medicine, Orthopedic Surgery Hipp, John; Baylor College of Medicine, Orthopedic Surgery Sonnet, Corinne; Baylor College of Medicine, Cell and Gene Therapy Fuentes, Angie; Baylor College of Medicine, Orthopedic Surgery Nistal, Rita; Baylor College of Medicine, Cell and Gene Therapy Davis, Alan; Baylor College of Medicine, Pediatrics-Hematology Oncology; Baylor College of Medicine, Cell and Gene Therapy; Baylor College of Medicine, Orthopedic Surgery Olabisi, Ronke; Rice University, Bioengineering West, Jennifer; Rice University, Bioengineering Olmsted-Davis, Elizabeth; Baylor College of Medicine, Pediatrics-Hematology Oncology; Baylor College of Medicine, Orthopedic Surgery; Baylor College of Medicine, Cell and Gene Therapy
Keywords:	heterotopic ossifcation, critical size defect, bone repair

Cell Based Gene Therapy for Repair of Critical Size Defects in the Rat Fibula.

ZaWaunyka Lazard[1], Michael Heggeness, M.D., Ph.D.[2], John Hipp, Ph.D.[2], Corinne Sonnet, Ph.D.[1], Angie Fuentes[2], Rita Nistal[1], Alan R. Davis, Ph.D. [1,2,3], Ronke Olabisi, Ph.D.[4] Jennifer L. West, Ph.D.[1,4] and [*]Elizabeth Olmsted-Davis, Ph.D.[1,2,3]

[1]Center for Cell and Gene Therapy; Departments of [2]Orthopedic Surgery and [3]Pediatrics-Hematology Oncology, Baylor College of Medicine, Houston, TX 77030, USA; [4]Department of Bioengineering, Rice University, 6500 Main St. MS 142, Houston, TX 77030

[*] Correspondence to: Dr. Elizabeth A. Olmsted-Davis, One Baylor Plaza Alkek N1010, Houston, TX 77030, tel. (713)798-1238, fax (713)798-1230, edavis@bcm.edu.

Keywords:

- **heterotopic ossification**
- **critical size defect**
- **bone repair**

Includes 5 figures

Contract grant sponsor:

Contract grant number: DAMD W81XWH-07-1-0215, DARPA W911NF-09-1-0040

Abstract:

More than a decade has passed since the first experiments using adenovirus transduced cells expressing bone morphogenetic protein 2 were performed for the synthesis of bone. Since this time, the field of bone gene therapy has tackled many issues surrounding safety and efficacy of this type of strategy. We present studies examining the parameters of the timing of bone healing, and remodeling when heterotopic ossification (HO) is used for bone fracture repair using an adenovirus gene therapy approach. We use a rat fibula defect, which surprisingly does not heal even when a simple fracture is introduced. In this model the bone quickly resorbs, most likely due to the non-weight bearing nature of this bone in rodents. Using our gene therapy system robust HO can be introduced at the targeted location of the defect resulting in bone repair. The HO and resultant bone healing appeared to be dose dependent, based on the number of AdBMP2 transduced cells delivered. Interestingly, the HO undergoes substantial remodeling, and assumes the size and shape of the missing segment of bone. However, in some instances we observed some additional bone associated with the repair, signifying that perhaps the forces on the newly forming bone are inadequate to dictate shape. In all cases, the HO appeared to fuse into the adjacent long bone. The data collectively indicates that the use of BMP2 gene therapy strategies may vary depending on the location and nature of the defect. Therefore additional parameters should be considered when implementing such strategies.

Introduction:

Successful bone repair of non unions remains a complex challenge in orthopedics today. Segmental bone loss resulting from trauma, cancer progression and various bone diseases are treated with bone grafting procedures that occur approximately 500,000 times annually in the United States. [Laurencin et al., 2006] Around 11% of the non fatal injuries in the United States involve long bone fractures[Vyrostek et al., 2004] and on average non union rates occur in about 10% of these cases, varying with the intervention treatment and type of long bone involved. [Giannoudis and Atkins, 2007; Tzioupis and Giannoudis, 2007] All of these factors contribute to a significant toll on the patients, through lengthy recovery times, changes in quality of life, and enormous expense associated with the course of treatment.

Bone distraction osteogenesis, free vascularized bone transfer, limb shortening, and autologous bone grafts are common methods used to manage post-traumatic segmental bone defects in any of the long bone segments. Specific conditions like mechanical instability, axial deviation, bone defect size and presence of infection must be addressed with the treatment being customized to each specific case. Distraction osteogenesis, with either the lengthening or bone transport technique, uses the Ilizarov apparatus to stabilize the limb and treat very large defects, up to 30 cm. However, this procedure is plagued with long treatment duration and numerous complications including delayed union at the docking site and devascularization of the transport segment. [DeCoster et al., 1999] The complication rate (major and minor) associated with the Ilizarov technique has been reported to reach as high as 87%. [Motsitsi, 2008] Vascularized bone transplantation can be performed with iliac crest, fibula, or rib but it has significant drawbacks involving donor site morbidity and increased fracture risk. [DeCoster et al., 2004] Limb shortening is restricted to bone defects less than 3 cm and has the shortest

treatment time, but it is also associated with excessive soft-tissue swelling and loss of limb function.[Watson et al., 1995]

Today the gold standard of care for segmental bone loss has become autologous bone graft, but it is limited by graft material availability. Therapies are also plagued with a plethora of complications and drawbacks. Infection, implant failure, dysfunctional limb, unplanned additional surgical procedure, high cost, and prolonged treatment time are only a few of the shortcomings associated with these treatments. [DeCoster et al., 2004; Finkemeier, 2002; Sen and Miclau, 2007] A 30% failure rate is associated with the surgical treatments for segmental bone defects.[Sorger et al., 2001]

Bone graft materials are selected based on their osteogenic, osteoinductive and osteoconductive qualities that would produce the best healing and mechanical stability for each individual case. Osteoinduction refers to the ability of the material to stimulate the host precursor cells to form new bone through their differentiation into chondroblasts or osteoblasts. The osteoinductive capacity of a graft depends on the amount and type of growth factors and cytokines present.

One of the most promising growth factors currently being tested is bone morphogenetic protein 2 (BMP2), which can induce both orthotopic and *de novo* bone formation at targeted locations. Recombinant human rhBMP-2 and rhBMP-7 are approved for clinical application and are commercially available, although neither has been determined to be efficacious in long bone repair by the FDA. One problem associated with the use of the recombinant proteins, beyond the expense and extremely high amount that must be delivered for any effect, is their extremely short half lives in vivo at approximately 24 hours [Jeon et al., 2007; Winn et al., 2000]. Further, because of their short retention at the target site additional carrier materials must be implanted

as well, thus increasing the risk of infection and making placement of the material difficult.[Haidar et al., 2009; Hollinger et al., 1998]

Many have attempted to deliver the BMP2 through gene therapy means in order to overcome delivery of protein that has limited efficacy. These approaches employ either retroviral transduced cells or the direct use of adenovirus with both methods having serious limitations. The delivery of retroviral transduced cells, which carry one to two copies of the BMP2 gene, provide low levels of the protein locally and allow for these genetically modified cells expressing BMP2 to be incorporated into the bone which increases the overall risk of unwanted long term adverse reactions [Moutsatsos et al., 2001]. Researchers have also attempted to introduce non-integrating vectors ,such as adenovirus or adeno-associated virus [Gafni et al., 2004; Lieberman et al., 1998], directly into the animal which has a large number of associated problems, including poor transduction efficiencies [Olmsted et al., 2001] and diffusion of the free virus expressing BMP2 to other tissues such as the liver and lungs [Baltzer et al., 2000; Gelse et al., 2001]. The injection of the free virus results in limited to no efficacy along with undetectable amounts of protein being expressed at the desired site, as well as significant risk to other tissues such as the liver.

To circumvent these problems we have employed a cell based gene therapy approach, which eliminates the use of free virus in the organism and ensures reliable, efficient transduction and/or expression of the BMP2 at the target site. Further, the BMP2 transgene cannot integrate into the chromosome, and with the use of a first generation vector the transduced cells are rapidly cleared by the immune system. [Fouletier-Dilling et al., 2007]. Again, because the cells are transduced *ex vivo*, with a replication defective adenovirus, the resultant cells are not considered to be infectious or contain any infectious material, thus there is minimal risk associated with the use of this gene therapy system. Additionally, this system provides a

sufficient local concentration of the BMP2 at the target site but the transgene does not integrate into the chromosome, so there is no long term risk associated with chronic BMP2 expression, or other gene disruption from the insertion. Finally, in our previous studies of heterotopic ossification, we have determined that the cells do not incorporate into the final bone structures and are only acting to deliver the BMP2. This importantly avoids potential long term adverse reactions arising from the inclusion of the foreign materials in the skeletal bone.

In the studies presented here, we are harnessing the bone induction capability of recombinant adenoviral transduced cells to safely and efficaciously deliver BMP2. This cell based gene therapy system provides sufficient BMP2 protein *in vivo* at a specific targeted location to induce rapid repair of a critical size defect introduced into the rat fibula. This circumvents the need for releasing carriers and supraphysiological concentrations of BMP2. Furthermore, the rat fibula model is somewhat unique in that it is fused at the ends to the adjacent tibia, thus creating a non-weight bearing environment. We have noted that even a simple fracture introduced into the fibula does not heal, but rather undergoes extensive resorption leaving an approximate 10 mm size defect. Thus repair of this bone would represent an extremely challenging environment. In the studies presented here, we demonstrate the parameters required by this system for bone healing and find that complete healing occurred by 6 weeks in 100% of the animals. Further, we followed the animals for an additional 6 weeks beyond this point to confirm that the fibula was stable and no additional changes resulted post healing.

Materials and Methods

Cell Culture

A human fibroblast cell line (MRC5) was acquired from the American Type Culture Collection (Manassas, VA) and propagated in Dulbecco's modified Eagle's medium (DMEM). The medium was supplemented with 10% fetal bovine serum (Hyclone, Logan, UT), penicillin (100 units/mL), streptomycin (100µg/mL), amphotericin B (.25µg/mL) (Invitrogen Life Technologies, Gaithersburg, MD) and tetracycline (3mg/L) (Sigma, St. Louis, MO). MRC5 cells are not capable of inducing bone formation before transduction.

W20-17, a murine stromal cell line, was obtained as a gift from Genetic Institute, Cambridge, MA and was propagated as described by [Thies et al., 1992]. The W20-17 cells were briefly grown in supplemented DMEM and cultured at a subconfluent density in order to maintain the phenotype. All cell types were grown at 37℃ and 5% CO_2 in humidified air.

Adenovirus Transduction

A replication-defective E1-E3-deleted human adenovirus type 35 fiber protein (Ad5F35) were constructed to contain cDNAs for BMP2 in the E1 region of the virus [Olmsted-Davis et al., 2002] or did not contain any transgene in this region, AdEmpty. The resultant purified viruses, AdBMP2 and AdEmpty cassette, had viral particle (VP)-to-plaque-forming unit (PFU) ratios of 1:77 and 1:111 respectively, and all viruses were confirmed to be negative for replication-competent adenovirus.[Olmsted-Davis et al., 2002] Cells were transduced as previously described with AdBMP2 or AdEmpty cassette at a viral concentration of 2500 VP/cell [Olmsted-Davis et al., 2002] [Fouletier-Dilling et al., 2007]. MRC5 cells were transduced with either AdEmpty or AdBMP2 in DMEM supplemented with 2% FBS at a concentration of 2500 viral

particles per cell. Adenovirus was allowed to incubate overnight at 37℃, humidified atmosphere, 5% CO_2.

Quantification of BMP2

BMP2 protein was measured in culture supernatant taken from cells 72 hours after transduction with AdBMP2 and culture supernatant was collected and assayed for BMP2 protein using a Quantikine BMP2 immunoassay ELISA kit (DBP200; R&D Systems, Minneapolis, MN). BMP2 protein activity was quantified in culture supernatant collected from cells after transduction with AdBMP2 or AdEmpty cassette or no virus, and a portion incubated with W20-17 bone marrow stromal cells, which rapidly increases alkaline phosphatase expression. Alkaline phosphatase activity is readily quantified. [Blum et al., 2001] Briefly, W20-17 cells were plated in 24 well plates at subconfluent densities (5 X 10^4 cells/cm2) and 24 hours later the media was replaced with 200µL of fresh media and 200µL of conditioned culture media from various cells doses. W20-17 cells were then assayed for alkaline phosphatase activity 72 hours after the addition of conditioned culture supernatant using a chemiluminescence procedure.[Olmsted et al., 2001] Cellular alkaline phosphatase was extracted by washing the cells with PBS and cells were lysed with three cycles of freeze thaw in 100µL/cm^2 of 25mM Tris-HCL, pH 8.0 and Triton X-100. For detection of alkaline phosphatase 2µL of CSPD® ready-to-use with Sapphire II enhancer (Tropix, Bedford, MA) in an eppendorf tube, vortexed and incubated at room temperature for 30 seconds. The light output from each sample was integrated for 10 seconds after a 2 second delay by a Glomax 20/20 luminometer.(Promega, Madison, WI). Alkaline phosphatase detection signal was recorded in relative luminescence units (RLU).

Critical Size Defect Model

The critical size defect was introduced into the rat fibula. Adult homozygous Athymic RNU Nude rats weighing (200-300g) were administered buprenorphine at 2mg/kg by subcutaneous injection into the right thigh one hour prior to surgery. The rats underwent general anesthesia through the use of an animal vaporizer that dispensed isoflurane at 2-4% initial induction and 1-2% throughout the surgery. Each animal was shaved, disinfected with Hibiclens and isolated to a sterile surgical field that included a surgical drape that allowed only the left hind limb to be exposed. A lateral incision in the skin of about 2cm was performed on the lower leg, along with a smaller incision into the gastrocnemius muscle. This muscle was retracted in order to expose the fibula and an osteotomy was performed to create a 2-4 mm segmental defect on the diaphysis of the fibula. Cells were then introduced into the defect void by placement into a sutured muscle pocket. Animals (n=8) were euthanized and tissues isolated at various time points as indicated in the text. All animal studies were performed in accordance with the standards of Baylor College of Medicine, Department of Comparative Medicine, after review and approval of the protocol by the Institutional Animal Care and Use Committee (IACUC).

Radiographic Analysis of the New Bone:

Hind limbs were harvested and radiographically analyzed using an XPERT model faxitron (Kubtec, Fairfield, CT) in biplanar projections. Samples were set at an exposure time of 15 seconds and acceleration voltage of 30kV. Bone healing was evaluated with radiographs at the termination of each study.

Qualitative radiographic analyses were performed using microcomputed tomography (MicroCT) system (eXplore Locus SP: GE Healthcare, London, ON, Canada) at 14µm resolution. Bone density was determined with a density calibration phantom. Three-dimensional reconstructions and cross-sections of the hind limb were generated to identify the defect void and new bone.

Histological Analysis of the New Bone:

Animals (n=8) were euthanized at weekly intervals starting at 2 weeks and ending at 12 weeks. Hind limbs were isolated; formalin fixed, and decalcified paraffin embedded. Serial sections (5µm) were prepared that encompassed the critical defect site. Hematoxylin and eosin staining was performed on every fifth slide to locate the newly forming endochondral bone. All sections were analyzed by light microscopy.

Results

Model of Critical Size Defect

Varying sizes of bone were removed from the rat fibula starting with a simple fracture (1mm), and systematically increasing in one millimeter increments to a maximum of 10 mm. The rat fibula was selected over other potential bones because unlike in humans, in rodents this bone is uniquely fused to the adjacent tibia. Therefore, a critical defect can readily be introduced without need for additional fixation. After 2 weeks bone healing was radiologically evaluated using microcomputational tomography (μCT). Surprisingly, in all cases 1 mm, 2 mm, 5 mm, and 10 mm defects (Fig. 1A-D, respectively) we observed a similar size defect of approximately 10 mm or the maximum size introduced into the bone, and the bone ends appeared to be pointed, suggesting that the bone was undergoing significant resorption. Rotation of the μCT images indicated that the bone ends were healed with no apparent sign of an open bone marrow cavity. This indicates that in all cases the bone was not only unable to repair, but that it no longer could maintain normal bone remodeling and had initiated resorption. These results imply that any defect introduced into this model is a significant challenge for bone repair.

Dose Response to AdBMP2 Transduced Cells

We next defined the dose of AdBMP2 transduced cells required to provide optimal healing of the bone defect. Fibroblasts were transduced with AdBMP2 at 2500vp/cell [Gugala et al., 2003] and BMP2 protein as well as activity was quantified 72 hours later. Total BMP2 protein within the culture supernatant was approximately 18.6 nanograms per 1 x 10^6 cells (Fig 2A). Cells transduced with AdEmpty, as well as untransduced cells, did not produce BMP2. Interestingly, a standard dose of recombinant BMP2 protein used to induce bone formation in a

rat critical size defect was approximately 12 ugs [Endo et al., 2006]. Since 5 x 10^6 BMP2-producing cells is adequate to heal the bone completely (Fig. 3A), and we have determined that the transduced cells are present at a maximum of 5 days [Fouletier-Dilling et al, 2007]. This means that a maximum of 93 ng is sufficient to completely heal the bone in this model. This is 130 times less than the amount of protein used in other rat defect studies with recombinant BMP2 suggesting that the prolonged local generation of BMP2 is critical to success due to the short half life of the protein. [Endo et al., 2006]

Further, BMP2 protein activity, as determined by the elevation in the BMP2 responsive protein alkaline phosphatase [Blum et al., 2001], showed that this BMP2 being made is active (Fig. 2B). At no time did we observe either BMP2 activity or protein in culture supernatant isolated from the AdEmpty cassette cells or cells alone. Various numbers of the AdBMP2 transduced cells were next injected simultaneously with the introduction of a 3 mm bone defect in the fibula. The cells were injected into the void region, and surrounding muscle tissues of the rats (n=5), and potential bone formation allowed to progress for two weeks. Representative images of the resulting new bone are shown in Figure 3. As seen in Figure 3A, the new bone formation varied drastically with cell numbers. At no time did we observe bone formation or healing in the samples receiving 5 x 10^4 cells, suggesting that there is a threshold amount of BMP2 required for inducing bone formation. Alternatively, there was no statistical difference between the two highest cell numbers or doses (3B), indicating that there is a maximum bone formation response that can be achieved with this system. No bone formation was observed in with the 5 x 10^4 cell dose, whereas there is a significant 10 fold change in bone volume between the 5 x 10^5 and 5 x 10^7 cell doses. There was significant difference between the highest doses 5 x 10^6 and 5 x 10^7 suggesting that there this may be a maximum response to BMP2. For that reason, we used this dose for all subsequent experiments.

Bone Healing of the Fibula Defect:

We next determined the ability of the therapy to heal the critical size defect over 12 weeks. Figure 4 shows there is substantial bone formation at 2 weeks using this dose of cells, which appears to quickly resorb and by 4 weeks the new bone more closely resembles the fibula that it is replacing. However, as seen in the cross sectional μCT (Fig. 4F) new bone appears to be immature in nature. Although it spans the defect and is contiguous with the skeletal bone, it has not remodeled to have contiguous cortices, which suggests that this may not be well integrated at this stage. Alternatively, by 6-12 weeks a cortical bone structure begins to appear in the newly formed bone (Fig. 4H-J), suggesting that the bone is being remodeled and most likely fused. Bone healing and remodeling appears to be complete by 6 weeks (Fig. 4H) with little additional remodeling occurring at weeks 9 through 12. Interestingly, there appears to be additional bone attached to the skeletal bone (Fig. 4C-E), or actual residual heterotopic ossification that has not been resorbed. Additionally, some samples appeared to have a small amount of residual heterotopic ossification which was not attached to the fibula, but remained in the muscle between fibers.

We next looked at the bone architecture by analyzing cross-sectional cuts through the bone. The architecture appeared to change dramatically over the course of bone healing. Changes in bone architecture are a component of bone remodeling and aid in determining if the new bone has truly fused to the skeletal bone. Fusion at the defect site is a critical parameter in this system, because the majority of the new bone is made *de novo*, as heterotopic ossification, and it must fuse to the skeletal bone to complete healing. At 2 weeks the new bone is found throughout the skeletal defect (Fig. 4F); however, it appears to be immature bone, which has not remodeled or integrated into the adjacent skeletal bone. This is in contrast to the adjacent skeletal bone, which has well defined cortices and a hollow bone marrow cavity. Thus although

there is new bone, it does not appear to be well fused into the skeletal bone, or healed to the point such that it is one contiguous remodeled structure. However, by 6 weeks portions of the new bone appear to be remodeled with defined cortical bone and the tentative fusion site are less apparent (Fig. 4H), suggesting that the bone is integrated and almost completely healed. By 9 to 12 weeks, we observed integrated structures with the only abnormality being the additional small amounts of bone on the outer cortex (Fig. 4I-J).

We next examined the bone healing through histological analysis to confirm the remodeling and fusion of the newly formed bone with the skeletal bone. This requires bone remodeling to replace the woven bone and lamellar bone junction with integrated remodeled bone. Photomicrographs from representative samples of the healing fibulas show substantial immature bone that completely fills and surrounds the defect (Fig. 5). Over time however, the bone remodels considerably and new cartilage is no longer present in the tissues (Fig. 5B). By 6 weeks, the bone appears to be considerably more mature, with thicker cortical area that are contiguous with the skeletal cortical bone (Fig. 5C). Interestingly, the adjacent cortical bone appears to have a significant gap, which may represent either an area where the bone is vascularized, as evidenced by the pooling of blood or alternatively, a defect introduced during healing (Fig. 5C). However, this defect was not observed through radiograph analysis (Fig. 4C), suggesting that it comprises a relatively small region of the new bone. It is also of interest to note that in the serial sections where this cortex appears uniform and contiguous, the adjacent cortex now appears ruffled. This indicates that although it is healing, the new shape of the bone does not exactly mimic the original fibula. At 9 and 12 weeks, there is once more additional bone on the exterior of the fibula. However, the interior cortex appears uniform and similar to the normal fibula (figure 5D and E).

Discussion

These studies are the first to introduce a cell-based gene therapy system into a rat critical size defect model and have it lead to rapid replacement and repair of the bone. HO can successfully be induced and directed to heal a critical size defect even in bone conditions that favor bone resorption. The HO, once touching the skeletal bone, can prevent rapid resorption and enhance the bone formation, remodeling, and fusion. The overall complete healing occurs rapidly from 2 to 6 weeks with 100 percent healing and repair completed by 6 weeks. Interestingly, little remodeling or additional resorption appears to occur after this time. In many cases after the initial resorption, there are small amounts of bone either heterotopic or orthotopic that are associated with the structures and appear to persist. This may be due in part to the non-weight bearing nature of this bone.

The rat fibula was selected for this model based on the unique fusion of this bone to the adjacent tibia. Thus, the tibia functions as an external support and no additional fixation is required, allowing this to be a very fast and reliable model. To our surprise, studies to determine the critical distance that would be unable to heal on its own showed even a simple fracture led to rapid resorption and non-union of this bone. Interestingly, since this bone is non-weight bearing in the rodent due to the fusion with the tibia, the rapid resorption may be a result from the lack of forces on this bone. Similar phenomenon has been reported in cases where heterotopic ossification has become extensive enough to become weight bearing, leading to the almost complete resorption of the normal skeletal bone. Further, it has long been known that disuse of skeletal bone during immobilization can lead to elevated resorption. Therefore this model, beyond its versatility, becomes one of the most challenging of all bone repair models for the investigation of bone healing. With bone remodeling favoring resorption, contribution to new

bone formation is challenging and thus may be even more difficult to obtain fusion and complete repair.

Complete bone healing could be reliably achieved using a minimal dose of 5 x 10^6 AdBMP2 transduced cells. This number of cells yields approximately 93ngs of total BMP2 protein within culture supernatant over a five day period. Although lesser numbers of AdBMP2 transduced cells (5 x 10^5) or BMP2 (9 ngs) did result in heterotopic bone formation, it was not enough to reliably heal the fibula defect. Smaller doses, such as 1ng, were unable to induce HO. Delivery of additional cells beyond 5 x 10^6 resulted in a similar volume of bone, suggesting that there is an upper threshold at which BMP2 receptors are saturated and no additional response will occur. Further, the volume of bone obtained when 5 x 10^6 AdBMP2 transduced cells were delivered to the defect was larger than required for complete healing, and substantial resorption was observed within the first 2-4 weeks as the fibula regained its physiological shape.

Interestingly, recombinant BMP2 studies in rat shows that minimal bone formation is detected at protein levels less than 10 ugs [Vogelin et al., 2005], which is 130 times more BMP2 than we require for complete healing (Figure 2 and 3). This indicates that the BMP2 protein produced by the adenovirus transduced cells is likely more active or potent than the purified recombinant protein. In addition, this concentration is roughly in the range of physiological concentrations of BMP2, revealing that this system is very unique and perhaps should not be compared to systems employing the recombinant protein [Sciadini and Johnson, 2000; Vogelin et al., 2000; Vogelin et al., 2005]. The ability to generate, *in vivo*, biologically active BMP2 in the physiological range similar to what would be expected during bone fracture [Kloen et al., 2003; Kloen et al., 2002; Kugimiya et al., 2005] or reduction of blood flow [Yao et al., 2010] suggests

that the BMP2 produced *in vivo* in the eukaryotic cells may be mimicking physiological scenarios that lead to repair of fractures.

The kinetics of bone healing appears to be similar to fracture callus, with a large disorganized structure within the defect area initially formed and successive remodeling and resorption to produce a structure similar to the original fibula. The initial new bone was observed within 10 days of delivery, with the first emergence of a remodeled bone with cortical appearance and inner marrow cavity appearing at 6 weeks. However, approximately half of the samples at 6 weeks still had one cortical bone interface that did not appear contiguously remodeled yet (Fig. 4H), suggesting that the bone had not completely remodeled yet. However, at 9 weeks, all samples appeared to be well remodeled with visible contiguous cortical bone, suggesting that at this point all defects were reliably healed. We observed little change from 9 weeks to 12 weeks; although there was additional bone observed associated with the newly formed skeletal bone. The majority of the bone remodeling and resorption occurred within the first 4 weeks, where the callus-like structure resorbs and begins to form bone in the shape of the original fibula.

Histological analysis of the bone healing within the defect supports the subsequent findings. A large amount of mature bone and cartilage that extend away from the defect site are observed at 2 weeks (Fig. 5A). By 6 weeks and beyond, the bone was more restricted to the defect region (Fig. 5C-E). Although substantial immature woven bone was observed at 4 weeks, by 6 weeks remodeled bone with defined cortical structures could be seen (Fig. 5B-C), suggesting that substantial remodeling and maturation was occurring between 4 and 6 weeks. Again little change occurs histologically between 9 and 12 weeks, suggesting that the bone was maintained and healing was complete. Interestingly, in these tissues the cortical bone appeared to be contiguous. Since the exact shape of the original fibula was not achieved, this may

suggest that the signals which would direct and define the exterior cortices may be lacking in this model.

In conclusion, bone healing of a critical size defect in the rat fibula could be rapidly achieved through injection of a cell based gene therapy system. This system delivered 130 times less BMP2 protein compared to studies using recombinant protein as the osteoinductive agent and was able to induce bone within a physiological range of BMP2 concentration. Thus, this cell based approach is reliable, efficacious and importantly has additional safety in that no free virus or infectious agents of any kind would be delivered to patients. These studies are the first step in developing a cell based gene therapy which effectively harnesses the capacity of BMP2 to generate bone at target locations and rapidly repair skeletal bone.

Acknowledgments

This work was supported in part by grants from (Department of Defense DAMD W81XWH-07-1-0215, and Defense Advanced Research Agency, DARPA W911NF-09-1-0040) to E.A.O.

References:

Baltzer AW, Lattermann C, Whalen JD, Ghivizzani S, Wooley P, Krauspe R, Robbins PD, Evans CH. 2000. Potential role of direct adenoviral gene transfer in enhancing fracture repair. Clin Orthop Relat Res:S120-5.

Blum JS, Li RH, Mikos AG, Barry MA. 2001. An optimized method for the chemiluminescent detection of alkaline phosphatase levels during osteodifferentiation by bone morphogenetic protein 2. J Cell Biochem 80:532-7.

DeCoster TA, Gehlert RJ, Mikola EA, Pirela-Cruz MA. 2004. Management of posttraumatic segmental bone defects. J Am Acad Orthop Surg 12:28-38.

DeCoster TA, Simpson AH, Wood M, Li G, Kenwright J. 1999. Biologic model of bone transport distraction osteogenesis and vascular response. J Orthop Res 17:238-45.

Endo M, Kuroda S, Kondo H, Maruoka Y, Ohya K, Kasugai S. 2006. Bone regeneration by modified gene-activated matrix: effectiveness in segmental tibial defects in rats. Tissue Eng 12:489-97.

Finkemeier CG. 2002. Bone-grafting and bone-graft substitutes. J Bone Joint Surg Am 84-A:454-64.

Fouletier-Dilling CM, Gannon FH, Olmsted-Davis EA, Lazard Z, Heggeness MH, Shafer JA, Hipp JA, Davis AR. 2007. Efficient and rapid osteoinduction in an immune-competent host. Hum Gene Ther 18:733-45.

Gafni Y, Pelled G, Zilberman Y, Turgeman G, Apparailly F, Yotvat H, Galun E, Gazit Z, Jorgensen C, Gazit D. 2004. Gene therapy platform for bone regeneration using an exogenously regulated, AAV-2-based gene expression system. Mol Ther 9:587-95.

Gelse K, Jiang QJ, Aigner T, Ritter T, Wagner K, Poschl E, von der Mark K, Schneider H. 2001. Fibroblast-mediated delivery of growth factor complementary DNA into mouse joints induces chondrogenesis but avoids the disadvantages of direct viral gene transfer. Arthritis Rheum 44:1943-53.

Giannoudis PV, Atkins R. 2007. Management of long-bone non-unions. Injury 38 Suppl 2:S1-2.

Gugala Z, Olmsted-Davis EA, Gannon FH, Lindsey RW, Davis AR. 2003. Osteoinduction by ex vivo adenovirus-mediated BMP2 delivery is independent of cell type. Gene Ther 10:1289-96.

Haidar ZS, Hamdy RC, Tabrizian M. 2009. Delivery of recombinant bone morphogenetic proteins for bone regeneration and repair. Part B: Delivery systems for BMPs in orthopaedic and craniofacial tissue engineering. Biotechnol Lett 31:1825-35.

Hollinger JO, Schmitt JM, Buck DC, Shannon R, Joh SP, Zegzula HD, Wozney J. 1998. Recombinant human bone morphogenetic protein-2 and collagen for bone regeneration. J Biomed Mater Res 43:356-64.

Jeon O, Song SJ, Kang SW, Putnam AJ, Kim BS. 2007. Enhancement of ectopic bone formation by bone morphogenetic protein-2 released from a heparin-conjugated poly(L-lactic-co-glycolic acid) scaffold. Biomaterials 28:2763-71.

Kloen P, Di Paola M, Borens O, Richmond J, Perino G, Helfet DL, Goumans MJ. 2003. BMP signaling components are expressed in human fracture callus. Bone 33:362-71.

Kloen P, Doty SB, Gordon E, Rubel IF, Goumans MJ, Helfet DL. 2002. Expression and activation of the BMP-signaling components in human fracture nonunions. J Bone Joint Surg Am 84-A:1909-18.

Kugimiya F, Kawaguchi H, Kamekura S, Chikuda H, Ohba S, Yano F, Ogata N, Katagiri T, Harada Y, Azuma Y, Nakamura K, Chung UI. 2005. Involvement of endogenous bone morphogenetic protein (BMP) 2 and BMP6 in bone formation. J Biol Chem 280:35704-12.

Laurencin C, Khan Y, El-Amin SF. 2006. Bone graft substitutes. Expert Rev Med Devices 3:49-57.

Lieberman JR, Le LQ, Wu L, Finerman GA, Berk A, Witte ON, Stevenson S. 1998. Regional gene therapy with a BMP-2-producing murine stromal cell line induces heterotopic and orthotopic bone formation in rodents. J Orthop Res 16:330-9.

Motsitsi NS. 2008. Management of infected nonunion of long bones: the last decade (1996-2006). Injury 39:155-60.

Moutsatsos IK, Turgeman G, Zhou S, Kurkalli BG, Pelled G, Tzur L, Kelley P, Stumm N, Mi S, Muller R, Zilberman Y, Gazit D. 2001. Exogenously regulated stem cell-mediated gene therapy for bone regeneration. Mol Ther 3:449-61.

Olmsted-Davis EA, Gugala Z, Gannon FH, Yotnda P, McAlhany RE, Lindsey RW, Davis AR. 2002. Use of a chimeric adenovirus vector enhances BMP2 production and bone formation. Hum Gene Ther 13:1337-47.

Olmsted EA, Blum JS, Rill D, Yotnda P, Gugala Z, Lindsey RW, Davis AR. 2001. Adenovirus-mediated BMP2 expression in human bone marrow stromal cells. J Cell Biochem 82:11-21.

Sciadini MF, Johnson KD. 2000. Evaluation of recombinant human bone morphogenetic protein-2 as a bone-graft substitute in a canine segmental defect model. J Orthop Res 18:289-302.

Sen MK, Miclau T. 2007. Autologous iliac crest bone graft: should it still be the gold standard for treating nonunions? Injury 38 Suppl 1:S75-80.

Sorger JI, Hornicek FJ, Zavatta M, Menzner JP, Gebhardt MC, Tomford WW, Mankin HJ. 2001. Allograft fractures revisited. Clin Orthop Relat Res:66-74.

Thies RS, Bauduy M, Ashton BA, Kurtzberg L, Wozney JM, Rosen V. 1992. Recombinant human bone morphogenetic protein-2 induces osteoblastic differentiation in W-20-17 stromal cells. Endocrinology 130:1318-24.

Tzioupis C, Giannoudis PV. 2007. Prevalence of long-bone non-unions. Injury 38 Suppl 2:S3-9.

Vogelin E, Brekke JH, Jones NF. 2000. [Heterotopic and orthotopic bone formation with a vascularized periosteal flap, a matrix and rh-BMP-2 (bone morphogenetic protein) in the rat model]. Mund Kiefer Gesichtschir 4 Suppl 2:S454-8.

Vogelin E, Jones NF, Huang JI, Brekke JH, Lieberman JR. 2005. Healing of a critical-sized defect in the rat femur with use of a vascularized periosteal flap, a biodegradable matrix, and bone morphogenetic protein. J Bone Joint Surg Am 87:1323-31.

Vyrostek SB, Annest JL, Ryan GW. 2004. Surveillance for fatal and nonfatal injuries--United States, 2001. MMWR Surveill Summ 53:1-57.

Watson JT, Anders M, Moed BR. 1995. Management strategies for bone loss in tibial shaft fractures. Clin Orthop Relat Res:138-52.

Winn SR, Hu Y, Sfeir C, Hollinger JO. 2000. Gene therapy approaches for modulating bone regeneration. Adv Drug Deliv Rev 42:121-38.

Yao Y, Bennett BJ, Wang X, Rosenfeld ME, Giachelli C, Lusis AJ, Bostrom KI. 2010. Inhibition of bone morphogenetic proteins protects against atherosclerosis and vascular calcification. Circ Res 107:485-94.

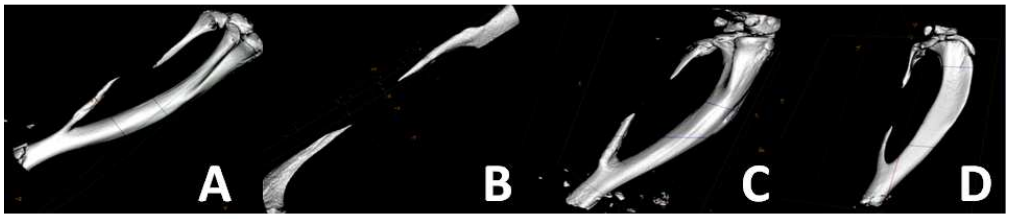

Figure 1: Representative three dimensional reconstructions of rat fibulas through microcomputational analysis.
Varying sizes of defects (1 mm - 10 mm) were surgically introduced into rat fibulas and two weeks later analyzed for the presence of bone repair. The results depicted show an approximately 10 mm defect independent of the original defect size (A) 1 mm, (B) 2 mm, (C) 5 mm and (D) 10 mm.

254x190mm (96 x 96 DPI)

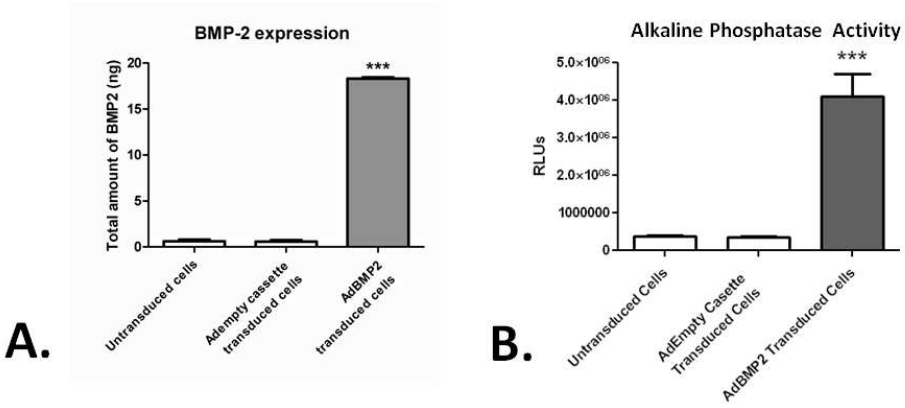

Figure 2: Quantification of BMP2 protein and activity from adenovirus transduced cells.
A. BMP2 activity in culture supernatant collected 72 hours after transduction with AdBMP2- or AdEmpty cassette-transduced cells (25000vp/cell) was quantified using an ELISA. BMP2 protein is represented as total protein produced by 5 x 106 cells. Error bars represent means ± SD for n=5. A student t-Test was applied to demonstrate significance.
B. Alkaline phosphatase activity in W20-17 cells after addition of conditioned media from AdBMP2- or AdEmpty cassette-transduced cells (25000 vp/cell). To demonstrate endogenous levels of alkaline phosphatase we included the cells alone. Alkaline phosphatase activity is depicted as the average relative chemiluminescence units (RLU), where n=3. Error bars represent means ± SD for n=3. A Student t-Test was applied to demonstrate significance.

254x190mm (96 x 96 DPI)

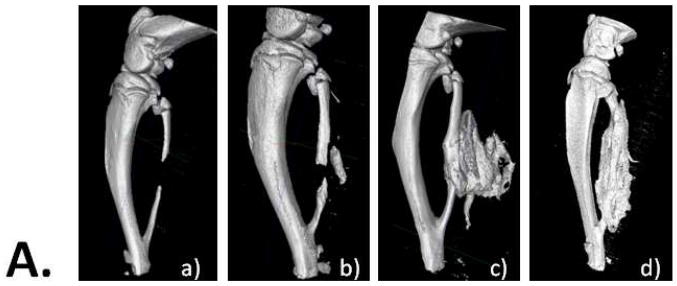

Figure 3: Resultant bone formation from the introduction of adenovirus transduced cells into the defect site.
A. Representative three dimensional surface renderings obtained from micro computational analysis of the resultant bone repair two weeks after introduction of critical size defect in the rat fibula and delivery of varying numbers of AdBMP2 transduced cells; (a) 5 x 104 cells (b) 5 x 105 (c) 5 x 106 (d) 5 x 107.

254x190mm (96 x 96 DPI)

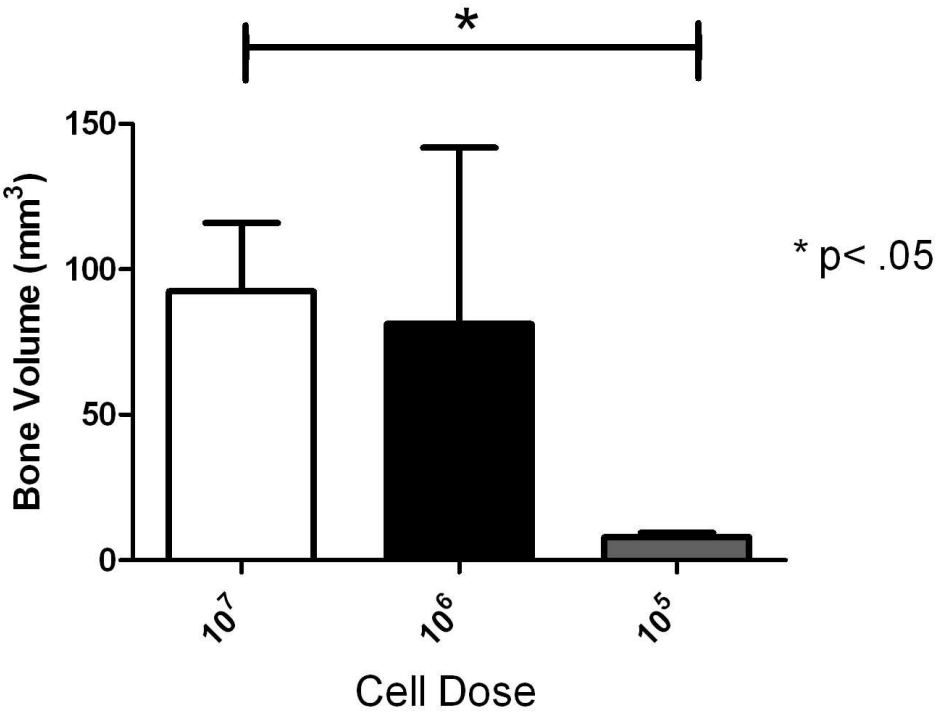

B. Quantification of the bone repair using microcomputational analysis. Bone volume of the newly forming bone as depicted in Figure 3A, was calculated for each cell dose (n=5 per group). The means and standard deviations for each group were calculated and compared using a one-way analysis of variance.
116x91mm (300 x 300 DPI)

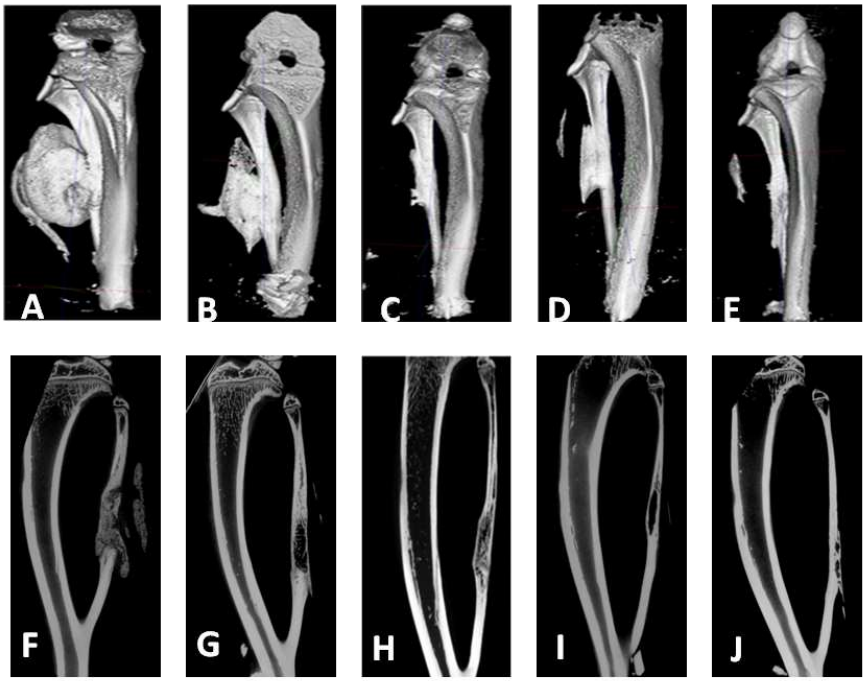

Figure 4: Micro-computational analysis of bone healing over time. Representative three dimensional surface renderings (A-E) or two dimensional reconstructions (F-J) of bone healing over time; (A and F) 2 weeks; (B and G) 4 weeks; (C and H) 6 weeks; (D and I) 9 weeks; and (E and J) 12 weeks after introduction of the AdBMP2 transduced cells in the fibula defect; n=9 per group.
254x190mm (96 x 96 DPI)

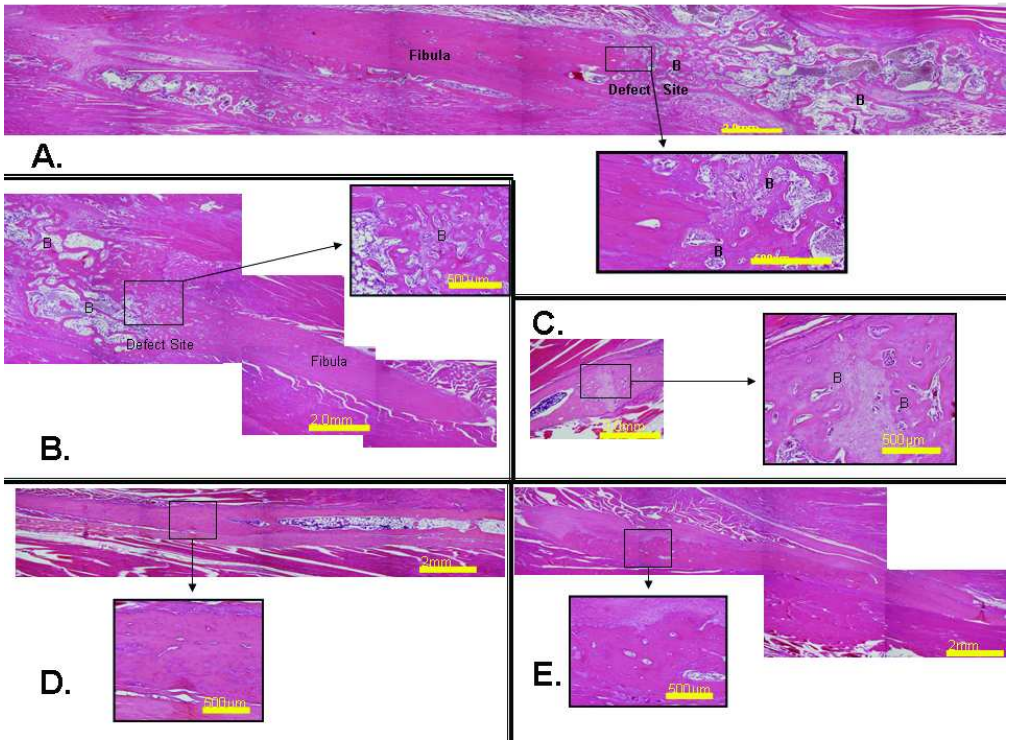

Figure 5: Representative photomicrographs of the fibula defect at various times after introduction of the AdBMP2 transduced cells. Tissues were formalin fixed decalcified, paraffin embedded and serial sectioned (5 µm) through the entire fibula region. Every fifth section was hematoxylin and eosin stained, and images taken which were representative of the defect region in particular the junction with the fibula at various times, (A) 2 weeks, (B) 4 weeks, (C) 6 weeks, (D) 9 weeks, and (E) 12 weeks. The appearance of bone is identified with [B].
254x190mm (96 x 96 DPI)

Sensory Nerve Induced Inflammation Contributes to Heterotopic Ossification

Elizabeth Salisbury[1,2], Eric Rodenberg[1] , Corinne Sonnet[1], John Hipp[4], Francis Gannon[3,4], Tegy Vadakkan[6], Mary Dickinson[1,6], Elizabeth A. Olmsted-Davis[1,2,4,7] , and Alan R. Davis[1,2,4,7]

[1]Center for Cell and Gene Therapy; [2] Translational Biology and Molecular Medicine and Departments of [3]Pathology, [4]Orthopaedic Surgery, [5]Neuroscience, [6]Biophysics and [7] Pediatrics, Baylor College of Medicine, Houston, TX 77030, USA

Number of text pages: 25
Number of figures: 6 figures and 1 supplemental figure

Corresponding author: Alan R. Davis
Baylor College of Medicine
One Baylor Plaza, Alkek N1010
Houston, TX 77030
713-798-1237 (phone)
713-798-1230 (fax)
ardavis@bcm.edu

Grant support: US Department of the Army (DAMD W81XWH-07-1-0214, DAMD W81XWH-07-1-0215), NBIB (EB005173), NIH (T-32 HL092332-06), American Heart Association (AHA 10815339F), Kirschstein-NRSA (T32 HL092332-08)

Abstract

Heterotopic ossification (HO), or bone formation in soft tissues, is often the result of traumatic injury. Much evidence has linked the release of BMPs (Bone Morphogenetic Proteins) upon injury to this process. HO was once thought to be a rare occurrence, but recent statistics from the military suggest that as many as 60% of traumatic injuries, resulting from bomb blasts, have associated HO. In this study, we attempt to define the role of peripheral nerves in this process. Since BMP2 has been shown previously to induce release of the neuroinflammatory molecules, substance P (SP) and calcitonin gene related peptide (CGRP), from peripheral, sensory neurons, we examined this process *in vivo*. These neuroinflammatory molecules are rapidly expressed within the tissues, upon delivery of BMP2, and remain elevated throughout bone formation. Animals lacking functional sensory neurons ($TRVP1^{-/-}$) were unable to upregulate SP and CGRP in response to BMP2, and the resultant HO in these animals was significantly inhibited, suggesting that neuroinflammation plays a functional role. Additionally, mast cells, known to be recruited by SP and CGRP, were significantly elevated 48 hours after induction of HO, and were localized to the nerve structures and undergoing degranulation. When degranulation was inhibited using cromolyn, HO was again reduced significantly to levels similar to those observed in animals lacking TRVP1-containing neurons. Immunohistochemical analysis revealed nerves expressing the stem cell markers, nanog and Klf4, as well as the osteoblast marker osterix, after BMP2 induction, in mice treated with cromolyn. The data collectively suggests that BMP2 can act directly on sensory neurons to induce neurogenic inflammation, resulting in nerve remodeling and the migration/release of osteogenic, as well as other, stem cells from the nerve. Further, blocking this process significantly reduces HO, suggesting that the stem cell population contributes to bone formation.

Introduction

Bone morphogenetic proteins, named for their original isolation from ground bone[1], are a family of factors involved in patterning of the early embryo, bone, vessels [2], nerves [3] , blood [4], and, most recently, fat [5, 6]. The BMPs appear to serve a similar role in the adult, where they have been shown to regulate the expansion and differentiation of progenitors for these same tissues [7]. One of the best studied of the BMPs, BMP2, is a highly conserved protein that has been shown to be the only common link between the various forms of heterotopic ossification (HO) [8 9 10].

HO, or bone formation at non-skeletal sites, is a disorder resulting from traumatic injury [11], with approximately 5% of all traumatic injuries leading to HO. HO has been linked specifically to the nervous system, as it appears after injury of the central nervous system (CNS) [12]. Maintenance of skeletal bone has been demonstrated to involve the CNS, through hypothalamic control of a number of neuroendocrine factors believed to directly regulate osteoblast function [13 14 15 16 17]. However, it is unclear that this mechanism results in the formation of ectopic bone. Some of the most compelling data linking HO formation to changes in the peripheral (PNS) or central nervous system comes from recent statistics from the military, which suggest that 60% of all combat injuries have associated HO[18]. This is presumably because these are mostly blast or burn injuries, both having a significant impact on the PNS and CNS.

Little is known about the causes of HO, beyond the common link to changes in BMP signaling. BMP2 has been shown to be elevated upon muscle injury and changes in blood flow, and BMP2 is released during bone injury [19 20 21 22]. Recently, BMP2 has also been shown to directly induce release of neuroinflammatory proteins from sensory neurons. Studies revealed the rapid up-regulation of substance P (SP) and calcitonin gene related peptide (CGRP) in sensory neuron cultures, after addition of recombinant BMP2 [23].

The afferent, sensory fibers of the PNS release SP and CGRP leading to the induction of neuroinflammation. These sensory neurons are stimulated by noxious mechanical, thermal, or chemical stimuli, providing feedback on pain and temperature [24], both locally and centrally through electrical signaling. The vanilloid (capsaicin) receptor TRPV1 (transient receptor potential cation channel V1) is a nociceptive ion channel located on sensory nerve endings that is activated by some of these noxious stimuli and involved in the mediation of pain [25 26]. Capsaicin, the compound in hot chili peppers, is one chemical stimulus, which can activate this channel, causing it to open, leading to an influx of calcium and sodium ions into the sensory neuron and triggering its depolarization. At normal levels, capsaicin binding transmits the sensation of pain. However, high doses of capsaicin lead to a massive influx of ions, resulting in death of sensory neurons expressing TRPV1. TRPV1 sensory neurons have been linked to a number of activities involving tissue regeneration and maintenance [27], including repair of bone fractures, which were shown to be significantly inhibited when these nerves were ablated with capsaicin [28].

Morrison *et al* [29] isolated cells indistinguishable from neural crest stem cells from fetal peripheral nerves. Recently [30], such cells have been shown to be the origin of melanocytes in the skin in the adult. In addition, the bone tumor Ewing's sarcoma is composed of poorly differentiated cells that bear no relationship to mesenchymal cells, but show a definite relationship to neural crest stem cells [31 32]. This, coupled with the fact that some of the bones of the skull have been shown, using tracking techniques, to originate from the neural crest [33] , opens the question of whether osteogenic progenitors may have an alternative niche, in addition to the bone marrow and periosteum. We provide evidence in these studies that suggest that such a site may indeed be local peripheral nerves.

We developed a model of rapid, *de novo* bone formation, or heterotopic ossification, which relies on expression of physiological levels of BMP2 at the site of bone formation [34 35 36].

Upon delivery of adenovirus-transduced cells expressing BMP2 within the muscle, a cascade of endochondral bone formation occurs over seven days, resulting in mature bone and bone marrow [37] [38]. In the studies described here, we have used this model to elucidate the manner in which peripheral nerves participate in HO.

Materials and Methods

Cell Culture: A murine C57BL/6-derived cell line (MC3T3-E1) was grown in αMEM supplemented and cultured at a subconfluent density to maintain the phenotype. All cell types were grown at 37°C and 5% CO_2 in humidified air.

Adenoviruses and cell transduction: Replication defective E1-E3 deleted first generation human type 5 adenovirus (Ad5) were constructed to contain cDNAs for BMP2 in the E1 region of the virus [34] or did not contain any transgene in this region, Adempty. MC3T3-E1 cells (1×10^6) were transduced with Ad5-BMP-2 or Ad5-empty control virus at a concentration of 5000 vp/cell with 1.2% GeneJammer, as described previously [39].

Heterotopic bone assay: The transduced cells were resuspended at a concentration of 5×10^6 cells/100 μL of PBS and then delivered through intramuscular injection into the hind limb quadriceps muscle of C57BL/6 or $TRVP1^{-/-}$ mice. (8–12 weeks old; Jackson Laboratories, Bar Harbor, ME). Sample sizes are indicated in figure legends. Animals were euthanized, as indicated in the text, either at daily intervals, or 10 days after injection of the transduced cells. Hind limbs were harvested and either placed in formalin or quick frozen and stored at -80°C. All animal studies performed were in accordance with standards of the Baylor College of Medicine, Department of Comparative Medicine, after review and approval of the protocol by the Institutional Animal Care and Use Committee (IACUC).

Cromolyn administrations: Intraperotoneial injections of sodium cromoglycate (C0399; Sigma-Aldrich, St. Louis, MO) were administered daily (8mg/kg/day) for five days prior to intramuscular injection of transduced cells, and then continued daily throughout the time course of the heterotopic bone assay. Control animals were given intraperotoneial injections of the vehicle, phosphate buffered saline (PBS), following the same treatment regimen as experimental animals. Animals were sacrificed at specified time points following injection of transduced cells.

Immunohistochemical Analysis: Mouse hind limbs were isolated, formalin fixed and cut in half prior to decalcification, processing, and paraffin embedding. The tissues were serial sectioned (5μm), and every fifth slide subject to hematoxylin and eosin staining as previously described [37]. Serial unstained slides were used for immunohistochemical staining (either single- or double-antibody labeling), using methods outlined previously. For double-antibody labeling, samples were treated with both primary antibodies simultaneously, followed by washing and incubation with respective secondary antibodies, used at 1:500 dilution, to which Alexa Fluor 488, 594, or 647 was conjugated. Primary antibodies were used as follows: Substance P, rat monoclonal, used at 1:250 dilution (Santa Cruz Biotechnology, Inc, Santa Cruz, CA, USA) and CGRP, rabbit polyclonal, used at 1:250 dilution (Biomol/Enzo LifeSciences, Plymouth Meeting, PA, USA) neurofilament, mouse monoclonal, (Sigma, St Louis, MO, USA), used at 1:200 dilution, Klf4, goat polyclonal (R&D Systems, Minneapolis, MN,USA), used at 1:200 dilution, nanog, goat polyclonal (Novus Biologicals, Littleton, CO, USA), osterix, goat or rabbit polyclonal (Santa Cruz Biotechnology, Inc, Santa Cruz, CA, USA) used at 1:200, and VWF, rabbit polyclonal, (Chemicon, Billerica, MA, USA), used at 1:250. Primary antibodies were either diluted in PBS and 10% serum of the species in which the secondary antibody was generated, or for mouse primary antibodies, staining was performed using the M.O.M. Kit (Vector Labs, Burlingame, CA,

USA). Tissues were mounted and counterstained using Vectashield mounting medium containing DAPI (Vector Laboratories, Burlingame, CA). Stained tissue sections were examined using an Olympus BX41 microscope equipped with a reflected fluorescence system, using a 20x/0.75 NA objective lens 10X, 40X, 100X. Stained tissue sections were examined by confocal microscopy (LSM 510 META, Zeiss, Inc., Thornwood, NY, USA) using a 20×/0.75NA objective lens.

Toluidine blue staining: Decalcified, paraffin embedded tissue sections were stained with toluidine blue, to specifically identify mast cells. Toluidine blue O (Sigma, Chemical Company, St Louis, MO, USA) was reconstituted in 70% ethanol, and then diluted at a ratio of 1:10 in 1% sodium chloride (pH=2.3) for subsequent staining. After deparaffinization and hydration, sections were stained in the working solution of toluidine blue for 10 minutes, washed, dehydrated, and cover-slipped with resinous mounting medium. The number of toluidine blue (TB) positive cells in an area of the tissue was calculated by adding the number of positive cells counted in each of the fields taken within the area. The area fraction of TB^+ cells was defined as the total number of TB^+ cells within the area divided by the number of fields taken in that area. The TIFF images of the histological sections were first inverted using ADOBE Photoshop. In the inverted images, the mast cells appeared as bright spots. The number of mast cells in each inverted image was counted by segmenting the cells using FARSIGHT (RPI, Troy, New York). The area fraction was measured for five different fields, and the average area fraction was calculated for control and BMP-treated tissues for every fifth slide sectioned throughout the entire hind limb. The area fractions of TB^+ cells in the control and the BMP-treated tissues on day 2 were 3 and 8.33, respectively. Based on the Student's *t* test, the *p* value for the day 2 data was 0.02.

Protein Extraction and Analysis: Protein from the entire quadriceps muscle, injected with either Ad5BMP2 or Ad5empty transduced cells, was isolated using the Total Protein Extraction Kit (Millipore, Billerica, MA), following manufacturer's instructions. Muscle samples (n=4) were collected every day, for 6 days following injection. Total protein concentrations of each sample were determined using the BSA Protein Assay Kit (Pierce/ ThermoScientific, Rockford, IL). Quantification of protein levels of both Substance P and CGRP were assayed by Enzyme Immunoassay (EIA) (EK-061-05 and EK-015-09; Phoenix Pharmaceuticals, Inc., Burlingame, CA). For each EIA assay, samples were equally loaded based on the total protein concentration, and measured in duplicate. Results from each day were averaged, and the difference in protein levels in control and BMP2 samples assessed by standard *t*-test analysis. The differences in protein levels over time were analyzed by one-way analysis of variance tests (ANOVA) and post-hoc Bonferroni multiple comparisons tests comparing time points, using Stata Ver II (College Station, TX).

Microcomputed tomography

Micro-CT exams were obtained of the left and right legs at 15 μm resolution (eXplore Locus SP; GE Healthcare, London, ON, Canada). A hydroxyapatite phantom was scanned alongside each specimen and was used to convert the scan data from arbitrary units to units of equivalent bone density. The scans were thresholded to exclude any tissue with a density less than 100 mg/cc, and the tissue volume within the region of interest was calculated as a measure of the total amount of mineralized tissue. The resulting data were analyzed by one-way analysis of variance to identify differences.

Results

Induction of substance P and CGRP through delivery of AdBMP2 transduced cells:

To determine if BMP2 directly activates expression of the neuroinflammatory proteins SP and CGRP during heterotopic ossification, proteins were isolated from tissues at daily intervals, starting 24 hours after delivery of AdBMP2 or Adempty (control virus) transduced cells, through the appearance of heterotopic bone. Quantification of protein levels of SP and CGRP within the tissues, through ELISA, is shown in figure 1A and B, respectively. Both proteins appear to be significantly elevated ($p \leq 0.0005$), compared to controls, within 24 hours after induction of HO, and again at 72 hours ($p \leq 0.005$) and 6 days ($p \leq 0.05$) after induction. Expression, therefore, appeared somewhat cyclical, and statistical analyses, using a one-way ANOVA with a post-hoc Bonferroni test for comparison between time points, verified a significant drop in SP and CGRP between days 1 and 2 ($p \leq 0.005$). This was followed by a significant rise between days 2 and 3 ($p \leq 0.005$). The data suggests that BMP2 induced a substantial and immediate release of these proteins, which was attenuated, but then continued for the remainder of endochondral bone formation, through the appearance of mineralized bone (Figure 1).

Tissues were next immunostained for the presence of SP and CGRP and analyzed to determine if the expression of these factors was associated with nerves throughout the entire hind limb, or limited to the region of new bone formation. Figure 2 shows representative images of the expression of SP and CGRP within the tissues isolated 4 days after receiving either AdBMP2 or Adempty transduced cells. By day 4 of HO, delivery cells are no longer found within the tissues, and the control appears as normal muscle (Figure 2D). However, there is a nidus of cartilage forming in tissues undergoing HO (Figure 2A). Figure 2 shows the positive expression of SP (green) or CGRP (red) in these tissues. As seen in figure 2, panels D-F, we observed a small amount of positive expression associated with a mature nerve structure within control tissues, but expression was not found within the muscle itself. In contrast, in tissue receiving

BMP2, expression was co-localized with the region undergoing cartilage formation and was limited to this region. This suggests that the expression of these factors is associated with BMP2, as predicted, and the continued expression of these factors was localized to new cartilage and bone formation.

Inhibition of HO in animals lacking TRVP1: The induction of neuroinflammatory mediators occurs through activation of sensory neurons by localized stimulus, or, in this case, secretion of BMP2. To determine if induction of neuroinflammation is contributing to HO, bone formation was quantified in animals that lacked TRPV1 ($TRVP1^{-/-}$), resulting in a functional loss of activity of sensory neurons. These $TRVP1^{-/-}$ animals lack a functional cationic channel on peripheral, sensory nerve terminals, which regulate neurogenic inflammation. We quantified the changes in SP and CGRP protein expression within tissues isolated from these knockout animals, and observed a significant suppression compared to the wild type counterpart (supplemental data 1), although we did observe a slight increase in their expression upon delivery of BMP2.

HO was induced in both $TRVP1^{-/-}$ and wild type mice (n=7), and, after 10 days, the resultant bone formation was quantified through micro-computed tomography (μCT). Figure 3A shows a representative three dimensional reconstruction of the bone formation. Heterotopic bone volume within $TRVP1^{-/-}$ mice was inhibited significantly ($p \leq 0.05$), as compared to wild type mice (Figure 3B).

Neuroinflammatory associated changes in mast cells:

The reduction of HO when there is a lack of functional TRVP1 signaling suggests that this pathway may be functionally important to the process of HO. The next step in neuroinflammatory signaling involves recruitment of mast cells and their resultant degranulation, for the release of key enzymes involved in processing proteins essential for inflammatory signaling and recruitment. To determine whether mast cells were recruited to the site of new

bone formation, muscle tissues from the hind limbs of wild type mice injected with AdBMP2 or Adempty transduced cells were isolated at daily intervals and then serially sectioned in entirety for quantification. There appears to be a trend toward more mast cells within the tissues undergoing HO, as compared to the control tissues (figure 4A). However, only day 2 shows a statistically significant increase in the number of mast cells. It is intriguing that we observed the most significant difference at these early stages, since this appears to parallel our findings for the release of SP and CGRP within the tissues, suggesting mast cells may be recruited after release of these factors.

Since mast cells are known to migrate throughout the tissues, co- localization with specific tissue structures was also noted. As seen in figure 4C, mast cells appeared to be scattered throughout the control tissues. However, within the tissues receiving AdBMP2 transduced cells, mast cells associated only with the nerves (figure 4B), in tissues isolated 2 days after induction of bone formation. As bone formation continues, the mast cells within the tissues receiving BMP2 continue to be localized within the nerve itself; however, a subset also appear within the vessel structures (data not shown). We did not see mast cells localizing within the nerve structures in control tissues at any time point.

Mast cell degranulation leads to the release of degradative enzymes, such as tryptase and chymase. These enzymes are known to degrade or process other proteins, leading to their activation. Many of the enzymes are involved in tissue remodeling, including the nerve structure itself. To determine if mast cell degranulation could be a factor in heterotopic ossification, animals were pretreated with the drug sodium cromoglycate (cromolyn), which has been shown to prevent mast cell degranulation. Following the pretreatment with either cromolyn or a vehicle control (PBS), HO was induced and the resultant bone formation quantified 10 days later. Figure 5A shows representative images of three dimensional reconstructions of the resultant HO formation after cromolyn or control, PBS treatment. As can be seen in figure 5B, quantification

of bone volume of the HO shows a significant ($p \leq 0.05$) decrease in animals after cromolyn treatment. The observed decrease in HO formation after cromolyn treatment was similar to that observed in the TRVP1 null mice, thus supporting the idea that suppression of this pathway inhibits HO.

The data collectively suggests a molecular model in which sensory neurons signal to induce neuro-inflammatory mediator expression and mast cell migration and degranulation, which ultimately facilitate HO. Since others have shown that progenitors reside within the nerve sheath [30] and can expand upon nerve remodeling after injury, we analyzed the nerves isolated in hind limb tissues from cromolyn or vehicle treated animals after induction of HO. We hypothesized cromolyn treatment would block nerve remodeling, and thus, the ultimate release of progenitors perhaps residing within the nerve. The tissues were immunostained for expression of a variety of stem cell markers, and, intriguingly, we observed changes in the subset of markers related to pluripotency. Figure 6A shows representative photomicrographs of tissues immunostained for expression of Nanog and Krüppel-like family of transcription factor 4 (Klf4) within the tissues isolated two days after induction of HO. As seen in 6A, in animals that received cromolyn, cells positive for these factors were observed throughout the nerve (Fig 6A; c,d), as demonstrated by neurofilament staining (Fig 6A; b,f). However, in tissues isolated from animals that received vehicle, these markers were significantly reduced, to completely absent throughout the nerve (Fig 6A; g,h). We observed $nanog^+$ and $Klf4^+$ cells within tissues isolated from wild type animals undergoing HO, but such cells are rare and are often not co-localizing with the nerve. Both these markers have been implicated in maintenance of the pluripotential phenotype observed in embryonic stem (ES) cells, with Klf4 actually enhancing the expression of the nanog gene in ES cells. Interestingly, the osteoblast specific transcription factor osterix was also found associated with the nerve sheath (figure 6B). Osterix expression was observed in the nerve by co-staining with the neural marker neurofilament (Figure 6B; g, h, i), in tissues

isolated 2 days after BMP2 induction, in the presence of cromolyn. These osterix positive cells also appeared to co-localize with a portion of the primitive stem cell factors, suggesting that a subset of the cells may be undergoing differentiation (Figure 6B, panels a-f).

Discussion

Heterotopic ossification is a disorder involving rapid bone formation within muscle, tendon, and ligaments, adjacent to skeletal bone, and it has been linked to an elevation in BMP2 signaling. Further, the incidence of HO appears to be dramatically increased in individuals who have sustained traumatic injury to the central nervous system. Here we determined whether localized changes in BMP signaling, which lead to heterotopic bone formation, can also alter peripheral nerve signaling through induction of neuroinflammation. Our results suggest that in the presence of BMP2, sensory neurons express mediators of neuroinflammation, resulting in the recruitment of mast cells and remodeling of the nerve structure.

BMP2 has been shown previously to induce the expression of the neuroinflammatory mediators, substance P and CGRP, in sensory neuron cultures. Here we quantified changes in these mediators, *in vivo,* after delivery of cells expressing BMP2. We found a significant and immediate elevation of both proteins, in relation to the control, which received the same cells transduced with an Adempty virus. Interestingly, we observed a strong correlation in elevation of these mediators, immediately following our delivery of BMP2. However, as the process continued over time, we observed a cyclical pattern in the expression of these mediators, with a significant decline in expression on day 2, followed by a significant rise in expression on day 3, and a trend towards another increase in expression by day 6. Although BMP2 would presumably be expressed for the first 3-4 days, prior to the rapid clearance of the cells [36], the kinetics of BMP2 receptor signaling in this model is unclear. Intriguingly, one of the first steps is the rapid formation of brown adipocytes within the tissues [37]. We have previously shown brown

adipocytes to be necessary for patterning of the new bone, by their unique capacity to regulate the oxygen microenvironment, not only by stimulation of new vessels, but also by uncoupling of aerobic respiration and "burning" of oxygen [37]. The result of this uncoupling is a release of energy as heat, which could potentially re-stimulate sensory neurons to respond and release substance P and CGRP. This could potentially explain the observed cyclical nature of the response, suggesting secondary or tertiary signaling events.

Performing the assay in animals lacking TRPV1, we saw a significant decrease in the volume of heterotopic bone formed, compared to animals with functional TRVP1. The suppression, rather than complete ablation, suggests that other TRVP family members present on sensory neurons may also contribute to the induction of HO. Although we do not rule out alterations in other peripheral nerve signaling to the central nervous system in these animals, both substance P and CGRP were found to be significantly decreased in the TRVP1$^{-/-}$ mice. We still observed a trend towards an increase in substance P and CGRP, upon addition of the AdBMP2 transduced cells. However, this was not above the normal background levels observed in wild type mice, so it is unclear whether this contributes to HO.

Mast cells are known to be recruited to nerves during times of neuroinflammation. Upon degranulation, mast cells release a number of digestive factors, chymase, tryptase, and other enzymes, which can cleave proproteins, leading to their activation. These factors appear to be essential for tissue remodeling of not only the nerve, but also, other surrounding tissues, including the vasculature [24 40 41 42 43]. Nerve remodeling is thought to be part of neurite outgrowth, or the ability to remodel and extend neurons. Perhaps this process is utilized to innervate the newly forming HO. Alternatively, Adameyko *et al* recently demonstrated the presence of a stem cell population residing within peripheral nerves that would migrate from the nerve, to undergo melanocyte differentiation [30]. We quantified the number of mast cells after induction of HO and found a significant elevation in this population within 48 hours, when

compared to tissues receiving the control cells. However, we did observe an upward trend in the number of mast cells on all days. Further, we observed the mast cells, within the first 48 hours, associating with the nerves and within the nerves, as compared to control tissues where the mast cells were usually located randomly throughout the tissues. Although not shown here, we did observe the mast cells associating with vessels, as well as nerves, later in the time course, suggesting that there is also a secondary vascular remodeling that may be triggered through this process. In line with these results, mast cells have also been observed in the human, genetic disease of HO, fibrodyplasia ossificans progressiva [44].

Additionally, mast cells, like platelets, store serotonin, presumably derived from the gut, and release it in an active form upon degranulation [45]. Serotonin, which has recently been linked to skeletal bone remodeling [14], is then capable of stimulating sympathetic neurons, which can ultimately regulate adipose production. Serotonin released by the gut has been reported to favor bone resorption during bone remodeling, whereas serotonin released in the hypothalamus appears to enhance bone formation and increase osteogenesis. Although it is still unclear how serotonin release contributes to HO, we have previously reported that brown adipocytes are made rapidly in the local tissues, presumably through activation of sympathetic neurons [46]. Thus, it seems likely that serotonin release may aid in the production and activation of adipocytes necessary for creating a microenvironment conducive for formation and patterning of bone.

We next looked at whether the nerve remodeling was releasing cells that were essential to bone formation. As noted above, it has been previously demonstrated that precursors in peripheral nerves are the origin of skin melanoctyes. Therefore, mast cell degranulation, and subsequent nerve remodeling, was blocked using cromolyn. We observed a decrease in HO, similar to that seen in studies using the TRVP1$^{-/-}$ mice. We next analyzed the nerves from these animals and found an increase in cells expressing markers of early stem cells (nanog and Klf4).

These primitive markers were sporadic in the nerves of untreated animals, but completely covered the nerve in the cromolyn treated animals. This not only suggests that the early tissue changes lead to expansion of these cells, but also that the pool size of these cells within the nerve of untreated animals is extremely low, due to concomitant and rapid migration and differentiation. However, blockade of these latter steps with cromolyn leads to accumulation of these cells expressing primitive markers within the nerve.

To our surprise, we observed osterix positive cells on the nerve as early as day 2, in the presence of cromolyn. There were also cells that expressed primitive stem cell factors, which appeared to simultaneously express osterix, suggesting that these cells are osteoblast precursors. The majority of osterix positive expression was associated with the nerve. We also observed Klf-4^{+} and nanog^{+} cells that were not associated with osterix, suggesting that these cells may have other potentials. Besides osteoblasts, another possible fate of these cells may be brown adipocytes, which we have shown previously to be critical for reduction of the oxygen tension in the microenvironment for cartilage formation [37] and for secreting VEGF for vessel formation [38]. It has recently been noted that the *Misty* mouse phenotype [47], which is deficient in brown fat, is caused by a mutation in dock 7 [48] , a neuronal stem cell migration factor. It is intriguing to speculate that brown fat progenitors may also reside in peripheral nerves, particularly since TRPV1 responds to heat [25]. Further, we previously demonstrated the rapid formation of new vessels early after BMP2 induction [38], suggesting that several types of tissues are being assembled simultaneously during this period. Osterix has previously been suggested to play a role in osteoblast lineage commitment of progenitors, suppressing the adipose phenotype [49]. Perhaps the early osterix expression, 4 days prior to the appearance of osteoid matrix, may be part of a regulatory mechanism to preserve these cells, for future osteogenic fate. Finally, although not highlighted in this manuscript, we did observe osterix positive cells that co-aligned with early endothelial markers, such as flk 1, that we have previously identified

as characteristic of this early vasculogenesis [38]. This notion also supports the work of Louney *et al* [50], suggesting that osteoblast progenitors reside within the newly forming vessels, have a Tie 2 marker, and are not derived from marrow [51].

This study is the first step in identifying a potential direct role for the peripheral nervous system in the induction of heterotopic ossification. The data suggests that early neuroinflammation, elicited in the presence of BMP2, may be capable of expanding a population of cells within the nerve, which can migrate and potentially contribute to a number of structures, rapidly assembling to produce HO. Suppression of these steps significantly decreases HO formation. Although it is unclear what affects this may have on the adjacent skeletal bone, the data suggests that there is direct communication with the hypothalamus, which could, in part, signal to impact bone remodeling. Understanding these earliest steps of HO will, for the first time, provide us novel targets for therapeutic intervention, which may ultimately lead to effective treatments. Finally, it is conceivable that such a mechanism could play a role in many other disease states, including neurofibromatosis and vascular calcification.

Acknowledgments

This work was supported by grants from the US Department of the Army, Orthopedic Trauma to ARD (DAMD W81XWH-07-1-0214) and EAOD (DAMD W81XWH-07-1-0215), as well as a grant from NBIB (EB005173) and from the NIH (T-32 HL092332-06) to ER, and a Pre-doctoral fellowship from the American Heart Association (AHA 10815339F) and Kirschstein-NRSA (T32 HL092332-08) to ES. We thank Hua Chen of the Vector Development Laboratory, Baylor College of Medicine for vector preparation.

Figure 1: Quantitation of substance P and CGRP protein by ELISA. Soft tissues, which encompass the site of new bone formation, were isolated at daily intervals from animals receiving either AdBMP2 (BMP2) or Adempty (control) transduced cells, and protein extracts were generated. **A.)** Substance P total protein was quantified and statistically significant changes between the groups, as denoted by an asterisk, determined using a standard t-test; n=4. **B.)** CGRP total protein was quantified and statistically significant changes between the groups, as denoted by an asterisk, determined using a standard t-test; n=4. * denotes statistical significance.

Figure 2: Photomicrographs of substance P and CGRP protein expression in tissues isolated four days after induction of HO. Tissues receiving cells transduced with AdBMP2 (BMP2) or Adempty cassette (control) were isolated four days after induction and immunostained with antibodies against substance P and CGRP. Expression of these factors was found to co-localize with the area of newly forming bone, but was minimal in tissues receiving the Adempty cassette transduced cells. Hematoxylin and eosin stained serial sections, adjacent to the section used for immunostaining four days after receiving **(A)** AdBMP2 transduced cells or **(D)** Adempty cassette transduced cells. Positive staining in the region of new bone (**B and C**) or nerve (**E and F**) for CGRP (B and E; red color) or substance P (C and F; green color).

Figure 3: Microcomputational analysis of heterotopic ossification ten days after induction with AdBMP2 transduced cells, in C57/BL6, wild type or $TRVP1^{-/-}$ mice. **(A)** Three dimensional reconstructions of representative samples for each group. **(B)** Quantitation of bone volume and statistically significant changes between the groups was determined using a one-way analysis of variance; n=7. * denotes statistical significance.

Figure 4: Quantitation of mast cells in tissues surrounding the area of new bone formation. Tissue sections were stained with the mast cell stain, toluidine blue. Photomicrographs of random fields (5 per section) were taken at 10X magnification, for every fifth slide, throughout the entire hindlimb. Each field equals $5.2mm^2$. **(A)** Quantification of the average number of mast cells within the tissues at daily intervals after induction of HO. Statistically significant changes were determined using a standard t-test; n=3 biological replicates. Seven slides were analyzed per tissue, and 5 fields per slide (35 images quantified per sample/time point). * denotes statistical significance. **(B)** Representative photomicrographs of tissues isolated two days after receiving AdBMP2 (BMP2) or Adempty (control) transduced cells, stained with toluidine blue. Positive cells are highlighted with arrows.

Figure 5: Microcomputational analysis of heterotopic ossification ten days after induction with AdBMP2 transduced cells, in mice pre-treated with either cromolyn or vehicle control (PBS). **(A)** Three dimensional reconstructions of representative samples for each group. **(B)** Quantitation of bone volume and statistically significant changes between the groups was determined using a one-way analysis of variance; n=9. * denotes statistical significance.

Figure 6. Peripheral nerves contain primitive stem cell markers and osterix after BMP2 induction in the presence of cromolyn.
A. Photomicrographs of tissues isolated two days after induction of HO. Tissues from animals receiving cells transduced with AdBMP2 and pre-treated with either cromolyn (a-d) or vehicle control (e-h) were isolated two days after induction, and immunostained with antibodies against stem cell markers, Klf4 and Nanog. Expression of these factors was found to co-localize to nerves residing within the area of new bone formation. Nerves were identified by hematoxylin and eosin staining of a serial section adjacent to the immunostainned tissues (**a** and **e**) and by

neurofilament (NF) staining (**b** and **f**; green color). Positive staining for Klf4 (**c**; red color) or Nanog (**d**; red color) was observed throughout the nerves in tissues isolated from animals receiving cromolyn at 2 days after induction. In comparison, the nerves in animals receiving vehicle control appeared to lack positive staining for either Klf 4 (**g**; red color) or nanog (**h**; red color).
B. Photomicrographs of osterix expression within tissues isolated two days after BMP2 induction in the presence of cromolyn. Images of osterix expression (**g**; osterix red color, DAPI blue color) associated with the nerve (**h**; neurofilament, NF, green color). **i**, osterix and NF, is a merger of g and h. Images of the expression of **a, d** osterix (green, DAPI blue) and **b**, Klf4 (red) or **e**, nanog (red). **c**, osterix and Klf4, is a merger of a and b. **f**, osterix and nanog is a merger of d and e.

Supplemental data 1: Quantitation of substance P and CGRP protein by ELISA. Soft tissues, which encompass the site of new bone formation, were isolated from C57/BL6, wild type (wt) or $TRVP1^{-/-}$ animals three days after receiving either AdBMP2 (BMP2) or Adempty cassette (control) transduced cells. Protein extracts were generated from these tissues. **A.)** Substance P total protein was quantified and statistically significant changes between the groups was determined using a standard t-test; n=4. **B.)** CGRP total protein was quantified and statistically significant changes between the groups was determined using a standard t-test; n=4. * denotes statistical significance between groups receiving the different transduced cells. # denotes statistical significance between wild type and $TRVP1^{-/-}$ mice. ns means not significant.

References:

1. Urist MR: Bone: formation by autoinduction, Science 1965, 150:893-899

2. Smadja DM, Bieche I, Silvestre JS, Germain S, Cornet A, Laurendeau I, Duong-Van-Huyen JP, Emmerich J, Vidaud M, Aiach M, Gaussem P: Bone morphogenetic proteins 2 and 4 are selectively expressed by late outgrowth endothelial progenitor cells and promote neoangiogenesis, Arterioscler Thromb Vasc Biol 2008, 28:2137-2143

3. Anderson RM, Stottmann RW, Choi M, Klingensmith J: Endogenous bone morphogenetic protein antagonists regulate mammalian neural crest generation and survival, Dev Dyn 2006, 235:2507-2520

4. Bhatia M, Bonnet D, Wu D, Murdoch B, Wrana J, Gallacher L, Dick JE: Bone morphogenetic proteins regulate the developmental program of human hematopoietic stem cells, J Exp Med 1999, 189:1139-1148

5. Tseng YH, Kokkotou E, Schulz TJ, Huang TL, Winnay JN, Taniguchi CM, Tran TT, Suzuki R, Espinoza DO, Yamamoto Y, Ahrens MJ, Dudley AT, Norris AW, Kulkarni RN, Kahn CR: New role of bone morphogenetic protein 7 in brown adipogenesis and energy expenditure, Nature 2008, 454:1000-1004

6. Sottile V, Seuwen K: Bone morphogenetic protein-2 stimulates adipogenic differentiation of mesenchymal precursor cells in synergy with BRL 49653 (rosiglitazone), FEBS Lett 2000, 475:201-204

7. Yanagita M: BMP modulators regulate the function of BMP during body patterning and disease progression, Biofactors 2009, 35:113-119

8. Shore EM, Kaplan FS: Inherited human diseases of heterotopic bone formation, Nat Rev Rheumatol 6:518-527

9. Kaplan FS, Pignolo RJ, Shore EM: The FOP metamorphogene encodes a novel type I receptor that dysregulates BMP signaling, Cytokine Growth Factor Rev 2009, 20:399-407

10. Kaplan FS, Xu M, Seemann P, Connor JM, Glaser DL, Carroll L, Delai P, Fastnacht-Urban E, Forman SJ, Gillessen-Kaesbach G, Hoover-Fong J, Koster B, Pauli RM, Reardon W, Zaidi SA, Zasloff M, Morhart R, Mundlos S, Groppe J, Shore EM: Classic and atypical fibrodysplasia ossificans progressiva (FOP) phenotypes are caused by mutations in the bone morphogenetic protein (BMP) type I receptor ACVR1, Hum Mutat 2009, 30:379-390

11. Vanden Bossche L, Vanderstraeten G: Heterotopic ossification: a review, J Rehabil Med 2005, 37:129-136

12. Baird EO, Kang QK: Prophylaxis of heterotopic ossification - an updated review, J Orthop Surg Res 2009, 4:12

13. Oury F, Yadav VK, Wang Y, Zhou B, Liu XS, Guo XE, Tecott LH, Schutz G, Means AR, Karsenty G: CREB mediates brain serotonin regulation of bone mass through its expression in ventromedial hypothalamic neurons, Genes Dev 24:2330-2342

14. Ducy P, Karsenty G: The two faces of serotonin in bone biology, J Cell Biol 191:7-13

15. Shi Y, Oury F, Yadav VK, Wess J, Liu XS, Guo XE, Murshed M, Karsenty G: Signaling through the M(3) muscarinic receptor favors bone mass accrual by decreasing sympathetic activity, Cell Metab 11:231-238

16. Takeda S, Karsenty G: Molecular bases of the sympathetic regulation of bone mass, Bone 2008, 42:837-840

17. Fu L, Patel MS, Bradley A, Wagner EF, Karsenty G: The molecular clock mediates leptin-regulated bone formation, Cell 2005, 122:803-815

18. Forsberg JA, Pepek JM, Wagner S, Wilson K, Flint J, Andersen RC, Tadaki D, Gage FA, Stojadinovic A, Elster EA: Heterotopic ossification in high-energy wartime extremity injuries: prevalence and risk factors, J Bone Joint Surg Am 2009, 91:1084-1091

19. Beiner JM, Jokl P: Muscle contusion injury and myositis ossificans traumatica, Clin Orthop Relat Res 2002, S110-119

20. Johnson RC, Leopold JA, Loscalzo J: Vascular calcification: pathobiological mechanisms and clinical implications, Circ Res 2006, 99:1044-1059

21. Sucosky P, Balachandran K, Elhammali A, Jo H, Yoganathan AP: Altered shear stress stimulates upregulation of endothelial VCAM-1 and ICAM-1 in a BMP-4- and TGF-beta1-dependent pathway, Arterioscler Thromb Vasc Biol 2009, 29:254-260

22. Kwong FN, Harris MB: Recent developments in the biology of fracture repair, J Am Acad Orthop Surg 2008, 16:619-625

23. Bucelli RC, Gonsiorek EA, Kim WY, Bruun D, Rabin RA, Higgins D, Lein PJ: Statins decrease expression of the proinflammatory neuropeptides calcitonin gene-related peptide and substance P in sensory neurons, J Pharmacol Exp Ther 2008, 324:1172-1180

24. Schaible HG, Del Rosso A, Matucci-Cerinic M: Neurogenic aspects of inflammation, Rheum Dis Clin North Am 2005, 31:77-101, ix

25. Szallasi A, Cortright DN, Blum CA, Eid SR: The vanilloid receptor TRPV1: 10 years from channel cloning to antagonist proof-of-concept, Nat Rev Drug Discov 2007, 6:357-372

26. Khairatkar-Joshi N, Szallasi A: TRPV1 antagonists: the challenges for therapeutic targeting, Trends Mol Med 2009, 15:14-22

27. Razavi R, Chan Y, Afifiyan FN, Liu XJ, Wan X, Yantha J, Tsui H, Tang L, Tsai S, Santamaria P, Driver JP, Serreze D, Salter MW, Dosch HM: TRPV1+ sensory neurons

control beta cell stress and islet inflammation in autoimmune diabetes, Cell 2006, 127:1123-1135

28. Apel PJ, Crane D, Northam CN, Callahan M, Smith TL, Teasdall RD: Effect of selective sensory denervation on fracture-healing: an experimental study of rats, J Bone Joint Surg Am 2009, 91:2886-2895

29. Morrison SJ, White PM, Zock C, Anderson DJ: Prospective identification, isolation by flow cytometry, and in vivo self-renewal of multipotent mammalian neural crest stem cells, Cell 1999, 96:737-749

30. Adameyko I, Lallemend F, Aquino JB, Pereira JA, Topilko P, Muller T, Fritz N, Beljajeva A, Mochii M, Liste I, Usoskin D, Suter U, Birchmeier C, Ernfors P: Schwann cell precursors from nerve innervation are a cellular origin of melanocytes in skin, Cell 2009, 139:366-379

31. Hu-Lieskovan S, Zhang J, Wu L, Shimada H, Schofield DE, Triche TJ: EWS-FLI1 fusion protein up-regulates critical genes in neural crest development and is responsible for the observed phenotype of Ewing's family of tumors, Cancer Res 2005, 65:4633-4644

32. Cavazzana AO, Miser JS, Jefferson J, Triche TJ: Experimental evidence for a neural origin of Ewing's sarcoma of bone, Am J Pathol 1987, 127:507-518

33. Jiang X, Iseki S, Maxson RE, Sucov HM, Morriss-Kay GM: Tissue origins and interactions in the mammalian skull vault, Dev Biol 2002, 241:106-116

34. Olmsted-Davis EA, Gugala Z, Gannon FH, Yotnda P, McAlhany RE, Lindsey RW, Davis AR: Use of a chimeric adenovirus vector enhances BMP2 production and bone formation, Hum Gene Ther 2002, 13:1337-1347

35. Gugala Z, Olmsted-Davis EA, Gannon FH, Lindsey RW, Davis AR: Osteoinduction by ex vivo adenovirus-mediated BMP2 delivery is independent of cell type, Gene Ther 2003, 10:1289-1296

36. Fouletier-Dilling CM, Gannon FH, Olmsted-Davis EA, Lazard Z, Heggeness MH, Shafer JA, Hipp JA, Davis AR: Efficient and rapid osteoinduction in an immune-competent host, Hum Gene Ther 2007, 18:733-745

37. Olmsted-Davis E, Gannon FH, Ozen M, Ittmann MM, Gugala Z, Hipp JA, Moran KM, Fouletier-Dilling CM, Schumara-Martin S, Lindsey RW, Heggeness MH, Brenner MK, Davis AR: Hypoxic adipocytes pattern early heterotopic bone formation, Am J Pathol 2007, 170:620-632

38. Dilling CF, Wada AM, Lazard ZW, Salisbury EA, Gannon FH, Vadakkan TJ, Gao L, Hirschi K, Dickinson ME, Davis AR, Olmsted-Davis EA: Vessel formation is induced prior to the appearance of cartilage in BMP-2-mediated heterotopic ossification, J Bone Miner Res 2010, 25:1147-1156

39. Fouletier-Dilling CM, Bosch P, Davis AR, Shafer JA, Stice SL, Gugala Z, Gannon FH, Olmsted-Davis EA: Novel compound enables high-level adenovirus transduction in the absence of an adenovirus-specific receptor, Hum Gene Ther 2005, 16:1287-1297

40. Richardson JD, Vasko MR: Cellular mechanisms of neurogenic inflammation, J Pharmacol Exp Ther 2002, 302:839-845

41. Kleij HP, Bienenstock J: Significance of Conversation between Mast Cells and Nerves, Allergy Asthma Clin Immunol 2005, 1:65-80

42. Kulka M, Sheen CH, Tancowny BP, Grammer LC, Schleimer RP: Neuropeptides activate human mast cell degranulation and chemokine production, Immunology 2008, 123:398-410

43. Johnson D, Weiner HL, Seeldrayers PA: Role of mast cells in peripheral nervous system demyelination, Ann N Y Acad Sci 1988, 540:727-728

44. Gannon FH, Glaser D, Caron R, Thompson LD, Shore EM, Kaplan FS: Mast cell involvement in fibrodysplasia ossificans progressiva, Hum Pathol 2001, 32:842-848

45. Theoharides TC, Bondy PK, Tsakalos ND, Askenase PW: Differential release of serotonin and histamine from mast cells, Nature 1982, 297:229-231

46. Salisbury E, Sonnet, C, Heggeness, M, Davis, AR, Olmsted-Davis, EA: Heterotopic ossification has some nerve Critical Reviews™ in Eukaryotic Gene Expression 2010.

47. Sviderskaya EV, Novak EK, Swank RT, Bennett DC: The murine misty mutation: phenotypic effects on melanocytes, platelets and brown fat, Genetics 1998, 148:381-390

48. Blasius AL, Brandl K, Crozat K, Xia Y, Khovananth K, Krebs P, Smart NG, Zampolli A, Ruggeri ZM, Beutler BA: Mice with mutations of Dock7 have generalized hypopigmentation and white-spotting but show normal neurological function, Proc Natl Acad Sci U S A 2009, 106:2706-2711

49. Cheng SL, Shao JS, Charlton-Kachigian N, Loewy AP, Towler DA: MSX2 promotes osteogenesis and suppresses adipogenic differentiation of multipotent mesenchymal progenitors, J Biol Chem 2003, 278:45969-45977

50. Lounev VY, Ramachandran R, Wosczyna MN, Yamamoto M, Maidment AD, Shore EM, Glaser DL, Goldhamer DJ, Kaplan FS: Identification of progenitor cells that contribute to heterotopic skeletogenesis, J Bone Joint Surg Am 2009, 91:652-663

51. Kaplan FS, Glaser DL, Shore EM, Pignolo RJ, Xu M, Zhang Y, Senitzer D, Forman SJ, Emerson SG: Hematopoietic stem-cell contribution to ectopic skeletogenesis, J Bone Joint Surg Am 2007, 89:347-357

A.

Substance P Protein Expression

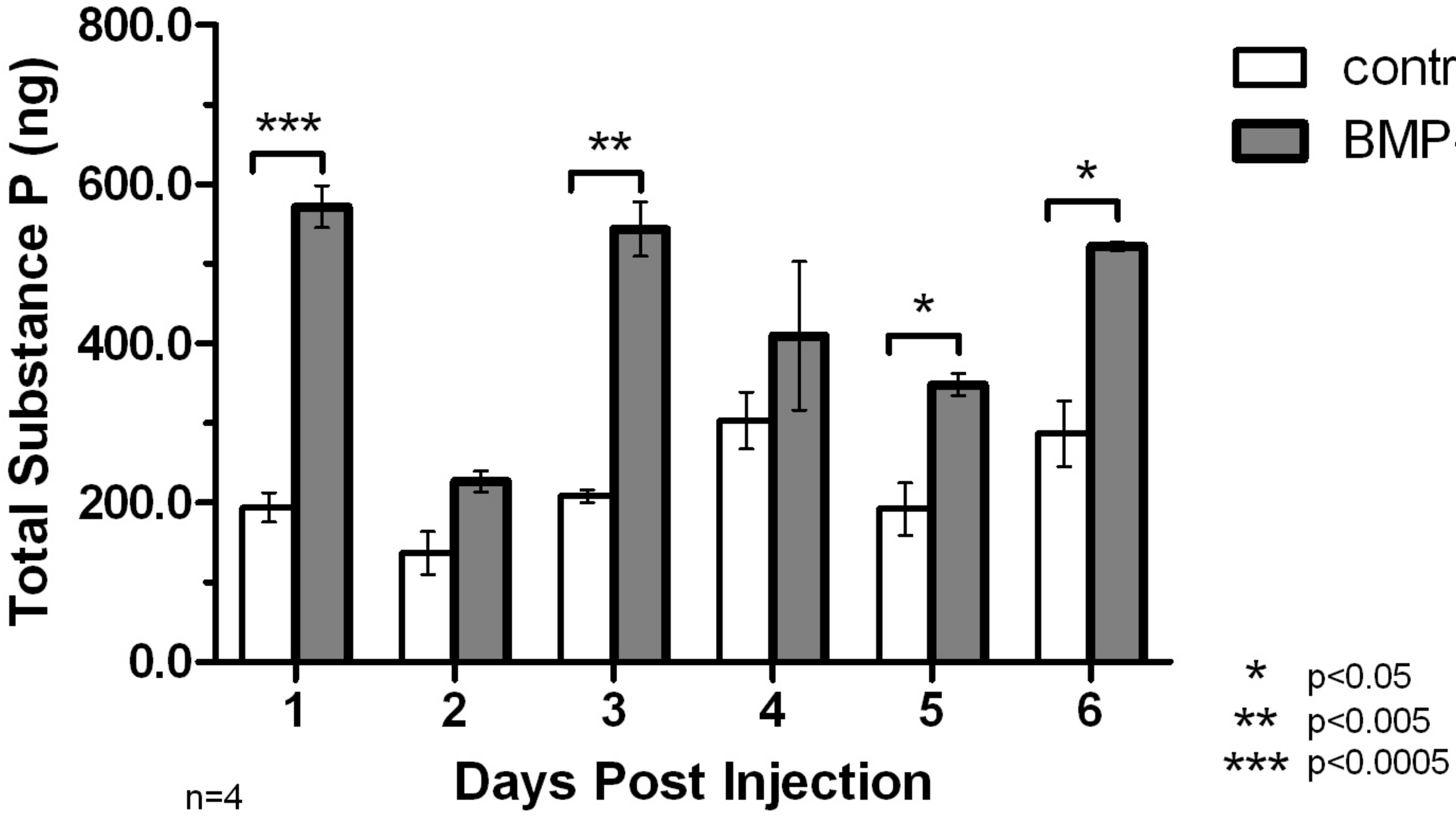

B.

CGRP Protein Expression

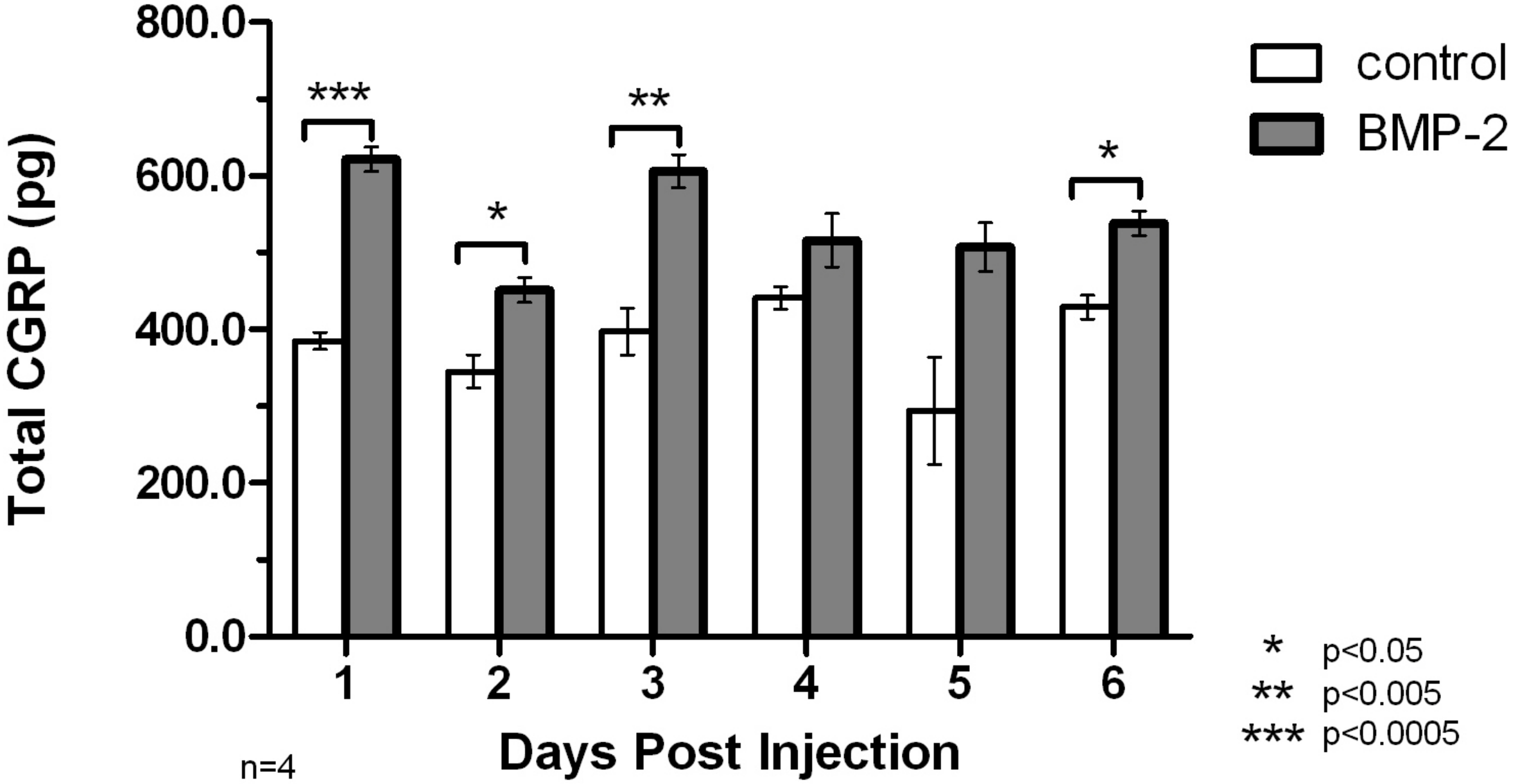

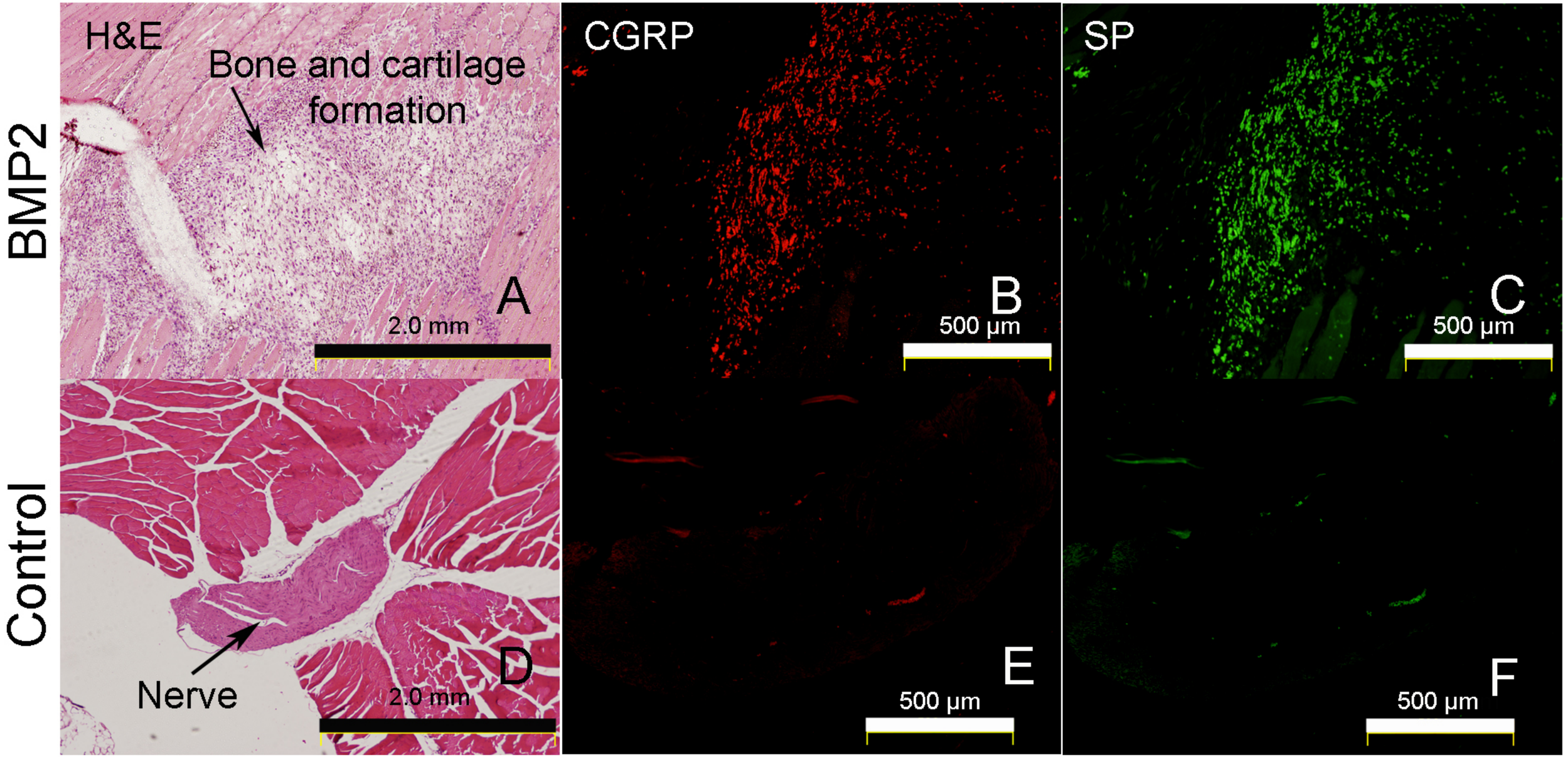
BMP2
Control
H&E
Bone and cartilage formation
A
2.0 mm
CGRP
B
500 µm
SP
C
500 µm
Nerve
D
2.0 mm
E
500 µm
F
500 µm

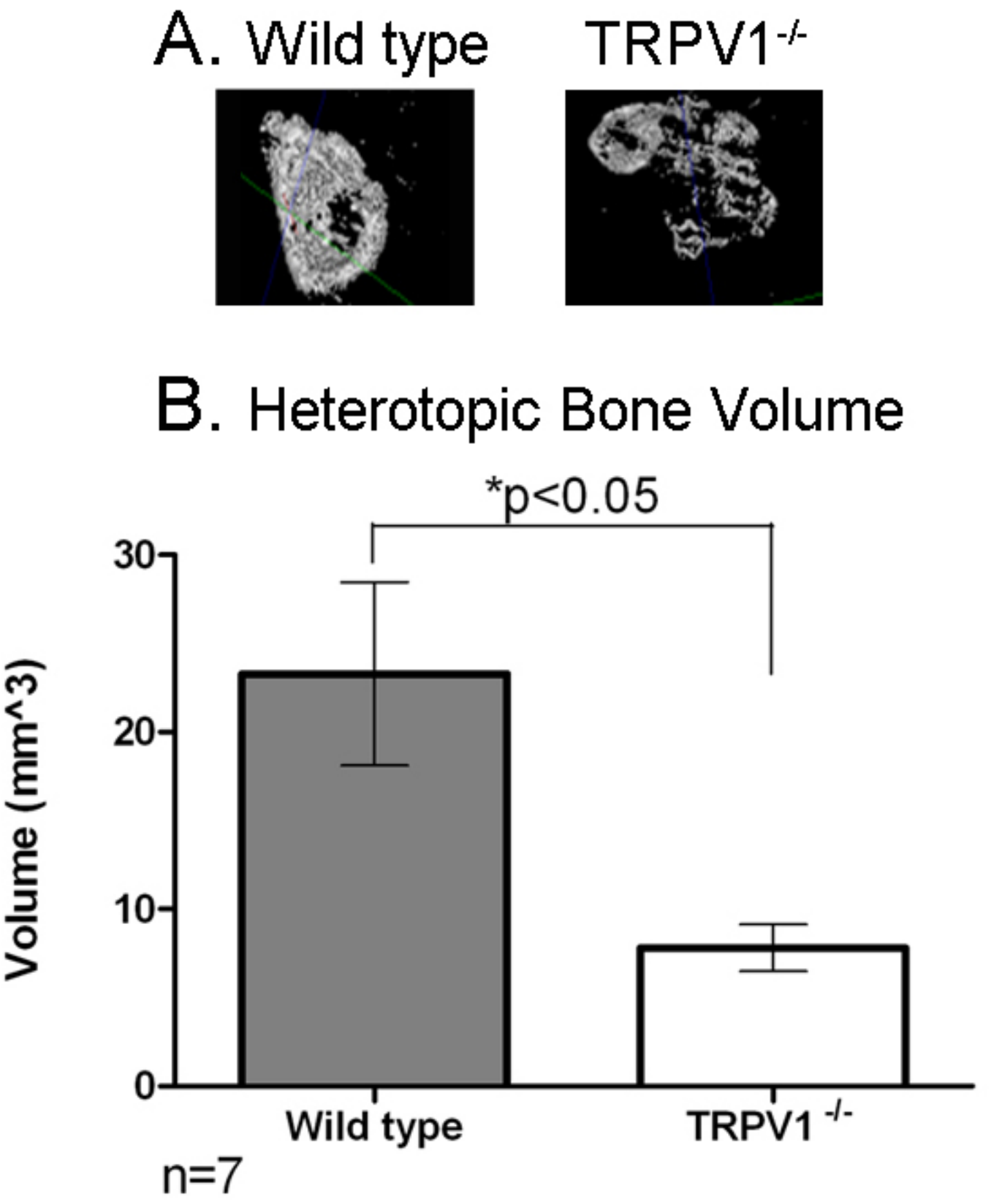
A. Wild type
TRPV1 -/-
B. Heterotopic Bone Volume
*p<0.05
Volume (mm^3)
30
20
10
0
Wild type
TRPV1 -/-
n=7

A.

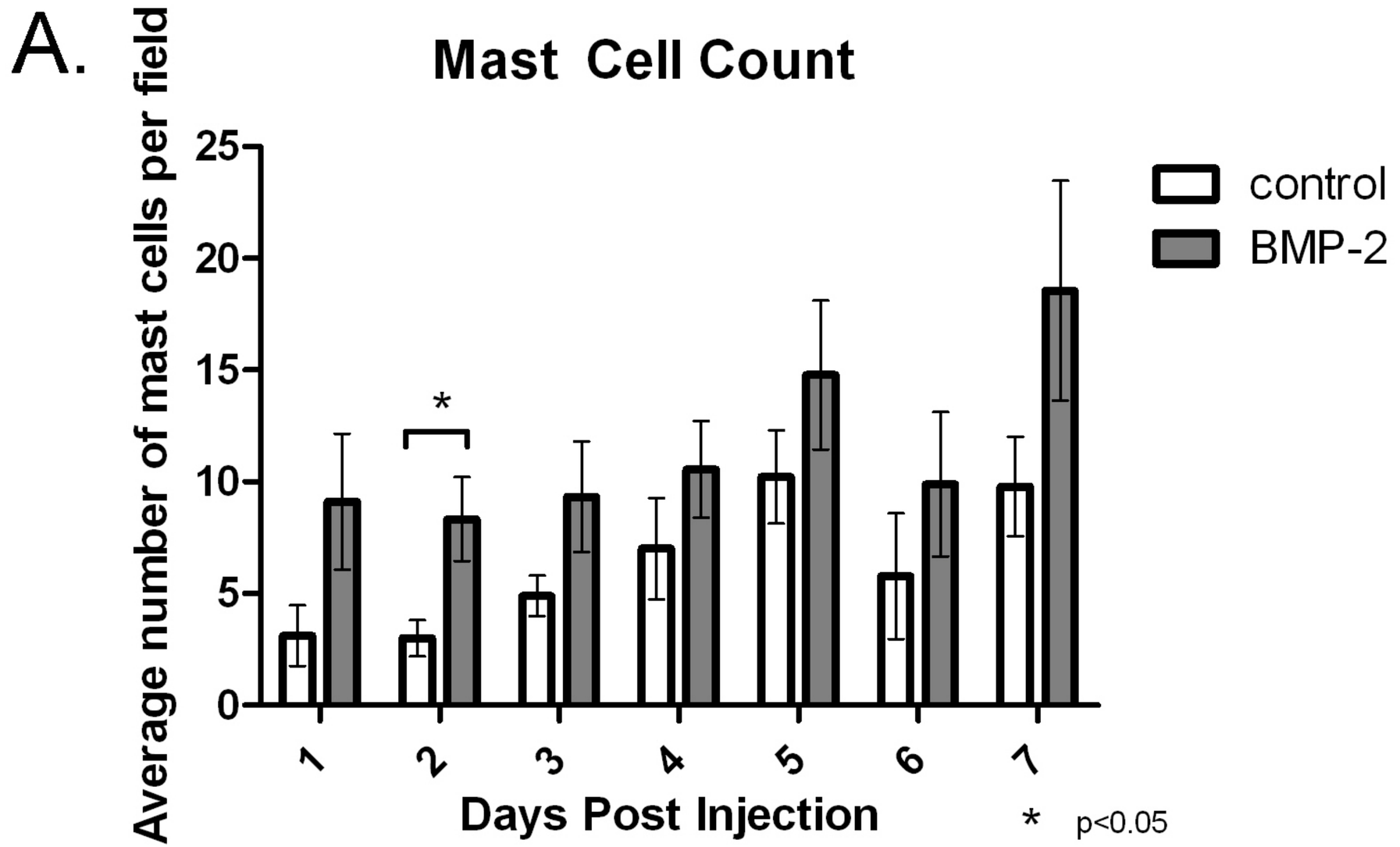
Mast Cell Count
Average number of mast cells per field
25
20
15
10
5
0
*
1
2
3
4
5
6
7
Days Post Injection
control
BMP-2
* p<0.05

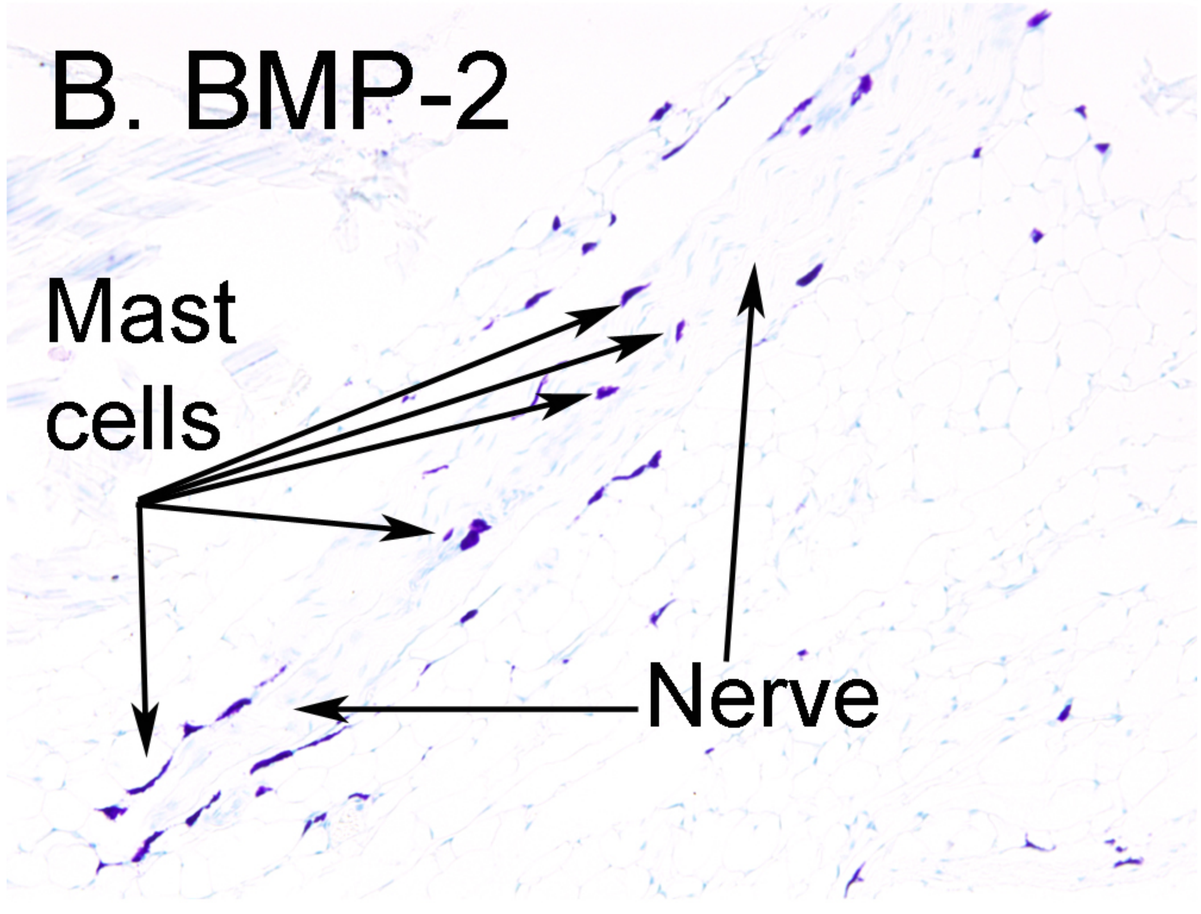
B. BMP-2
Mast cells
Nerve

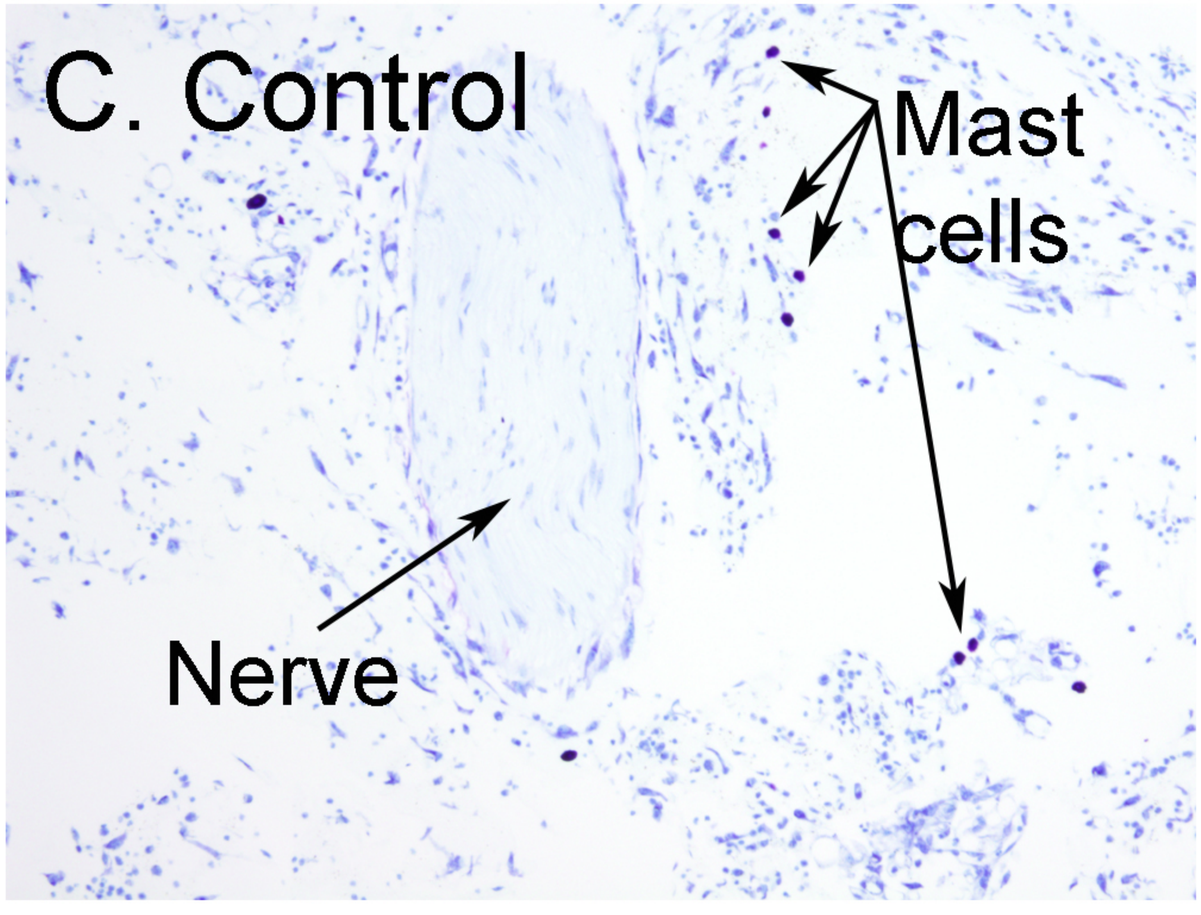
C. Control
Mast cells
Nerve

A. Control

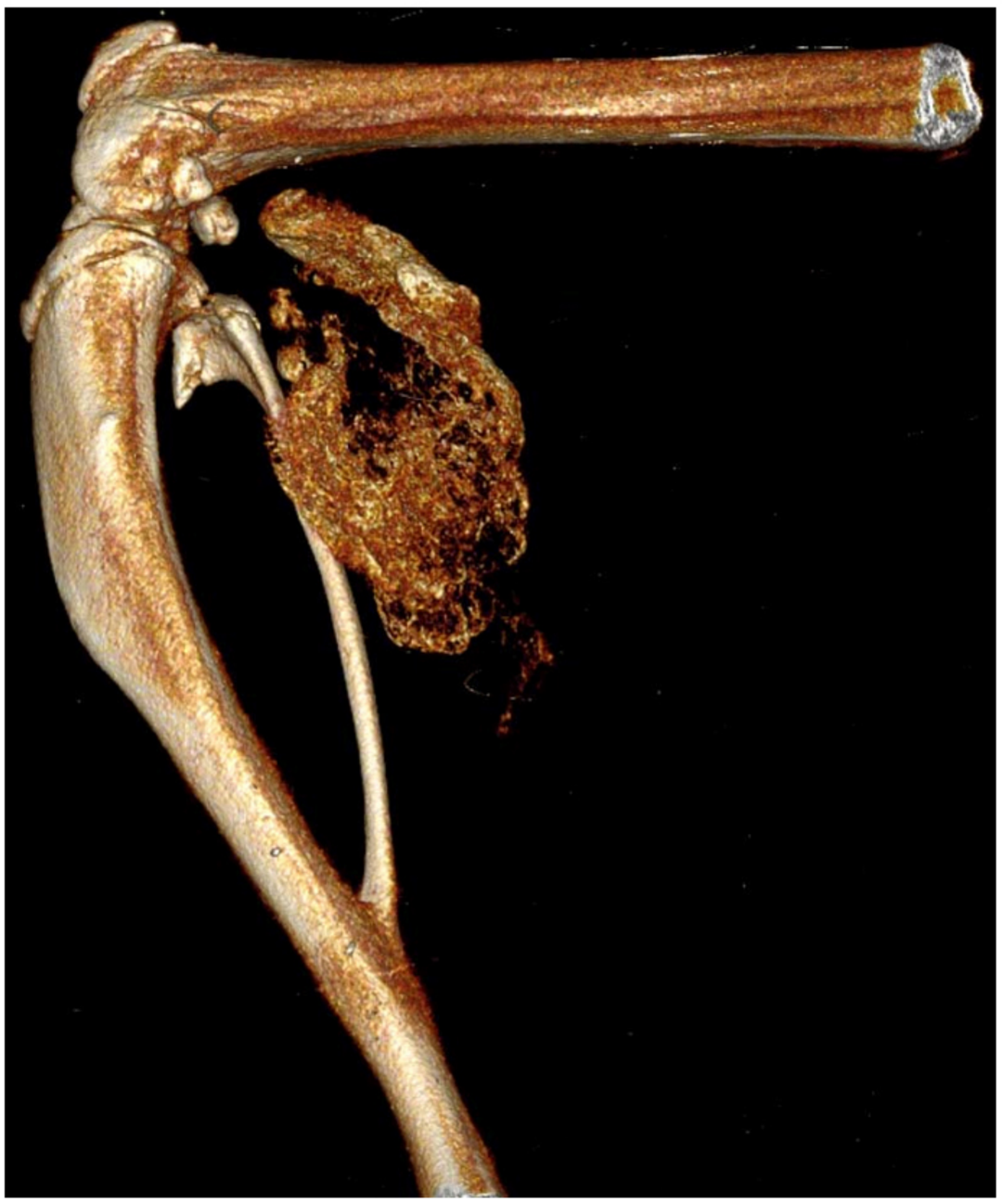

Cromolyn

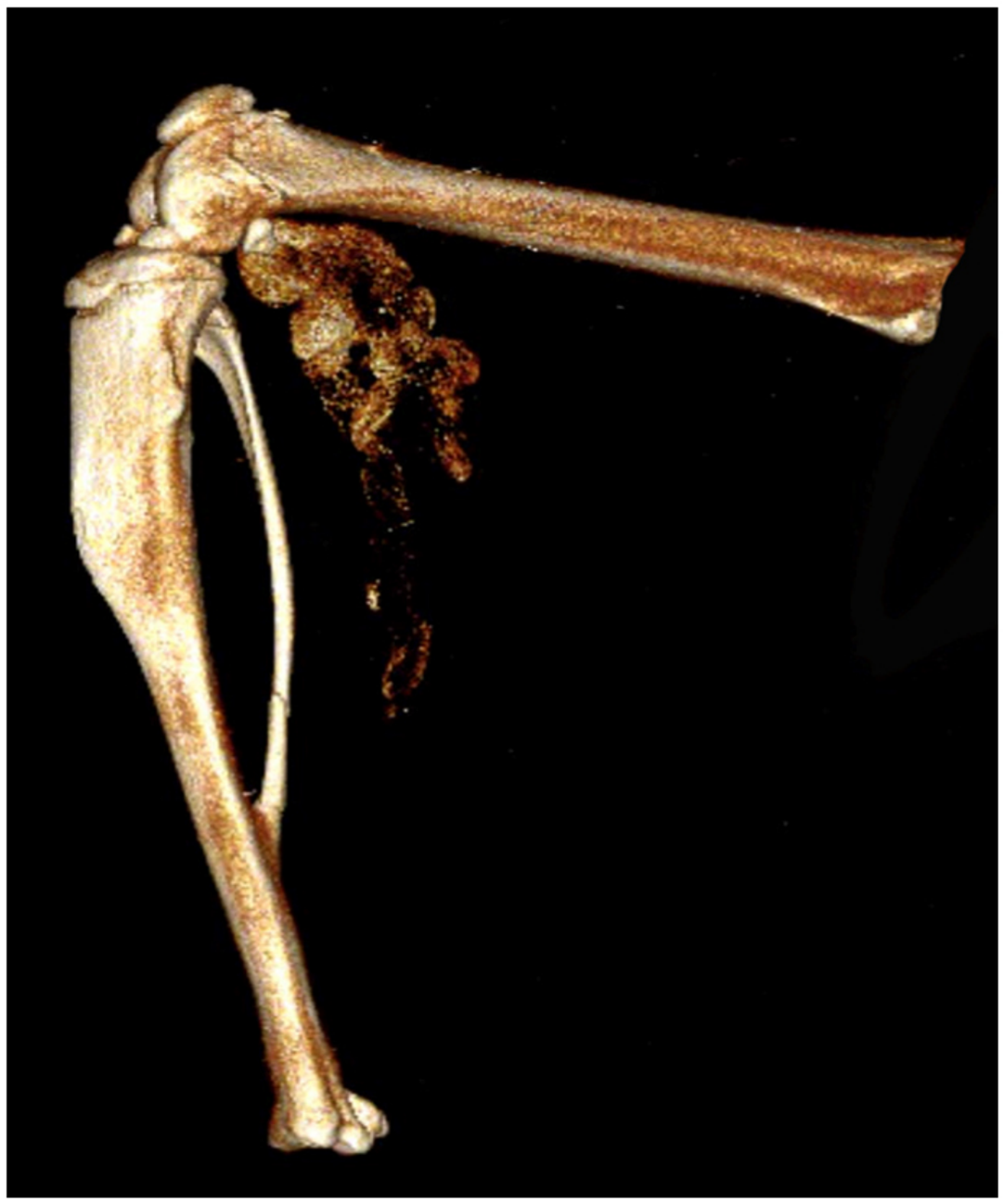

B. Heterotopic Bone Volume

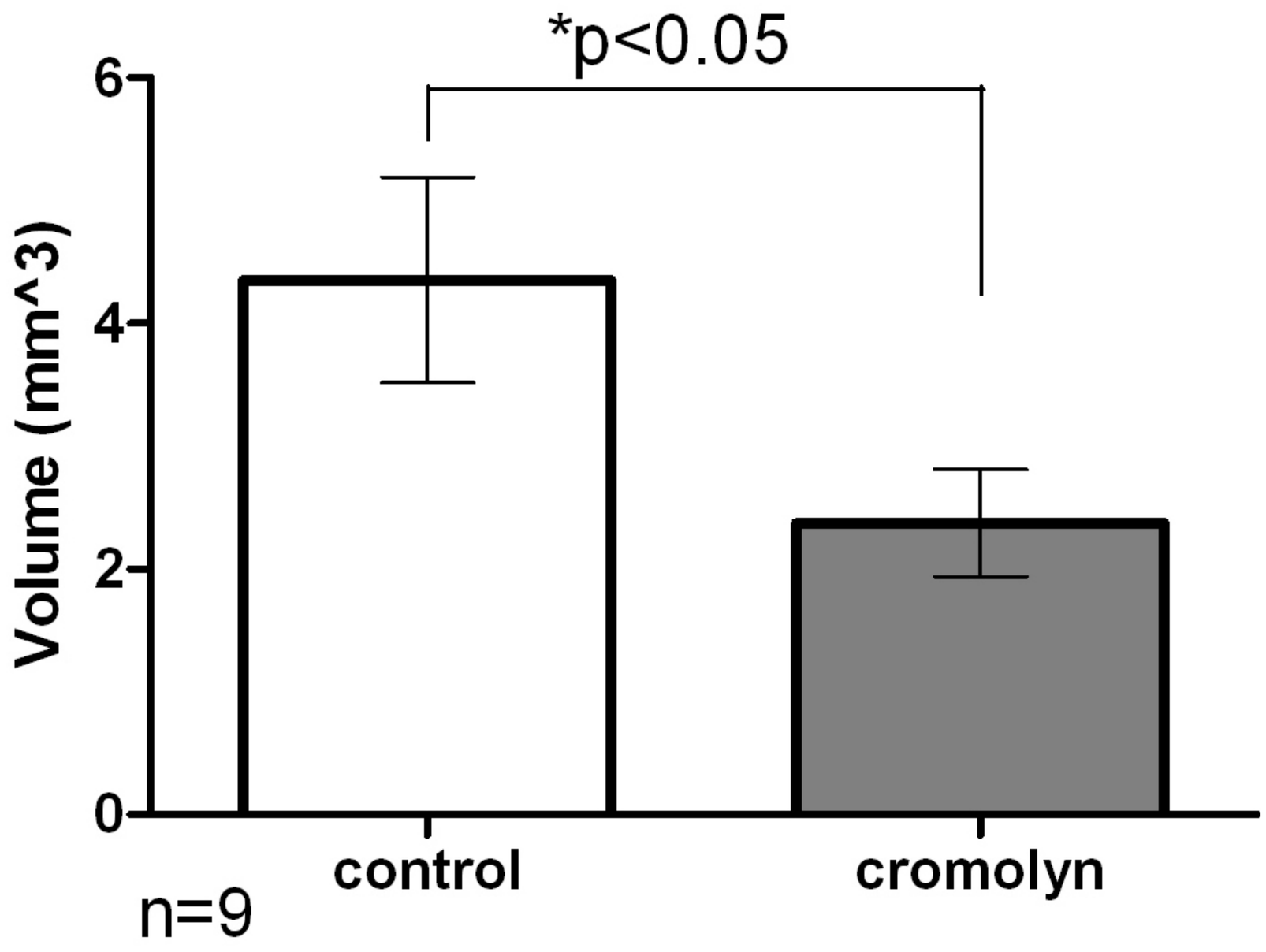

A.

BMP2 +Cromolyn

BMP2

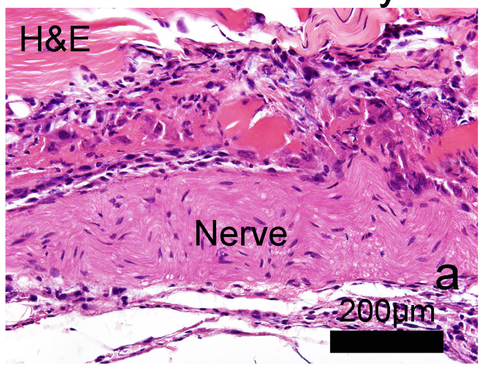

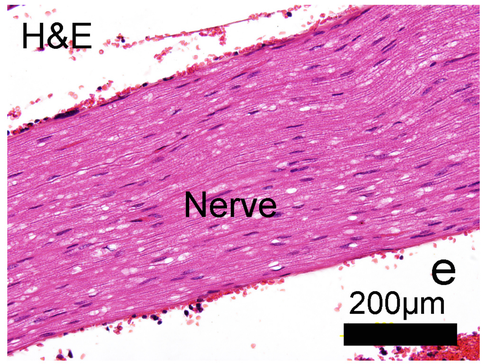

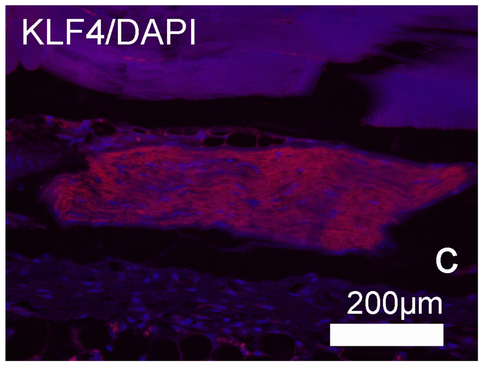

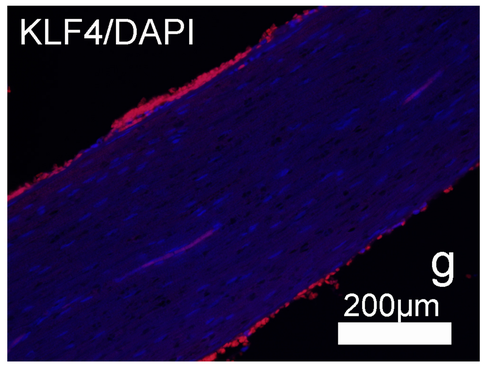

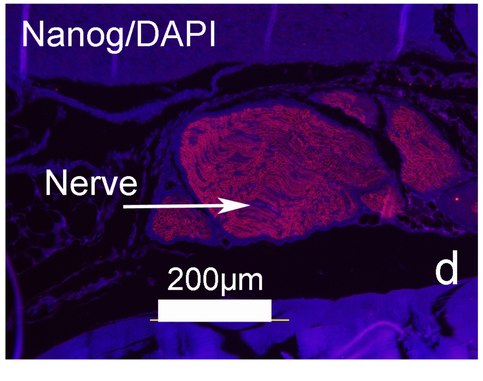

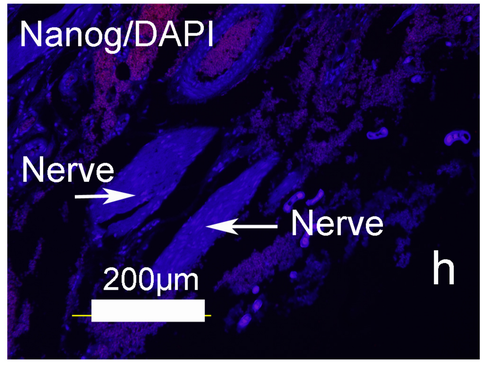

B.

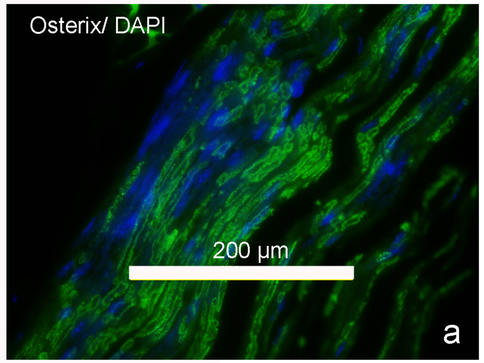

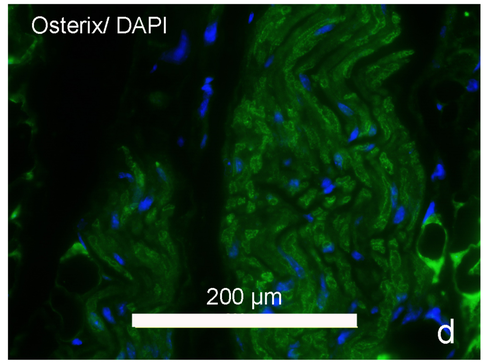

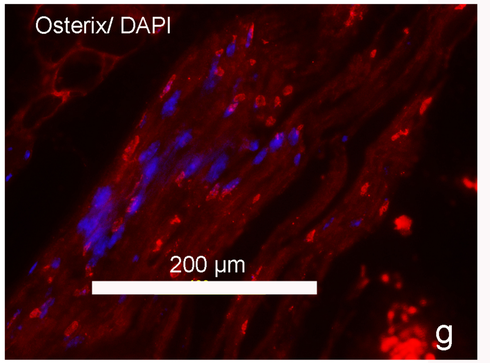

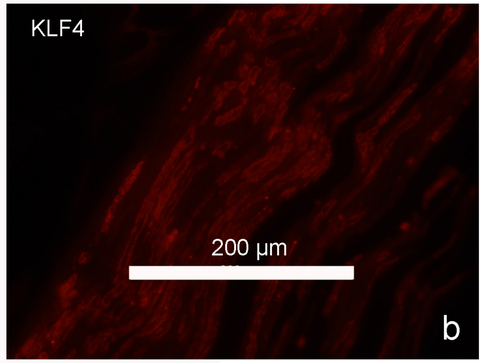

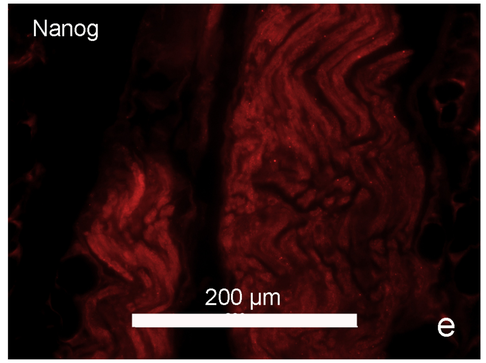

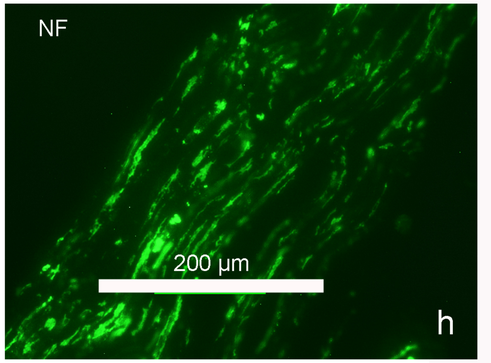

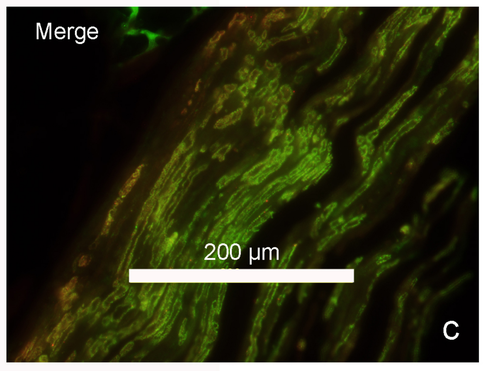

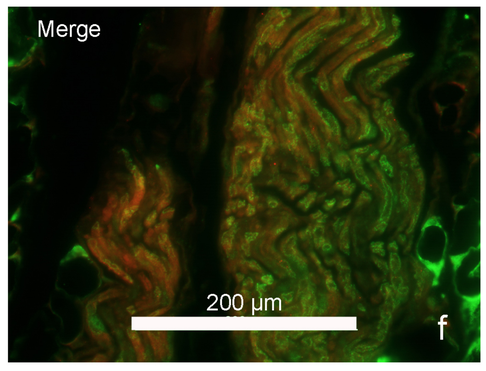

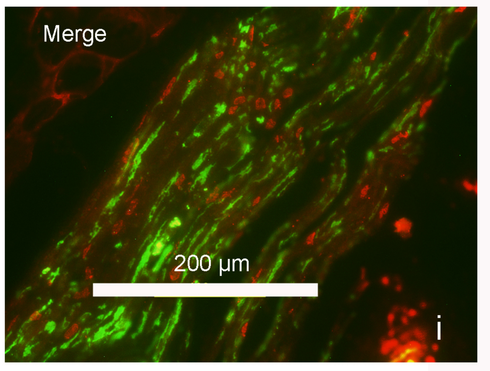

Osterix
DAPI
KLF4
Merge

Osterix
DAPI
Nanog
Merge

Osterix
DAPI
Neurofilament
Merge

A.

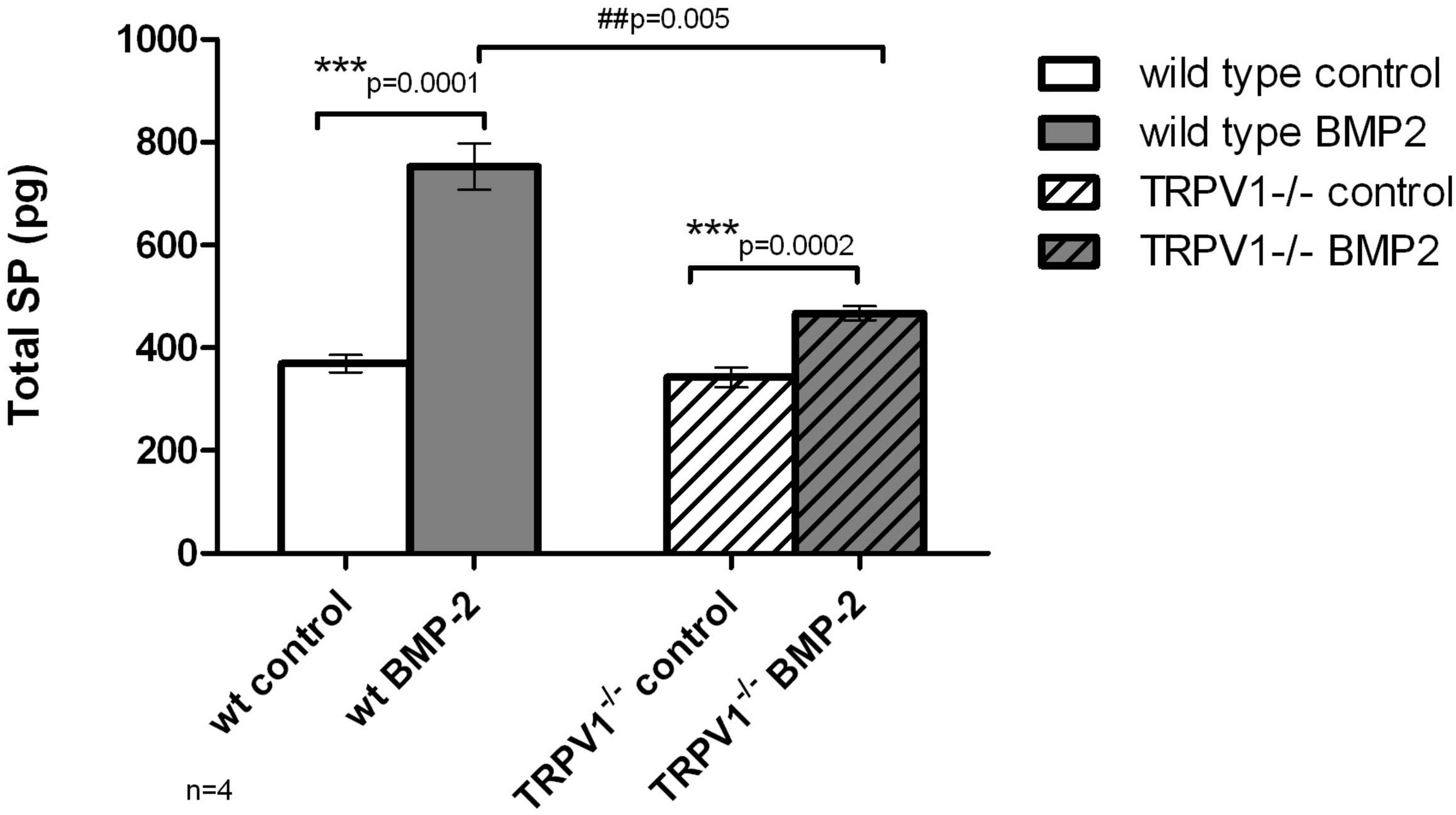
SP Protein Expression Day 3
Total SP (pg)
1000
800
600
400
200
0
***p=0.0001
##p=0.005
***p=0.0002
wild type control
wild type BMP2
TRPV1-/- control
TRPV1-/- BMP2
wt control
wt BMP-2
TRPV1-/- control
TRPV1-/- BMP-2
n=4

B.

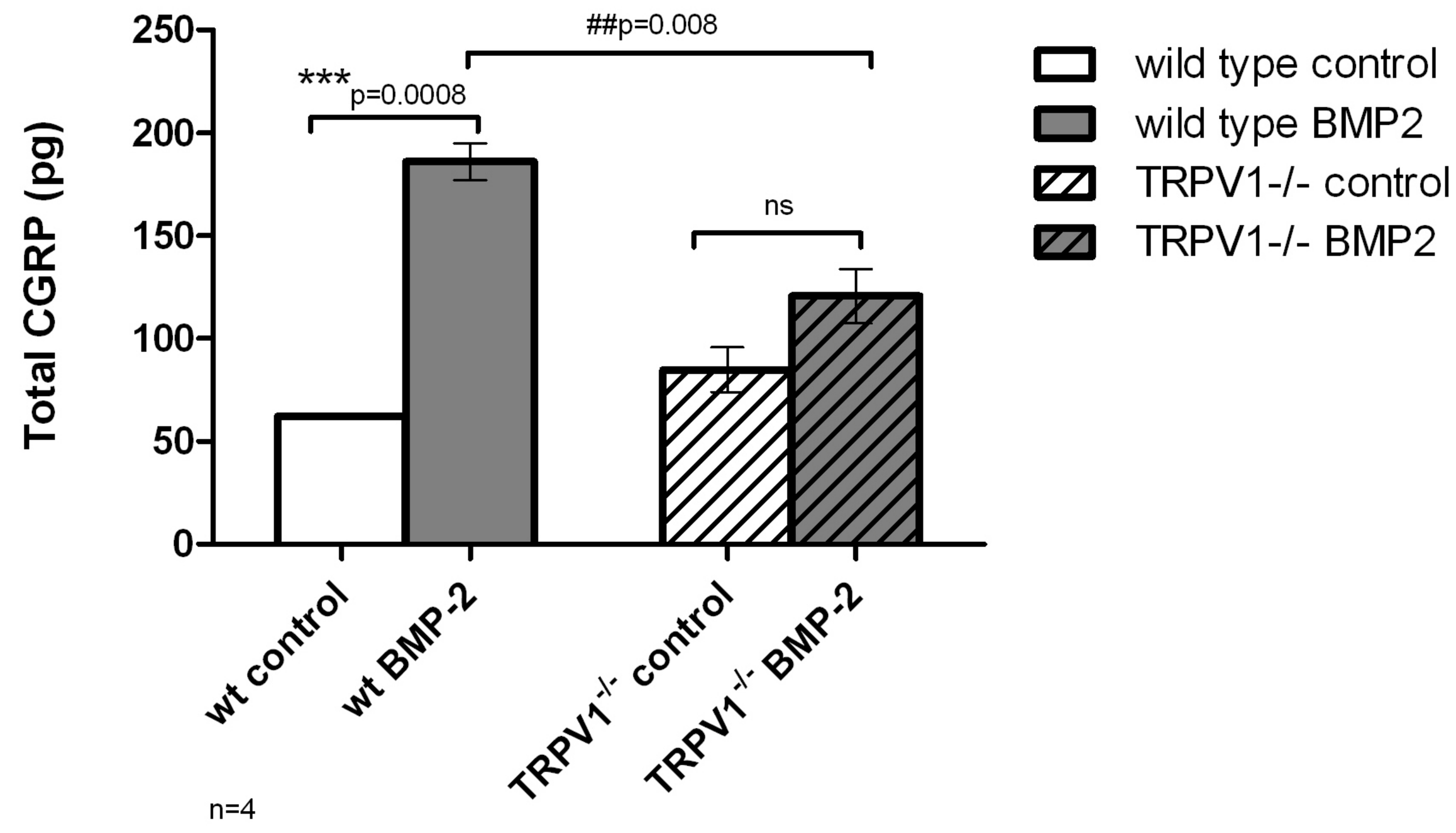
CGRP Protein Expression Day 3
Total CGRP (pg)
250
200
150
100
50
0
***p=0.0008
##p=0.008
ns
wild type control
wild type BMP2
TRPV1-/- control
TRPV1-/- BMP2
wt control
wt BMP-2
TRPV1-/- control
TRPV1-/- BMP-2
n=4